MANCHESTER METROPOLITAN UNIVERSITY

The impact of emissions of nitrogen oxides from aviation on tropospheric chemistry – the counterbalancing roles of ozone and methane

by

Agnieszka Maria Skowron

A thesis submitted in partial fulfilment for the degree of Doctor of Philosophy

in the

Faculty of Science and Engineering
School of Science and the Environment

November 2013

Abstract

Aviation is a unique anthropogenic emission source in that it is the only man-made source of emissions injected directly to the remote and uncontaminated regions of the atmosphere. It constitutes a relatively small fraction of total anthropogenic climate impact. However, with the potential increase in growth of air traffic and potential reductions of emissions in other sector, the importance of aircraft contribution to anthropogenic climate change may increase in the future.

Aviation NO_x emissions result in a short-term increase in tropospheric ozone (warming) and the long-term destruction of a small amount of ambient methane (cooling), positive and negative radiative forcing responses. In addition, the methane reduction results in a long-term reduction in tropospheric ozone (cooling) and a long-term reduction in water vapour in the stratosphere (cooling) from reduced oxidation of methane, both negative radiative forcing effects. The aircraft net NO_x response (the sum of all these components) is thought to result in a positive (warming) radiative forcing under constant emissions assumptions. The quantification of aircraft NO_x effects requires spatio-temporal analyses of its dependencies, which is challenging and result in significant variations in aircraft NO_x 'impact'.

An investigation of a series of different factors influencing the effect of aircraft NO_x emission on climate was performed using the global chemistry transport model (MOZART-3) in combination with a radiative transfer model (Edwards–Slingo), and rationale of the existing uncertainties associated with aircraft NO_x estimates was conducted. A wide spectrum in the magnitude and balance of chemical responses from aircraft NO_x perturbations, affecting Global Warming Potential estimates, was observed. The derived aircraft net NO_x radiative forcing was found to be as low as -0.4 and as high as 19.9 $mWm^{-2}/Tg(N)yr^{-1}$. The balance between aircraft ozone and methane changes proved to be experiment-specific, and it was observed to depend on background conditions due to surface emissions or region of emission, aircraft NO_x emission inventory, or size of aircraft NO_x emission rate. Thus, it was shown that it is impossible to define a unique GWP for aviation NO_x. Moreover, an aviation NO_x GWP increases with reduction of aircraft NO_x emissions and decreases with increased aircraft NO_x emissions.

Acknowledgements

It was a special journey, full of many people and many experiences.
It has been a pleasure.

First, and foremost I would like to thank my supervisors: David Lee and Ivar Isaksen, for their understanding and patience, for source of endless inspiration and most importantly, for giving me freedom to explore. I am also grateful to Dave Raper for his positive attitude and support in administrative formalities.

This work was made possible through a Studentship funded by Dalton Research Institute (MMU) during first years and the UK Department for Transport at later stage of this study. Christine Ingley and Anne-Marie Walsh are especially acknowledged for giving me ability to wade through all the forms of application, registration, suspension and so forth.

I would like to thank many of you for your support and motivation during recent years, especially: Ling Lim and Stacy Walters for setting up and testing CRAY-CX1, Sandra Fletcher for further assistance and Ruben Rodriguez de León for guarding RTM model. I also would like to thank Jérôme Hilaire, who introduced me to MOZART. I am grateful to Mike Jenkin, who unravelled organic chemistry for me and to Roger Kingdon for FACSIMILE exercises. Special thanks go to Jan Fuglestvedt for these few words, during one of the meetings, which awakened my 'NO_x imagination'.

There were ups and downs, but all is possible, when you believe in it. The spirit of people who surrounded me during this time kept me high. I am grateful to my Family and Friends – thanks you I had no choice – just to look ahead. I also would like to thank all in CATE for this warm and agreeable atmosphere.

Last, but definitely not least are Artur and Tymon – your smiles have rescued me!

Contents

List of Figures

List of Tables

Abbreviations

AEDT	Aviation Environmental Tool
AEM	Advanced Emission Model
AERO2K	Global Aviation Emission Inventory
AGWP	Absolute Global Warming Potential
AR4	Assessment Report 4
AR5	Assessment Report 5
CAEP	Committee on Aviation Environmental Protection
CCM	Climate Chemistry Model
CH_4	methane
CO	carbon monoxide
CO_2	carbon dioxide
CTM	Chemical Transport Model
DU	Dobson Unit
ECMWF	European Center for Medium-range Weather Forecasts
EU ETS	European Union Greenhouse Gas Emission Trading Scheme
FAST	Future Aviation Scenario Tool
GCM	General Circulation Model
GFDL	Geophysical Fluid Dynamics Laboratory
GTP	Global Temperature Change Potential
GWP	Global Warming Potential
IPCC	Intergovernmental Panel on Climate Change
ISCCP	International Satellite Cloud Climatology Project
JPL	Jet Propulsion Laboratory
LTO	Landing and Take-Off phases of aircraft operations
LOSU	Level of scientific understanding
MATCH	Model of Atmospheric Transport and Chemistry
MOZART	Model of OZone And Related Tracers
N	nitrogen
N_2O	nitrous oxide
NASA	National Aeronautics and Space Administration
NCAR	National Centre for Atmospheric Research
NMVOC	Non–methane volatile organic compounds
NO	nitric oxide, nitrogen monoxide

NO_2	nitrogen dioxide
NO_x	nitrogen oxides
NOAA	National Oceanic and Atmospheric Administration
O_3	ozone
OAG	Official Aviation Guide
OPE	Ozone Production Efficiency
PIANO	Project Interactive Analysis and Optimization Model
POET	Precursors of Ozone and their Effect on the Troposphere
ppbv	parts per billion by volume
ppmv	parts per million by volume
pptv	parts per trillion by volume
QUANTIFY	Quantifying the Climate Impact of Global and European Transport Systems
RCP	Representative Concentration Pathways
REACT4C	Reducing Emissions from Aviation by Changing Trajectories
RF	Radiative Forcing
RTM	Radiative Transfer Model
SHADOZ	Southern Hemisphere Additional Ozonesondes
SWV	Stratospheric Water Vapour
TAR	Third Assessment Report
TOPSE	Tropospheric Ozone Production about the Spring Equinox
TRADEOFF	Aircraft emissions: Contributions of different climate components to changes in radiative forcing – TRADEOFF to reduce atmospheric impact
TROPOS	Two–Dimensional Global Tropospheric Model
UNFCC	United Nations Framework Convention on Climate Change
UTLS	Upper Troposphere Lower Stratosphere
WDCGG	World Data Centre for Greenhouse Gases
WOUDC	World Ozone and Ultraviolet Radiation Data Centre

Chapter 1

Introduction

1.1 Climate change issue – science and policy

Climate refers to an average condition of the atmosphere (weather) over 30 years, which is a traditional mean time for defining climate (Seinfeld and Pandis, 2006), for a certain region. Climate change is understood as both changes in its variables (the fundamental climate variable is the global annual mean surface temperature) and changes in the variance of these variables. Natural variations have existed for millennia: during the last 160 000 years, prior the preindustrial era, CO_2 concentrations varied from 180 ppmv to 300 ppmv, while CH_4 was as low as 0.3 ppmv and as high as 0.7 ppmv (Harvey, 2000). Human activity in the past 200 years has enhanced the CO_2 and CH_4 concentrations: in 2010 the global annual mean of CH_4 was 1.8 ppmv (Dlugokencky et al., 2011) and CO_2 reached 400 ppmv level in 2013 (Jones, 2013). The rate of human induced changes significantly exceeds the rate of change from natural variations (Seinfeld and Pandis, 2006).

The United Nations Framework Convention on Climate Change (UNFCCC) defines climate change as "a change of climate that is attributed directly or indirectly to human activity that alters the composition of the global atmosphere and that is in addition to natural climate variability observed over comparable time periods" (Article 1, 1992). Emissions of greenhouse gases affect atmospheric concentrations; altered atmospheric

concentrations change the heat balance, and perturbed heat balance modifies the climate and sea level.

Climate response is a result of climate forcing: the former is often represented by global mean surface temperature change; the latter is a change imposed on the Earth's energy budget and expressed in watts per square meter. The relation between a global mean surface temperature change and a global mean radiative forcing was assumed to be approximately linear (e.g., Hansen et al., 1997):

$$\Delta T_s = \lambda RF, \tag{1.1}$$

where λ is the climate sensitivity parameter. Thus, the radiative forcing became a convenient tool for the first-order projection of climate impact.

The Intergovernmental Panel on Climate Change (IPCC) stated in its Fourth Assessment Report (AR4) that "warming of the climate system is unequivocal, as is now evident from observations of increases in global average air and ocean temperatures, widespread melting of snow and ice and rising global average sea level" and that "most of the observed increase in global average temperatures since the mid-20th century is very likely (> 90%) due to the observed increase in anthropogenic greenhouse concentrations" (Solomon et al., 2007).

To tackle the climate change issue, in 1992 most countries (195) signed an international agreement – the United Nations Framework Convention on Climate Change (UNFCCC). The "stabilization of greenhouse gas concentrations in the atmosphere at a level that would prevent dangerous anthropogenic interference with the climate system" was the main aim of the Rio Convention (Article 2, 1992). In order to "strengthen the global response to climate change", the Kyoto Protocol was adopted in 1997 (UNFCCC, 1998) and came into force in 2005. In the first commitment period, 2008–2012, the industrialized countries agreed to reduce their greenhouse gas emissions by 5.2% compared with the year 1990. During the second period, 2013–2020, the reduction of greenhouse gas emissions was committed to be at least 18%, compared with 1990. The composition of countries in the above commitment periods differs. The greenhouse gases included in the first commitment period of the Kyoto Protocol are carbon dioxide (CO_2), methane (CH_4), nitrous oxide (N_2O), sulphur

hexafluoride (SF_6), hydrofluorocarbons (HFCs) and perfluorocarbons (PFCs). In the second commitment period nitrogen trifluoride (NF_3) was added to the 'basket' of six greenhouse gases (Annex A, Doha Amendment, 2012). These gases are converted into a common scale called 'CO_2 equivalence'[1] in order to determine the target.

The Kyoto Protocol excludes the short-lived species and their precursors (such as CO, NMVOC, NO_x, aerosols, SO_2) even though they contribute significantly to climate forcings. The transport sector is in a peculiar position, as a significant fraction of its emissions constitutes non-CO_2 substances. In 2000, the largest contribution of nitrogen oxides (NO_x) emissions belonged to global transportation and constituted 37% of total anthropogenic NO_x emissions (Fuglestvedt et al., 2010) and 31% of total anthropogenic O_3 forcing is contributed by transport sector (Fuglestvedt et al., 2008).

1.2 Aviation climate impact

The end of 1990s brought two notable evaluations. In 1998, the European assessment on the impact of aircraft emissions on atmosphere (Brasseur et al., 1998) was released, the following year, the Intergovernmental Panel on Climate Change (IPCC) published a Special Report on 'Aviation and the Global Atmosphere' (Penner et al., 1999). The latter one highlighted that aviation represents a small but potentially significant impact on climate forcing and that the uncertainty in an overall magnitude of those forcing arises mostly from non-CO_2 effects. Despite the length of time and improvements in understanding various atmospheric processes and interactions due to aircraft emissions, today this statement seems to be still valid. The level of scientific understanding (LOSU[2]) is 'high' only for aircraft CO_2. LOSU of aircraft NO_x impact is assigned to be 'medium-low', followed by 'low' for water vapour, soot and sulphate aerosols, linear contrails and 'very low' for aircraft induced cirrus cloudiness (Lee et al., 2009).

Aviation, as a part of anthropogenic activity, emerges as a unique sector since it is the only man-made source injected directly to the 'clean' and remote regions of the atmosphere, the upper troposphere and lower stratosphere (UTLS). The effectiveness

[1] CO_2-equ = E_x * M_x, where E_x is emissions of gas x and M_x is adopted normalized metric; under existing scheme M_x = GWP(100).

[2] LOSU – a subjective measure in assessing uncertainties applied in IPCC analysis; the four-grade system updated by IPCC AR4 consist of 'high', 'medium', 'medium-low', 'low' measures.

of some of the emitted substances at these altitudes (8–12 km) is much greater compared with those emissions near Earth's surface in terms of, e.g., O_3 production. An aircraft emissions alter the Earth's radiative balance and therefore climate, through chemical and aerosol effects (Figure 1.1). These effects arise from three types of processes: direct emissions of radiatively active substances (e.g., CO_2, H_2O); emissions of substances that trigger the production or destruction of radiatively active substances (e.g., NO_x); emissions of substances that initiate the production of aerosol particles or modify the properties of natural clouds (e.g., contrails) (Penner et al., 1999).

The number of aircraft emissions and effects, applicable for climate forcings, has been identified:

- emissions of CO_2 (positive climate forcing),
- emissions of NO_x (produce tropospheric O_3 (positive climate forcing) and reduce the ambient CH_4 (negative climate forcing)),
- emissions of H_2O (positive climate forcing),
- formation of persistent linear contrails (positive climate forcing),
- aviation induced cirrus clouds (positive climate forcing),
- emissions of sulphate particles (negative climate forcing),
- emissions of soot particles (positive climate forcing).

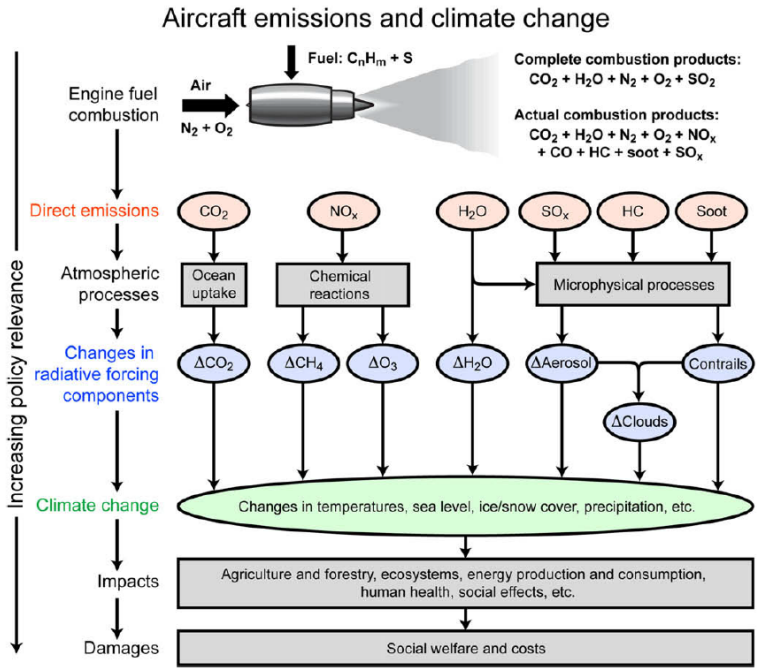

Figure 1.1: Scheme presenting the main emissions from aviation and the atmospheric processes that influence the radiative forcing, which affect climate, which, in turn, lead to social damage (Figure from Lee et al. (2009) based on Prather et al. (1999) and Fuglestvedt et al. (2003)).

The total aircraft forcings were estimated to be 48 mW m^{-2} for air traffic in 2000 (Sausen et al., 2005) and 55 mW m^{-2} ($\pm$ 32 mW m^{-2}) for air traffic in 2005 (Lee et al., 2009). Aviation represents a relatively small fraction of total anthropogenic RF, between 3.5% and 4.9% in the year 2005 (Lee et al., 2009). However, taking into account the average rate of air passenger traffic growth in the recent years, 5.3% yr^{-1} between 2000 and 2007 (Airbus, 2007) and potential reductions of emissions in other sector, the importance of aircraft contribution to anthropogenic climate change may increase in the future and it might reach 4.0–4.7% in 2050, as estimated by Lee et al. (2009).

Since 2012, the CO_2 emissions from civil aviation are included in the EU Emissions Trading Scheme (EU ETS). All airlines received allowances to cover their emissions for flights to and from European airports. It is currently not certain, how the non-CO_2 effects might be captured, in order to offset the growth of aircraft emissions (Forster et al., 2006).

Aviation activity alters atmospheric composition that consequently affects planetary energy balance and hence contributes to anthropogenic climate change. Air traffic consists of various components in its emissions and effects, where NO_x emissions, despite being carefully investigated for the last decades still remains among scientifically active areas. Aircraft NO_x emissions initiate a series of complex chemical interactions resulting in positive and negative forcing effects, which quantification requires temporal and spatial perception of its dependencies. It is challenging, especially when evaluations further down the steps in the cause–effect [3] chain are undertaken, as under existing default metric and framework of emission trading policy it is difficult to include these kinds of peculiarities. Is there at all a physical and robust possibility in applying the aircraft NO_x effect into the 'time-integrated forcing' concept?

In order to better understand the 'aircraft NO_x phenomenon' and potentially unravel the uncertainties associated with aviation NO_x estimates this study was established.

[3] 'Cause–effect' chain is the schematic path from emission to climate change and impact as presented by Fuglestvedt et al. (2003) (see also Figure 1.1). The further steps down, the policy relevance increases, as well as uncertainty of estimations.

1.3 Research questions

The main research questions addressed within this thesis are:

- Do the surface emissions of ozone precursors influence the effect of aircraft NO_x emissions?
- Can aircraft inventories explain the variation in estimates of aircraft NO_x impact on radiative forcing?
- Why is there a significant discrepancy in the reported values of an aircraft NO_x global warming potential?
- What are the variations of the effect of regional aircraft NO_x emissions?

1.4 Thesis structure

The details regarding tropospheric chemistry and aircraft NO_x emissions impacts on atmospheric composition, along with presentation of climate metrics employed in this study are given in Chapter 2. The description of models and methodology are introduced in Chapter 3 and the validation of applied methods given in Chapter 4. Furthermore, investigations on how different factors influence the effect of aircraft NO_x emissions on climate include: surface emissions of ozone precursors (Chapter 5), aircraft inventories (Chapter 6), size of aircraft NO_x emission (Chapter 7, 8 and 9), regions (Chapters 8 and 9). The summary of the main results is presented in Chapter 10, followed by conclusions and recommendations for future work in Chapter 11.

Chapter 2

Chemical cycles, effects of aircraft nitrogen oxides emissions on chemical system and measures to capture their impact on climate

This chapter introduces the details of the relevant tropospheric and stratospheric chemistry, showing the scheme which leads to formation and destruction of ozone and how aircraft nitrogen oxides emissions alter the chemical composition of the atmosphere. Furthermore, an overview of climate metrics used within this study is given.

2.1 Relevant atmospheric chemistry

2.1.1 Production of hydroxyl radical

A central role in tropospheric chemistry is played by the hydroxyl (OH) radical, which is the dominant (OH is unreactive toward O_2) oxidant in the troposphere. Photolysis of O_3, at wavelengths shorter than 319 nm, leads to production of excited $O(^1D)$ oxygen atoms, which either react with an inert molecule, most often it is N_2 or O_2, to reform O_3, or collides with water molecule to form two OH radicals:

$$O_3 + h\lambda \ (\lambda < 319 \text{ nm}) \rightarrow O(^1D) + O_2 \quad (2.1)$$
$$O(^1D) + M \rightarrow O(^3P) + M \quad (2.2)$$
$$O(^3P) + O_2 + M \rightarrow O_3 + M \quad (2.3)$$
$$O(^1D) + H_2O \rightarrow OH + OH \quad (2.4)$$

The efficiency of O_3 photolysis depends on intensity of solar flux and $O(^1D)$ to OH conversion depends on concentrations of water vapour, which, in turn, is determined by temperature and relative humidity.

2.1.2 Chemical cycles

Hydroxyl radical reacts rapidly with hydrocarbons, its reaction with carbon monoxide (CO) and methane (CH_4) constitute the main removal path of these two trace gases. The oxidation of CO and CH_4 generates the peroxy radicals, HO_2 and CH_3O_2, which react with NO to produce NO_2 :

$$CO + OH \rightarrow CO_2 + H \quad (2.5)$$
$$H + O_2 + M \rightarrow HO_2 + M \quad (2.6)$$
$$NO + HO_2 \rightarrow NO_2 + OH \quad (2.7)$$

$$CH_4 + OH \rightarrow CH_3 + H_2O \quad (2.8)$$
$$CH_3 + O_2 + M \rightarrow CH_3O_2 + M \quad (2.9)$$
$$CH_3O_2 + NO \rightarrow CH_3O + NO_2 \quad (2.10)$$
$$CH_3O + O_2 \rightarrow CH_2O + HO_2 \quad (2.11)$$
$$NO + HO_2 \rightarrow NO_2 + OH \quad (2.12)$$

In the presence of sunlight, the photochemical cycle of NO and NO_2 persists and the formation of O_3 occurs. Once generated, O_3 reacts with NO to reform NO_2:

$$NO_2 + h\lambda \ (\lambda < 424 \text{ nm}) \rightarrow NO + O(^3P) \quad (2.13)$$
$$O(^3P) + O_2 + M \rightarrow O_3 + M \quad (2.14)$$
$$O_3 + NO \rightarrow NO_2 + O_2 \quad (2.15)$$

Ozone production and destruction depends on various conditions, such as solar radiation, temperature, background levels of NO_x and HO_x, concentrations of CO, CH_4, H_2O. The described above mechanisms are specific for an intermediate NO_x levels, ~50–1000 pptv (Royal Society, 2008), which characterize the net O_3 formation.

However, the oxidation of CO and CH_4 also initiates reactions that lead to net O_3 removal. At low NO_x levels, which correspond to remote regions of the atmosphere, the peroxy radicals are removed by forming hydrogen peroxide and methyl hydroperoxide:

$$HO_2 + HO_2 \rightarrow H_2O_2 + O_2 \quad (2.16)$$

$$CH_3O_2 + HO_2 \rightarrow CH_3OOH + O_2 \quad (2.17)$$

This leads to O_3 loss, because the cycle was initiated by O_3 photolysis. Also an additional process occurs:

$$HO_2 + O_3 \rightarrow OH + 2O_2 \quad (2.18)$$

which, at the expense of O_3, regenerates OH.

At high NO_x levels, which correspond to locations close to pollution sources or the lowermost stratosphere, the formation of nitric acid (HNO_3) and peroxynitric acid (HO_2NO_2) becomes the major termination reactions:

$$OH + NO_2 + M \rightarrow HNO_3 + M \quad (2.19)$$

$$HO_2 + NO_2 + M \rightarrow HO_2NO_2 + M \quad (2.20)$$

Under this regime, the addition of NO_x decreases the number of free radicals and consequently decreases the production rate of O_3. However, the elevated concentrations of CO or CH_4 or additions of non-methane VOC, efficiently compete with above reaction and lead to an increase of O_3 formation rate.

In the stratosphere, the chlorinated compounds are highly reactive toward O_3:

$$Cl + O_3 + M \rightarrow ClO + O_2 \quad (2.21)$$

The rapid ClO_x cycle is characterized by ClO formation and its loss with O and NO. If the ClO reacts with O, the catalytic O_3 depletion occurs. If ClO reacts with NO:

$$ClO + NO \rightarrow Cl + NO_2 \qquad (2.22)$$

the null cycle with respect to O_3 destruction takes place, as the rapid O_3 reformation occurs through reactions 2.13, 2.14.

2.1.3 Effect of aircraft NO_x emissions on tropospheric chemistry

Aircraft NO_x ($NO + NO_2$) emissions, injected directly to relatively 'clean' regions of atmosphere, alter the budgets of O_3 and CH_4, both important greenhouse gases. The NO_x mixing ratios in the upper troposphere and lower stratosphere (UTLS) are around 50–200 pptv (Derwent et al., 1999); at these levels of NO_x, the net O_3 production increases almost linearly with an increasing NO_x background concentrations (Figure 2.1). As result of an injection of aircraft NO_x emissions, the catalytic production of O_3 occurs (reactions 2.12, 2.13, 2.14, 2.15). The UTLS in mid-latitudes is the most efficient in O_3 production per NO_x molecule due to the low NO_x backgrounds, low HO_x concentration and high NO/NO_2 ratio (Derwent et al., 1999). Ozone lifetime at flight altitudes is of the order of weeks, thus the aircraft O_3 perturbation is distributed heterogeneously, concentrated mainly in the Northern Hemisphere, where most of the aircraft NO_x emission occur.

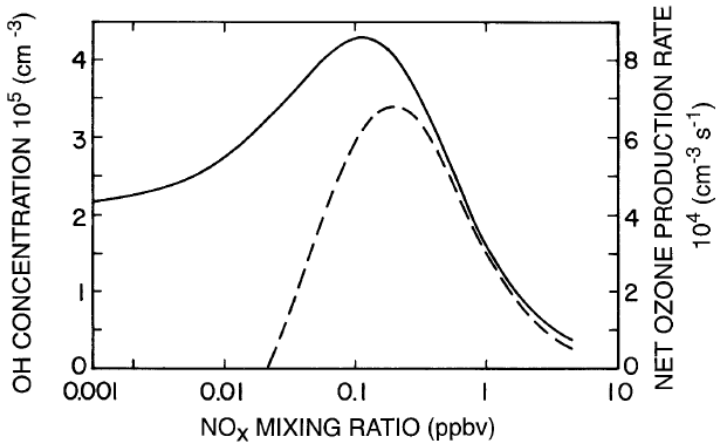

Figure 2.1: Model calculated OH concentration (solid line) and photochemical net O_3 production rate (dashed line) as a function of NO_x background concentrations. The represented conditions are for lower troposphere at mid-latitudes during the spring time (Figure from Brasseur et al. (1998) based on Ehhalt and Rohrer (1994)).

Air traffic also changes the oxidizing capacity of the atmosphere: enhanced NO_x and O_3 changes the HO_2/OH ratio, in favour of OH (reaction 2.7). Additionally, the increase of O_3 might lead to further OH production through O_3 photolysis (reactions 2.1, 2.4). In turn, modified OH concentrations influence ambient CH_4, as the reaction of CH_4 with OH is the principal loss process for atmospheric CH_4. Enhanced OH reduces CH_4 lifetime and concentration (reaction 2.8). The aircraft perturbation of long-lived CH_4 (lifetime of the order of decade) is distributed uniformly across the globe.

In the stratosphere, NO_x is a source of O_3 depletion through the catalytic NO_x cycle; additional NO_x emissions result in a net loss of HO_x (reaction 2.19, 2.20) followed by a decrease of net O_3 production.

2.2 Metrics for climate impacts

Metrics constitute tools for quantifying and comparing the potential impact of emissions of various gases on climate. It places substances with different radiative properties and lifetimes on a common scale; thus it enables definition of climate targets, trading or comparison of the emissions from different sources and regions. A given metric does not define policy, but constitutes a tool, which makes possible the implementation of a policy. Different policy goals and frameworks require different metric concepts (e.g., Manne and Richels, 2001, Shine et al., 2007).

Two metrics are adopted in this study: radiative forcing (RF) and global warming potential (GWP). Despite other concepts existing, the evaluation of the 'integrated forcings' mode for aircraft NO_x emission is needed due to few and disparate estimates available in the literature (see Chapter 7.1 for more details). Also, the usage of GWPs is consistent with the approach undertaken by the existing emission trading policy, the Kyoto Protocol.

Alternatives to the GWP, including either popular, but conceptually different approach, global temperature change potential (GTP), are also presented. However, many of the alternative metric concepts utilize, like GWP, the time-integrated dimension; therefore, any 'their issues' cannot be solved in isolation to 'GWP issues'.

2.2.1 Radiative forcing

There are various sources of energy in the Earth's atmosphere; however, the Sun is its main (99.97%) contributor. The gas species and particles, of which the Earth's atmosphere is composed, cause that about 52% of incoming short-wave solar radiation is absorbed, scattered or reflected; the rest reaches the Earth's surface; which, in turn, is either reflected, or absorbed by surface (Figure 2.2). The heated surface radiates the outgoing long-wave radiation, which either radiates to higher altitudes through the 'atmospheric window' (8–12 μm), or is absorbed by lower atmosphere. The 93% of the absorbed radiation is re-emitted by atmosphere back to the surface. This "net trapping of infrared radiation" is the so-called 'greenhouse effect' (Harvey, 2000). The major greenhouse gases are water vapour (H_2O), carbon dioxide (CO_2), ozone (O_3), methane (CH_4) and nitrous oxide (N_2O). Anthropogenic activities alter the natural composition of the atmosphere, by production of greenhouse gases and its precursors, which leads to modification of the Earth's energy budget.

Radiative forcing (RF) is an accepted measure of the strength of the perturbation of Earth–atmosphere system caused by natural agents and human activity. The Third Assessment Report of the IPCC (Ramaswamy et al., 2001) defines RF as "the change in net (down minus up) irradiance (solar plus long-wave; in Wm^{-2}) at the tropopause after allowing for stratospheric temperatures to readjust to radiative equilibrium, but with surface and tropospheric temperatures and state held fixed at the unperturbed values". This is the most common way in deriving the radiative forcings, employed also in this study.

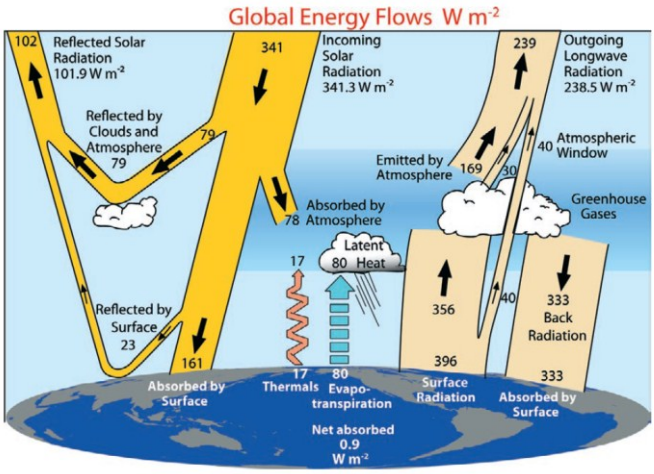

Figure 2.2: The Earth's energy budget (Figure from Trenberth et al., 2009).

2.2.2 Global Warming Potential

The formulation of global warming potential (GWP) is based on a concept of Ozone Depletion Potential (Wuebbles, 1983) and other GWP-like approaches (e.g., Derwent et al., 1990, Fisher et al., 1990, Lashof and Ahuja, 1990).

The GWP method was introduced by the IPCC in 1990 as a "simple approach (…) to illustrate the difficulties inherent in the concept" (Houghton et al., 1990). Despite GWP was not intended to be a default tool used in policy, it was soon embraced by Kyoto Protocol in order to serve the needs of a multi-gas treaty. On the other hand, it is questionable to what extent the presence of GWP itself, affected the current framework of Kyoto Protocol agreement (Skodvin , 1999, Shine, 2009).
The GWP is currently employed to translate the emissions of non-CO_2 greenhouse gases into a CO_2-equivalency, allowing consideration of various options (in terms of greenhouse gases emissions reduction) and feasibility of multi-component policy.

The GWP is a ratio of the RF from the emission of a gas x relative to that of a reference gas (normally it is CO_2) for a nominal kg release of both gases, integrated over a given time horizon:

$$\mathrm{GWP(H)_x} = \frac{\int_0^H \mathrm{RF_x(t)c_x dt}}{\int_0^H \mathrm{RF_{CO2}(t)c_{CO2} dt}} = \frac{\mathrm{AGWP_x}}{\mathrm{AGWP_{CO2}}}, \tag{2.23}$$

where H is the defined time horizon, RF_x and RF_{CO2} are the radiative forcings arising from unit increase in atmospheric abundances of the gas x and CO_2, respectively, c_x and c_{CO2} are the time-dependent decays in the concentrations of pulses of the injected gases. GWP is a dimensionless value. GWP is a purely physical metric defined by radiative forcing measure.

Since the GWP concept was introduced it became widely accepted and utilized (e.g, Derwent et al., 2001, Wild et al., 2001, Berntsen et al., 2005, Derwent et al., 2008, Myhre et al., 2011, Fry et al., 2012, Köhler et al., 2012, Skowron et al., 2013).

As well as its applicability has been debated at the same time (e.g., Wigley et al., 1998, Smith and Wigley, 2000a, b, Fuglestvedt et al., 2000, O'Neill, 2000, Godal and Fuglestvedt, 2002, O'Neill, 2003, Shine, 2009, Tanaka et al., 2010).

The voices of criticism, coming from scientists and economists, highlight several limitations associated with usage of GWP concept, e.g.:

- equal weights are given to emissions over all defined time horizon (Michaelis et al., 1992),
- it does not account the effects beyond the defined time horizon,
- it considers constant background conditions over time, whilst for the policy, the transient background would be more relevant (Tanaka et al., 2010),
- emissions of gases with equal GWPs might have different climate impacts (e.g., Smith and Wigley, 2000a); the same GWP for a gas with high RF but short lifetime and for a gas with low RF but long lifetime will lead to different impact on temperature (Shine et al., 2005b),
- it does not take into account any specific climate target, e.g., 2°C temperature limit (Manne and Richels, 2001, Shine et al., 2007, Manning and Reisinger, 2011, Smith et al., 2012, Tanaka et al, 2013),
- as a cost-benefit approach (Tol et al., 2012), it is not very consistent with UNFCCC's cost-effectiveness approach (Tanaka et al., 2010),
- scientifically unjustified choice of 100 year time horizon (Fuglestvedt et al., 2003, Shine, 2009), even though a GWP value significantly depend on a time horizon.

Despite the objections, GWP, due to its transparency and simplicity in application and calculation, gained prevalence among the user community; whether it is a sufficient reason of applicability belongs to a separate discussion.

The formulation of GWP relies on a global input parameter; while it is adequate for a long-lived (well-mixed) species, it becomes problematic for short-lived substances (e.g. Berntsen et al., 2005, Shine et al., 2005a, Isaksen et al., 2009). "Unlike the Kyoto gases, it is certainly generally not possible to prescribe a single value of the GWP for short-lived emissions, which are independent of location and conditions at the time of emissions" (Fuglestvedt et al., 2010). The research challenges regarding aircraft NO_x GWPs are presented in Chapter 7.1.

2.2.3 Alternative metric concepts

The most popular alternative metric is Global Temperature Change Potential (GTP) proposed by Shine et al. (2005b). It is defined as a global mean surface temperature change at a given point in time after a unit emission release, relative to that of CO_2. Similarly to the GWP, it is a purely physical metric; however, it goes one step further in the cause–effect chain, as it accounts for the thermal inertia of the climate system. The GTP is an end-point metric, thus the GTP values for short-lived species over long-time horizons are lower than the equivalent GWP values (the GWP which through its integrated nature retains memory of short-lived effect long after the emission occurred). GTP falls under the cost-effectiveness approach (Shine et al., 2007, Tol et al., 2012) and is considered by some to be more (than GWP) suitable for climate stabilization policy (Tanaka et al., 2013), when a temperature target is considered.

There are series of other metrics that attempt to address different aspects of shortcomings of the GWP. The combinations of GWP and GTP were proposed: the Temperature Proxy Index (TEMP) (Tanaka et al., 2009) and Mean Global Temperature change Potential (MGTP) (Gillet and Matthews, 2010) (known also as integrated Global Temperature change Potential (iGTP) (Peters et al., 2011) or (IGTP) (Azar and Johansson, 2012). These metrics refer to integrated temperature change under time dependent emission scenarios. It has been presented that time-dependent concepts, where the time horizon follows the "proximity to the policy target" (Manne and Richels, 2001, Shine et al., 2007, Tanaka et al, 2009, Berntsen et al., 2010) might suit better to a specific climate targets. In order to explore the different aspects of regional patterns of responses and its consequences the non-linear damage function was applied (Shine et al., 2005a, Lund et al., 2012) or Absolute Regional Temperature Potential (ARTP) has been developed (Collins et al., 2013). The GWP and GTP for bioenergy (GWP_{bio}, GTP_{bio}) have been proposed by Cherubini et al. (2011, 2012) to account for CO_2 emissions from biomass for energy combustion.

The perception of economists on metric design is based on different optimization scenarios. The cost-benefit approach relies on a ratio of marginal damage from the emission of the substance to that damage from an emission of CO_2 and is known

as Global Damage Potential (GDP) (Kandlikar et al., 1995). The cost-effectiveness approach is more complex as it aims to minimize the cost of emission reduction from all substances under the process of fulfilment of the optimization scenario; it is known as 'price ratio' (Manne and Richels, 2001), as well as Global Cost Potential (GCP) (Tol et al., 2012).

A 'single-basket' approach embedded in the Kyoto Protocol is not necessarily the only framework possible and propositions of other perspectives, like a multi-basket approach, gas-by-gas approach or regional agreements, have been suggested as well (Rypdal et al., 2005, Daniel et al., 2012). It would be constructive if future climate policies give the possibility for revision and updates of existing tools (Tanaka et al., 2010). Implementation of any changes will bring the cost for society (Godal and Fuglestvedt, 2002, Shine, 2009); however, on a global scale the cost is relatively small especially when it is related to the benefits arising from adoption a multi-gas mitigation scenario (O'Niell, 2003, Johansson et al., 2006, Smith et al., 2012). However, any change in metric, whatever the benefit, will be subject to political inertia, when adoption by the policy community is concerned.

2.3 Radiative forcings from aircraft NO_x emissions

The impact of aviation NO_x emissions on tropospheric ozone (O_3) has been investigated since the 1970s (Hidalgo and Crutzen, 1977). Despite the length of time over which this effect has been explored, it still represents an active research area. One distinct milestone was the IPCC Special Report on 'Aviation and the Global Atmosphere' (Penner et al., 1999), which highlighted the finding that whilst NO_x emissions from the existing fleet of subsonic aircraft resulted in a small enhancement in tropospheric O_3, there was also a small but significant reduction in ambient CH_4 (for an equilibrium calculation of constant emissions). Since CH_4 has a lifetime of approximately 8–12 year, it takes some time to respond to an additional NO_x injection. The IPCC thus established a positive ozone radiative forcing (RF) and a negative RF associated with a NO_x increase from aircraft.

Wild et al. (2001) also distinguished that with this long-term CH_4 decrease, a small decrease in O_3 also emerged (again, for equilibrium conditions). However, it has taken some time to realise that this O_3 reduction could be significant over the longer time-period and that the overall RF response from aircraft NO_x arises from one positive and two negative RF responses. More recently, Myhre et al. (2011) presented a number of model responses to an aircraft NO_x increase and also highlighted a fourth RF response in that a decrease in CH_4 also ultimately resulted in a small negative RF response from water vapour in the stratosphere (Myhre et al., 2007). Any CH_4 response takes decades to come to an equilibrium response, thus it can enter the stratosphere where it can be oxidised to water vapour. The water vapour (from CH_4 oxidation reaction) results in a positive forcing in the stratosphere, so that any decrease in CH_4 will result in a reduction in water vapour forcing in the stratosphere and can therefore be considered as a negative RF from aviation NO_x.

Despite the magnitudes of positive and negative radiative forcing are roughly the same (from equilibrium run of present-day aircraft emissions), they do not cancel in climate terms. The complexity of NO_x–O_3–CH_4 system is intensified not only through different signs of responses of its components (mixture of positive and negative forcings) or different timescales of responses (positive forcing is short-term, negative responses are long-term), but also by differences of their spatial extents. Whilst short-term O_3 increase is regional, the CH_4, CH_4-induced O_3 and stratospheric water vapour (SWV) act on a global scale. The latitudinal imbalance occurs, with positive net (O_3 + CH_4) forcing observed in the Northern Hemisphere and negative in the Southern Hemisphere (Prather et al., 1999).

The other impacts resulting from aircraft NO_x emissions, like formation of nitrate aerosols (Kärcher, 1996, Unger et al., 2011) or indirect formation of sulphate aerosols (more efficient, via increased OH, conversion of SO_2 to sulphuric acid) (Pitari et al., 2002) are not so well known and are not taken into account in this study.

The recent investigations regarding the impacts of aircraft NO_x emissions on atmosphere and climate from various modelling studies are presented in Chapter 6.1.

Chapter 3

Models description, methodology and experimental design

The main model employed for this study is the 3D Chemistry Transport Model (CTM), MOZART-3 and it constitutes the foundation of Chapters 5, 6, 7, 8, 9. The 2D CTM, TROPOS was utilized for an additional analysis, presented in Chapter 4, in order to illustrate the long-term processes distinctive for NO_x–O_3–CH_4 system.

In this chapter, the descriptions of models along with the methodology undertaken at each main step of calculation are presented. The general bases of experimental design (3D CTM, MOZART-3, set up) are introduced.

3.1 Models description

3.1.1 2D Chemistry Transport Model, TROPOS

The 2D Chemistry Transport Model, TROPOS is a latitudinally-averaged two-dimensional Eulerian global tropospheric chemistry model extensively evaluated by Hough (1989, 1991). The model's domain extends from pole-to-pole (24 latitudinal grid cells) and from the surface to an altitude of 24 km (12 vertical layers). TROPOS is driven by chemistry, emissions, transport, removal processes and upper boundary

conditions. The transport is based on circulation derived by Plumb and Mahlmann (1987), who utilized the output from a General Circulation Model (GCM) (Mahlmann et al., 1980). The temperature fields are from Barnett and Corney (1985) and Oort (1983) and are interpolated onto the model's grids with a monthly temporal resolution. Differential equations, which describe the combined chemistry and transport, are solved using a variable-order Gear's method.

There are 56 chemical species in the chemical mechanism of the model, which consists of 91 thermal reactions, 27 photolytic reactions and 7 more reactions, which include nighttime NO_3 chemistry. There are no fixed concentrations within the modal domain other than the upper boundary conditions, which are specified for long-lived species and for gases that the stratospheric region acts as a source. The model contains three cloud layers, where cloud cover is predicted based on the routine of Buriez et al. (1998), which depends on relative humidity.

Table 3.1: Annual emissions used in 2D CTM, TROPOS.

Scenario / Annual emissions	2000 IPCC–TAR
NO_x total [Tg(N)/yr]	45.7
anthropogenic [Tg(NO_2)/yr]	33.0
biomass burning[Tg(NO_2)/yr]	7.1
lightning [Tg(N)/yr]	5.0
CO total [Tg(CO)/yr]	1575.0
anthropogenic [Tg(CO)/yr]	650.0
biomass burning [Tg(CO)/yr]	700.0
NMVOC total [Tg(C)/yr]	779.7
isoprene [Tg(C)/yr]	450.1

A series of updates has been conducted for this study, among which the most important are: budgets of surface emission and aircraft emissions (Table 3.1), thermal and photolysis reactions rates (Tables A.1, A.2, in Appendix A), cross sections, quantum yields for $O(^1D)$ production from O_3 photolysis (Figure 3.1). The latter was especially important, as while the previous parameterisation assumed the $O(^1D)$ production to be 0 for wavelengths greater than 310 nm, the new one leads to the existence of the 'tail' in the $300 \leq \lambda \leq 330$ nm region (Sander et al., 2003; details are presented in Appendix B). Taking into account that intensity of the solar actinic flux in the troposphere and lower stratosphere increases rapidly with $\lambda \geq 290$ nm, this update was of importance.

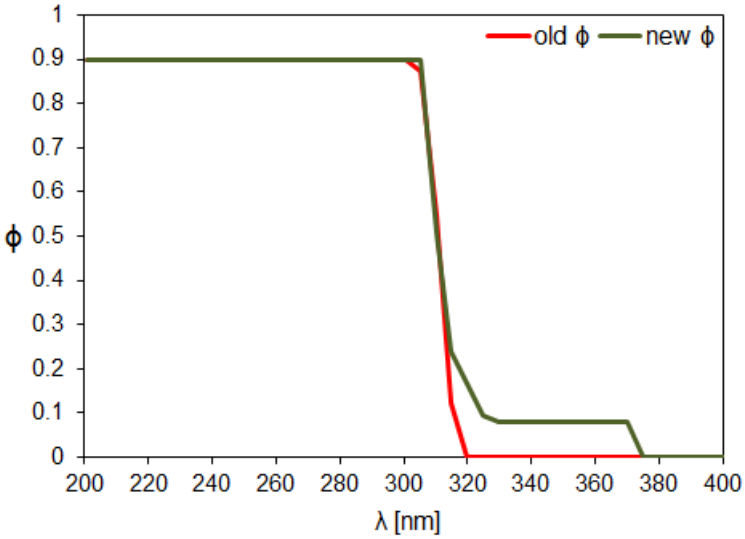

Figure 3.1: Quantum yields for $O(^1D)$ formation from O_3 photolysis as a function of wavelength.

A 2D CTM has the disadvantage of not fully representing atmospheric transport (it cannot describe the variability of concentrations around latitude circles or species (e.g. NO_x) are transported to restricted regions), but has the advantage of a complex chemical scheme and being computationally efficient, such that the long-term (e.g., 100 years) integrations can be performed.

TROPOS was exploited in a number of investigations related mainly with chemistry of ozone precursors both, in the past (Hough and Johnson, 1991, Johnson et al., 1992, Johnson and Derwent, 1996) and quite recently (Skowron et al., 2009).

3.1.2 3D Chemistry Transport Model, MOZART-3

The Model for Ozone and Related Tracers, version 3 (MOZART-3) is a 3D Chemistry Transport Model (CTM) designed to simulate atmospheric ozone and its precursors; it was comprehensively evaluated by Kinnison et al. (2007). This model, with an extension to the middle atmosphere, is based on earlier versions of global tropospheric models: MOZART-1 (Brasseur et al., 1998b) and MOZART-2 (Horowitz et al., 2003). MOZART has been developed jointly by the National Center for Atmospheric Research (NCAR), the National Oceanic and Atmospheric Administration (NOAA), the Max–Planck Institute of Meteorology (MPI–Hamburg), the Geophysical Fluid Dynamics Laboratory (GFDL) and Princeton University. However, version 3 of this model was released by NCAR.

MOZART-3 is built on the framework of the transport model MATCH (Model for Atmospheric Transport and Chemistry) (Rasch et al., 1997) and accounts for advection, convection, boundary layer exchanges, wet and dry deposition. Using the flux-form semi-Lagrangian scheme of Lin and Rood (1996), the vertical velocities are derived based on divergence of the horizontal velocity fields. Convection fluxes are derived using shallow and mid-level convection scheme of Hack (1994) and deep convective routine of Zhang and MacFarlane (1995). The planetary boundary layer exchanges are parameterised based on Holstag and Boville (1993) formulations. Wet deposition is taken from Brausser et al. (1998b) and surface dry deposition from Müller (1992).

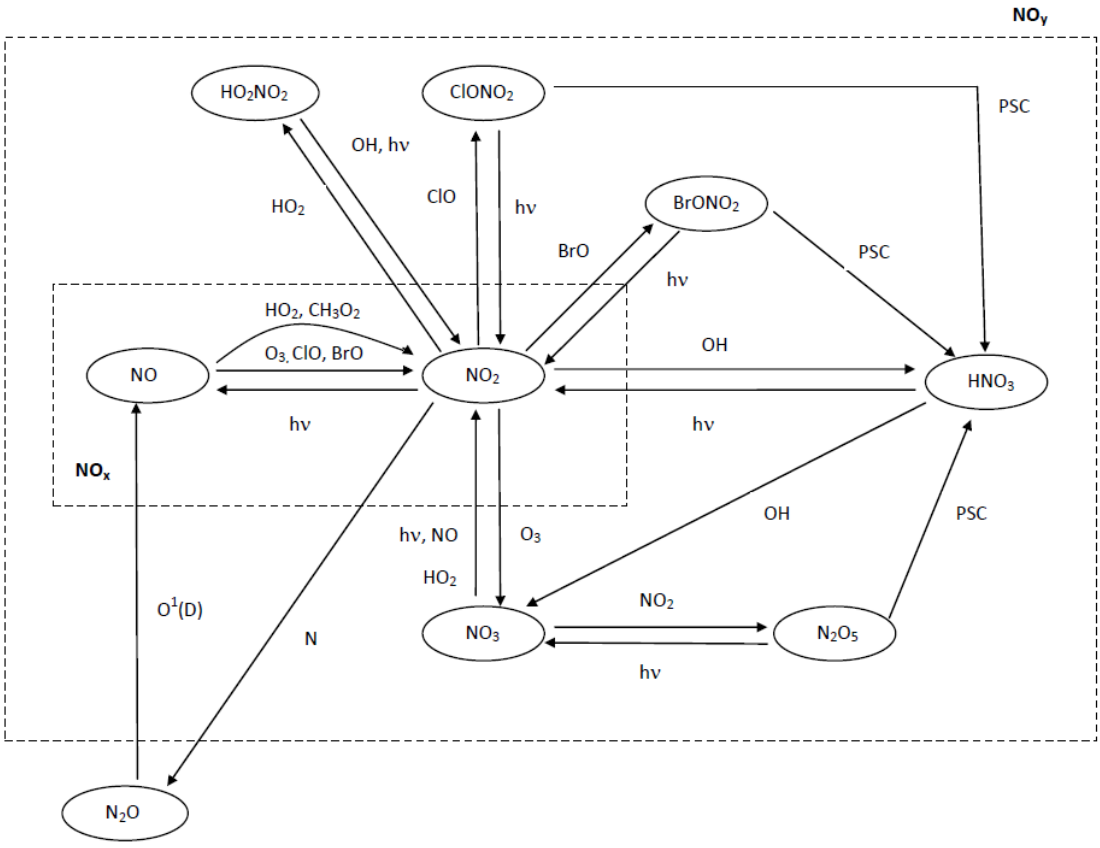

Figure 3.2: NO_x and NO_y family represented in MOZART-3 (Figure adapted from Seinfeld and Pandis (2006)).

MOZART-3 reproduces detailed chemical and physical processes from the troposphere through the stratosphere. The chemical mechanism includes 108 species, 218 gas-phase reactions, 71 photolytic reactions (including the photochemical reactions associated with organic halogen compounds) and 17 heterogeneous reactions. The species included within this mechanism are members of the O_x, NO_x, HO_x, ClO_x and BrO_x chemical families, along with CH_4 and its degradation products. As an example of the

complexity of chemical scheme represented in MOZART-3, the scheme of NO_x and NO_y chemistry is presented in Figure 3.2. The kinetic and photochemical data are based on the NASA/JPL evaluation (Sander et al., 2006). The non-methane hydrocarbon oxidation scheme is based on three separate lumped hydrocarbons (one representing aromatic species – TOLUENE, one representing alkanes with four or more carbons – BIGALK and one representing alkenes with four or more carbons – BIGENE). The lightning parameterisation is based on Price et al. (1997), which defines the NO_x production from lightning as a function of the location of convective clouds top heights. The vertical profile of lightning NO_x follows the C-shaped formulations (Pickering et al., 1998), which reduces these emissions close to the surface.

MOZART-3 has been extensively used for different application studies, e.g., influence of El Niño and La Niña events on dynamical, thermal and chemical structure of the middle atmosphere (Sassi et al., 2004), specificity of stratospheric O_3 and downward O_3 transport in the UTLS region during the sudden stratospheric warming event in January 2004 (Liu et al., 2009), forecast study of the ozone hole over Antarctica in 2008 (Flemming et al., 2011), estimations of Ozone Depletion Potentials for n-propyl bromide (Wuebbles et al., 2011), assessment of the impact of present-day aircraft NO_x emissions on climate (Skowron et al., 2013) and others.

Chapter 3.3 presents details regarding the model's set-up, along with dynamical and emission data employed for this study.

3.1.3 Edwards–Slingo

The Edwards–Slingo is an offline radiative transfer model (RTM) (Edwards and Slingo, 1996). The model calculates the radiative fluxes and heating rates based on the δ-Eddington form of the two-stream equations in both, the long-wave and short-wave spectral regions. The version of the model used in this study was developed in the UK Met Office and it has been set up and maintained by Dr Ruben Rodriguez de León of MMU. Cloud treatment is set up based on averaged ISCCP D2 data (Rossow and Schiffer, 1999), which are used to determine the position and amount of ice clouds and water in the atmosphere. Climatological fields of temperature and specific humidity are determined by ERA-Interim data (Dee et al., 2011). Well mixed concentrations of

CO_2 (379 ppmv), CH_4 (1774 ppbv), and N_2O (319 ppbv) are specified. While H_2O, CO_2, N_2O, O_3, CH_4 are defined in the long-wave, H_2O, CO_2, O_3, O_2 are defined in the short-wave. This model does not include concentrations of aerosol, halocarbons and chlorofluorocarbons. The Edwards–Slingo radiation code was employed in number of studies (Edwards and Slingo, 1996, Stevenson et al., 1998, 2006, Myhre et al., 2009).

3.2 Methodology

3.2.1 Chemical perturbations

The O_3 lifetime is of an order of weeks in the troposphere, thus its concentrations modelled by the CTM are expected to be in steady state condition from a few years run under the constant emission scenario. The O_3 monthly averages from MOZART-3 output for meteorological years 2000 and 2006 are exploited within this thesis.

A one year CTM simulation is not long enough to obtain the change in CH_4 concentration, as it takes decades for CH_4 to come into equilibrium with the perturbed OH fields (this is because CH_4 lifetime is ~8.7 years (Denman et al., 2007)). Thus, to obtain the steady state concentrations of CH_4 in the perturbation runs the change in CH_4 lifetime owing to reaction with OH was computed for each experiment. Then, based on Fuglestvedt et al. (1999), it was multiplied by the reference CH_4 concentration and a feedback factor of 1.4 (Prather et al., 2001) to reflect the effect of changes of CH_4 on its own lifetime (α):

$$[CH_4]_{ss} = [CH_4]_{ref} * (1 + 1.4 * \Delta\alpha_0/\alpha_{ref}) \quad (3.1)$$

where $\Delta\alpha_0 = \alpha_{per} - \alpha_{ref}$ and $[CH_4]_{ref}$ is a reference run concentration.

The CH_4-induced O_3 is derived based on an assumption that 10% increase of CH_4 leads to 0.64 DU increase of O_3 (Prather et al., 2001).

3.2.2 Radiative forcing calculations

The short-term O_3 radiative forcings (RF) are derived off-line using the Edwards–Slingo radiation code (see Chapter 3.1.3 for more details about the model). The calculations are based on a monthly O_3 MOZART-3 output. The O_3 background and aircraft perturbations, as calculated by MOZART-3, were converted into mass mixing ratios and interpolated onto the Edward–Slingo horizontal and vertical resolution. To account for a stratospheric adjustment a 20% reduction was implemented to the O_3 RF, according to the work of Stevenson et al. (1998).

The radiative forcings of CH_4 are calculated using a simplified expression defined in Ramaswamy et al. (2001), which accounts the N_2O overlap:

$$\Delta F = 0.036\ (\sqrt{M} - \sqrt{M_0}) - (f(M,N_0) - f(M_0,N_0)), \quad (3.2)$$

$$f(M,N) = 0.47\ \ln[1 + 2.01 \times 10^{-5}\ (MN)^{0.75} + 5.31 \times 10^{-15}\ M(MN)^{1.52}] \quad (3.3)$$

where M is CH_4 in ppbv, N is N_2O in ppbv and subscript 0 denotes unperturbed concentration.

The CH_4-induced O_3 has a characteristic RF of 42 mW m^{-2} DU^{-1} (Ramaswamy et al., 2001). The impact of CH_4 change on stratospheric water vapour (SWV) is also included in the calculations and as reported by Myhre et al. (2007) the RF of SWV is assessed to be 0.15 times that of CH_4 RF.

3.2.3 Global Warming Potential calculations

The calculations of Global Warming Potentials (GWP) are based on a methodology described by Fuglestvedt et al., (2010).

The temporal evolution of net RF following the NO_x emission is needed in order to calculate GWP. It can be assumed that the constant one year emission is a step emission and the successive decay occurs of the resulting forcing from the end of the year onwards.

The temporal evolutions of O_3, CH_4-induced O_3 and CH_4 can be described by:

$$\Delta F\,(t) = \Delta F^{SS}\,(1 - \exp(-\,t/\alpha)) \quad \text{for } t < 1 \tag{3.4}$$

$$\Delta F\,(t) = \Delta F^{SS}\,(1 - \exp(-\,1/\alpha))\,\exp((-\,(t-1)/\,\alpha) \quad \text{for } t \geq 1 \tag{3.5}$$

where ΔF^{SS} is a steady state forcing and α is lifetime (primary-mode lifetime in case of CH_4-induced O_3 and CH_4).

For CH_4-induced O_3 only $t \geq 1$ applies. The first equation describes the effects at the first year, when the emission occurs; the second equation describes the long-term decay of the first year effect.

The AGWP can be calculated through:

$$AGWP\,(H) = \Delta F^{SS}\,(1 - \alpha(\exp\,(-\,(H - 1\,)/\alpha) - \exp(-\,H/\alpha))) \tag{3.6}$$

where H is the time horizon.
When lifetime is short compared to the time horizon (e.g. for O_3) the integrated forcing is equal to $\Delta F^{SS} \cdot 1$ year.

The CO_2 AGWPs used for GWP calculations are taken from IPCC AR4 (Forster et al., 2007) and constitute 2.47×10^{-14}, 8.69×10^{-14} and 28.6×10^{-14} $Wm^{-2}yr(kgCO_2)^{-1}$ for 20, 100 and 500 years respectively.

This method of GWP calculations was applied for both, 'aircraft – no aircraft' and 'incremental aircraft – aircraft', types of experiments (the first one is presented in Chapter 6; the second one in Chapters 7, 8, 9). It is worth to keep in mind that whilst these two different settings are in agreement from analytical point of view, they differ in their experimental design (reference perturbation) and consequently in the resultant sensitivities of O_3 response, which means that they cannot be directly comparable (more details regarding this issue is presented in Chapter 7.4).

3.3 Experimental design

The 3D CTM, MOZART-3, simulations constitute the basis of each experiment performed for this thesis. The applied horizontal resolution is T42 (~ 2.8° x 2.8°) for all experiments and the vertical domain extends from the surface to 0.1hPa with 60 hybrid layers (Figure 3.3). The transport of chemical compounds is driven by the meteorological fields from European Centre for Medium Range Weather Forecast (ECMWF), reanalysis ERA-Interim data for the years 2000–2006 (Dee et al., 2011). The dynamical input for MOZART-3 consists of wind speed[1], temperature, pressure, specific humidity, surface geopotential height, wind surface stress, surface heat and moisture fluxes, solar radiation flux, snow height, soil moisture fraction.

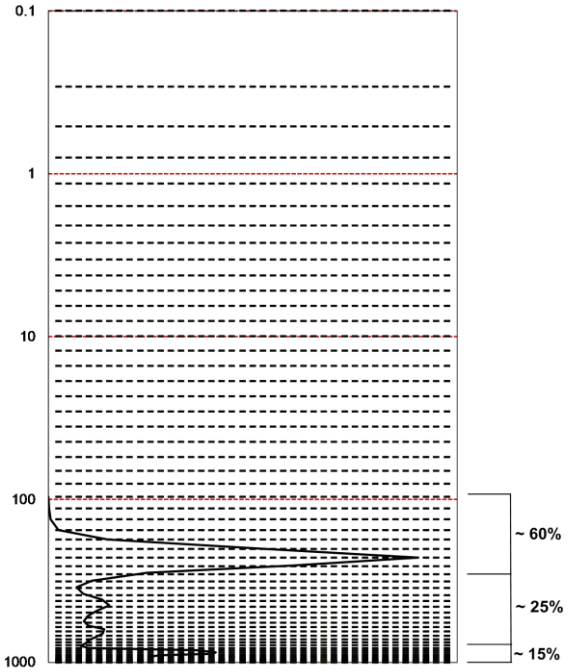

Figure 3.3: The MOZART-3's vertical domain. The black lines indicate model's 60 hybrid sigma pressure layers and red lines show the 1000, 100, 10, 1 and 0.1 pressure (hPa) levels. The schematic illustration of a vertical profile of aircraft NO_x emissions in MOZART-3 is presented.

There are several advantages of usage of ERA-Interim reanalysis data. It is proved to be a high-quality product, which resolves the deficiencies (e.g., representation of hydrological cycles or stratospheric circulation) encountered in previous, ERA-40, data (Dee et al., 2011). The distribution of long-lived tracers, mean age of air in the

[1] It is represented by three variables: zonal wind (U) [m/s], meridional wind (V) [m/s] and vertical wind velocity (OMEGA) [Pa/s].

stratosphere or CH_4 photochemical lifetime is the best represented in MOZART-3 when is driven by ECMWF reanalysis, than by e.g., the operational data (Kinnison et al., 2007). Also, ECMWF products are widely used in the community (e.g., Stordal et al., 2006, Hoor et al., 2009, Myhre et al., 2011, Hodnebrog et al., 2012), which makes this study more consistent in comparison with another studies.

The anthropogenic and biomass burning surface emissions are taken from Lamarque et al. (2010) and represent year 2000. The biogenic surface emissions come from the European Union project POET (Precursors of Ozone and their Effects on Troposphere) (Granier et al., 2005). Table 3.2 presents details regarding surface emissions from different sources and for different species. The most populated regions: Europe, U.S., Southeast Asia are the main source of anthropogenic CO and NO_x emissions; the most of biomass burning emissions comes from equatorial Africa (Figure 3.4). The main source of biogenic emissions comes from isoprene.

Table 3.2: Annual emissions used in 3D CTM, MOZART-3.

Scenario / Annual emissions	2000 IPCC–AR5
NO_x total [Tg(N)/yr]	37.1
anthropogenic [Tg(NO_2)/yr]	26.5
biomass burning[Tg(NO_2)/yr]	4.5
lightning [Tg(N)/yr]	4.8
CO total [Tg(CO)/yr]	1245.9
anthropogenic [Tg(CO)/yr]	606.2
biomass burning [Tg(CO)/yr]	459.2
NMVOC total [Tg(C)/yr]	768.5
isoprene [Tg(C)/yr]	473.9

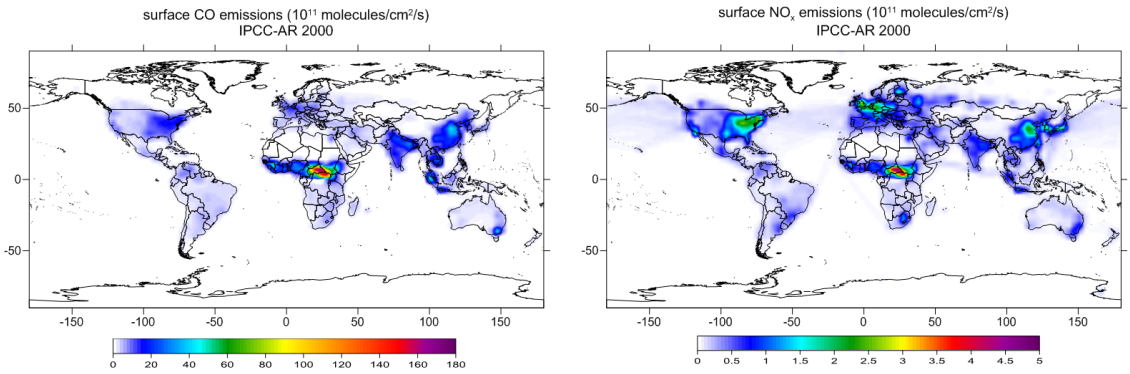

Figure 3.4: Distribution of surface (anthropogenic + biomass burning) emissions of CO (left panel) and NO_x (right panel) in 2000 based on IPCC–AR5 dataset.

Aircraft emissions in MOZART-3 are represented by the REACT4C inventory (http://www.react4c.eu) for the year 2006 (CAEP/8 movements), which is 2.33 Tg(N) yr^{-1}. Most of the aircraft NO_x emissions are concentrated in the upper troposphere lower stratosphere (UTLS) of Northern Hemisphere (Figure 3.5). The largest source regions are Europe, North Atlantic, North America and Southeast Asia. The NO_x and CO emissions are implemented into MOZART-3: the 1°x1° geographical spacing and 23 regular altitudinal layers of original data are interpolated to CTM's T42 resolution and 60 irregular vertical layers; also unit conversion from kg/yr to mol/cm^3/s and from km to hybrid sigma pressure is conducted. More details regarding REACT4C dataset and aircraft inventory peculiarities, in general, are presented in Chapter 6.

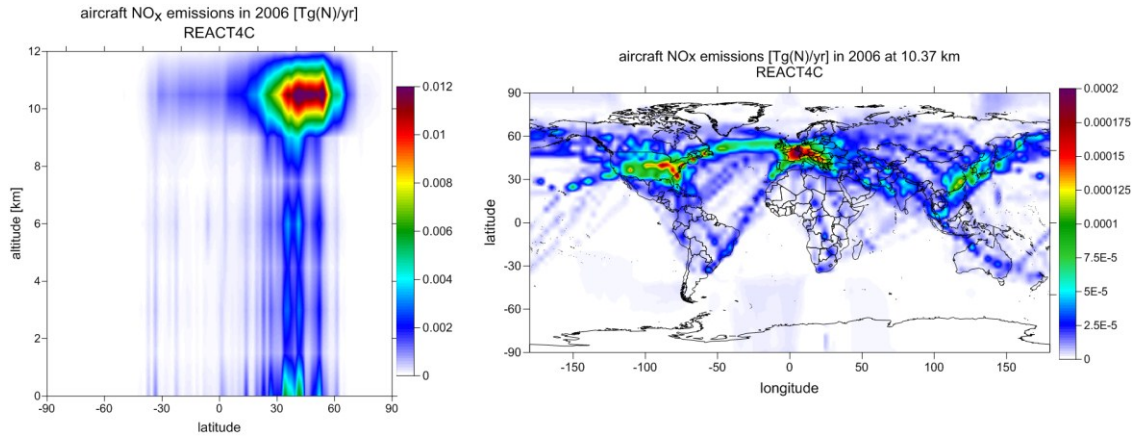

Figure 3.5: Latitudinal distribution (left panel) and geographical distribution at 10.37 km (right panel) of aircraft NO_x emissions [Tg(N) yr^{-1}] in 2006 based on REACT4C dataset.

The effect of aircraft NO_x emissions is estimated based on simulations with and without emissions (Chapters 5, 6) or additional aircraft NO_x rates which are added to existing emissions (incremental emissions – base emissions) (Chapters 7, 8, 9). Each experiment taken into account for analysis was preceded by a spin-up, which varied from one year (Chapters 5, 6) to five years (Chapters 7, 8, 9).

The 'aircraft – no_aircraft' is not the sole way in assessing the impact of emissions on climate: the small perturbation approach (Hoor et al., 2009) or tagging approach (Grewe et al., 2012) also exists. The latter might be interesting for mitigation studies, when possible compensations from other emission sectors are investigated, e.g., by applying tagging method one can be able to assess how O_3 changes induced by NO_x from lightning (for aircraft it is one of the possible compensating NO_x source) are modified by aircraft emissions. However, it is not within the scope of this study.

Chapter 4

The legitimacy of applied methodology and MOZART-3 usage

4.1 Introduction

The ability of MOZART-3 to represent the atmospheric processes and constituents was extensively evaluated by Kinnison et al. (2007) and was shown in number of publications (Sassi et al., 2004, Flemming et al., 2011), with a special attention paid to the upper troposphere and lower stratosphere region (Gettelman et al. 2004, Park et al., 2004, Pan et al., 2007, Liu et al., 2009). Through these publications the capability of MOZART-3 in reproducing the atmospheric composition, both globally and seasonally, with a good accuracy was proved. However, while the chemical tropopause exchanges are qualitatively well represented in MOZART-3, quantitatively the trace gas profiles show some discrepancies. The main factor which determines the model's accuracy of chemical distribution in UTLS region is meteorological data: MOZART-3 driven by the ECMWF reanalysis winds has shown the greatest agreement with observational data (Kinnison et al., 2007).

In this chapter MOZART-3 output and observational fields of O_3, NO_2, CO, NO_x, NO_y, CH_4, and PAN are compared for the years 2000 and 2006. Furthermore, the justification of methodologies applied in this study is presented.

4.2 Methodology

4.2.1 Measurement data

The summary of the geographical distributions of the selected observational stations and regions is presented on Figure 4.1.

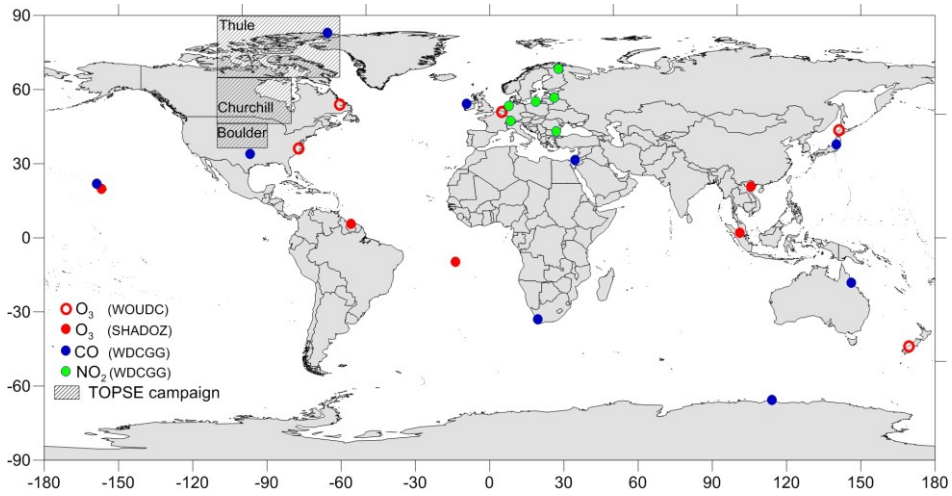

Figure 4.1: Locations of WOUDC and SHADOZ ozonesonde stations, WDCGG stationery stations and geographical regions covered by aircraft TOPSE campaign.

World Data Centre for Greenhouse Gases (WDCGG) is part of the Global Atmosphere Watch (GAW) program of the World Meteorological Organization (WMO) and is led by the Japanese Meteorological Agency. This observational network consists of stationary and mobile (aircraft, ship) stations, and in addition ice core data are also available. In this study data from the stationary stations across the globe are used. The monitored CO and NO_2 values are employed for this study. The temporal resolution varies from daily to monthly values, depending on the location. The data were downloaded on 21st (CO data) and 23rd (NO_2 data) of May 2013 from the WDCGG website http://ds.data.jma.go.jp/gmd/wdcgg/cgibin/wdcgg/catalogue.cgi/.

World Ozone and Ultraviolet Radiation Data Centre (WOUDC) is another project of the Global Atmosphere Watch (GAW) program of the World Meteorological Organization (WMO) and it is operated by the Meteorological Service of Canada. WOUDC provides the O_3 and ultraviolet radiation observations which are represented by more than 400 stations. The observations have been run for more than 50 years and they consist of total column ozone, the vertical profiles from ozonesondes, lidar

measurements and the umkehr technique. For purpose of this study the ozonesondes data for selected ozone stations for year 2006 was utilized. The daily profiles for selected months, January, April, July, October, were employed here. The data was downloaded on 20th of May 2013 from the WOUDC FTP server: ftp://woudc:woudc*@ftp.tor.ec.gc.ca/.

Southern Hemisphere Additional Ozonesondes (SHADOZ) project was originated by NASA/Goddard Space Flight Centre and other U.S. and international investigators in 1998. The main aims are to provide the climatological profiles of tropical ozone in the equatorial zone and to validate and refine satellite remote sensing techniques for estimating tropical ozone estimations. Currently the observational network consists of eleven stations which launch ozonesondes. For the purpose of this study five stations, which provide ozone profiles for year 2006, were chosen. The daily profiles for selected months, January, April, July, October, were employed here. The data were downloaded on 10th of May 2013 from the SHADOZ/Data Archive website http://croc.gsfc.nasa.gov/shadoz/.

TOPSE campaign (Tropospheric Ozone Production about the Spring Equinox) was undertaken in spring 2000. This aircraft campaign covered the continental part of North America with a latitudinal range from 37°N to 90°N and from 100 ft to 25000 ft in altitude. TOPSE measurements give a unique view on the spatial and temporal distribution of ozone and ozone precursors. The gridded climatologies and the regional profiles are provided; the latter was utilized in this study. The 3 regions are defined in TOPSE campaign: Boulder (37–47°N, 250–270°E), Churchill (47–65°N, 250–280°E) and Thule (65–90°N, 250–300°E). The O_3, NO_x, NO_y, CO, CH_4, PAN constituents were chosen for analysis. The data was downloaded on 9th of May 2013 from the website of the Atmospheric Chemistry Division at NCAR http://www.acd.ucar.edu/gctm/data/.

4.2.2 CTM's data

The 2D CTM, TROPOS, was employed for long-term (100 years) integrations, starting in January 2000 and finishing in December 2100. The constant surface emissions were applied, which represents year 2000; the aircraft NO_x emissions constitute the QUANTIFY dataset for year 2000 (more details regarding this dataset are presented in

Chapters 6.2.1 and 6.3.1). The quarterly averages were taken into account for analysis. The aircraft emissions were implemented in two ways, as a constant emission (see Chapter 4.5) and as a pulse emission (see Chapter 4.6).

The 3D CTM, MOZART-3, set up is described in detail in Chapter 3.3. The monthly averages, starting in January and finishing in December, representing meteorological years 2000 (Chapters 4.3, 4.4, 4.5, 4.6) and 2006 (Chapter 4.3) are exploited in comparison with observational data and the inter-CTM comparison.

4.3 Comparison of modelled, by 3D CTM MOZART-3, atmospheric constituents with measurement data

Time series of CO and NO_2 for year 2006 (based on WDCGG data) and monthly O_3 profiles for year 2006 (based on WOUDC and SHADOZ data) were analysed, along with O_3 and its precursors at Northern mid-latitudes and polar region during the spring 2000 (based on TOPSE campaign data). The selected stations and regions are presented in Figure 4.1. This is the first time, when ground CO and NO_2 concentrations modelled by MOZART-3 are compared with measurements, as well as TOPSE data are plotted against MOZART-3 constituents.

In general, the magnitudes and temporal variations of NO_2 and CO are well reproduced by the model, despite some discrepancies being apparent. The distributions of NO_2 concentrations over Europe (represented by 6 ground stations) reveal good agreement with modelled mixing ratios (Figure 4.2). In most cases, differences of the mean of NO_2 for the year 2006 do not exceed 15%. The exception is at stations Zoseni and Burgas, where MOZART-3 annual mean is overestimated by 43% and underestimated by 34%, respectively. While at Zoseni the differences are observed during winter months, at Burgas the spring and autumn time causes discrepancies. This might originate from anthropogenic emission input dataset.

The CO observational stations (represented by 9 ground stations) are more spread over the globe. Again the model and observational data are in good agreement and seasonal dependencies are reproduced well by MOZART-3 (Figure 4.3). However, some tendencies are noticeable. The modelled mean of CO concentrations for year 2006 at

high and mid-northern latitudes are similar to the observed data and the differences are in the range of 2%. At the tropical northern station modelled values are underestimated by 13% compared the measurements. The MOZART-3 data show consistently greater CO concentration over southern latitudes than observations, whose annual mean differences range from 14% at Casey Station, 17% at Cape Ferguson to 28% at Cape Point. This was also pointed out by Emmons et al. (2010), but for MOZART-4; the possible reason for this behaviour might be attributed to biomass burning emissions.

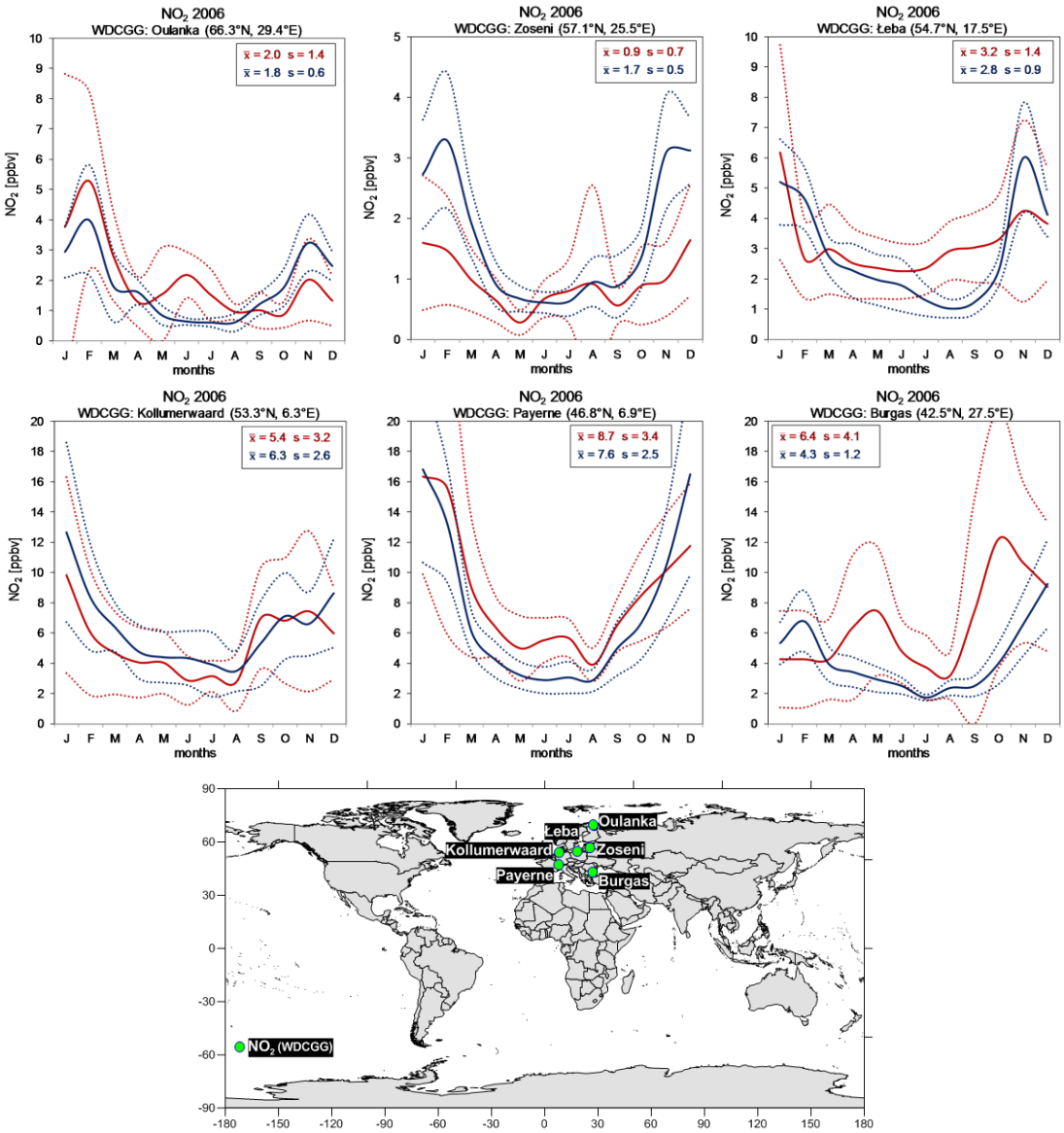

Figure 4.2: Time series of NO_2 [ppbv] concentrations in 2006 from 6 WDCGG ground stations (red lines) and the corresponding time series simulated by MOZART-3 (blue lines). The dotted lines show the standard deviation range (observational ranges are based on hourly data, modelled ranges are based on monthly data from surface to ~1km). WDCGG and MOZART-3 annual means and their standard deviations are provided for each location. The map shows the locations of ground stations.

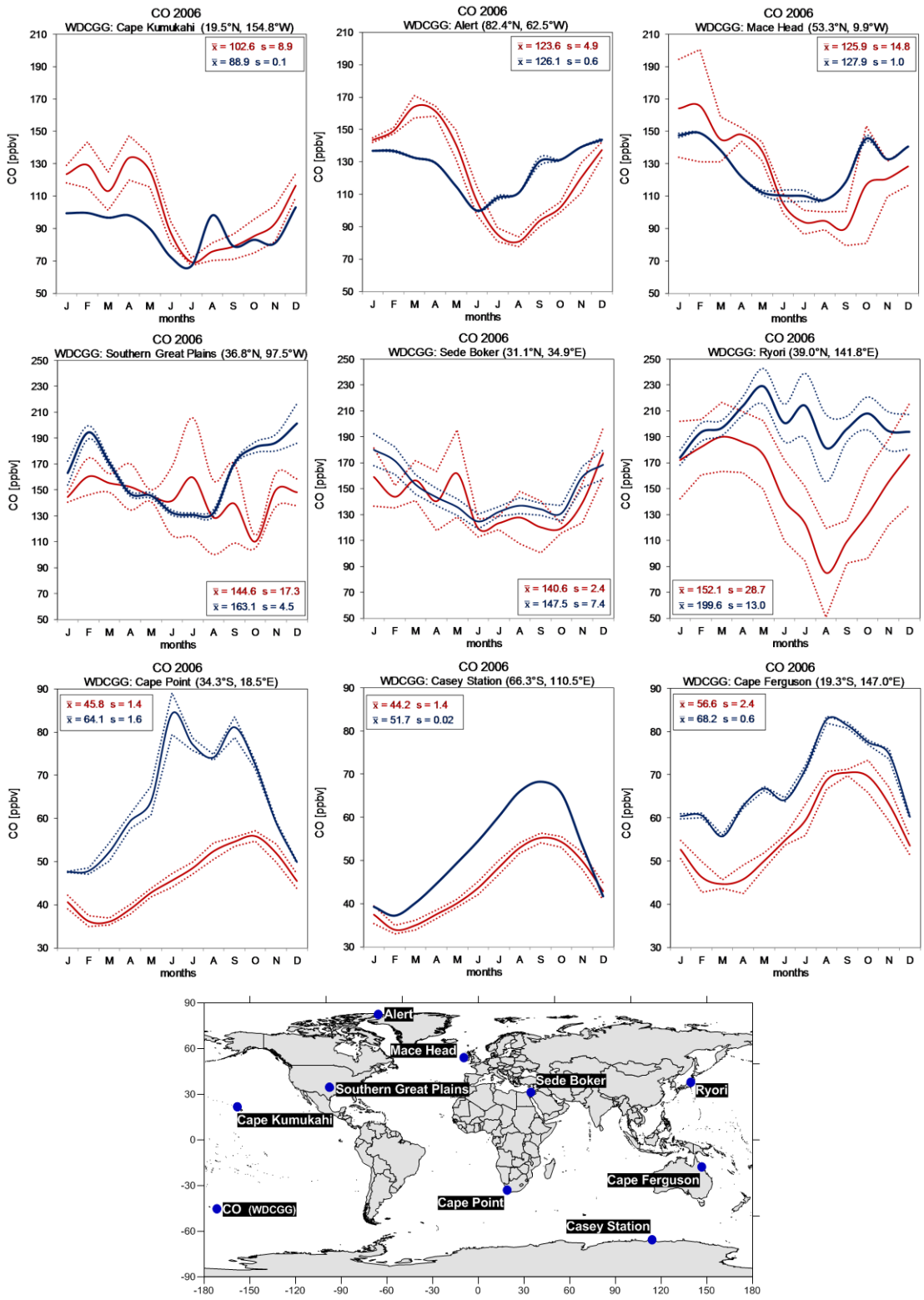

Figure 4.3: Time series of CO [ppbv] concentrations in 2006 from 9 WDCGG ground stations (red lines) and the corresponding time series simulated by MOZART-3 (blue lines). The dotted lines show the standard deviation range (observational ranges are based on hourly data, modelled ranges are based on monthly data from surface to ~1km). WDCGG and MOZART-3 annual means and their standard deviations are provided for each location. The map shows the locations of ground stations.

This range of differences is expected among short-lived species, especially in the low troposphere (the height of ground stations did not exceed 500 m). The variability of NO_x concentrations near the surface is very large, especially in the industrialized areas, e.g., Burgas. Taking this into account, and that there are only few point observations of NO_x, it is challenging to translate it into regional or global scale concentrations.

The monthly O_3 profiles from 9 ozonesonde stations were compared with O_3 from MOZART-3 simulations, both represents year 2006 (Figure 4.4). The good accuracy in reproducing vertical distribution of O_3 in troposphere and stratosphere is shown for mid- and high latitudes of both hemispheres. The Pearson's correlation coefficients are above 0.82 (N=1692) for the domain 1000–10 hPa. However, the larger vertical dispersion in the upper troposphere is observed among some of the MOZART-3 profiles. This is especially pronounced in the tropical tropopause represented by Paramaribo, Hilo, Ascension Island, Ha Noi, Kuala Lumpur. In the 250–150 hPa region the modelled values reach their overestimations in April at Paramaribo station with its 45 ppbv (58%) of O_3 difference. The larger O_3 mixing ratios in the upper troposphere in MOZART-3 have already been pointed out by van Noije et al. (2006) and Kinnison et al. (2007). It is explained through excessive downward transport of O_3 across the tropopause caused by too strong Brewer Dobson circulation in MOZART-3, which is a one of the difficulties when the accurate representation of dynamical and transport processes in the UTLS needs to be modelled (Schoeberl et al., 2003).

The TOPSE aircraft campaign is extremely useful as it gives the unique opportunity to validate the simulated O_3 and its precursors during the springtime in the mid- and high northern latitudes. The observational and modelled data for 7 altitudinal bands are shown at Figure 4.5. The accuracy of simulated concentrations is generally good and the Pearson's correlation coefficients (N=126) are usually high, above 0.9 for O_3, CH_4, CO and NO_y and 0.7 for NO_x and PAN. There is a certain pattern, which may be noticed: the oxidised nitrogen species (NO_x, NO_y and PAN) are overestimated by MOZART-3 near the surface, which is observed especially in Boulder region. This discrepancy is decreasing with height, when the distance from anthropogenic emissions is increasing. For example, the modelled NO_x at the surface is 7 times larger than the observed concentrations, becoming consistent within 10% one layer (1.5 km) higher (in Churchill region). On the contrary, the CO and CH_4 concentrations are slightly underestimated in MOZART-3 in each region for each altitudinal band. However,

the differences are relatively small and did not exceed 1.5% for CH_4 in each region and for CO 15% in Thule and Churchill, 25% in Boulder. Concentrations of O_3 are the best reproduced in Thule and Churchill (differences are within 10%) and relatively poorer accuracy is observed in the Boulder region (differences are within 25%). Most of the concentrations simulated by the model lie within 1-σ of the observational data (PAN is an exception near the surface).

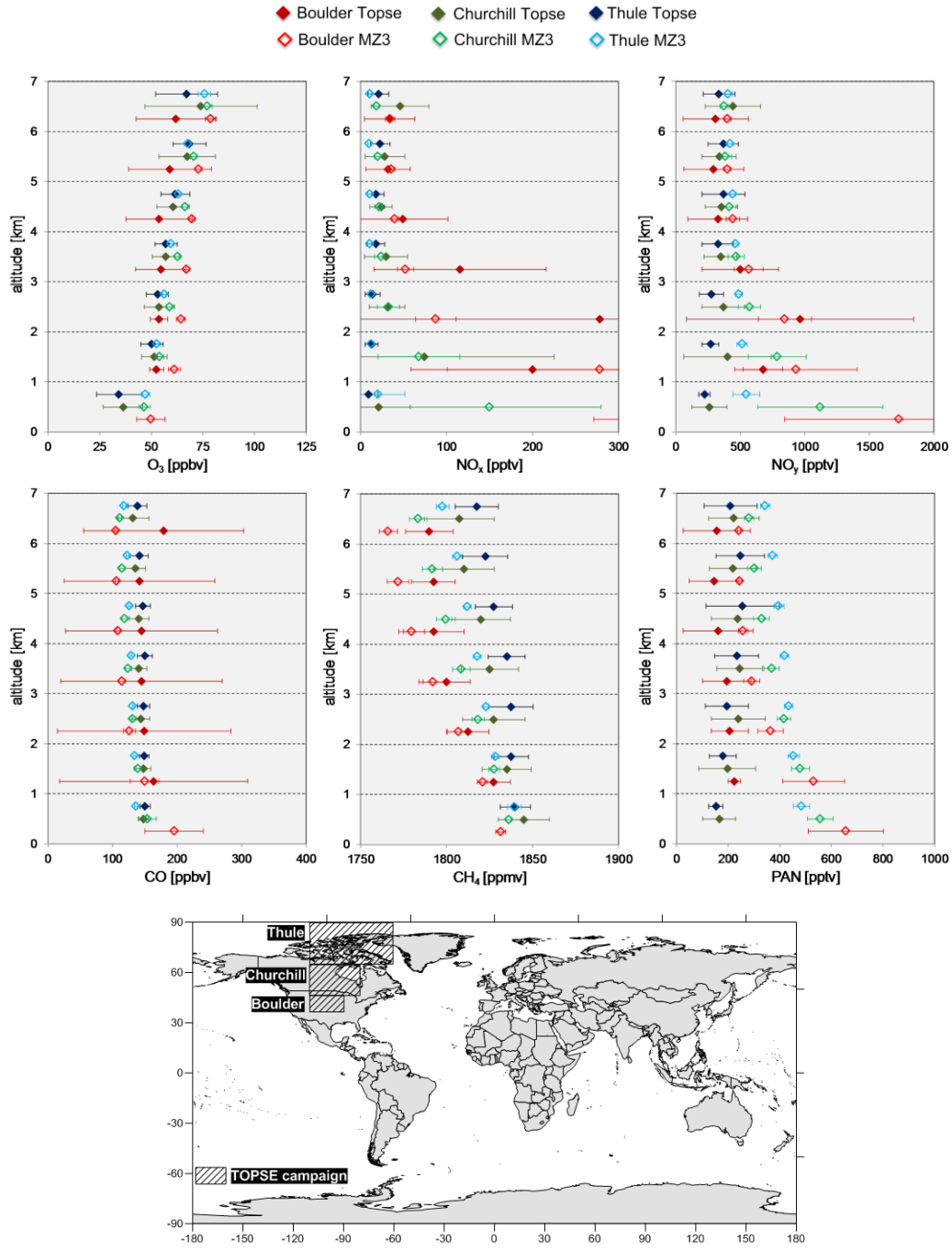

Figure 4.5: Comparison of O_3, NO_x, NO_y, CO, CH_4, PAN concentrations between measurements taken during the TOPSE campaign and MOZART-3. The means (dots) and standard deviations (lines) constitute an average of 4 months (February, March, April, May) of year 2000. The map shows the regions covered by the aircraft campaigne.

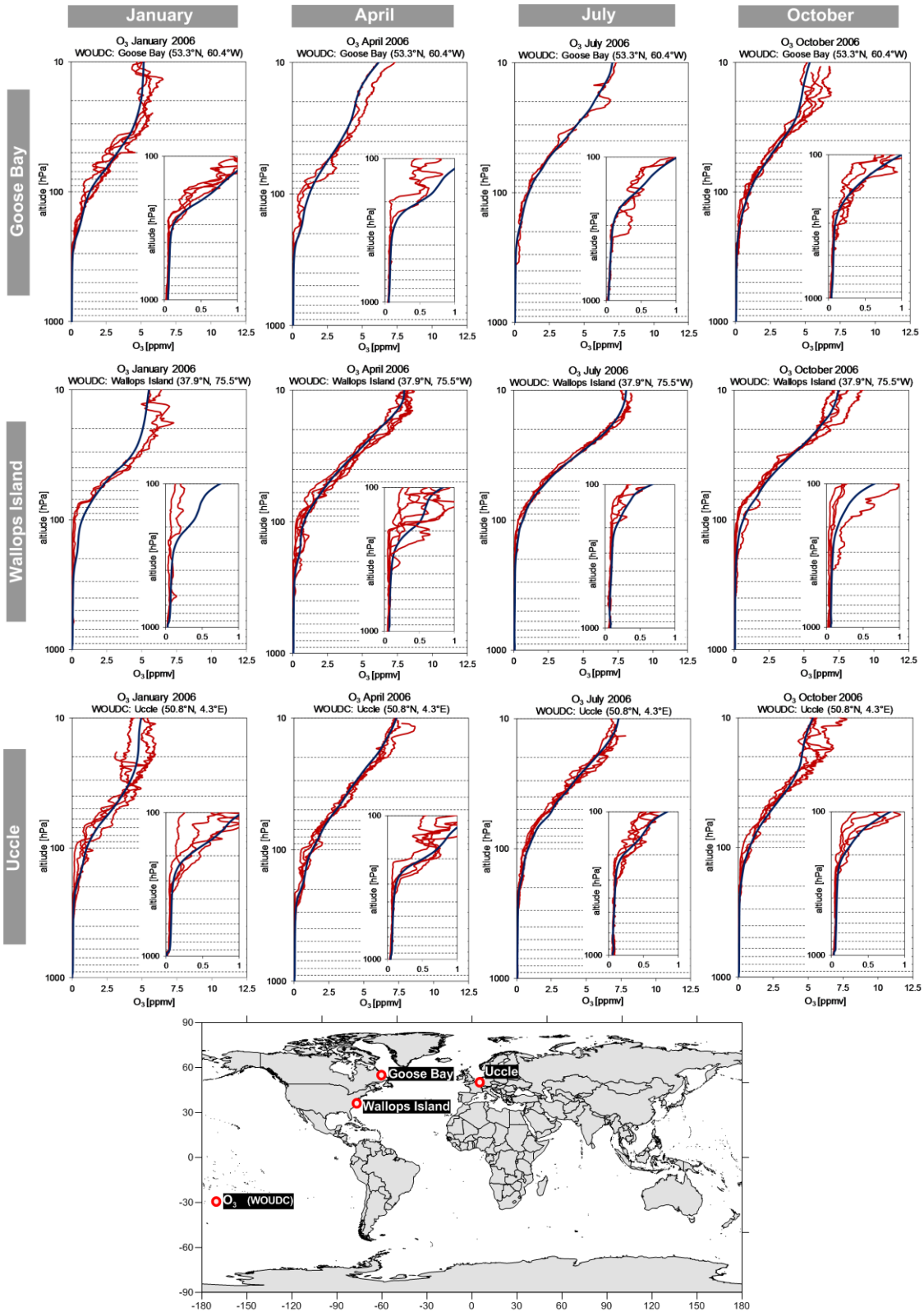

Figure 4.4: Vertical profiles of O_3 [ppmv] in 2006 measured at selected, 5 WOUDC and 4 SHADOZ, sonde stations (red line, daily data) and modelled by MOZART-3 (blue line, monthly data). The zoomed figures expose O_3 profiles in UTLS region. The map shows the locations of observational stations.

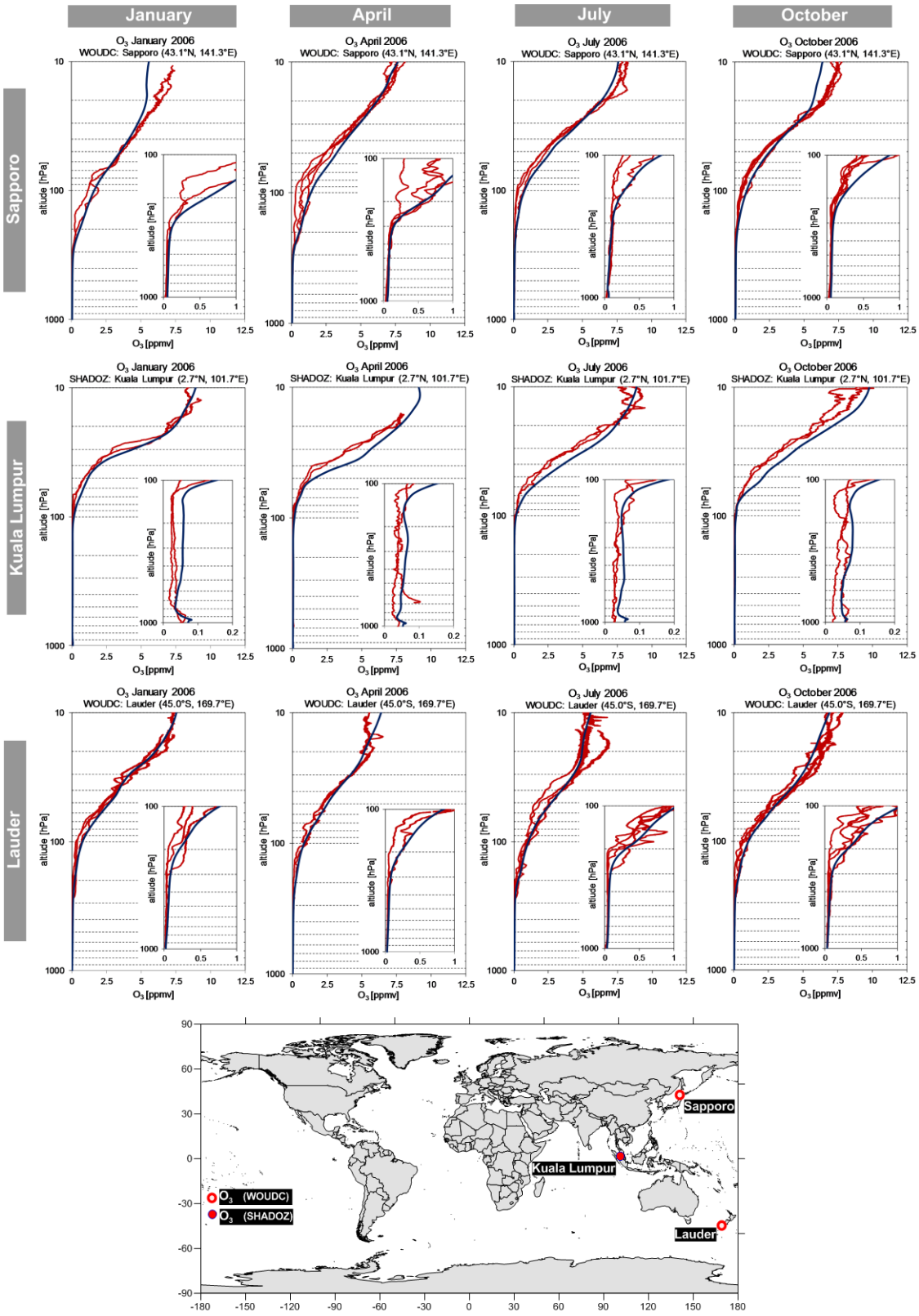

Figure 4.4: Figure 4.4 continuing.

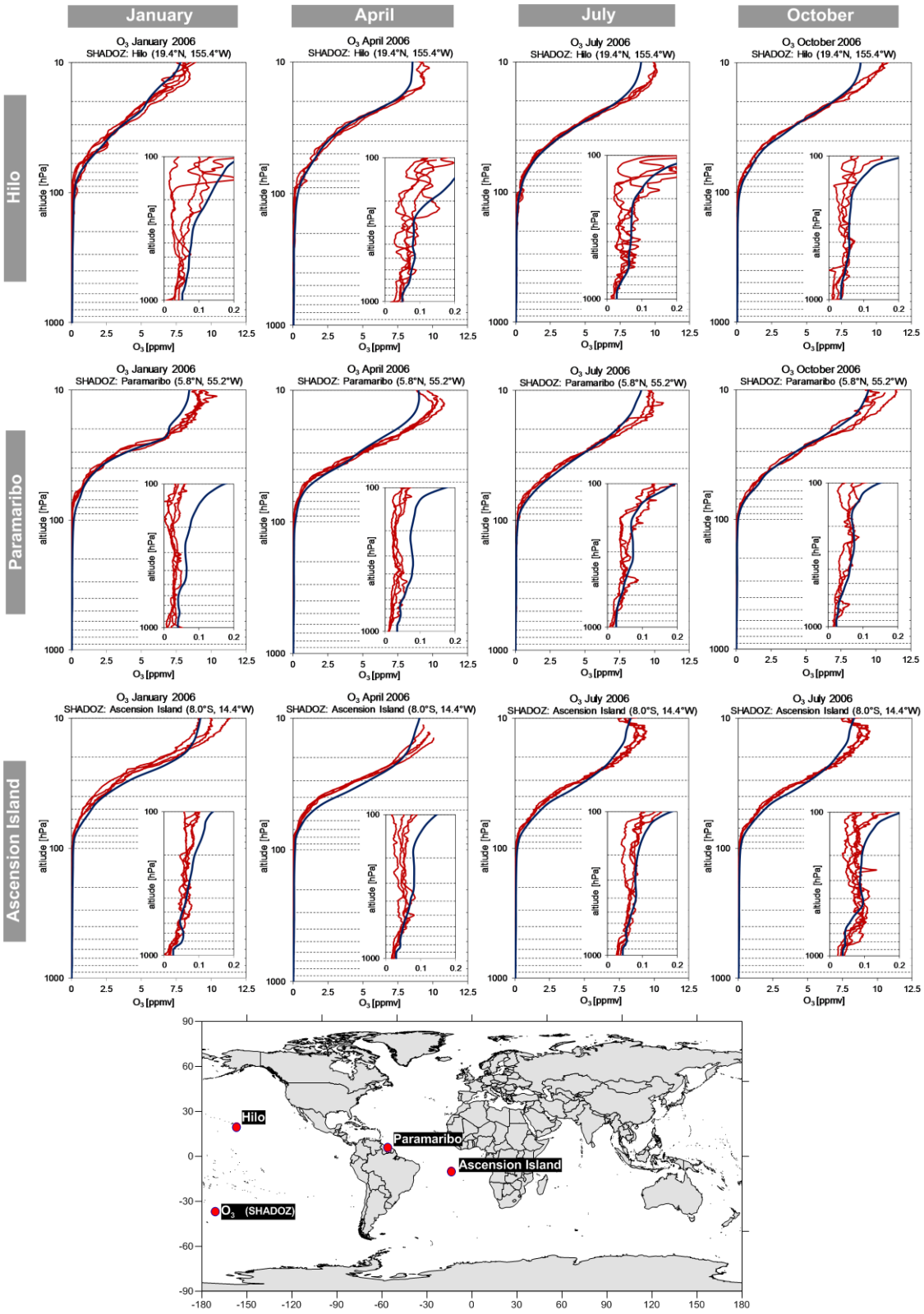

Figure 4.4: Figure 4.4 continuing.

4.4 The validity of 2-year MOZART-3's simulation in representing the aircraft O_3 response

The calculations of O_3 change, along with RFs, cover the surface to 1 hPa domain. Since some of the experiments are performed for 2 years (Chapters 5 and 6), the magnitude of aircraft stratospheric response is not fully representative (Figure 4.6). The stratospheric transport timescales are of several years (Stiller et al., 2012) and indeed the reliable aircraft O_3 response in the stratosphere is not observed until the 6th year of simulation, with magnitudes much more enhanced than for 2 years of aircraft perturbation runs (Table 4.1). The annual average stratospheric (100–1 hPa) O_3 column change in the 2nd year is positive (with July showing the most negative peak -0.0002 DU), whilst the 6th year shows negative O_3 change through all year (with greatest July depletion -0.0137 DU). Despite these significant differences in the aircraft stratospheric response between the 2nd and 6th years, the total O_3 change is not as much affected, as most of the mass of aircraft O_3 is concentrated in the upper troposphere lower stratosphere (UTLS) region. The difference in O_3 column change between the 2nd and 6th years is 5.1%, the differences in the resultant O_3 RF is -0.6%. Thus the O_3 changes derived from a 2 years simulation for a surface–1 hPa domain, as presented in Chapters 5 and 6, can be treated as reliable.

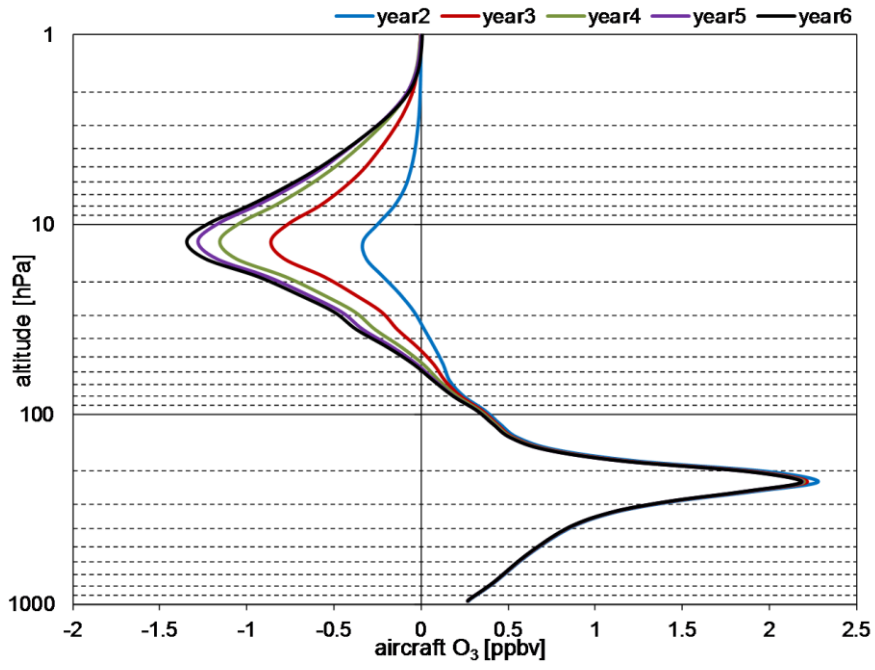

Figure 4.6: The globally and annually averaged vertical distributions of aircraft perturbations of O_3 concentrations for consecutive years of simulations.

Table 4.1: The global and annual mean O_3 column change (in DU) and RF (in mW m^{-2}) response due to aircraft O_3 for consecutive years of MOZART-3 simulations.

Year	aircraft O_3 [DU]			aircraft O_3 RF [mW m^{-2}]
	surf–100 hPa	100–1 hPa	total	Net
2nd	0.516	0.002	0.518	13.4
5th	0.503	-0.010	0.493	–
6th	0.503	-0.011	0.492	13.5

4.5 The CH_4 steady-state calculations in a 3D CTM

The CH_4 lifetime is of order of decade, ~8.7 years (Denman et al., 2007), 8.8 years in MOZART-3 for year 2000. Thus, simulations performed for 2–6 years, which are conducted in this study, are not long enough to observe the proper equilibrium CH_4 response to aircraft NO_x emissions. In order to calculate an accurate CH_4 response, the method defined by Fuglestvedt et al. (1999) and presented in Chapter 3.2.1 is applied. This method is widely exploited, e.g., Hoor et al. (2009), Myhre et al. (2011), Hodnebrøg et al. (2012), Köhler et al. (2012) and others, and it is caused by the fact that none of the 3D CTMs can afford long-term runs: the steady state of CH_4 would be reached after ~50 years of simulation.

In order to illustrate this long-term CH_4 behaviour, the 100-year integrations were performed with 2D CTM, which has this advantage of being computationally efficient. Figure 4.7 gathers together the 2D and 3D CTM runs with constant aircraft NO_x emissions: solid lines represent the O_3 and CH_4 responses in TROPOS, yellow dots show results observed in MOZART-3. It is shown that, due to differences in lifetimes of CH_4 and O_3, their responses to aircraft emissions act on a different timescales. While the O_3 response [1] in MOZART-3 is accurate, the CH_4 response is significantly underestimated. However, by using a one year perturbed CH_4 field (yellow CH_4 dot) together with the Fuglestvedt et al. (1999) method, the proper CH_4 response can be derived, as shown by the dashed yellow line in Figure 4.7. The difference between calculated and modelled steady state CH_4 is 3.1%. This shows that applied method is appropriate for steady state CH_4 calculations.

[1] The short-term O_3 response

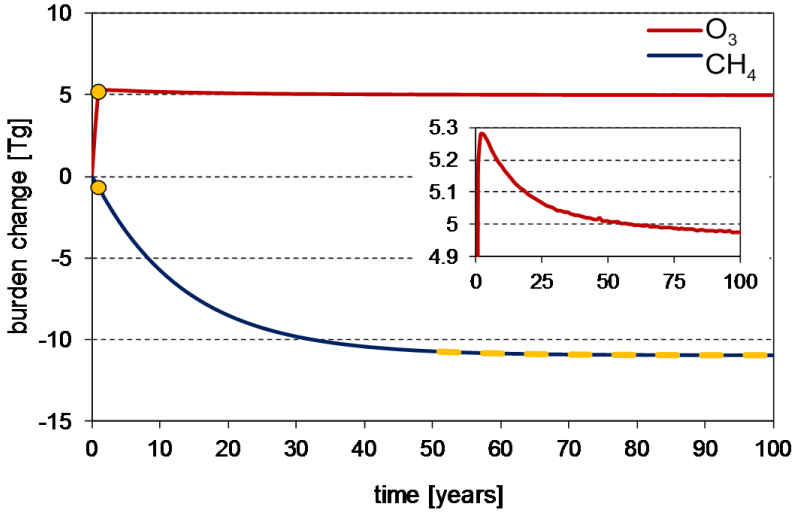

Figure 4.7: The response of O_3 and CH_4 to constant aircraft NO_x emissions as a function of time horizon. The solid lines present the species responses modelled by 2D CTM, TROPOS; yellow dots show the species responses modelled by 3D CTM, MOZART-3; dashed yellow line is the steady state CH_4 derived through MOZART-3 simulations and Fuglestvedt et al. (1999) method (more details in the text). The zoomed panel presents the long-term O_3 response.

The 100-years TROPOS integration under constant emission scenario visualises also, not observed in MOZART-3, the long-term behaviour of O_3 burden change (Figure 4.7, zoomed panel). The aircraft O_3 is weakening with time under a constant NO_x emissions scenario, following the accumulated decrease of ambient CH_4. The aircraft net NO_x calculations applied in this study account for this effect, as described in Chapter 3.2.

4.6 The response of NO_x–O_3–CH_4 system to an aircraft NO_x pulse emission

The pulse experiments have a specific structure (release and unconstrained observation) and are useful to study the mechanism of certain process. By conducting pulse experiments, the complex relationships between NO_x, O_3, OH and CH_4 can be observed in detail (Derwent et al., 2001, Wild et al., 2001, Stevenson et al., 2004).

When the aircraft NO_x pulse is applied, O_3 burden anomalies follow the emission pulse and peak on the same timescale as the NO_x source appears, then decay with a typical (a few weeks) O_3 lifetime. This is defined as the short-term O_3 change. After a few months (or years, depending on the temporal resolution of a NO_x pulse) the burden of O_3 becomes slightly negative, as a result of lowering backgrounds of CH_4 and CO,

both important precursors of O_3. This is defined as the long-term O_3 change and it decays with a CH_4 lifetime. The NO_x pulse is a source of increased OH (through positive anomalies of NO_x and O_3), which after a few months (years) after the pulse is weakening. This affects the main CH_4 oxidation path and causes the global depletion of CH_4, which builds up in the first few months (years) and then decay with an e-folding lifetime. The e-folding (also called primary mode or adjustment) lifetime is 1.4 greater than the average CH_4 atmospheric lifetime (Prather, 1994).

The pulse experiments require the freely interactive chemistry in order to perform it correctly. This raises a difficulty for 3D CTM, MOZART-3, where fixed boundary conditions exist for CH_4. Figure 4.8 shows what the 'risk' is of improper model settings. The aircraft NO_x pulse was applied for a period of a month (January) in two models: 2D CTM, TROPOS, which has surface CH_4 emissions (CH_4 flux) and to the 3D CTM, MOZART-3, which has defined fields of CH_4 as lower boundary conditions (CH_4 fixed). Whilst TROPOS ideally describe the mechanism of NO_x–O_3–CH_4 system, MOZART-3 presents the 'false' responses. The CH_4 depletion recovers just after the NO_x pulse disappears, which results in the prolonged positive O_3 anomaly and lack of long-term O_3. However, the framework of responses for O_3 are CH_4 between these two setting are in agreement in the year of pulse emissions. This is why the method described by Fuglestvedt et al., (2010) and presented in detail in Chapter 3.2.3 was applied to incremental aircraft NO_x experiments conducted with MOZART-3, so the temporal behaviour of species was possible to define.

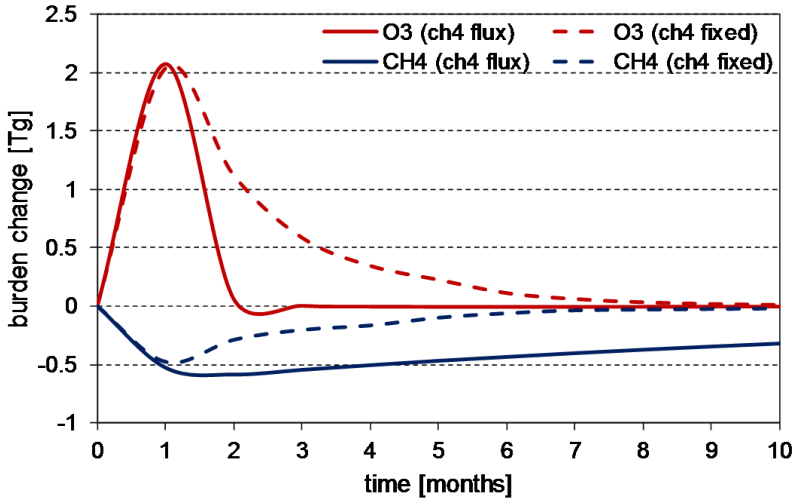

Figure 4.8: The response of O_3 and CH_4 to pulse aircraft NO_x emission under different CH_4 settings as a function of time horizon (solid lines are modelled by 2D CTM, TROPOS; dashed lines are the responses from 3D CTM, MOZART-3).

The cross checks between the 100 year integrations of 'real' NO_x pulses in 2D CTM and the methodology applied in 3D CTM were performed (the additional aircraft NO_x emissions were added for a period of year). Figure 4.9 shows that applied method is able to get away from constrained chemistry and to properly describe the temporal decay evolutions of O_3 and CH_4.

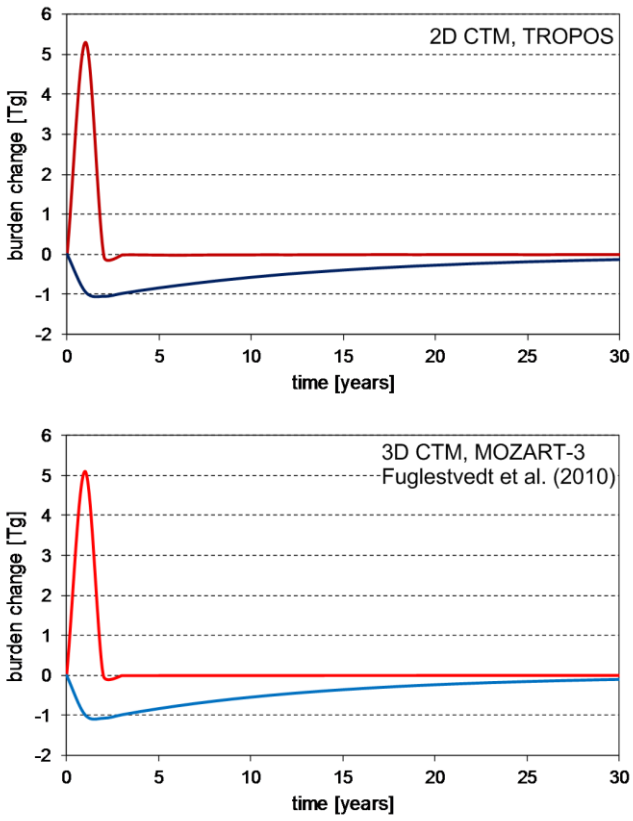

Figure 4.9: The response of O_3 and CH_4 to pulse aircraft NO_x emission simulated by TROPOS (upper panel) and MOZART-3 jointly with Fuglestvedt et al. (2010) methodology (bottom panel) as a function of time horizon.

Chapter 5

The influence of ozone precursor emissions on aircraft NO_x response

5.1 Introduction

The O_3 production from NO_x strongly depends on the 'state of the atmosphere' into which NO_x is injected (e.g., in the form of air traffic emissions) and it is a complex relation influenced by many factors, e.g., solar flux intensity, NO_x and HO_x background levels, concentrations of CO, CH_4, etc.. The 'state of the atmosphere' is defined mainly through surface emissions, of which anthropogenic activity is their principal source.

Changing emissions of any O_3 precursors: nitrogen oxides (NO_x), carbon monoxide (CO), non-methane volatile organic compounds (NMVOC) or methane (CH_4), affect the concentrations of gaseous species (O_3 and CH_4) and aerosols through the changes in oxidative capacity of the atmosphere (e.g., Unger et al., 2006, Shindell et al., 2009, Leibensperger et al., 2011). Reductions in surface NO_x emissions increase ambient CH_4 via a decrease in OH and decrease in the concentrations of tropospheric O_3, which, overall, produce a global positive radiative forcing, as O_3 outweighs CH_4 RF responses. However, the magnitude of responses strongly depends on location or sector of emission (e.g., Fuglestvedt et al., 1999, Fiore et al., 2002, Berntsen et al., 2005, Naik et al., 2005, West et al., 2007, Derwent et al., 2008, Fry et al., 2012). In contrast, the reductions of CO and NMVOC, causing the increase of OH and decrease of both

tropospheric O_3 and CH_4, lead to an overall negative climate forcings (Fiore et al., 2002, Naik et al., 2005, Fry et al., 2012). The reduction of global anthropogenic CH_4 emissions contributes to the most negative climate forcings among the O_3 precursors, due to direct reductions of ambient CH_4 (Fiore et al., 2002, Shindell et al., 2005, West et al., 2007, Fry et al., 2012). Thus, any modification of the surface emissions results in changes of the abundance of atmospheric species, which might affect the relation between aircraft NO_x emissions and O_3 production.

In this chapter, the aircraft NO_x impact on chemical composition of the troposphere is investigated under different background conditions. Usually this subject is studied in the light of air quality issues and potential climate change mitigation possibilities. Here, for the first time, the influence of perturbed surface NO_x, CO and NMVOC fluxes on the aircraft NO_x response is taken into account.

5.2 Methodology

5.2.1 Surface NO_x, CO and NMVOC emissions

Three different cases are investigated: global reduction of surface NO_x emissions (-30% NO_x), global reduction of surface CO emissions (-30% CO), global reduction of NMVOC emissions (-30% NMVOC), which are compared with surface emissions for year 2000 (base 2000). All other sources of emissions, including aircraft NO_x emissions were held constant for each experimental case.

The datasets representing historical surface emissions for the year 2000 are IPCC–AR5 and POET datasets (see Chapter 3.3 for more details). The reductions of O_3 precursor emissions are achieved by applying two Representative Concentration Pathways (RCP) scenarios for year 2100 (Lamarque et al., 2012): the anthropogenic and biomass burning emissions under RCP 8.5 2100 scenario for NO_x, CO emissions and RCP 4.5 2100 scenario for NMVOC surface emissions. Each of employed future scenarios predicts reductions of emissions, which constitute -32% of surface NO_x emissions, -33% of surface CO emissions and -33% of surface NMVOC emissions.

Figure 5.1 presents the distribution of differences in surface emissions between the base case and each experimental case. The most significant reductions of NO_x emissions are in East U.S., Europe and East Asia. The regions, where the greatest decrease of CO surface emissions are calculated for East U.S., North India, East Asia and equatorial Africa. Reductions of NMVOC surface emissions are the largest in East Asia, equatorial Africa, East U.S. and Southeast Australia.

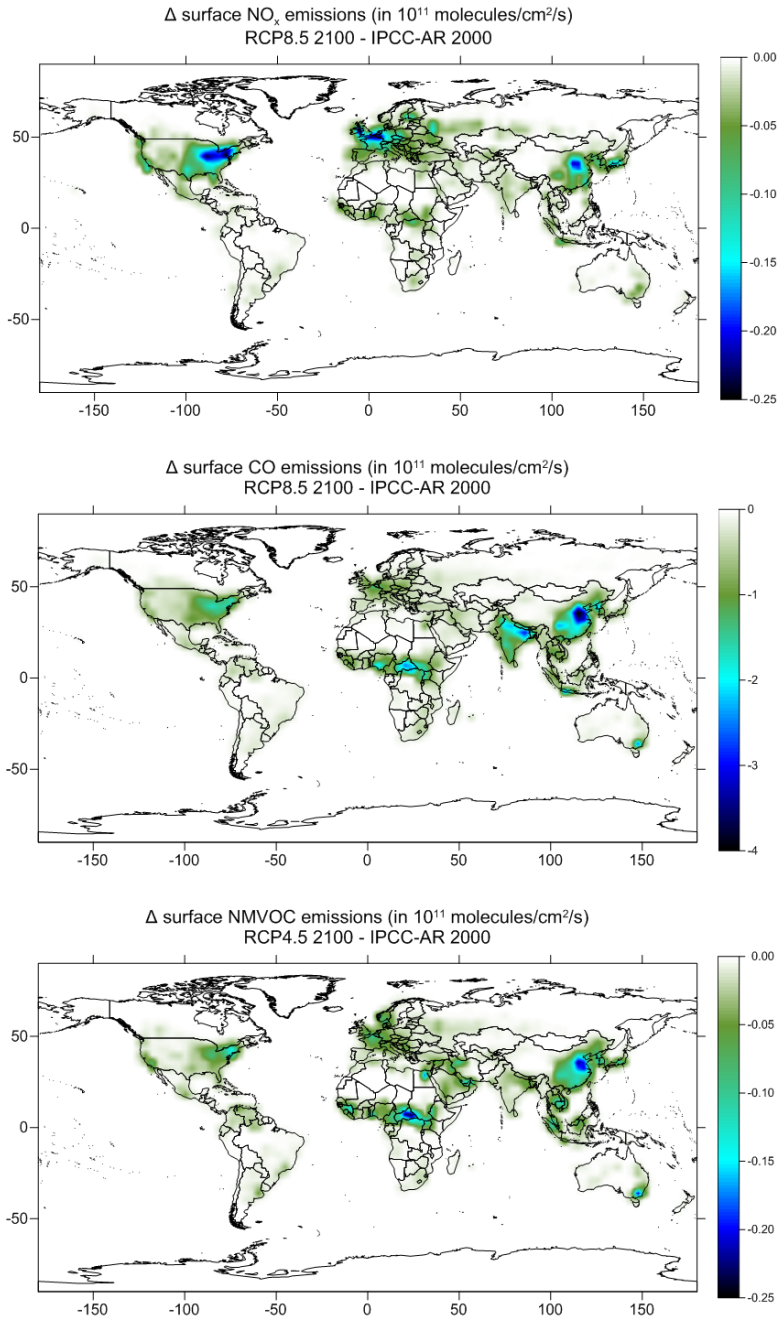

Figure 5.1: The difference (in 10^{11} molecules/cm^2/s) of the surface NO_x (upper panel), CO (middle panel) and NMVOC (bottom panel) emissions between RCP 8.5 2100 (in case of NO_x and CO), RCP 4.5 2100 (in case of NMVOC) and IPCC–AR5 2000 datasets.

5.2.2 Experimental design

The QUANTIFY 2000, aircraft emission dataset, was implemented into the 3D CTM, MOZART-3. Eight experiments were performed: four reference (no-aircraft) runs and four perturbation (aircraft) simulations, each starting in January 2000, finishing in December 2000 and preceded by one year spin-up. Each simulation represents specific background conditions (base 2000, -30% NO_x, -30% CO, -30% NMVOC). The aircraft perturbation is derived by extracting the difference between aircraft and no-aircraft experiments.

The model (3D CTM, MOZART-3) set-up used to perform simulations is presented in detail in Chapter 3.3. Details regarding the aircraft QUANTIFY dataset are provided in Chapters 6.2.1 and 6.3.1.

5.2.3 Additional surface and aircraft NO_x experiments

A series of surface NO_x emission reductions were employed in order to explore the strength of influences of background NO_x conditions on aircraft O_3 response and to confront it with aircraft NO_x emission rates. The reduction of surface NO_x emissions varied from -3% to -50% and future NO_x RCPs scenarios were applied: RCP 6.0 2010 (NO_x decreased by 3%), RCP 2.6 2020 (NO_x decreased by 7%), RCP 8.5 2050 (NO_x decreased by 14%), RCP 4.5 2050 (NO_x decreased by 23%), RCP 4.5 2100 (NO_x decreased by 50%); the aircraft NO_x emissions were held constant. The next series of experiments included modifications of aircraft NO_x emissions (REACT4C 2006 data), which were scaled globally and the reduced aircraft NO_x rates varied from 0.71 to 0.36 Tg(N)/yr; the surface NO_x emissions were held constant. The results from those additional experiments are presented in Figure 5.15.

5.3 Results

5.3.1 Background concentrations of NO_x, CO, OH, O_3 and CH_4 lifetime

The NO_x background is one of the important factors influencing O_3 production from aircraft injected NO_x. While the large concentrations of NO_x at lower altitudes are not conducive for aircraft O_3 change, the NO_x concentration in middle and upper troposphere are ideal for O_3 production, where the relation between injected NO_x and produced O_3 is almost linear (Figure 2.1 in Chapter 2.1.3). In MOZART-3 the annual averaged concentration of NO_x at 200–250 hPa is 85 pptv (Figure 5.2). Locally, at the tropical belt, NO_x can reach 200–400 pptv, with the greatest concentrations occurring over South Asia. This tropical zone is the main area of NO_x production from lightning (as modelled by MOZART-3), which is the major source of NO_x in the upper troposphere. The predominant sources of NO_x near ground are surface emissions.

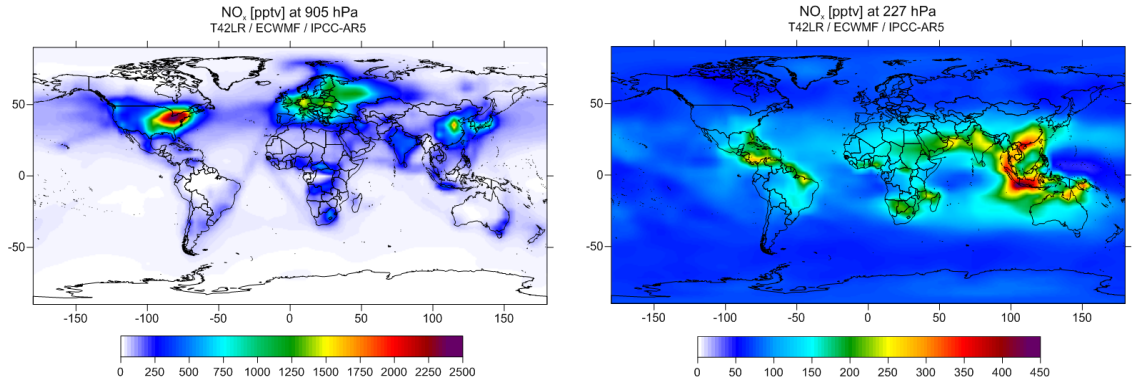

Figure 5.2: Distribution of concentrations of NO_x (in pptv) at 905 hPa (left) and 227 hPa (right) modelled by MOZART-3 CTM.

The reduction of surface emissions influences atmospheric constituents and affects not only the lower troposphere, but its effect is also observed in the upper troposphere (Table 5.1). In most cases, differences in the background of constituents due to modified surface fluxes, are more pronounced near ground (1000–900 hPa). The exception are the responses of CO to reductions in surface NO_x and NMVOC, and OH to reductions in surface CO and NMVOC emissions, where greater differences in the background conditions are calculated in the 250–200 hPa region compared to the 1000–900 hPa. The background concentrations of NO_x and O_3 are always more perturbed near ground than in the upper troposphere, e.g., the reduction of NO_x

emissions modifies the NO_x background by -47% in the 1000–900 hPa region and only by -8.1% in the 250–200 hPa region.

Table 5.1: The concentrations of NO_x, CO, OH and O_3 in the lower and upper troposphere for different background conditions.

Background constituents		Background conditions			
		Base 2000	-30% NO_x	-30% CO	-30% NMVOC
1000 - 900 hPa	NO_x [pptv]	278.7	148.6	280.7	309.4
	CO [ppbv]	102.0	107.4	80.1	98.9
	OH [10^6 mol cm^{-3}]	1.00	0.92	1.04	1.02
	O_3 [ppbv]	34.5	32.8	33.8	33.3
250 - 200 hPa	NO_x [pptv]	84.6	77.8	84.4	86.5
	CO [ppbv]	69.0	73.0	58.8	66.9
	OH [10^6 mol cm^{-3}]	0.97	0.91	1.02	0.98
	O_3 [ppbv]	161.7	158.6	159.3	160.5

Each of the experimental case affects the atmospheric constituents to different extent (Figure 5.3). The NO_x background changes are the largest for surface reduction of NO_x emissions: the annual and global NO_x field is reduced by -151.1 pptv (-49.1%) at 950 hPa and by -7.6 pptv (-8.1 %) at 227 hPa (at that level the most of aircraft NO_x emissions is emitted in MOZART-3). The ~30% reduction of surface CO emissions causes the increase of NO_x concentrations by 2.4 pptv (0.8 %) at 950 hPa and minimal decrease by -0.2 pptv (-0.2%) 227 hPa. The perturbed NMVOC surface fluxes increases NO_x background by 34.9 pptv (11.3%) at 950 hPa and 2.1pptv (2.2%) at 227 hPa.

The CO background is the most sensitive to CO reduction, which decreases CO concentration relatively uniformly throughout the troposphere and constitutes -9.6 ppbv (-14.5%) at 227 hPa. Also, the ~30% NMVOC reduction leads to a lowering of CO background by 2.0 ppbv (3.0%) at 227 hPa. The reduction of surface NO_x emissions causes increase of CO in the atmosphere, again very consistently throughout the troposphere, by 3.6 ppbv (5.6%), globally and annually, more CO at 227 hPa.

While perturbed NO_x and CO concentrations are the result of direct effect of modified surface fluxes, further changes of other constituents are expected to occur through chemical reactions. Indeed, we can observe modified fields of OH and O_3 (Figure 5.3). The OH field decreases with surface NO_x reduction (-5.4% at 227 hPa) and increases

with surface CO and NNMVOC reductions (5.0% and 1.4% at 227 hPa, respectively). The response of O_3 concentration to changes in surface emissions is negative for each case; the strongest O_3 decrease is observed for NO_x reduction (-1.7% at 227 hPa), the weakest for surface NMVOC reduction (-0.7% at 227 hPa).

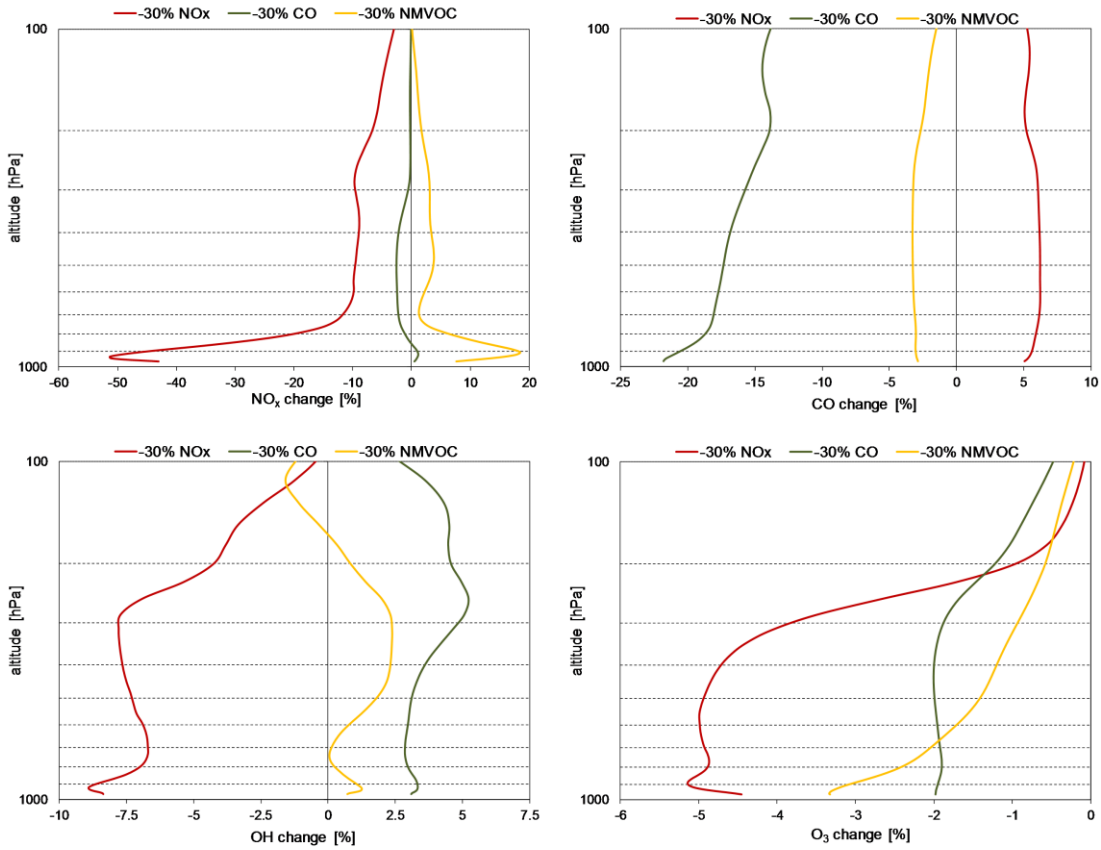

Figure 5.3: The globally and annually averaged vertical distributions of differences in concentrations of NO_x, CO, OH and O_3 for different background conditions compared to the base case.

The differences in the background responses exist not only in the vertical domain, but also spatial influences occur. Figure 5.4 and 5.5 presents the distributions of NO_x, CO, OH and O_3 relative changes at 227 hPa from modified surface emissions. The most uniformly distributed background response belongs to CO for each experimental case. The more regional responses concentrated mainly over continents, where the reduced sources are placed, are calculated for background changes of NO_x, OH and O_3 pronounced especially for surface NO_x reduction and to lesser extent for surface NMVOC reduction.

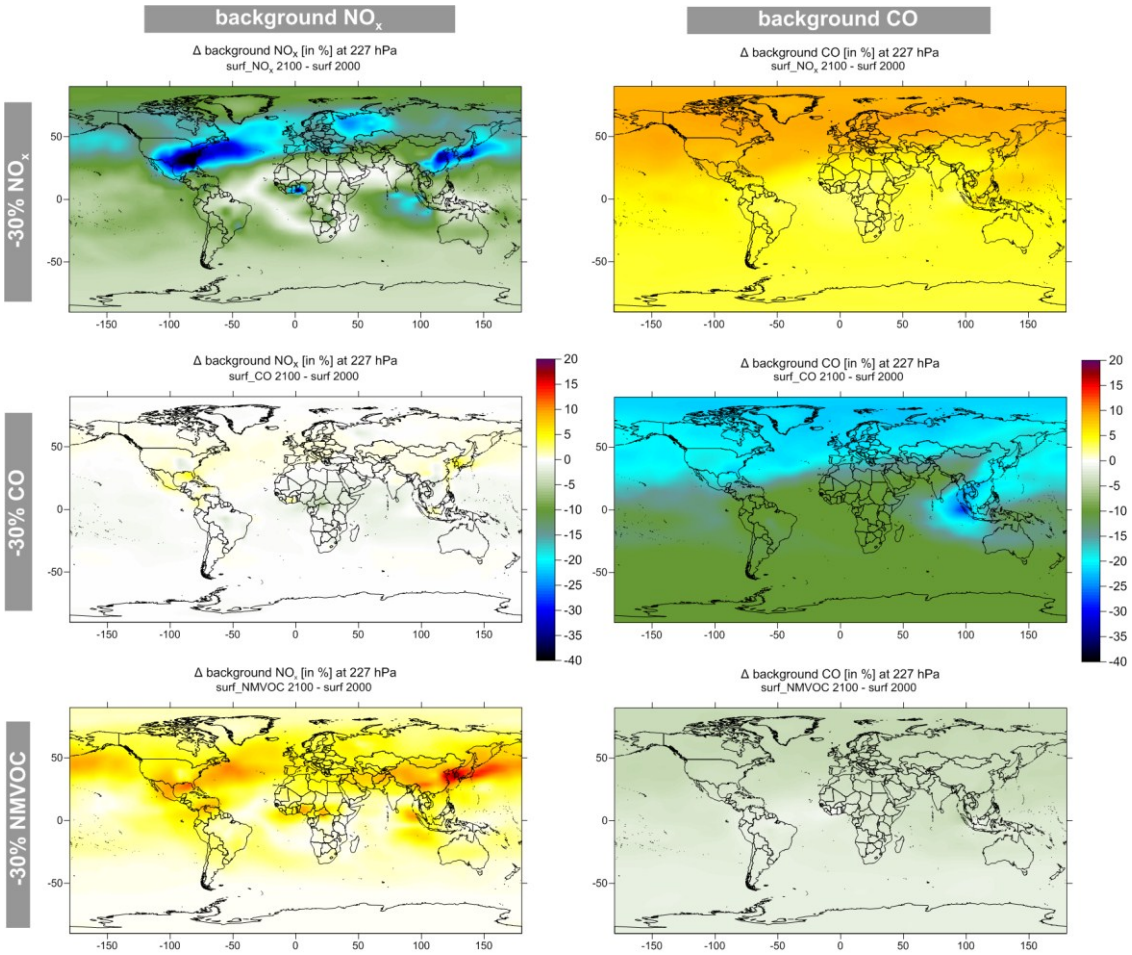

Figure 5.4: The annually averaged spatial distribution of relative changes (in %) of background constituents: NO_x (left column) and CO (right column) at 227 hPa due to reductions of surface NO_x emissions (upper row), reductions of surface CO emissions (middle row) and reductions of surface NMVOC emissions (bottom row).

The changes of atmospheric constituents are also influenced by seasons (Figure 5.6). In the upper troposphere larger perturbations for each of analysed species occur in summer months. The seasonal pattern looks different near the ground where winter months are more pronounced for species, for which the main source is surface emissions. Changes in OH and O_3 that depend purely on chemical reactions have smaller responses during winter months, when solar intensity in the Northern Hemisphere is much weaker than during the summer months.

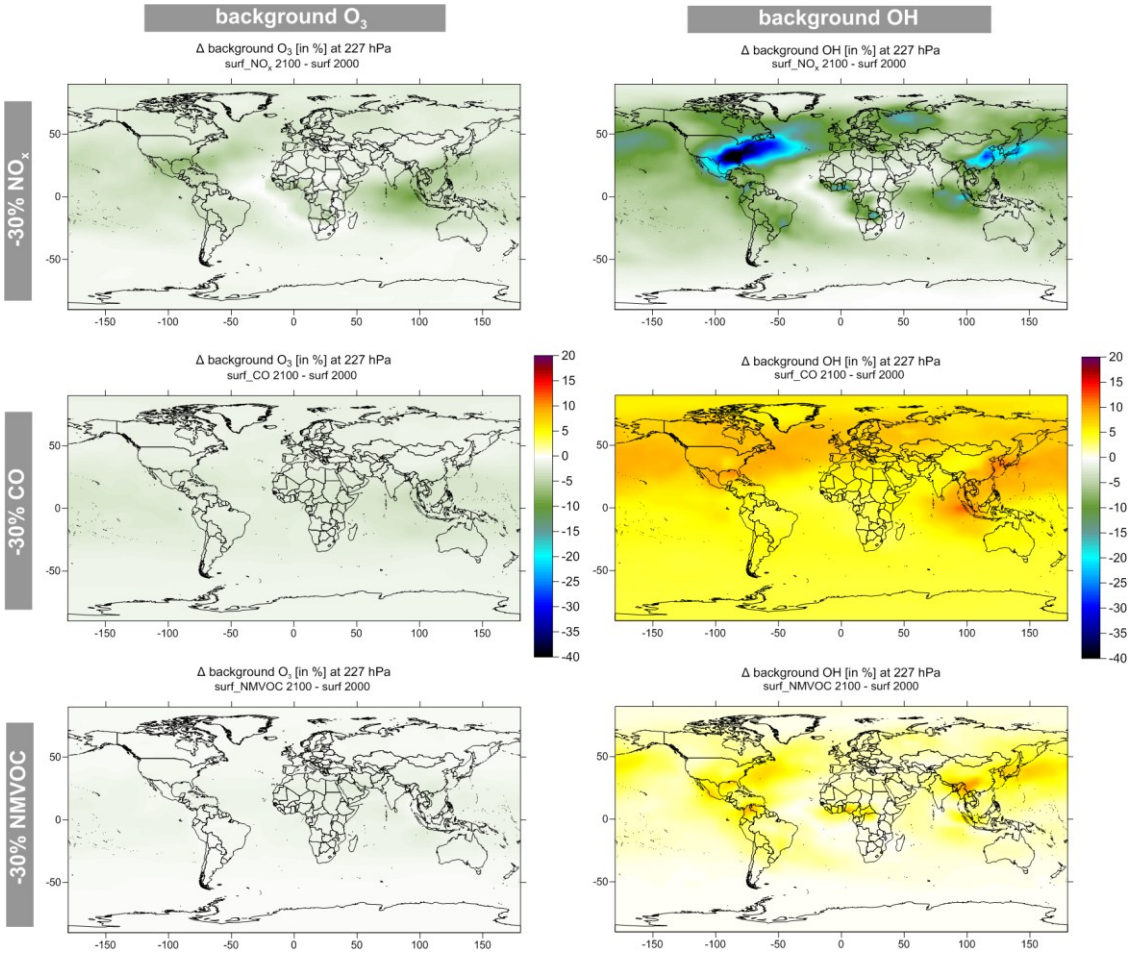

Figure 5.5: The annually averaged spatial distribution of relative changes (in %) of background constituents: O_3 (left column) and OH (right column) at 227 hPa due to reductions of surface NO_x emissions (upper row), reductions of surface CO emissions (middle row) and reductions of surface NMVOC emissions (bottom row).

The oxidizing capacity of the atmosphere is substantially affected, when the reductions of NO_x, CO and NMVOC are applied. This means that CH_4 lifetime must be also influenced. Figure 5.7 shows how CH_4 lifetime changes under different reduction cases. The CH_4 lifetime due to destruction by OH is 8.8 years for the base case. While the 30% reduction of NO_x introduces the greatest, the NMVOC reduction gives the weakest perturbations of CH_4 abundance compared to base case, where CH_4 lifetime changes by 7.0% (9.4 yr) and -0.7% (8.7 yr), respectively. The 30% reduction of surface CO emissions reduces CH_4 lifetime by 3.4% and it constitutes 8.5 years.

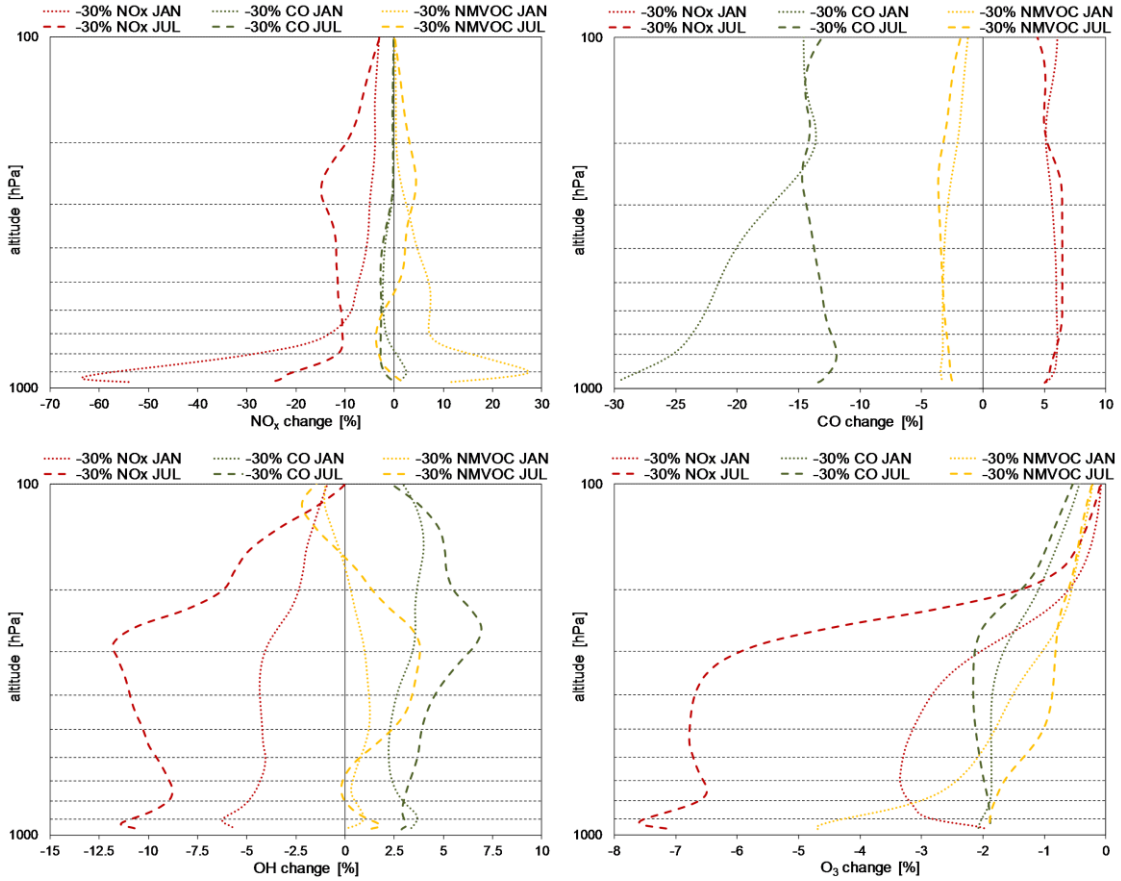

Figure 5.6: The vertical distributions of differences in concentrations of NO_x, CO, OH and O_3 in January (dotted lines) and July (dashed line) for different background conditions compared with base case.

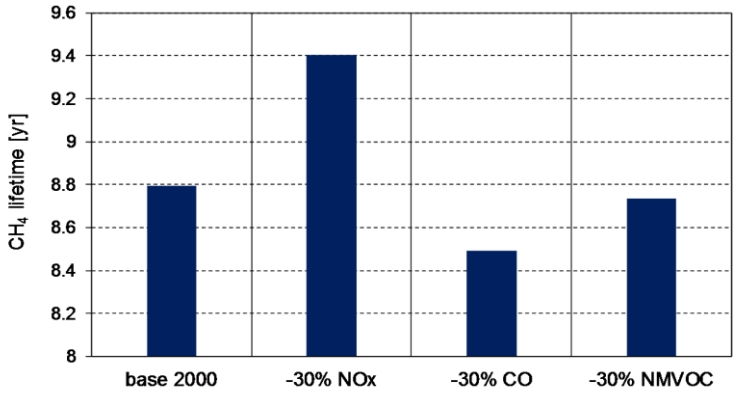

Figure 5.7: The CH_4 lifetime (in year) due to destruction by OH for a different background conditions.

5.3.2 Aircraft perturbation

Most of the NO_x and O_3 enhancement from aircraft NO_x emissions is concentrated in the Northern Hemisphere (Figure 5.8). Both species are short lived, order of days and weeks, respectively, thus their perturbation occurs where the main air traffic takes place. The O_3 production from NO_x emissions depends on the state of the atmosphere, thus by changing the background of constituents, the sensitivity of aircraft O_3 response should also change.

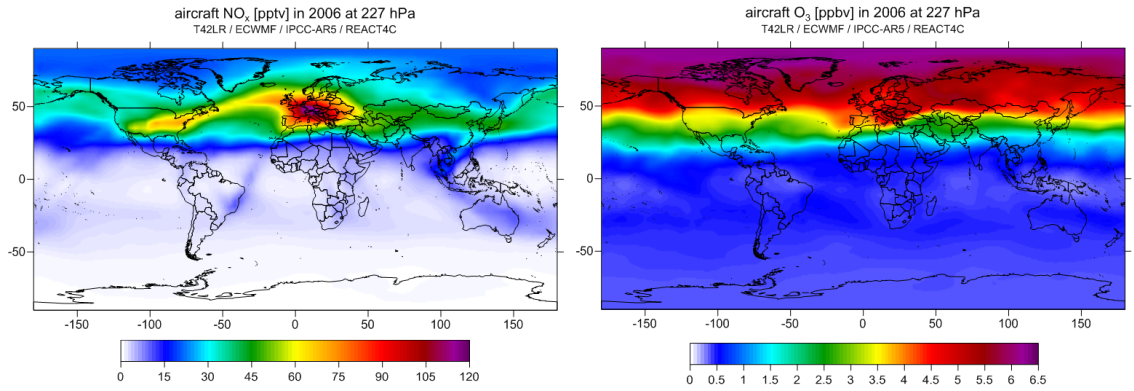

Figure 5.8: The annual mean perturbations of NO_x (left) and O_3 (right) at 227 hPa in a response to emissions of aircraft NO_x emissions modelled by MOZART-3 CTM.

Figure 5.9 shows the aircraft NO_x and O_3 for different background cases. While the aircraft NO_x response is only slightly affected, for aircraft O_3, significant changes are calculated. The reduction of surface NO_x brings increase of aircraft NO_x perturbation near ground and decrease, by 1.1% of aircraft NO_x response at 283–254 hPa. Generally, the small increase of aircraft NO_x perturbation is observed at 227 hPa for all experimental cases and the reduction of surface NMVOC gives the largest aircraft NO_x perturbation, which is 0.3 pptv (1.9%). The aircraft O_3 response from modifications of surface emissions is more significant than aircraft NO_x response. The most significant changes of aircraft O_3 are observed for reduction of surface NO_x, where the O_3 perturbation increases by 0.36 ppbv (17%) at 227 hPa. The reduction of surface CO and NMVOC causes decrease of aircraft O_3 perturbation, by -0.10 ppbv (-4.8%) and -0.12 ppbv (-5.5%), respectively, despite the increase of aircraft NO_x perturbation is observed.

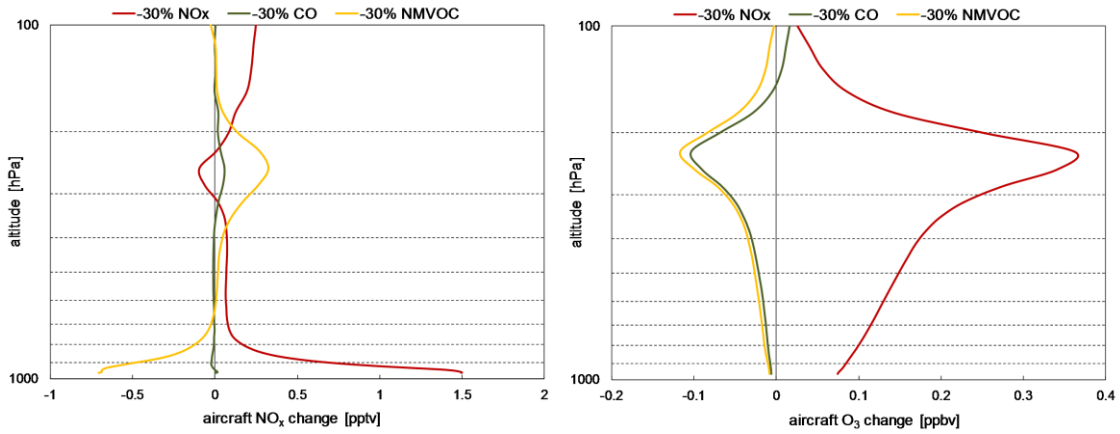

Figure 5.9: The globally and annually averaged vertical distributions of aircraft perturbations of NO_x (left column) and O_3 (right column) concentrations for different background conditions (upper row) and their absolute differences compared to the base case (bottom row).

The changes in surface emissions affect distributions of both aircraft NO_x and O_3 perturbations (Figure 5.10). The reduced surface NO_x emissions decreases aircraft NO_x response at 227 hPa with the negative peaks concentrated over east coast of North America and North Atlantic. The reduction of surface CO and NMVOC fluxes increases aircraft NO_x response at 227 hPa; this enhancement is much more pronounced for the 'NMVOC case' especially over Europe, the North Atlantic and Asia. The aircraft O_3 changes to different surface emissions are evenly distributed in the Northern Hemisphere, being positive for surface NO_x reduction and negative for surface CO and NMVOC reductions.

Similar to changes in background constituents, the aircraft responses have their seasonal dependencies (Figure 5.11). The aircraft NO_x perturbation are greater in January for each experimental case for both near ground and at flight levels (~300–200 hPa). The aircraft O_3 response is stronger in July for each surface conditions at flight levels; the reduction of surface NO_x is a source of increase of aircraft O_3, by 19.3%, in July at 227 hPa, on the contrary the reduction of surface NMVOC result in 5.7% decrease of aircraft O_3 response.

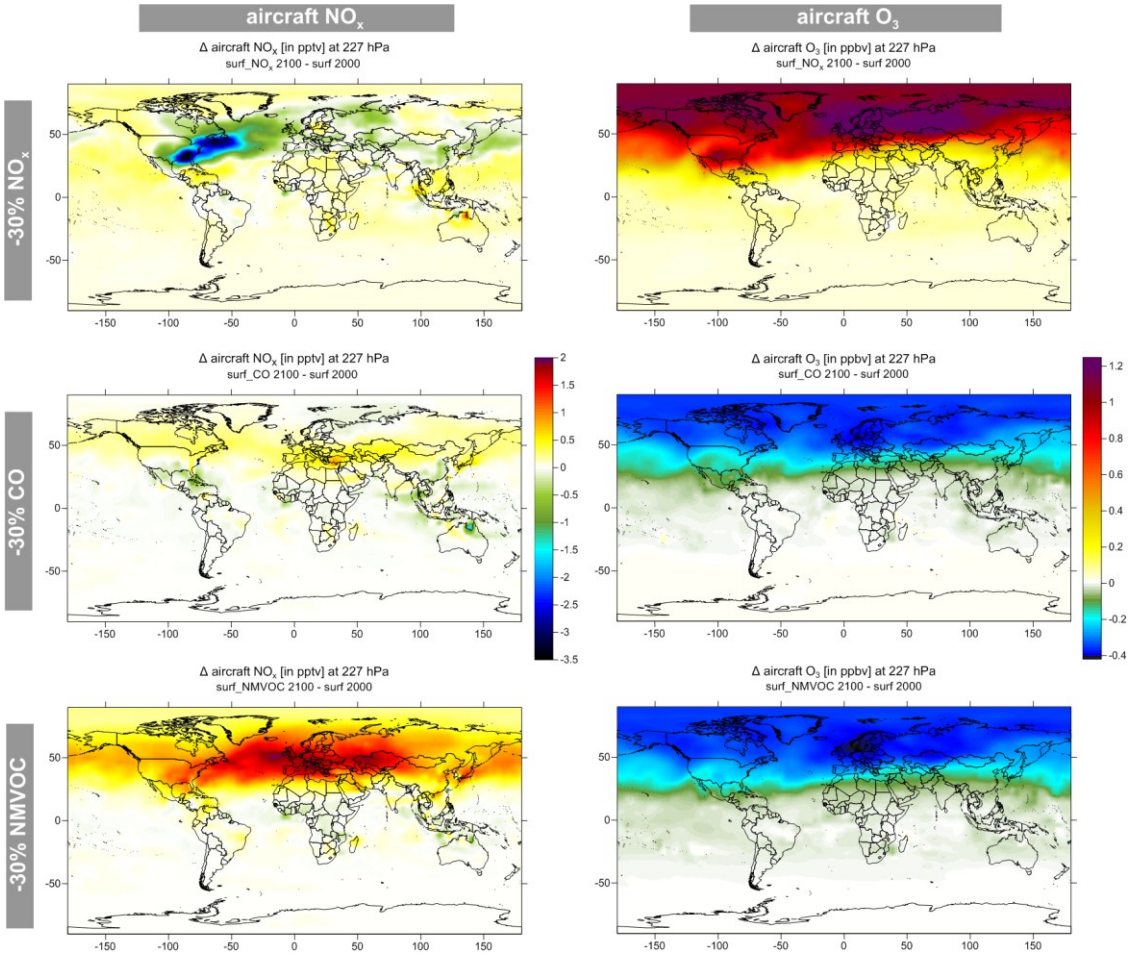

Figure 5.10: The annually averaged spatial distribution of absolute changes of aircraft perturbations of NO_x (upper row) and O_3 (bottom row) at 227 hPa due to reductions of surface NO_x emissions (left column), reductions of surface CO emissions (middle column) and combined reductions of surface NO_x CO emissions (right column).

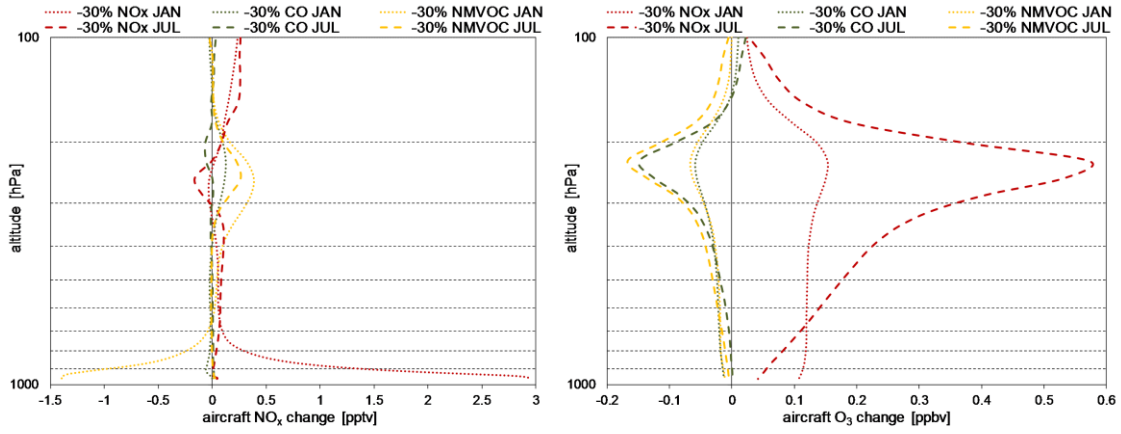

Figure 5.11: The vertical distributions of differences of aircraft perturbations of NO_x (left) and O_3 (right) in January (dotted lines) and July (dashed line) for different background conditions compared with base case.

5.4 Discussion

The perturbations of anthropogenic and biomass burning emissions substantially affect the background conditions of the atmosphere. The reductions of surface NO_x, CO and NMVOC directly affect concentrations of these gases and the decreases of NO_x, CO and NMVOC are observed, respectively. Reduction of surface NO_x decreases concentrations of OH, which consequently affect CO and CH_4 causing an increase in its abundance. On the contrary, reduction of CO leads to an increase of OH and decrease of CH_4 lifetime. The NMVOC reduction increases NO_x background via OH increase. The O_3 strongly follows the NO_x concentrations, thus its decrease is calculated for NO_x reduction. What also drives the O_3 production is abundance of CH_4 (and CO, NMVOC); the decrease of CH_4 lifetime with reduction of surface CO and NMVOC emissions (via OH) also decreases concentrations of O_3. These results are consistent with other studies (e.g., Fry et al., 2012, Shindell et al., 2009, West et al., 2007). The species' lifetimes influence the distribution, both spatial and vertical, of their changes to modified surface fluxes. The CO lifetime is longer than NO_x, OH and O_3, thus its changes are more uniformly distributed in the troposphere.

The resultant changes from surface emissions also extent to the upper troposphere, where aviation acts as the major pollutant source, which means that aircraft responses are also affected. Changes in aircraft response for perturbed background conditions are clearly observed (Table 5.2). The greatest aircraft O_3 burden change and CH_4 lifetime reduction are calculated for reduction of surface NO_x emissions. The reduced NMVOC fields gives the lowest O_3 response and the perturbed CO surface emissions results in the weakest CH_4 lifetime reduction due to aircraft NO_x emissions.

Table 5.2: The annual mean O_3 burden change (in Tg) and CH_4 lifetime change (in year) due to the aircraft NO_x emissions for different background conditions.

Background conditions	aircraft O_3 burden (Tg)	aircraft CH_4 lifetime (yr)
Base 2000	5.05	-0.073
-30% NO_x	6.07	-0.106
-30% CO	4.89	-0.067
-30% NMVOC	4.81	-0.069

The sensitivity of aircraft O_3 production strongly depends on the experimental case (Figure 5.12), with its relative values ranging from positive (for reduction of NO_x reduction) to negative (for reduction of CO and NMVOC emissions). The reduction of NO_x emissions leads to larger aircraft O_3 responses by 19.6% in July and by 11.9% in January. One of the main factors that drive this increase is 'cleaner' NO_x background: the decrease of NO_x concentration at 250–200 hPa reaches -12.3% in July and -4.2% in January. However, taking into account that O_3 production from injected NO_x is almost linear in the upper troposphere, there must be other agent influencing O_3 response, which is enhanced CO abundance (Figure 5.3). The role of CO is also observed when reduction of surface CO emissions is taken into account; here weaker aircraft O_3 is observed compared to base case (despite the fact that the NO_x background is almost not affected and the small increase of aircraft NO_x is observed, reaching 1.2% in January). This decline is rather constant through the year and it is -4.7% in July and -4.3% in January. All of these highlight importance of CO in O_3 production. The decrease of O_3 in case of surface NMVOC reduction, by -4.8% in January and -5.3% in July, is related with a decrease of CO background and an increase (reaching 3.8% in July) of NO_x background (via OH increase).

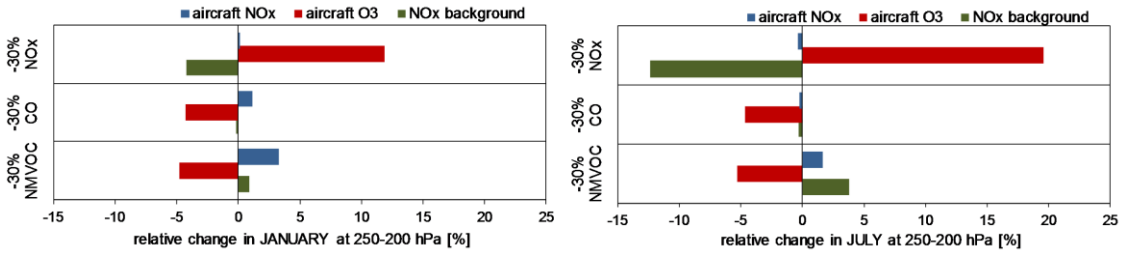

Figure 5.12: The relative changes of aircraft NO_x response (blue bars), aircraft O_3 burden (red bars) and NO_x concentrations (green bars) in 250–200 hPa domain for January (left) and July (right) due to different background conditions.

The disparate aircraft O_3 burden changes, as well as CH_4 abundance modified in each experimental case, both influence the magnitude of aircraft CH_4 reduction. Figure 5.13 shows that the reduction of CH_4 lifetime, due to aircraft NO_x emissions, is larger for reductions of surface NO_x, by 46.2% compared to the base case and lower, by -7.4% and -4.6%, for reductions of surface CO and NMVOC emissions, respectively.

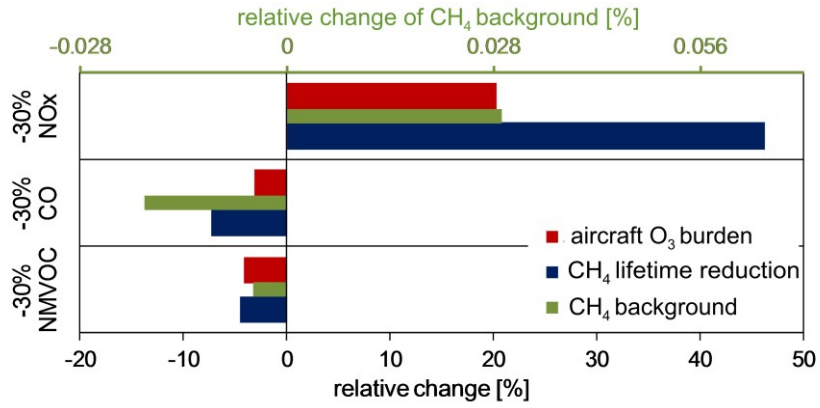

Figure 5.13: The global and annual relative changes of aircraft O_3 burden (red bars) and CH_4 lifetime reductions (blue bars) responses due to different background conditions.

Modifications of surface O_3 precursor emissions lead to different ratios of the CH_4 lifetime change to the O_3 burden change, which is specific for each background condition (Figure 5.14). The observed significant increase in the magnitude of aircraft O_3 response, in the case of reduced surface NO_x emissions, is substantially cancelled by efficient (due to increased CH_4 abundance) negative CH_4 response. The situation is different for reduction of surface CO emissions, where the decrease of aircraft O_3 response is greater than the increase (due to decreased CH_4 abundance) of CH_4 lifetime reduction. The CH_4/O_3 ratio almost does not change (-0.4%) for reduction of surface NMVOC emissions compared with the base case.

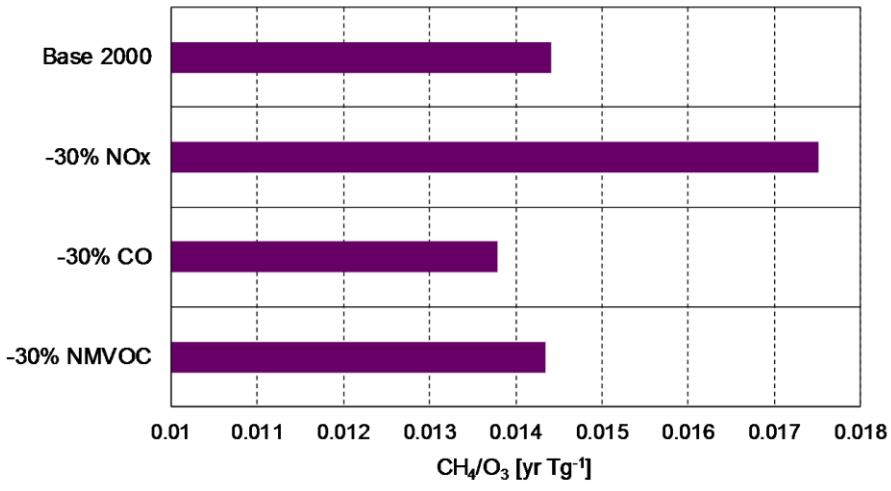

Figure 5.14: The absolute ratio of the CH_4 lifetime change to the O_3 burden change for different background conditions.

5.5 Summary

The modified surface NO_x emissions clearly affect the aircraft O_3 response (Figure 5.15): the smaller (cleaner) background NO_x leads to greater change of O_3 from injected NO_x, which is consistent with other studies on tropospheric non-linearities (Lin et al., 1988, Wu et al., 2009). The relation between the NO_x background change and aircraft O_3 response is linear up to 20% of the surface NO_x reduction; for surface NO_x rates greater than 20% the efficiency of O_3 change raises with greater surface NO_x reduction (the shape of this relation will depend on the initial background concentration). On the contrary, the relation between aircraft NO_x emissions change and aircraft O_3 response is linear for each aircraft NO_x rate: the aircraft O_3 response decreases with reduced amounts of injected NO_x. The modified aircraft NO_x emissions are always more efficient in influencing the aircraft O_3 change; however, not with the same degree. The reduced NO_x rates smaller than 5% give the similar strength in affecting aircraft O_3 response for both cases; the difference in O_3 change between surface and aircraft experiments are less than 1.5%. The NO_x rates greater than 5% show that the aircraft O_3 response is more sensitive to the aircraft NO_x reductions, than to the surface NO_x changes, e.g., for 50% reduction of surface and aircraft NO_x emissions, the aircraft O_3 changes by 32% and 43%, respectively. Therefore, the primary driver of aircraft induced O_3 are NO_x emissions; to the lesser, but still significant, extent it is influenced by NO_x background conditions.

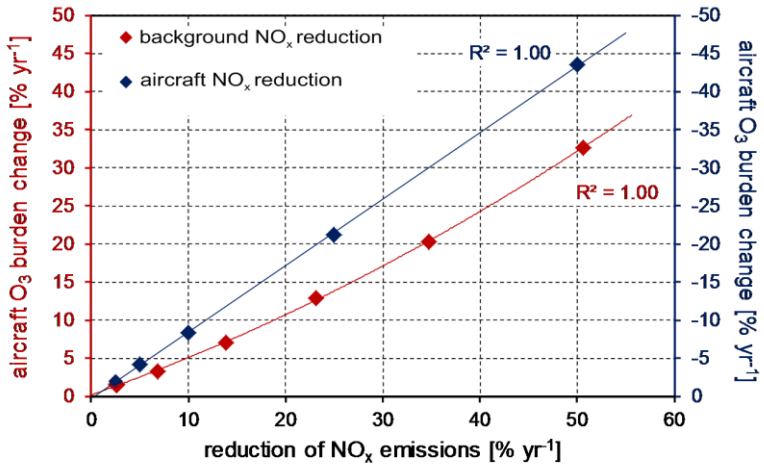

Figure 5.15: Scatter plot of aircraft O_3 burden changes (in %) against series of reduced aircraft (blue) and surface (red) NO_x rates of emissions (dots are individual experiments, line is the best fit line).

Chapter 6

The uncertainties associated with aircraft NO_x estimates arising from usage of different aircraft inventories

6.1 Introduction

The NO_x aircraft emissions alter the composition of atmosphere: enhance O_3 production and reduce CH_4 lifetime and concentration. These changes result in radiative forcings (RF) which consequently stimulate climate change. The comprehensive review, regarding aviation impact on atmosphere and climate, has been recently presented by Lee et al. (2010).

IPCC (1999) estimated that a global mean RF for O_3 to be 23 mWm^{-2} and reduction of CH_4 as -14 mWm^{-2} in year 1992. An updated study for year 2000 was presented by Sausen et al. (2005), which calculated the O_3 RF of 21.9 mWm^{-2} and the CH_4 RF of -10.4 mWm^{-2}. Recently, Lee et al. (2009) estimated O_3 and CH_4 RFs as 26.3 mWm^{-2} and -12.5 mWm^{-2}, consequently, for year 2005. The ensemble studies, as presented above, are relatively consistent in determining their RFs and give a global mean net positive RF form aircraft NO_x perturbation, varying from 9.0 mWm^{-2} to 13.8 mWm^{-2}.

Many studies have been published over the past years assessing the impact of aviation NO_x emissions on atmospheric chemistry and RF (Grewe et al., 1999, Isaksen et al., 2001, Grewe et al., 2002, Stordal et al., 2006, Gauss et al., 2006, Søvde et al., 2007, Hoor et al., 2009, Köhler et al., 2008, Myhre et al., 2011, Hodnebrog et al., 2011, 2012, Frömming et al., 2012). The NO_x estimates derived through modelling experiments, a mixture of Chemistry Transport Models (CTMs) and Climate Chemistry Model (CCM) give a diverse picture. The O_3 column change due to aircraft NO_x emissions can vary from 0.30 DU (Hoor et al., 2009) to 0.81 DU (Köhler et al., 2008). The methane lifetime change due to aircraft NO_x emissions ranges between -3.0% (Köhler et al., 2008) to -0.64% (Hoor et al., 2009). Consequently, the resultant RFs give broad spectrum of values as well. The short-term O_3 RFs fluctuate between 10.8 mWm^{-2} (Stordal et al., 2006, Hoor et al., 2009) and ~30 mWm^{-2} (Köhler et al., 2008, Hoor et al., 2009). The CH_4 RFs vary from -5.7 mWm^{-2} (Hoor et al., 2009) to -19.0 mWm^{-2} (Köhler et al., 2008). The reported aircraft net NO_x RFs are rather positive. However, the numbers can be as low as 0.0 mWm^{-2} (Köhler et al., 2008) or 0.8 mWm^{-2} (Hoor et al., 2009) and as high as 8.7 mWm^{-2} (Myhre et al., 2011) or ~7.0 mWm^{-2} (Hoor et al., 2009, Myhre et al.,2011, Stordal et al., 2006). All these numbers are derived based on a sustained present-day aircraft NO_x perturbations.

Holmes et al. (2011) gathered the published model results, quantified and distinguished the processes, which drive the uncertainties in RFs from aviation NO_x. The multi-model means of the short-term O_3 are of 27.3 ± 9.7 mW m^{-2} per Tg(N) yr^{-1}, the CH_4-induced O_3 RF are of -6.6 ± 3.3 mW m^{-2} per Tg(N) yr^{-1} and the CH_4 RF are of -16.1 ± 5.6 mW m^{-2} per Tg(N) yr^{-1}. The multi-model net NO_x RF turned out to be very uncertain and it is of 4.5 ± 4.5 mW m^{-2} per Tg(N) yr^{-1}. The uncertainties of the O_3 change to aviation NO_x emissions and the radiative efficiencies of O_3 are the main contributors to the uncertainty of the aircraft short-term O_3 estimates. The uncertainty in the aircraft CH_4 response originates, in 80%, from the uncertainty in the CH_4 change to aviation NO_x emissions. For the CH_4-induced O_3 response, the variance in its response is driven, in 50%, by the O_3 change in the CH_4 perturbation.

These studies are not always straightforward in comparison, since the models have varying degrees of complexity in terms of completeness of representation of tropospheric and stratospheric chemistry, horizontal and vertical resolution.

Holmes et al. (2011) highlighted factors, which drive the inter-model differences: these related to model response to aircraft emissions ('aviation factor'), e.g., the model's specific O_3, CH_4 change per unit emitted N and these related to general model response ('nonaviation factor'), e.g., the model's specific O_3 change per unit change of CH_4. Myhre et al. (2011) pointed out that the change in CH_4 lifetime per unit O_3 change is the dominant driver of inter-model disparities. However, these factors not necessarily must represent only a certain model's peculiarities. The various sensitivities of O_3 change per unit emitted N and CH_4 change per unit change of O_3 are also possible to observe with one model and the same amount of emitted aircraft NO_x, which will be shown below.

In this chapter, the NO_x impact on chemical composition of the troposphere is revisited and the individual RF responses (short-term O_3 increase, long-term CH_4 and O_3 decreases, CH_4 feedback effect on stratospheric water vapour) are estimated. Most importantly, the impact of using different emission inventories is investigated, as all previous comparative studies have utilised different models. Here, a novel approach for aircraft NO_x estimates is taken of using a single model with various aircraft emissions.

6.2 Methodology

6.2.1 Aircraft emission inventories

The aircraft inventory datasets are normally produced based on aircraft movement database, characteristic of a global fleet in terms of type of aircraft and engines, fuel-flow model, calculation of emissions at vertical scale from fuel flow, landing and take-off emissions (LTO). The aircraft movement databases are usually generated from a combination of flight plan data, flight operation data, radar data, Official Aviation Guide (OAG) data (www.oag.com) and idealized great circle routes analysis. Recent publication of Olsen et al. (2013) presents more details regarding aircraft inventories and their comprehensive comparison.
In this study, six different aircraft inventories were investigated:

AEDT (Aviation Environmental Tool), representing year 2006 (Wilkerson et al., 2010). The global aircraft data came from by Volpe National Transportation Systems

Centre. An individual flight by flight analysis were adopted in order to estimate the aircraft fuel burn and emissions. The 70–80% of global aircraft movements is based on a radar data for Europe and North America and for the remaining flight movements the OAG data were used.

AEM (Advanced Emission Model), representing year 2006 (www.eurocontrol.int/services/advanced-emission-model). AEM was developed and is maintained by EUROCONTROL. AEM is a stand-alone system, which calculates aviation emissions and fuel burn based on a few basic databases: aircraft, aircraft engines, fuel burn rates and emissions indices. AEM is design for analysis of the flight profile data, on a flight by flight bases, for different air traffic scenarios.

AERO2K inventory, representing year 2002 (Eyers et al., 2005), was developed under the EC 5th Framework Programme. The inventory is based on a radar tracked flight data for North America and Europe; the rest of the world is included through scheduled flights data from Back Aviation database (Back, 2002) and by routing information. The fuel burn and emissions for each flight were derived using means from the PIANO (www.piano.aero) aircraft performance model based on forty representative aircraft types.

REACT4C (EC 7th Framework Programme Reducing Emissions from Aviation by Changing Trajectories For the benefits of Climate), representing year 2006 (www.react4c.eu). The input data consist of the CAEP-8 comprehensive set of aircraft movements (the individual movements are for 6 weeks of the year, which then are scaled to a full year's movements). The base of air traffic movements are the radar data for flights for Europe and North America and the remaining global flight movements are covered by OAG. Two models were applied to generate this inventory: the fuel-flow model PIANO (Project Interactive Analysis and Optimization model) and global emissions model FAST (The Future Aviation Scenario Tool) (Owen et al., 2010), similarly as for QUANTIFY and TRADEOFF data presented below.

QUANTIFY (Quantifying the Climate Impact of Global and European Transport Systems), representing year 2000 (Owen et al., 2010). The dataset is based on the OAG data for scheduled flights and AERO2K's traffic for non-scheduled aircraft

movements. The QUANTIFY inventory, once released, was scaled to the International Energy Aviation (IEA) aviation fuel burn total for year 2000.

TRADEOFF – representing year 1992 (Gauss et al., 2006). This inventory consists of a flight track data from the EUROCONTROL and FAA from the year 1991/1992. Four months of aircraft movements: July 1991, October 1991, January 1992 and April 1992 were scaled in order to get a full year's movement. The global aircraft movement data are a mixture of air traffic control and scheduled data. Sixteen civil aircraft–engine type combinations account for the global fleet of aircraft.

Aircraft inventories used in this study are three dimensional gridded datasets, with a $1^{\circ}x1^{\circ}$ horizontal resolution and a varying, from 1km through 610m to 500 ft, vertical resolution. Table 6.1 gives an overview of the characteristics of each inventory. Military emissions have not been included in this study.

Table 6.1: The summary of specifications of aircraft inventories used in this study: AEDT, AEM, AERO2K, REACT4C, QUANTIFY and TRADEOFF.

Inventory	AEDT	AEM	AERO2K	REACT4C	QUANTIFY	TRADEOFF
Year	2006	2006	2002	2006	2000	1992
Fuel Tg/year	187	210	156	178	152	114
Distance billion km/year	38.9	43.6	33.2	38.9	30.5	17.4
CO_2 Tg/year	590	508	492	562	479	n/a
NO_x $Tg(NO_2)$/year	2.72	2.99	2.06	2.33	1.98	1.61
Vertical spacing	1km	500 ft	500 ft	610 m	610 m	610 m
Temporal resolution	Annual	Monthly	Monthly	Monthly	Monthly	Seasonal
Air traffic movements	Radar data, OAG	Radar data, OAG	Radar data, BACK	Radar data, OAG	OAG for schedule & AERO2K for non-schedule traffic	OAG, scheduled data
Modelling tool	SAGE, BADA	AEM, BADA	AERO2K, PIANO	FAST, PIANO	FAST, PIANO	FAST, PIANO

Air traffic movements incorporated to different aircraft inventories are based on similar methodologies: 4D radar data for Western Europe and North America and schedule data for the rest of the world. Usually, for most of the inventories, the few weeks of 4D 'real data' are considered, which are then scaled to represent the full year's movement. Only AEDT inventory includes 'as much real data as possible' (Wilkerson et al., 2010), where flight trajectories are analysed on a single flight basis. In addition, the track methodology employed in AEDT 2006 is an airways track method (instead of Great Circle analysis widely used for other inventories), which was proved to constitute a more precise representation of actual flight activity (Wilkerson et al. (2010), based on analysis of Eastern Europe, East Asia and Arctic, where most of the non-radar data occurs). This all makes aircraft AEDT 2006 inventory favourable, in terms of representing the air traffic movements, hence related aviation emissions, the most accurately.

6.2.2 Experimental design

The aircraft emission datasets were implemented into the 3D CTM, MOZART-3. Each dataset represents different years of aircraft movements, which results in different amounts of burned fuel ranging from 210 Tg yr^{-1} for AEDT (2006) to 114 Tg yr^{-1} for TRADEOFF (1992) which affects the emitted NO_x. In order to exclude the differences in the amount of injected NO_x, which consequently impacts O_3 response, the NO_x emissions of each inventory were scaled to the same global total as the REACT4C , which is 2.33 Tg (NO_2) yr^{-1}.

Seven experiments were conducted, one reference (no-aircraft) run and six perturbation (aircraft) runs, each starting in January 2000 and finishing in December 2000. Each of the simulations was preceded by one year spin-up. The aircraft perturbation is obtained by extracting the difference between aircraft and no-aircraft experiments. The validity of 2 years simulations is presented in Chapter 4.4. The details regarding model set-up, surface emissions and dynamical data applied for this study are described in Chapter 3.3. The detailed description of radiative forcings and global warming potentials calculations is presented in Chapter 3.2

6.2.3 Additional aircraft NO_x experiments – altitudinal regions

In order to examine the extent of importance of altitudinal and latitudinal locations in O_3 production, the incremental aircraft NO_x emissions (0.035 Tg(N) yr^{-1}) were applied for a period of a year to three altitudinal regions: 9–10 km, 10–11 km, 11–12 km and three latitudinal regions: Europe, Southeast Asia and North America (Figure 6.1). The additional NO_x emission corresponds to 38%, 12%, 130%, 32%, 28% and 30% of relative increases in the respective regions. The MOZART-3 setup is consistent with incremental aircraft NO_x experiments presented in Chapter 8 and it is described in details in Chapter 3. The aircraft inventory used for these runs is the REACT4C 2006 dataset

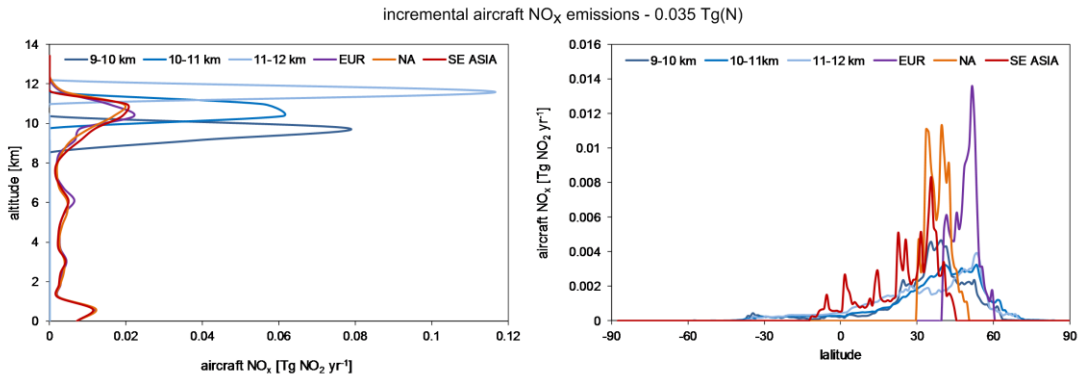

Figure 6.1: The vertical (left side) and latitudinal (right side) profiles of incremental aircraft NO_x emissions in six regions: 9–10 km, 10–11 km, 11–12 km, Europe (EUR), Southeast Asia (SE ASIA) and North America (NA).

6.3 Results

6.3.1 Aircraft NO_x emissions

As various methodologies have been applied to determine different inventories, the distribution of NO_x emissions reveals some discrepancies. The geographical distribution shows rather uniform picture (Figure 6.2). The image of altitudinal spacing reveals some discrepancies (Figure 6.3).

The main location of aircraft NO_x emissions is the Northern Hemisphere: emissions in 30–60°N and 0–30°N regions constitute 65% and 24%, respectively, for AEDT,

AEM and REACT4C inventories; AERO2K, QUANTIFY and TRADEOFF have more emissions in mid northern latitudes (68%) and less over the northern tropical region (21%). Most of aircraft NO_x emissions is present over North America, Europe and Southeast Asia. AERO2K, QUANTIFY and TRADEOFF have lower emissions, by ~4%, in 60–120°E region and more, by ~4%, in 120–60°W region than AEDT, AEM and REACT4C.

The largest part of the NO_x emissions are injected between 9 and 12 km for most of the inventories; AEDT and AEM have larger fraction of aircraft NO_x over 12 km than the other inventories. AERO2K's NO_x emissions at cruise altitudes represent only 43% of its total aircraft NO_x emissions (Figure 6.3), which, when compared with 57% of QUANTIFY, 58% of AEM, 59% of REACT4C and TRADEOFF and 63% of AEDT, is noticeably low. The 'missing' ~10% is hidden under AERO2K's relatively large NO_x emissions at mid-altitudes, which is 34%, while for all the rest of inventories it covers around 25%. The difference in the vertical structure of NO_x emissions between AERO2K and the other datasets is considerable. Also Olsen et al. (2012) and Wilcox et al. (2012) highlighted the peculiarity of AERO2K inventory in their inventory comparison and water vapour studies, respectively.

The normalized datasets (scaled to the same global total, which is 2.33 $Tg(NO_2)\ yr^{-1}$) also reveal discrepancies in altitudinal and latitudinal distributions of aircraft NO_x emissions (Figure 6.4, 6.5). The AERO2K's NO_x dominates by ~87% near ground and in mid-altitudes (till 9 km) reaching 261% at 2–3 km layer compared to AEDT inventory, along with significant lack of aircraft NO_x emissions ~56% in 9–13 km region (Figure 6.4). All FAST inventories (REACT4C, TRADEOFF, QUANTIFY) have ~21% more NO_x emissions at 10–11 km compared to AEDT and ~83% less at 11–13 km. The latitudinal distribution of aircraft NO_x emissions is rather consistent (Figure 6.5). It is observed that high northern and southern latitudes are causing the greatest relative differences. The longitudinal profiles (Figure 6.5) shows that AEDT has slightly more NO_x in Asia and a bit less NO_x in North America than AERO2K, QUANTIFY and TRADEOFF. The AEM and REACT4C inventories are the most consistent with AEDT dataset in terms of their latitudinal and longitudinal distribution.

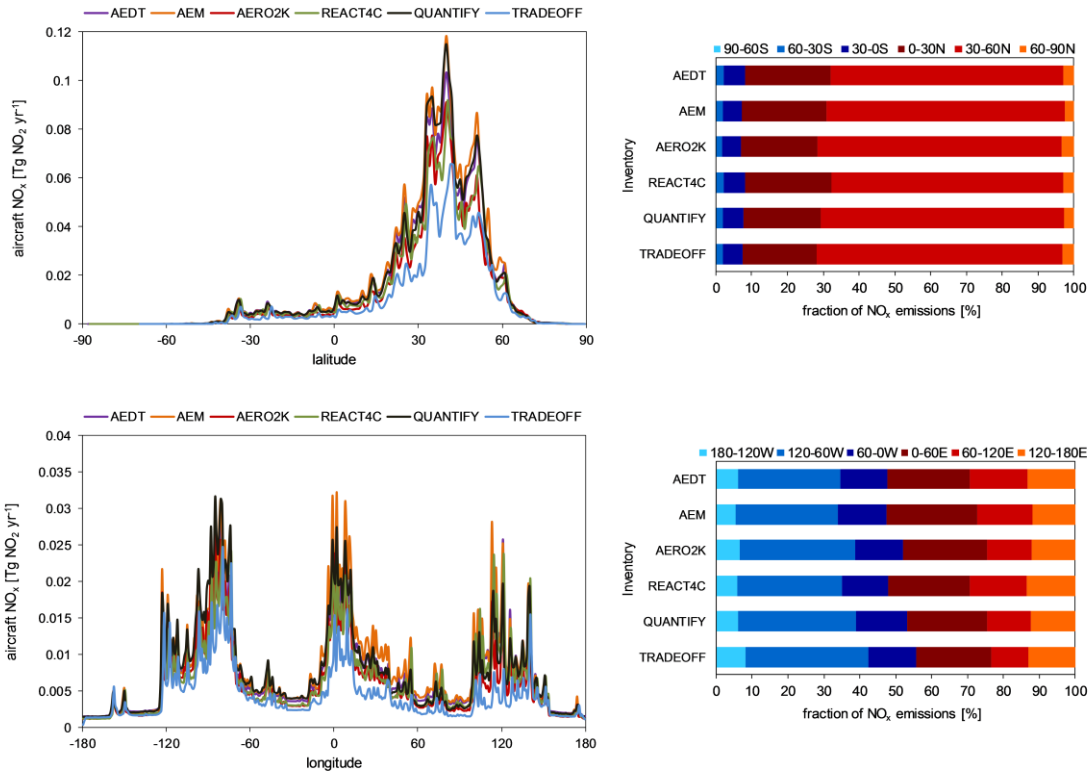

Figure 6.2: The globally and annually averaged latitudinal (upper row) and longitudinal (bottom row) distributions of aircraft NO_x emission (left column) and the fraction of aircraft NO_x emission occurring in latitudinal and longitudinal bands (right column) for different aircraft inventories: AEDT, AEM, AERO2K, REACT4C, QUANTIFY and TRADEOFF.

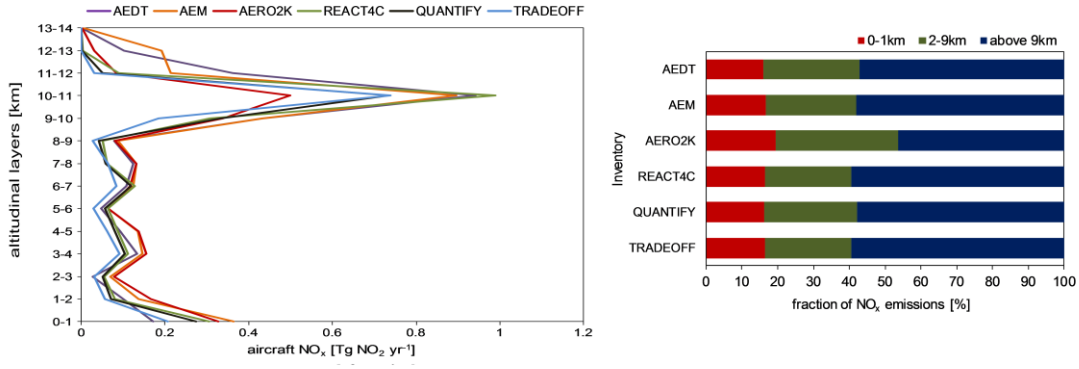

Figure 6.3: The globally and annually averaged altitudinal distributions of aircraft NO_x emission (left) and the fraction of aircraft NO_x emission occurring in three altitudinal bands (right) for different aircraft inventories: AEDT, AEM, AERO2K, REACT4C, QUANTIFY and TRADEOFF.

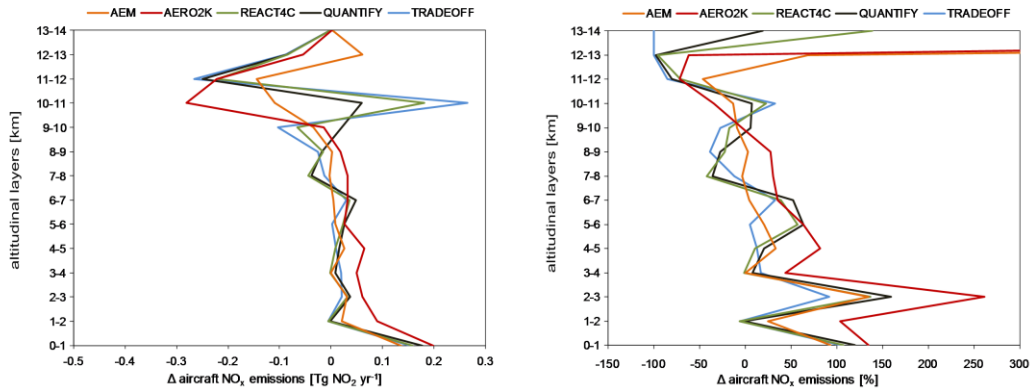

Figure 6.4: The vertical distributions of absolute (left) and relative (right) differences of normalized aircraft NO_x emissions; data from each scaled inventory is related to the scaled AEDT inventory.

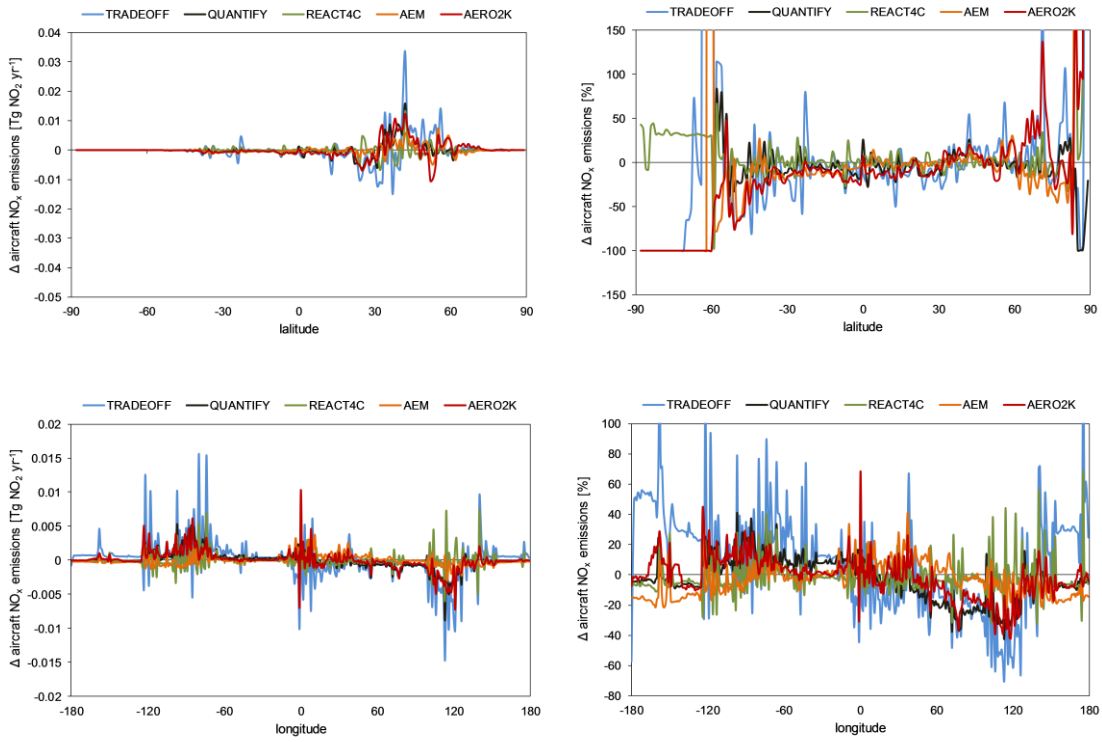

Figure 6.5: The latitudinal (upper row) and longitudinal (bottom row) distributions of absolute (left column) and relative (right column) differences of normalized aircraft NO_x emissions; data from each scaled inventory is related to the scaled AEDT inventory.

Despite the geographical distribution between AEDT and REACT4C is similar the differences exist in altitudinal domain. Thus, the region where most of the aircraft NO_x emissions are injected is divided into single vertical layers in order to estimate where the differences exist. Figure 6.6 shows that the REACT4C's main North Atlantic flight corridor, as well as emissions over Europe and United States, is concentrated

at 227 hPa. The AEDT's North Atlantic flights are one layer higher at 201 hPa. Different situation is distinguished for AERO2K's emissions, where the main concentration of European and North Atlantic flights is two layers lower than AEDT's emissions, at 254 hPa (Figure 6.7). AEDT has also more aircraft NO_x emissions over East Asia at 201 hPa than REACT4C and AERO2K. While REACT4C has these emissions at 254–283 hPa, the AERO2K data has observed deficiency of NO_x emissions over East Asia in all investigated vertical layers.

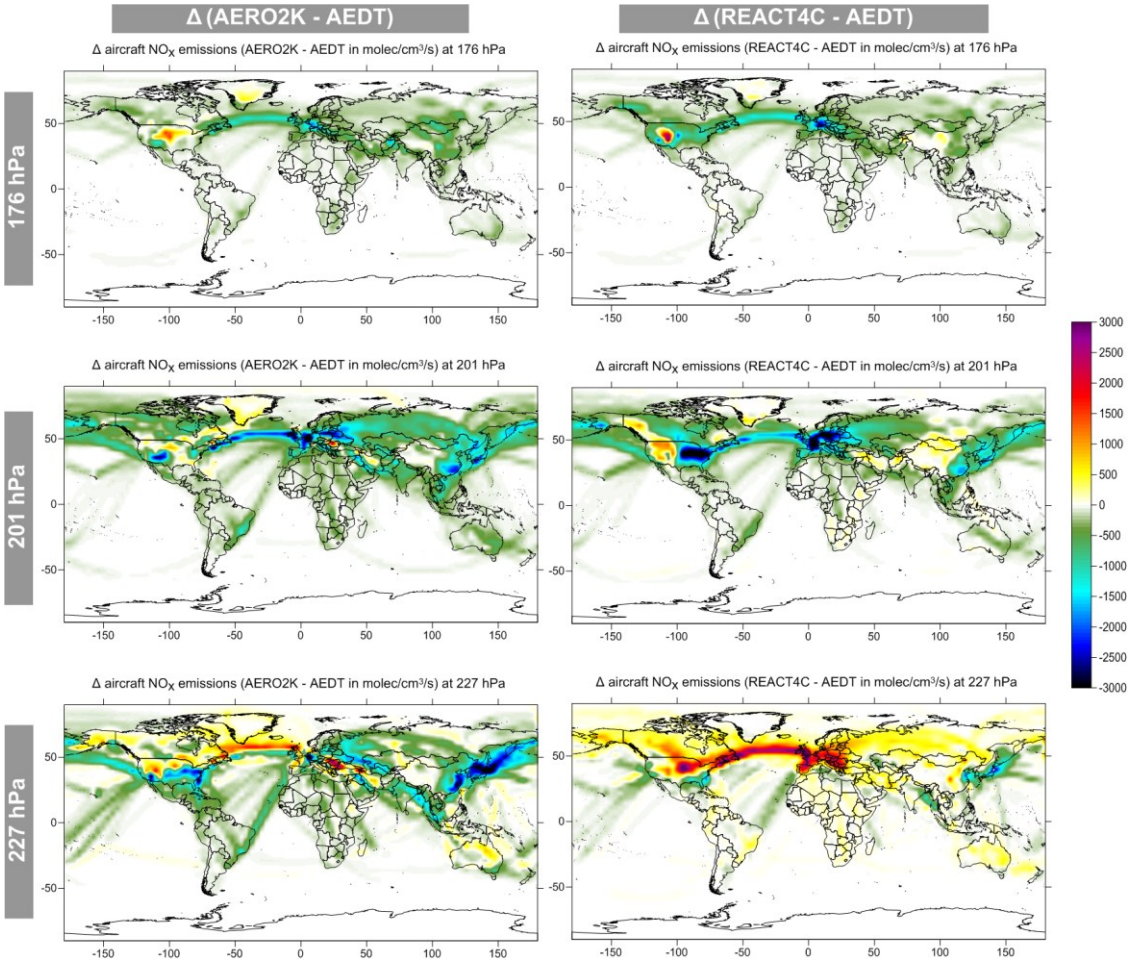

Figure 6.6: The differences (in molec/cm^3/s) in annual distributions of aircraft NO_x emissions at 176 hPa (upper row), 201 hPa (middle row), 227 hPa (bottom row) between AEDT and AERO2K (left column), REACT4C (right column) normalized inventories.

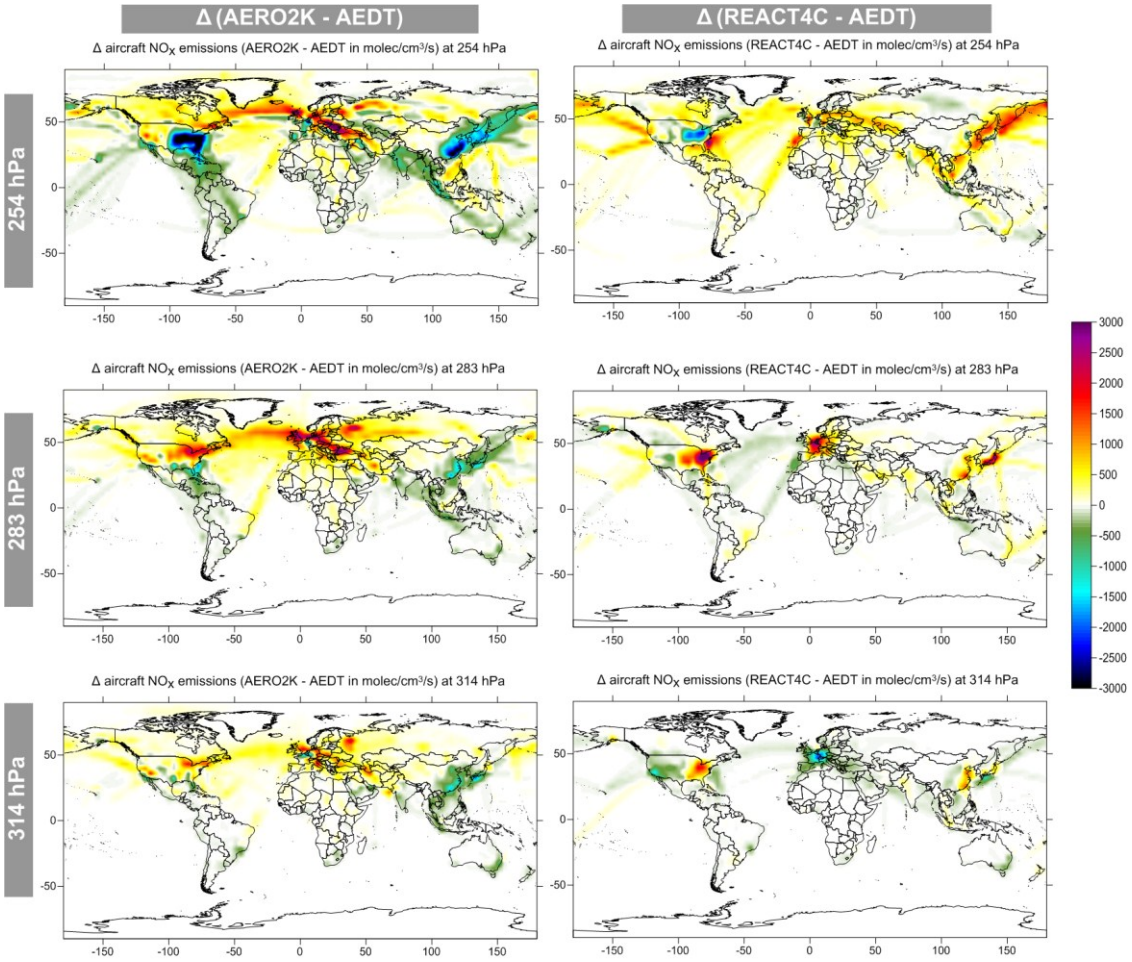

Figure 6.7: The differences (in molec/cm^3/s) in annual distributions of aircraft NO_x emissions at 254 hPa (upper row), 283 hPa (middle row), 314 hPa (bottom row) between AEDT and AERO2K (left column), REACT4C (right column) normalized inventories.

The original aircraft emission data have a regular vertical gridding (500ft, 610m or 1km), which are then interpolated by MOZART-3 to its irregular (with hybrid sigma layers every ~1 km in UTLS region) vertical spacing (Figure 3.3 in Chapter 3). Figure 6.8 shows the vertical distribution of aircraft NO_x emissions in MOZART-3 for the six normalized aircraft inventories. Each dataset represents the equal global total of aircraft NO_x (2.33 Tg (NO_2) yr^{-1}). The initial resolution of dataset plays an important role when it is redistributed into the lowest CTM's vertical layers. Since the vertical resolution in MOZART-3 near surface is high (~45 m), the datasets with higher resolution (AEM and AERO2K) have more aircraft NO_x emissions near ground (1000–950 hPa).

In MOZART-3 the most of aircraft NO_x emissions are injected in the 283–200 hPa region, where the emissions differ by 23% when the greatest (TRADEOFF) and

the smallest (AERO2K) numbers are considered. The peak of aircraft NO_x emissions is found to be at 227 hPa, with the greatest values occurring for REACT4C and TRADEOFF. AEDT and AEM have more emissions at 200 hPa and over, than other inventories, which gives the possibility of more efficient accumulation of N molecules (Seinfeld and Pandis, 2006).

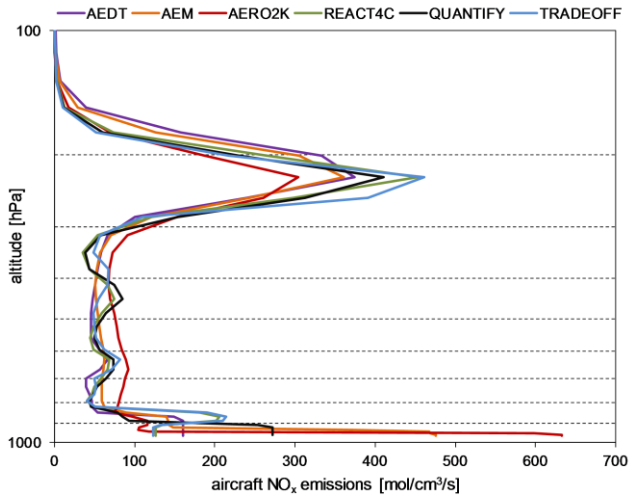

Figure 6.8: The globally and annually averaged vertical distribution of aircraft NO_x emissions redistributed into MOZART-3 vertical layers for six aircraft inventories: AEDT, AEM, AERO2K, REACT4C, QUANTIFY and TRADEOFF. The NO_x emissions are scaled to the same global total, which is 2.33 Tg(NO_2)/yr.

6.3.2 Chemical perturbation

Aviation NO_x emissions affects the NO_x–O_3–CH_4 system; its response presents Figure 6.9. The enhancements of NO_x and O_3 are calculated due to aircraft NO_x emissions, concentrated mainly at ~300–180 hPa, where most of the aviation emissions are injected. The positive peak of NO_x perturbation is observed at 227 hPa for all inventories; only AEDT and AEM have their maximum one level higher, at 201 hPa. This suggests that NO_x emissions at higher altitudes have a greater potential in perturbing NO_x fields, which indeed is confirmed by additional (as described in Chapter 6.2.3) experiments (Figure 6.10). The greatest NO_x perturbation is observed for AEDT and the smallest for AERO2K, which consequently affects the O_3 response, which follows similar pattern of differences between datasets. The peak of O_3 response is found to be at 227 hPa level for all inventories, with AEDT and AERO2K having the most different magnitudes. The enhanced O_3 changes the oxidizing capacity of the

troposphere; the OH/HO_2 ratio is perturbed: OH increases and HO_2 decreases. The positive OH response is observed through all tropospheric domain, the negative HO_2 response appears mainly at flight altitudes. While the impact of AERO2K inventory on NO_x and O_3 in UTLS region is relatively small, it is responsible for greater aircraft OH perturbation in mid-altitudes and consequently CO and CH_4 changes, than other datasets. The more efficient CO oxidation results in a greater AERO2K's HO_2 perturbation in mid-altitudes, than of other inventories.

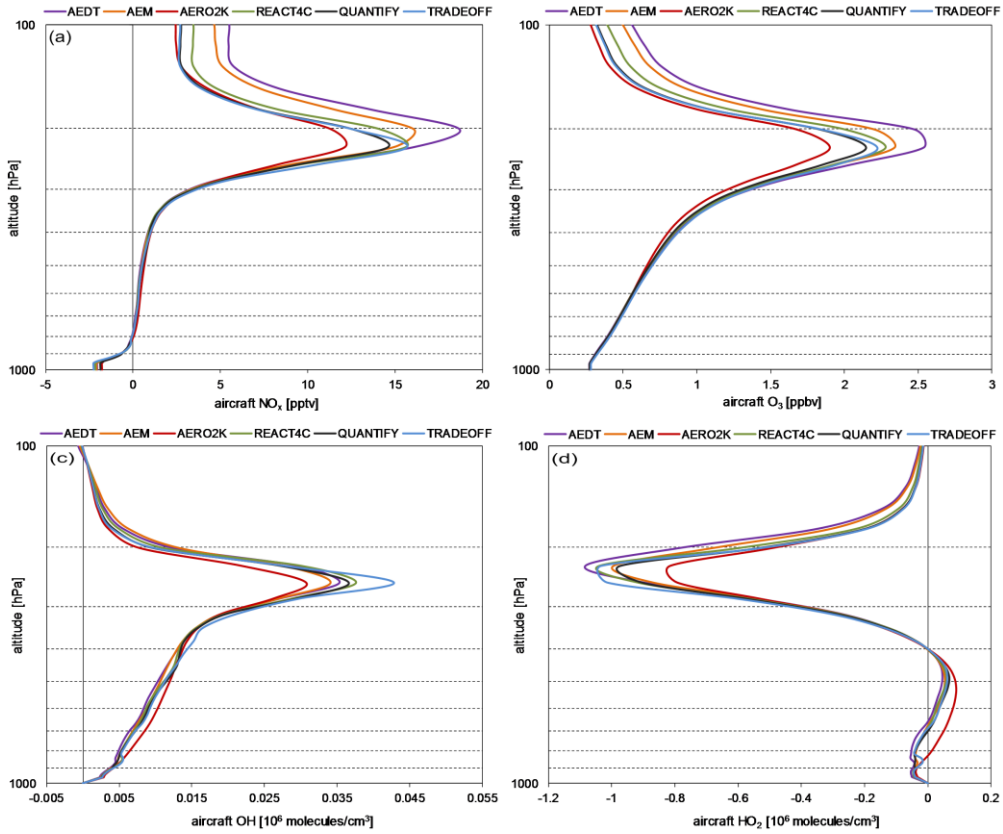

Figure 6.9: The globally and annually averaged vertical distributions of aircraft perturbations of NO_x (a), O_3 (b), OH (c) and HO_2 (d) concentrations for a six normalized aircraft inventories.

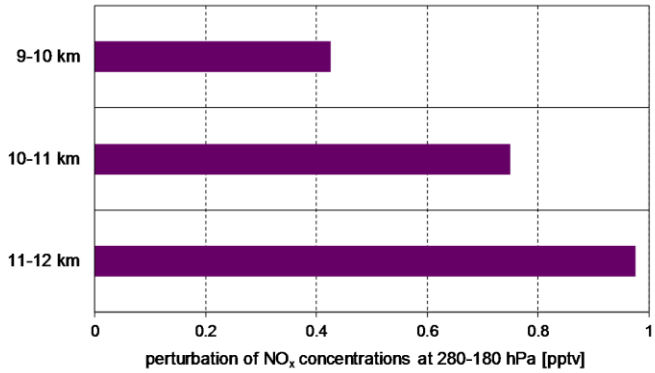

Figure 6.10: The perturbation of NO_x concentrations at 280–180 hPa (in pptv) due to 0.035 Tg(N)/yr incremental aircraft NO_x emissions in three altitudinal regions.

The spread in magnitudes of aircraft perturbations of NO_x and O_3 at 227 hPa for a series of aircraft inventories reveals regional patterns (Figure 6.11). The largest spread in aircraft NO_x perturbation is observed over Europe, North Atlantic, western and central areas of Asia and eastern coast of Asia. The largest differences in perturbed O_3 are concentrated uniformly in high northern latitudes.

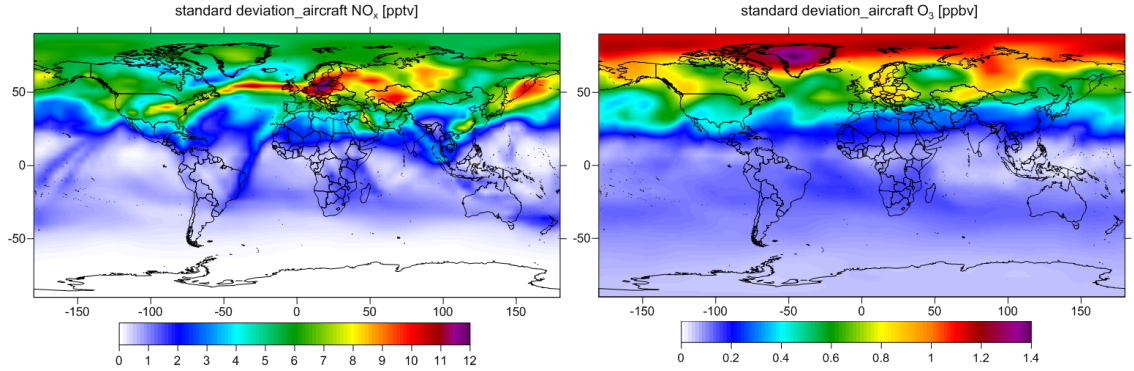

Figure 6.11: Standard deviation in annually averaged perturbations of NO_x (left) and O_3 (right) at 227 hPa for a series of aircraft inventories.

The same amount of emitted NO_x, but varying vertical distributions of NO_x emissions lead to significant differences in short-term O_3 response between inventories. Table 6.2 gives global and annual means of O_3 burden change and O_3 production efficiency values for six different inventories. The greatest burden change is observed for AEDT (5.6 Tg) and AEM (5.4 Tg) and the smallest for AERO2K (4.7 Tg). Also, QUANTIFY shows a relatively weaker O_3 response (5.0 Tg) compared with the other FAST inventories REACT4C and TRADEOFF (5.3 Tg and 5.2 Tg, respectively).

Table 6.2: The global and annual mean O_3 burden change (in Tg) and O_3 production efficiency (OPE; the number of O_3 molecules produced per emitted NO_x molecule) for a series of normalized aircraft inventories.

INVENTORY	O_3 Tg	OPE
AEDT	5.6	30.1
AEM	5.4	29.1
AERO2K	4.7	25.4
REACT4C	5.3	28.2
QUANTIFY	5.0	27.0
TRADEOFF	5.2	27.7

It has been shown that the O_3 production in the troposphere is sensitive to the height of the initial precursor emissions (Köhler et al., 2008). This is indirectly observed in these results, where more molecules of ozone are produced per molecule of N for inventories with greater amounts of NO_x emissions at higher altitudes, it being 30 for AEDT, 29 for AEM, 28 for REACT4C, 27 for QUANTIFY and TRADEOFF and 25 for AERO2K (Table 6.2). This shows that a lower potential, by 15%, is represented by AERO2K inventory compared to AEDT dataset in terms of ozone production, which is consistent with the spread of O_3 burden change.

The methane lifetime due to destruction by OH in a reference case was calculated as 8.88 years. In contrast to the O_3 responses, the CH_4 lifetime reductions are found to be quite uniform among different inventories (Table 6.3) ranging from -0.074 years for AERO2K and TRADEOFF, -0.073 years for REACT4C to -0.07 years for AEDT.

Table 6.3: CH_4 lifetime (in year) due to destruction by OH (between the surface and 1hPa) and the CH_4 lifetime change (in year) due to the aircraft NO_x emissions for a series of normalized aircraft inventories.

INVENTORY	CH_4 lifetime (year)	CH_4 lifetime change (year)
Reference run	8.882	
AEDT	8.813	-0.070
AEM	8.811	-0.071
AERO2K	8.808	-0.074
REACT4C	8.810	-0.073
QUANTIFY	8.809	-0.073
TRADEOFF	8.808	-0.074

6.3.3 Radiative forcing and global warming potential for aviation NO_x

The latitudinal distributions of short-term O_3 RF for the six normalized inventories are shown in Figure 6.12. The patterns of each inventories are consistent and they mimic the zonal-mean distributions of NO_x emissions (Figure 6.2) (as both are rather short-lived), with dominating role of short-term O_3 RF over Northern Hemisphere. There is relative agreement in the resultant short-term O_3 RF between inventories at high southern and northern latitudes; the tropical region (30°S–40°N) shows discrepancies (Figure 6.11). The largest spread in the short-term O_3 RF between

inventories are found to be over northern tropical belt (15–30°N), where locally the standard deviation reaches 3.0–3.5 mWm^{-2}, over Middle East, Pacific and North Africa. The AERO2K shows the greatest underestimations of short-term O_3 RFs among the investigated inventories (Figure 6.13).

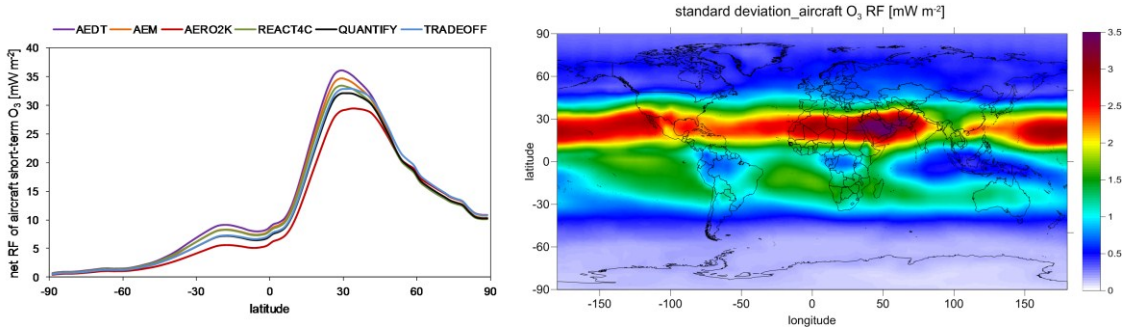

Figure 6.12: The zonal and annual mean radiative forcing ($mW\ m^{-2}$) from short-term O_3 (left) and the standard deviation in net radiative forcing from short-term O_3 (right) for a series of normalized aircraft inventories.

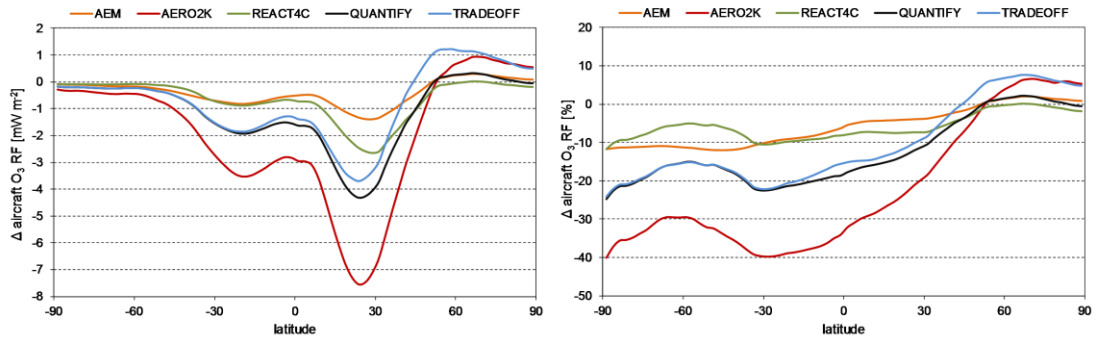

Figure 6.13: The zonal and annual means of the absolute (left) and the relative differences (right) in net radiative forcing from short-term O_3 between normalized AEDT and the rest of normalized inventories.

Table 6.4 presents the global and annual mean RF (mWm^{-2}) for short-term O_3, CH_4-induced O_3, CH_4, and stratospheric water vapour from aircraft NO_x perturbation for a series of normalized inventories. The spread of short-term O_3 values is of 2.8 mWm^{-2}, with AEDT and AERO2K resulting in highest and lowest numbers (the standard deviation is 1.0 mWm^{-2}, when all investigated inventories are considered). The CH_4 responses are much more consistent, the numbers differ by 0.4 mWm^{-2} and standard deviation is 0.2 mWm^{-2} (with values ranging from -7.1 mWm^{-2} for AERO2K and TRADEOFF and -6.7 mWm^{-2} for AEDT). The net aircraft NO_x RF values ranges from 3.6 mWm^{-2} for AEDT, 3.0 mWm^{-2} for AEM, 2.3 mWm^{-2} for REACT4C to 0.2 mWm^{-2} for AERO2K and the standard deviation constitute 1.2 mWm^{-2}.

Table 6.4: Radiative forcings (in mW m^{-2}) due to short-term O_3, CH_4-induced O_3, CH_4, stratospheric water vapour (SWV) and net NO_x (net of all 4 components) for six normalized aircraft inventories. The radiative forcings per unit emission of aircraft N (in mW m^{-2}/Tg(N) yr^{-1}) are presented in the brackets.

INVENTORY	Radiative forcings from aircraft NO_x emissions				
	Short-term O_3	CH_4-induced O_3	CH_4	SWV	Net NO_x
AEDT	14.3 (20.5)	-3.0 (-4.3)	-6.7 (-9.5)	-1.0 (-1.4)	3.6 (5.2)
AEM	13.8 (19.7)	-3.0 (-4.2)	-6.8 (-9.7)	-1.0 (-1.5)	3.0 (4.2)
AERO2K	11.5 (16.5)	-3.1 (-4.5)	-7.1 (-10.4)	-1.1 (-1.5)	0.2 (0.3)
REACT4C	13.4 (19.2)	-3.1 (-4.4)	-7.0 (-10.0)	-1.1 (-1.5)	2.3 (3.3)
QUANTIFY	12.8 (18.3)	-3.1 (-4.4)	-7.0 (-10.0)	-1.1 (-1.5)	1.7 (2.4)
TRADEOFF	13.1 (18.7)	-3.1 (-4.5)	-7.1 (-10.2)	-1.1 (-1.5)	1.8 (2.6)

Myhre et al. (2011) presented GWP values for aviation NO_x emissions using the same aircraft emissions, the same experimental design and a range of five models. The differences in their results constitute a good insight into uncertainties arising from usage of different global chemistry models. In contrast, the spread in results, which are presented here, gives range of differences that arise from usage of different aircraft inventories.

The resulting GWP values for three time horizons (20, 100 and 500 years) are presented in Table 6.5. The numbers show significant differences, which are enhanced with larger time horizons; however, the sign of calculated responses shows a consistently net positive value. The greatest differences come from the AEDT and AERO2K inventories, being 57%, 93%, 93% different for 20, 100, 500 time horizons, respectively. The increase of discrepancy with larger time horizons might be expounded by CH_4, as its response 'remains' for a few decades after NO_x emission.

The GWP decrease between a 20 year time horizon and a 100 year horizon is larger for inventories where the CH_4 lifetime reduction is more enhanced; it is 82% for AEDT, 83% for AEM, 85% for REACT4C, 87% for QUANTIFY and TRADEOFF, 97% for AERO2K. The 100 vs 500 year time horizons discrepancies are constant, 70%, for all inventories. Due to relatively short lifetimes of the net NO_x components the GWP (H=500) differs between inventory data only by the CO_2 integral in the denominator.

Table 6.5: Global Warming Potentials (GWP) for aircraft NO_x emissions for a series of normalized aircraft inventories for 20, 100 and 500 time horizon (sO_3 = short-term O_3, lO_3 = CH_4-induced O_3, CH_4 = CH_4 + SWV, net NO_x = sO_3 + lO_3 + CH_4). All values are given on a per kg N basis and are relative to CO_2.

INVENTORY	GWP(20)				GWP(100)				GWP(500)			
	sO_3	lO_3	CH_4	NO_x	sO_3	lO_3	CH_4	NO_x	sO_3	lO_3	CH_4	NO_x
AEDT	828	-140	-356	332	235	-50	-126	60	72	-15	-38	18
AEM	796	-137	-364	295	226	-49	-129	49	69	-15	-39	15
AERO2K	666	-146	-379	142	189	-52	-134	4	58	-16	-41	1
REACT4C	777	-143	-372	262	221	-51	-132	39	67	-15	-40	12
QUANTIFY	740	-143	-372	225	210	-51	-132	28	64	-15	-40	8
TRADEOFF	759	-146	-380	233	216	-52	-134	30	66	-16	-41	9

6.4 Discussion

Figure 6.15 shows the vertical profiles of the relative difference of NO_x, O_3 and OH responses to aircraft NO_x emissions to that of the AEDT inventory (chosen simply as it gives the largest overall response). The aircraft NO_x perturbation at 227 hPa is about 25% greater for AEDT than that for AERO2K. The difference rises with higher altitudes and constitutes 55% at 100 hPa. On the contrary, AERO2K's NO_x response significantly exceeds that of AEDT (and any other inventory) at mid altitudes, where the difference reaches 500% at 762 hPa. The response of the O_3 for these discrepancies is not comparable. It is found that AERO2K's O_3 response indeed dominates in the low-troposphere region (1000–600 hPa) but only by about 4%, whereas AEDT's prevalence at cruise altitudes reaches 25% and 50% at 100 hPa. The same pattern is observed for all inventories, just the scale of differences is smaller. The linear relation between additional NO_x and O_3 response is observed in the UTLS region, being the strongest at 227 hPa and becoming weaker at higher altitudes. The ratio of O_3 to NO_x for AERO2K's results is 1 at 227 hPa and 0.9 at 100 hPa (e.g. for AEM it is 1 at 227 hPa and 0.7 at 100 hPa, for REACT4C it is 1.5 at 227 hPa and 0.8 at 100 hPa).

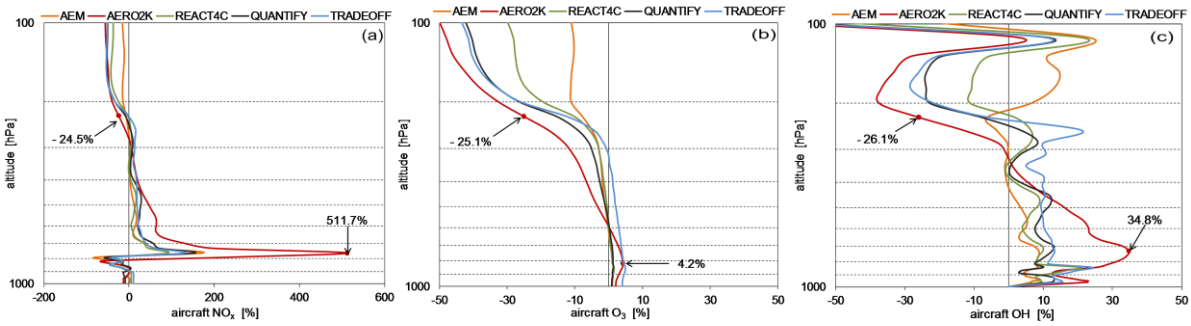

Figure 6.15: The globally and annually averaged vertical distributions of relative differences (in %) in aircraft perturbations of NO_x (a), O_3 (b) and OH (c) concentrations for a normalized aircraft inventories; results from each inventory were related to the results from AEDT.

Interestingly, the greatest O_3 aircraft perturbation did not introduce the largest CH_4 reduction, as might be expected from the chemistry. The vertical distribution of emissions might hide the explanation: a significant fraction of AERO2K's NO_x emissions occurs in the mid-troposphere. The ~4% domination of AERO2K's O_3 in 900–700 hPa region significantly modifies the oxidizing capacity of the low troposphere (there is more OH by about 30% than for AEDT, Figure 6.14). Annual mean concentrations of OH and CH_4 and temperature are greater at lower altitudes, which catalyse processes of OH production and CH_4 destruction.

Another consequence of AERO2K's enhancement of O_3 concentrations at lower altitudes is that this O_3 is not as radiatively efficient as O_3 at higher altitudes (Lacis et al., 1990, Köhler et al., 2008). Hence, despite the spread between O_3 burden of the two most differing inventories is 15%, the discrepancy of short-term O_3 RF reaches 20%.

It is worth to note, that not only the height is important, also the geographical distribution of aircraft NO_x emissions plays a certain role in terms of O_3 RF response. The NO_x emissions from low latitudes have a larger impact on climate forcings than the NO_x emissions from high latitudes (e.g., Fuglestvedt et al., 1999, Berntsen et al., 2005, Köhler et al., 2012). The AERO2K dataset has less, compared to other inventories, NO_x emissions at cruise altitudes over East Asia (Figure 6.6, 6.7), which was also noted by Olsen et al. (2013). However, what are the extents of influences of potentials hidden in geographical and altitudinal regions in terms of O_3 production?

The O_3 response differs from region to region, being the most pronounced at cruise altitudes, especially at 11–12 km and 10–11 km (Figure 6.16). The efficiency of O_3 production at 11–12 km exceeds the low latitude efficiency by 36%, the mid-latitude by 45% for North America and 51% for Europe and the lower flight altitudes efficiency, 10–11 km and 9–10 km, by 14% and 22%, respectively. The background conditions and the intensity of solar irradiance influence both, O_3 and CH_4 responses. The ratio of the CH_4 lifetime change to the O_3 burden change is specific for each region (Figure 6.17). The least efficient CH_4 loss occurs in altitudinal regions, 10–11 km and 11–12 km. The greatest efficiency in CH_4 lifetime reduction is observed in Southeast Asia. Interestingly the CH_4 loss efficiency changes significantly at 9–10 km compared to higher altitudinal layers.

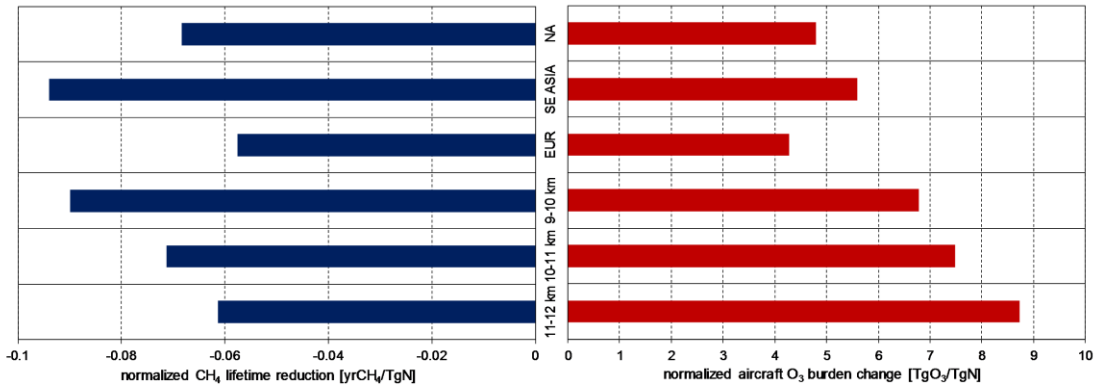

Figure 6.16: The normalized O_3 burden change (red bars) and CH_4 lifetime reduction (blue bars) due to 0.035 Tg(N)/yr incremental aircraft NO_x emissions in six regions.

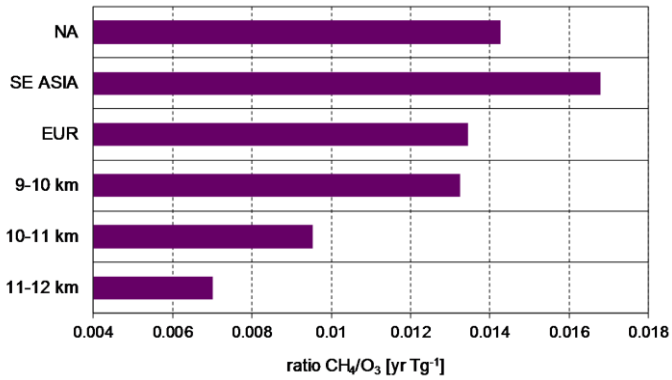

Figure 6.17: The absolute ratio of the CH_4 lifetime change to the O_3 burden change due to 0.035 Tg(N)/yr incremental aircraft NO_x emissions for six regions.

All these aspects reduce the potential of AERO2K in terms of its impact on tropospheric O_3 and its overall aircraft net NO_x RF response compared with other aircraft inventories. The AERO2K's ratio of the CH_4 lifetime change to the O_3 burden change is significantly greater than of other inventories (Figure 6.18).

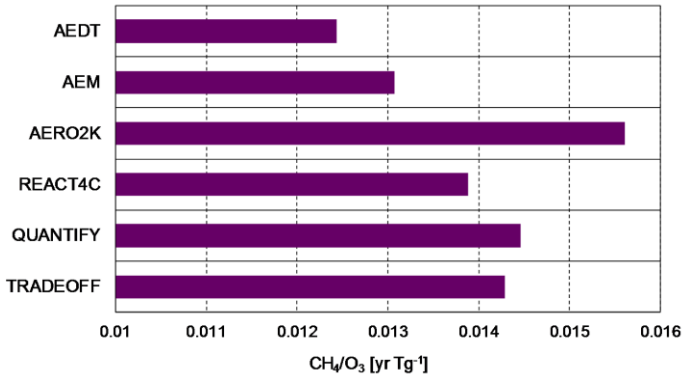

Figure 6.18: The absolute ratio of the CH_4 lifetime change to the O_3 burden change due to aircraft NO_x emissions for a series of normalized aircraft inventories.

6.5 Summary

Figure 6.19 presents a short-term O_3 RF and net NO_x RF responses normalized to 1 Tg of emitted aircraft N reported for a number of model simulations (Stordal et al. 2006, Hoor et al., 2009, Myhre et al., 2011, Hodnebrog et al., 2011, 2012). The above studies give an inter-model mean O_3 and NO_x RF values equal 22.2 and 5.0 mW m^{-2}/Tg(N) yr^{-1}, respectively. Most of the modelled short-term O_3 responses are placed within a one standard deviation range. On the contrary, the net NO_x RF values constitute a more diverse picture. This can be revealed by the inter-study differences in the components taken into account for net NO_x calculation. Myhre et al. (2011) highlighted that the ratio of the CH_4 lifetime change to the O_3 column change is very specific for each model, which also influence the net NO_x numbers. The results given by MOZART-3 are in good agreement with other modelling studies.

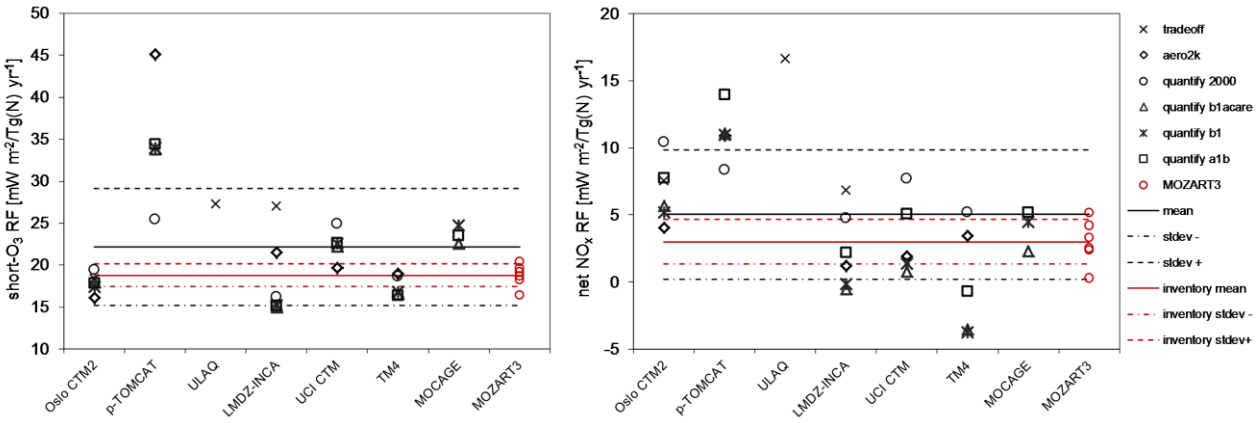

Figure 6.19: Global and annual radiative forcings from a short-term O_3 (left) and net NO_x (right) per unit emission of aircraft N (mW m^{-2}/Tg N yr^{-1}) as reported in literature (black font) and as a result of this study (red font). Each point represents a specific model study, solid lines denote the mean value, dashed lines show the one standard deviation range of results. The components included in 'net NO_x' values differ from study to study, as explained in the text.

The difference in RF values (20% for O_3 RF and 94% for net NO_x RF) between six aircraft inventories is of a smaller magnitude to that of uncertainties between models; however, it is still meaningful. Myhre et al. (2011) reported a 36% spread in O_3 RF values and 54% in net NO_x RF numbers between a set of five different models (note that Myhre et al. (2011) account for the time-history emissions (Grewe and Stenke, 2008) in their long term effects). Hoor et al. (2009) presented a 64% spread in O_3 RF and 89% in net NO_x (net is without SWV) values between five different models and Stordal et al. (2006) reported a 33% spread in O_3 RF and 59% in net NO_x RF (net is a sum of short-term O_3 and CH_4) numbers between three different models. This places the disparities between different inventories on the same scale of importance as inter-model differences.

Overall, the AERO2K inventory is significantly distinct from other inventories in terms of its impact on O_3 and net aviation NO_x. The spread between aircraft NO_x estimates emerging from usage of different aircraft inventories constitutes a significant range of uncertainty. An attention should be paid to formulating aircraft emission inventories where precise cruise altitudes are defined.

Chapter 7

New developments in global warming potentials for aviation NO_x emissions

7.1 Introduction

There are significant difficulties related to the inclusion of the effects from chemically active short-lived substances (e.g., ozone precursors or aerosols) into the Global Warming Potential (GWP) concept, which was initially designed for long-lived greenhouse gases. The substantial uncertainties associated with estimates of the climate impacts for these species and limited understanding of indirect effects makes the usage of GWP scientifically contentious (e.g., Isaksen et al., 2009). GWPs for NO_x emissions are described by Fuglestvedt et al. (2003) as one of the most "challenging and controversial".

Generally, the NO_x GWP metric value comprises the short-term O_3 effect, long-term CH_4 response and long-term CH_4 effect on O_3. Further indirect NO_x effects also occur, like nitrate formation, or CH_4 effect on stratospheric H_2O (the latter has usually been taken into account recently, in addition to the three 'default' components mentioned above, e.g., Myhre et al., 2011, Fry et al., 2012, Köhler et al., 2012). The short-term O_3 response is always positive; the CH_4 and CH_4-induced O_3 responses are always negative. However, the net effect is not always so clear in terms of magnitude, or even a sign.

The net NO_x value depends on the counterbalancing effects, which represent different temporal behaviours. Additionally, the climate forcings resulting from NO_x emission significantly depend on the location of emissions. Shine et al. (2005a) highlighted two dimensions of challenges related with defining a robust metric value for climate impact of NO_x emissions: metric design and differences among the models. The inclusion of non-linear and heterogeneous NO_x–O_3–CH_4 system into a concept leaning on global mean input, results in a substantial divergence in the calculated values available in the literature.

GWPs for aviation NO_x, based on a pulse emission, have been derived in a very limited number of evaluations. IPCC AR4 (Forster et al., 2007) identified only three studies: Wild et al. (2001), Derwent et al. (2001) and Stevenson et al. (2004), which yielded the GWP_{100} values of 130, 100 and -3, respectively. These GWPs have lately been re-evaluated by Fuglestvedt et al. (2010), yielding values of 71 and -2.1 (for Wild et al., 2001 and Stevenson et al., 2004, respectively). Recently Köhler et al. (2012) calculated aircraft NO_x GWP_{100} of 75, whilst Myhre et al. (2011) and Skowron et al. (2013) provided ranges of aircraft NO_x GWP_{100} varying from 67 to -21 and from 60 to 4, respectively.

It has been shown that the uncertainties in estimations in GWP from aviation NO_x might arise from different tropospheric NO_x background conditions (e.g., Holmes et al., 2011), model-specific CH_4 per O_3 response (Myhre et al., 2011), or usage of different aircraft inventories (Skowron et al., 2013).

These disparate, and relatively few estimates, of aircraft NO_x GWP are the inspiration of this study. In this chapter, the impact of different aircraft NO_x emission rates on NO_x–O_3–CH_4 system and its implication on aircraft NO_x GWP value are investigated.

7.2 Methodology

7.2.1 Incremental aircraft NO_x emissions

The incremental aircraft NO_x emissions were applied globally for a period of a year, having aircraft NO_x rates ranging from 0.007 to 9.3 Tg(N) yr^{-1}. The reference run for the incremental experiments constitute actual aircraft NO_x emissions for the year 2006, 0.71 Tg(N) yr^{-1}. These CTM simulations in conjunction with further calculations of the temporal evolution of aircraft perturbations following the additional aircraft NO_x injections (as described in Chapters 3.2.3 and 4.6) give a possibility of creating experiments analogous to pulses[1] (Figure 7.1) and are consistent with the 'transient' approach defined by Fuglestvedt et al. (2010).

Additionally, the corresponding aircraft NO_x emission rates (0.717–10 Tg(N) yr^{-1}) were employed for steady-state experiments where the reference run constitutes a background without aircraft emissions. These CTM simulations and further calculations of temporal evolution of aircraft perturbations are consistent with 'steady-state' approach defined by Fuglestvedt et al. (2010). The results of which will be employed and discussed later in this chapter.

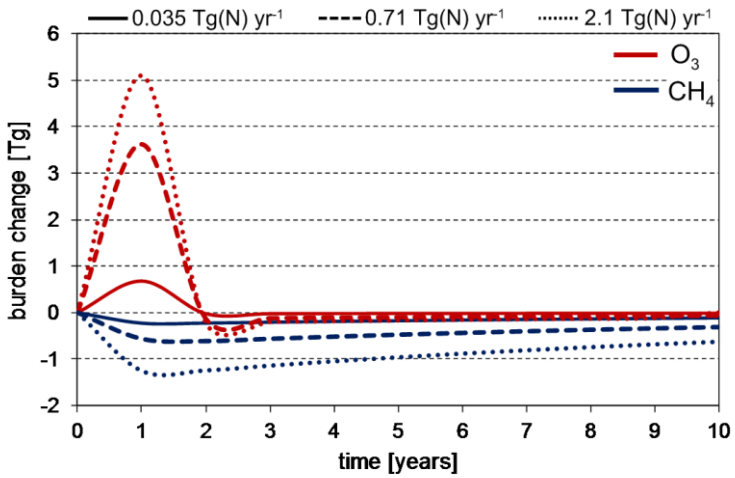

Figure 7.1: Temporal evolution of changes in the global burdens of O_3 (red) and CH_4 (blue) for different incremental aircraft NO_x emission rates: 0.035 Tg(N) yr^{-1} (solid line), 0.71 Tg(N) yr^{-1} (dashed line), 2.1 Tg(N) yr^{-1} (dotted line).

[1] Similarities: injection of additional aircraft NO_x emissions over the existing background aircraft emission; Distinctions: mathematical calculation, not modelled observation, of temporal behaviour of perturbations following additional aircraft NO_x emissions.
The justification of applied method is presented in Chapter 4.6.

7.2.1 Experimental design

The REACT4C inventory base case for 2006, and a series of globally-scaled datasets, were implemented into the 3D CTM, MOZART-3. Thirteen pulse-like experiments were performed, one reference (base aircraft emission) run and twelve perturbation (incremental aircraft emission) simulations, each starting in January 2006 and finishing in December 2006; each simulation was preceded by a multi-year spin-up, 2000–2005. The aircraft perturbation is derived by extracting the difference between 'incremental aircraft' and 'aircraft' experiments. Also thirteen steady-state experiments were performed, one reference (without aircraft emission) run and twelve perturbation (aircraft emission) simulations, each starting in January 2006 and finishing in December 2006; each simulation was preceded by a one-year spin-up, 2005. The aircraft perturbation is derived by extracting the difference between 'aircraft' and 'no aircraft' experiments.

The details regarding model set-up, aircraft emission dataset, surface emissions and dynamical data applied for this study are described in Chapter 3.3. The description of radiative forcings and global warming potential calculation is presented in Chapter 3.2.

7.3 Results

7.3.1 The non-linearity of NO_x–O_3–CH_4 system

The NO_x background concentrations (~50–200 pptv) in UTLS region are ideal for O_3 production, which increases almost linearly with additional NO_x (Figure 2.1). The linear relation between additional NO_x and O_3 was shown previously (e.g., Isaksen et al., 1999, Köhler et al., 2008), with some evidence of the decline of O_3 production with larger aircraft NO_x emissions (Rogers et al., 2002). Here, the successive additions, increasing in size, of different aircraft NO_x rates, reveal a dual nature of aircraft O_3 responses (Figure 7.2). Different incremental aircraft NO_x emissions yield different results, with O_3 saturating at higher NO_x emission rates. Overall, Figure 7.2 shows a strong non-linear O_3 response to aircraft NO_x perturbations observed on a global scale.

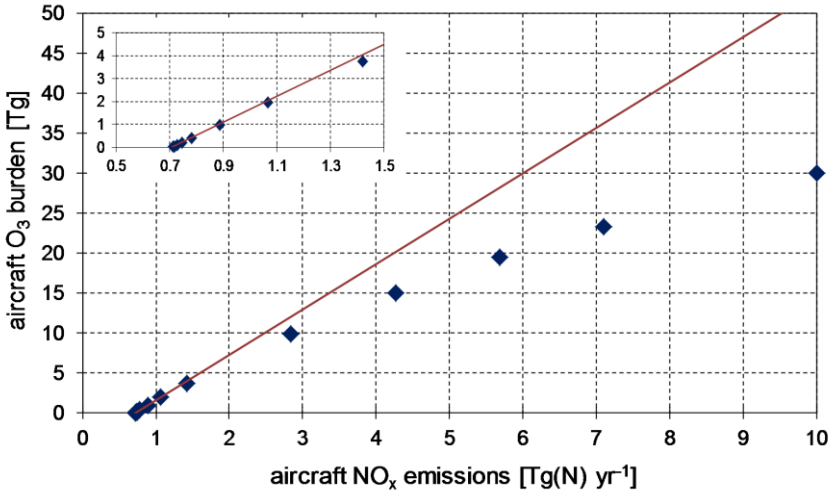

Figure 7.2: Scatter plots of aircraft O_3 burden change against series of aircraft NO_x emission rates (dots are individual experiments, line is a linear solution). The zoomed panel presents linear O_3 response due to small incremental aircrat NO_x perturbation.

The linear increase of O_3 burden with additional NO_x is observed for small incremental aircraft NO_x emission rates, up to ~1.42 Tg(N) yr^{-1} of total emitted NO_x, which is a 100% increase over the reference aircraft NO_x emission. The deviation from a linear solution varies with size of the incremental aircraft NO_x emission rate and is -7% for 0.71 Tg(N) yr^{-1}, -18% for 2.1 Tg(N) yr^{-1} and -36% for 6.4 Tg(N) yr^{-1} of additional NO_x injections. The CH_4 lifetime reduction also reveals the non-linear behaviour and with greater aircraft NO_x emission rates, a smaller CH_4 lifetime reduction is observed (Figure 7.3); however, it is less pronounced than for the O_3 burden changes shown in Figure 7.2. Again, the deviation from a linear solution varies with size of the incremental aircraft NO_x emission rate and constitutes 6% for 0.71 Tg(N) yr^{-1}, 13% for 2.1 Tg(N) yr^{-1} and 28% for 6.4 Tg(N) $yr^{-1}$of additional NO_x injections.

The ozone production efficiency (OPE, the number of O_3 molecules produced per emitted NO_x molecule) picture shows a significant saturation for emissions higher than 1.5 Tg(N) yr^{-1} (Figure 7.4). A relative decline of OPE occurs for emissions larger than 5.7 Tg(N) yr^{-1}. The same is found for CH_4 lifetime change per aircraft Tg(N) yr^{-1}; the CH_4 reduction increases with increasing aircraft NO_x emissions and follows OPE till around 100% increase of reference aircraft NO_x levels, which is ~1.5 Tg(N) yr^{-1}. Then the CH_4 lifetime reduction saturates at 1.9–3.7 Tg(N) yr^{-1} levels and starts to decline at aircraft NO_x rates greater than 5.7 Tg(N) yr^{-1}.

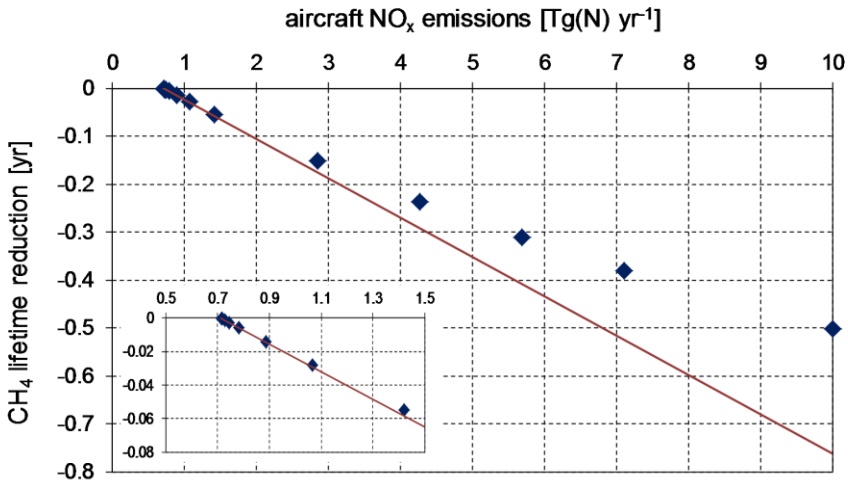

Figure 7.3: Scatter plot of aircraft CH_4 lifetime reduction against series of aircraft NO_x emission rates (dots are individual experiments, line is a linear solution). The zoomed panel presents linear CH_4 response due to small incremental aircrat NO_x emissions.

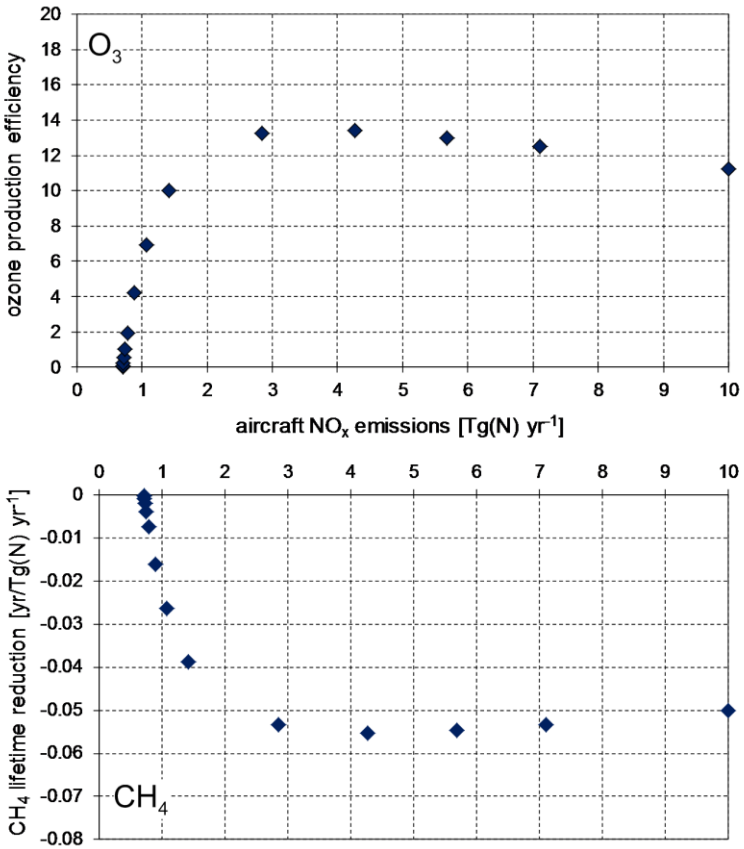

Figure 7.4: Scatter plots of aircraft O_3 production efficiency (upper) and normalized CH_4 lifetime reduction (bottom) against different sizes of aircraft NO_x emisison.

7.3.2 Variability of global warming potentials for aviation NO_x emissions

The aviation NO_x GWP values were derived for each incremental aircraft NO_x emission size for three time horizons, 20-, 100- and 500-years. With one model, a series of GWP numbers ranging from positive to negative is observed (Figure 7.5). The unique number for an aviation NO_x GWP does not exist, regardless of the time horizon taken into account and the net NO_x components.

The calculated values of GWPs for a 100-year time horizon (GWP_{100}) varies from 29, 22, 17 for 0.007, 0.07, 0.7 Tg(N) yr^{-1} of incremental aircraft NO_x emissions, respectively, to -1, -5 for 6.4, 7.1 Tg(N) yr^{-1} of additional aircraft NO_x, respectively. The aviation NO_x GWP_{20} values vary between 197 and 44 and for GWP_{500} ranges from 9 to -2. The difference in the reported numbers for net NO_x GWP_{20} reaches 78% and for net NO_x $GWP_{100,\ 500}$ the difference constitutes 115%. This significant diversity among net NO_x GWPs exists despite the observation that the discrepancies for single components are less pronounced: 44% for short-term O_3 GWP_{100}, 29% for CH_4-induced O_3 GWP_{100} and 33% for (CH_4+SWV) GWP_{100}.

The chemical components' lifetimes, which impact on the net NO_x effect are much shorter than the millennial scales of CO_2's persistence in the atmosphere. Thus, the aviation NO_x GWPs are declining rapidly in the first decades following the additional aircraft NO_x injection (Figure 7.6). The shape of the response (exponential decay with time) remains similar for each incremental NO_x emission size; however, the calculated numbers differ. The GWPs for aircraft NO_x rates not greater than 3.5 Tg(N) yr^{-1} remains positive for each time horizon. The GWPs for aircraft NO_x rates greater than 4.9 Tg(N)/yr of are positive for H=20, but for H=100 and H=500, either the value is 0, or the sign changes to negative. The difference in the calculated aircraft NO_x GWPs between 0.07 and 0.71 Tg(N) yr^{-1} NO_x rates is 15% for H=20 and it rises to 25% for H=100 and H=500. The disparity in GWPs between 0.71 and 6.4 Tg(N) yr^{-1} NO_x rates is 57% for H=20 and 105% for H=100, 500. For a small aircraft NO_x emission (and linear O_3 and CH_4 regime) the differences among reported GWP values stay in a reasonable range, but uncertainties increase substantially for greater incremental aircraft NO_x emission.

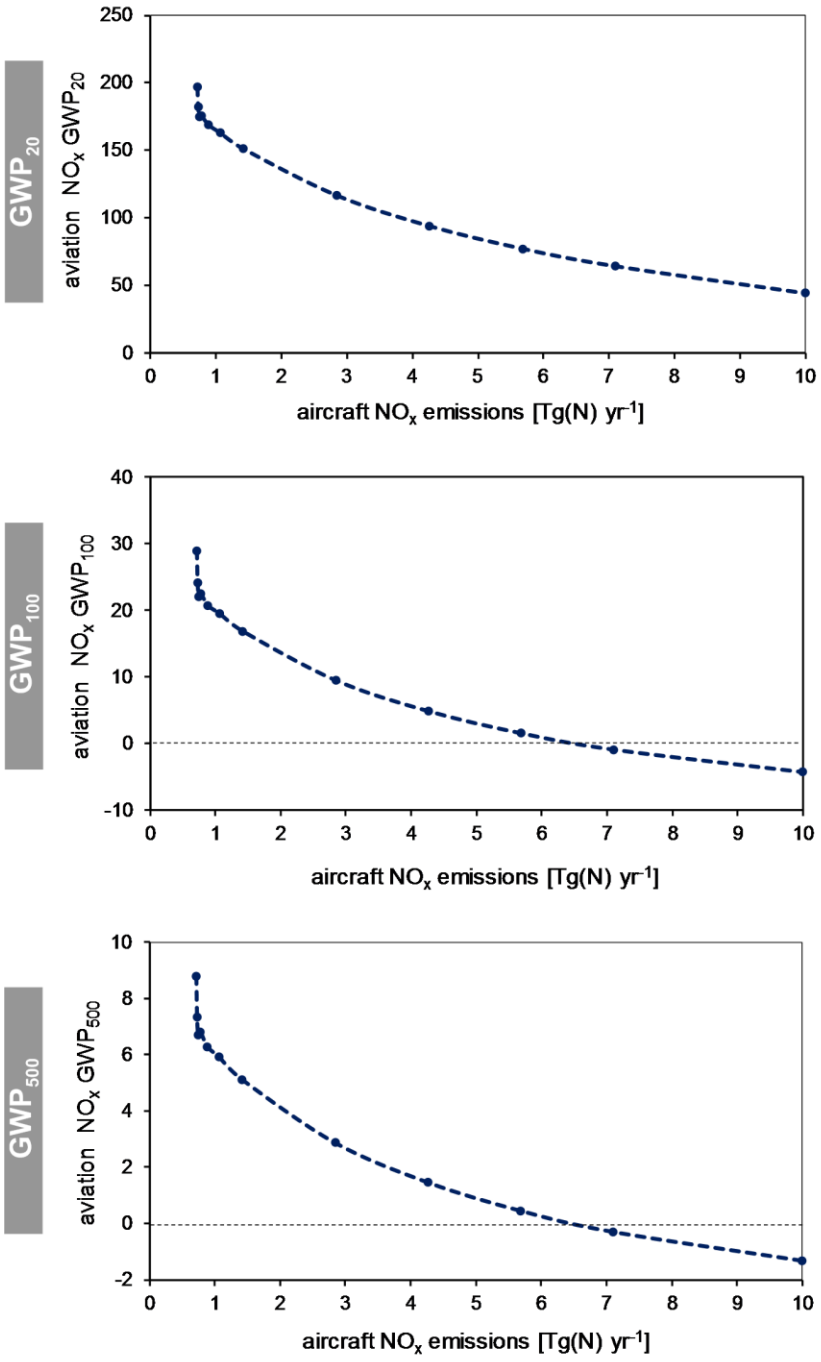

Figure 7.5: Calculated aviation net NO_x GWPs for a 20-, 100- and 500-year time horizons as a function of different global aircraft NO_x emission rates. Net NO_x=short-term O_3+ CH_4-induced O_3+CH_4+SWV. All values are on a per kg N bases and are relative to CO_2.

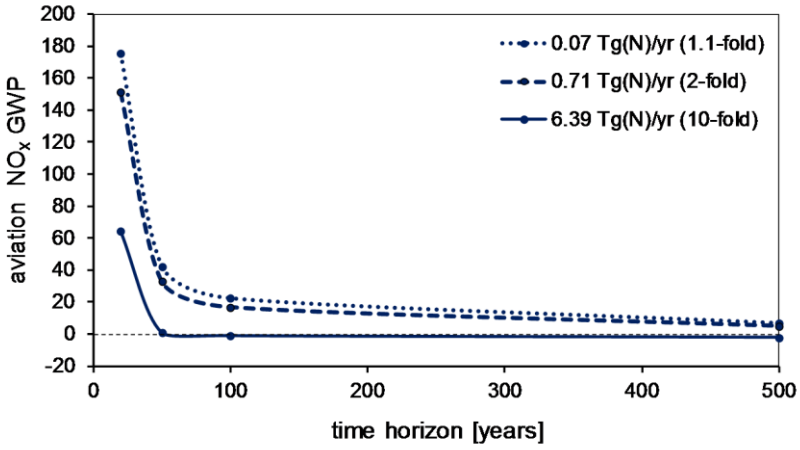

Figure 7.6: Calculated aviation NO_x GWPs for different incremental aircraft NO_x emission rates (1.1-times, 2-times and 10-times of the reference aircraft NO_x emission level) as a function of time horizon.

7.4 Discussion

The chemical and transport schemes within different models control the sensitivities of O_3 and CH_4 perturbations; this is potentially one of the reasons for the discrepancies found between reported aircraft NO_x GWP values (e.g., Fuglestvedt et al., 2010, Myhre et al., 2011). However, this study shows that even with one model a wide range of NO_x GWPs is achievable. The varying, with size of the injected aircraft NO_x emissions, O_3 and CH_4 responses and in a non-linear way, constitute another means of explaining variability among reported aircraft NO_x GWPs.

There is very limited number of studies that define GWPs for aviation NO_x emissions. IPCC AR4 (Forster et al., 2007) summarized them and only three values for GWP_{100} were presented: 130, 100 and -3 (Wild et al., 2001, Derwent et al., 2001, Stevenson et al., 2004). While the first two values are within the same range, the third number introduces confusion especially given that Stevenson et al. (2004) and Derwent et al. (2001) used the same model. Recently, these GWPs were re-evaluated by Fuglestvedt et al. (2010) yielding values: 71 for Wild et al. (2001) and -2.1 for Stevenson et al. (2004). Knowing that NO_x GWP varies with different aircraft NO_x rates (Figure 7.5), these differences might be explained by the size of a NO_x pulse applied in each study. Signals of ~0.7-times, ~1.5-times and 10-times greater than background (reference) aviation NO_x emissions were applied in Wild et al. (2001), Derwent et al. (2001) and Stevenson et al. (2004) experiments, respectively. This study

shows that by applying large pulse sizes, the O_3 response (and consequently CH_4, but to lesser extent) is pushed into saturation regime. Thus, the caution made by Stevenson et al. (2004) over the interpretation of their results is appropriate. The GWP_{100} value for the aircraft NO_x rate 10-times larger than the reference aircraft NO_x derived in this study is -1, which is comparable with Stevenson et al. (2004) work. The numbers of GWP_{100} for small aircraft NO_x rates calculated in this study are of 29–17, which are much smaller than Wild et al.'s value, 71; the background aircraft NO_x emissions and inter-model differences can play a role here.

The above GWP numbers are derived through pulse experiments, as the definition of GWP says (Chapter 2.2.2). Fuglestvedt et al. (2010) presented how to get a GWP from steady-state experiments and since then a series of additional estimations appeared as well (Köhler et al., 2008 (in Fuglestvedt et al., 2010), Myhre et al., 2011, Köhler et al., 2012, Skowron et al., 2013). On purpose, these steady-state GWP values, which varied from 75 to -27 (Chapter 7.1), were not compared with the above pulse GWP numbers. Whilst the 'pulse GWP' and 'steady-state GWP' are in agreement from mathematical point of view, when following method of Fuglestvedt et al. (2010), they differ in their experimental design, namely in their reference perturbation and consequently in the resultant sensitivities of chemical responses (e.g., Figure 5.15 in Chapter 5). Thus, it is questionable whether they might be directly compared. This issue is addressed in the following paragraph.

Indeed, the OPE per unit of emitted N is 17% greater for experiments where a background without aircraft emissions constitutes the reference case (steady-state approach); this discrepancy decreases to ~10% for larger aircraft NO_x emission rates (Figure 7.7). On the contrary, the CH_4 response is more pronounced, by ~15%, for pulse experiments for small aircraft NO_x emission rates. However the magnitudes of CH_4 lifetime reduction per emitted N differs by only ~1% for aircraft NO_x emission rates greater than 2.8 Tg(N) yr^{-1}. These peculiarities of the chemical system affect the GWP values, where net NO_x GWP_{100} for the steady-state approach are greater than 'pulse GWPs' by ~50–60% across various aircraft NO_x emissions rates (Figure 7.8). Thus, attention should be given to any methodological differences between aircraft estimates comparisons, where the results from various studies are taken into account.

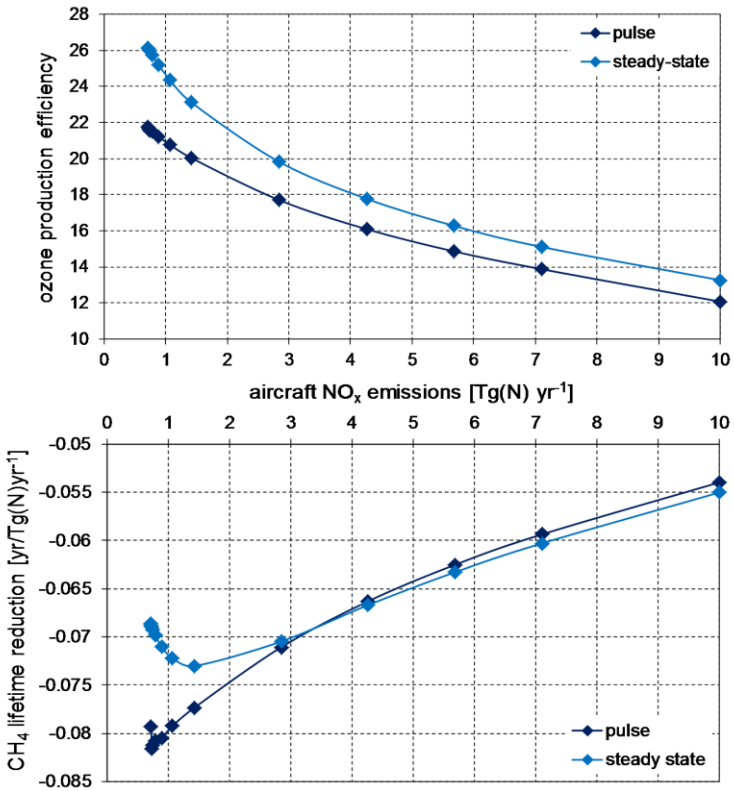

Figure 7.7: Scatter plots of O_3 production efficiency (upper) and CH_4 lifetime reduction (bottom) per unit of emitted N for steady-state (blue) and 'pulse' (dark blue) experiments against series of aircraft NO_x emission rates.

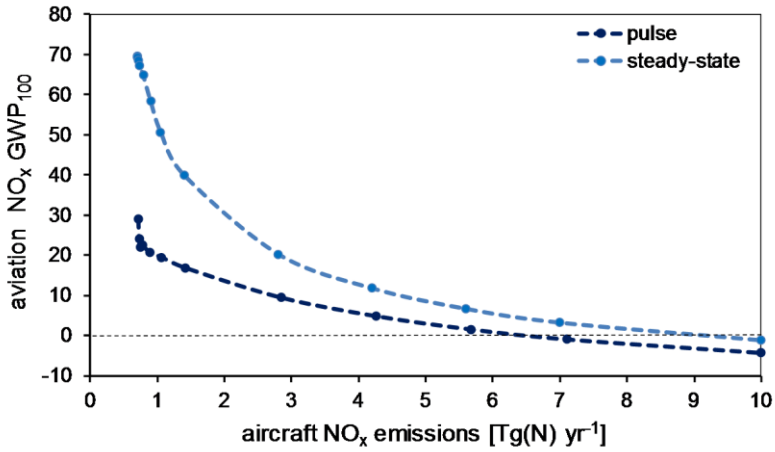

Figure 7.8: Calculated aviation NO_x GWPs for 100-year time horizons for steady-state (blue) and 'pulse' (dark blue) experiments as a function of different global aircraft NO_x emission.

There is significant variability of aircraft NO_x GWPs for each time horizon (Figure 7.5) driven by non-linearities of the chemical system. However, a unique value for GWP does not exist, even for a relatively small incremental aircraft NO_x emission rates. Taking into account only the linear regime of O_3 and CH_4 responses (experiments with

NO_x up to 1.42 Tg(N) yr^{-1}, which constitute a NO_x emission increase of 100%) the range of O_3 and CH_4 GWP values are admittedly limited, ΔO_3 GWP_{100} = 9%, Δ CH_4 GWP_{100} = 5% (Figure 7.9). The GWP diversity still remains significant for net NO_x estimates, where Δ net NO_x GWP_{100} = 30%. The decreasing OPE per unit emitted N with increasing aircraft NO_x emission rates drives the variability of aircraft O_3 GWP (Figure 7.10). The increasing CH_4 GWP with greater NO_x emission rates follows the weakening of CH_4 lifetime reduction per increasing aircraft N emission. When the CH_4 lifetime change per unit O_3 burden change is analysed, it is observed that each aircraft NO_x emission rate leads to a different ratio, even in the linear regime. Figure 7.11 reveals that weaker O_3 change with increasing aircraft NO_x emissions is more pronounced than the weakening of CH_4 reduction. Thus, the ratio is decreasing with greater aircraft NO_x emissions, similarly as it is observed for net NO_x GWPs. A strong correlation between the CH_4/O_3 ratio and aircraft net NO_x GWP was found (Figure 7.12): 97% of global aviation NO_x GWP_{100} variability can be explained by variance in CH_4/O_3 ratio resulting from application of different aircraft NO_x rates into a 3D CTM, MOZART-3.

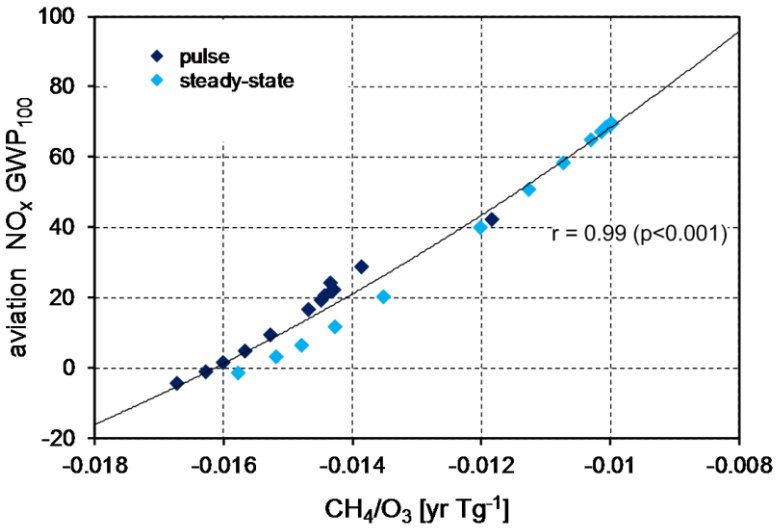

Figure 7.12: Scatter plot of net NO_x GWP_{100} for 'pulse' (dark blue) and steady-state (blue) experiments against corresponding ratio of CH_4 lifetime change per O_3 burden change (dots are the individual experiments, line is the best fit curve).

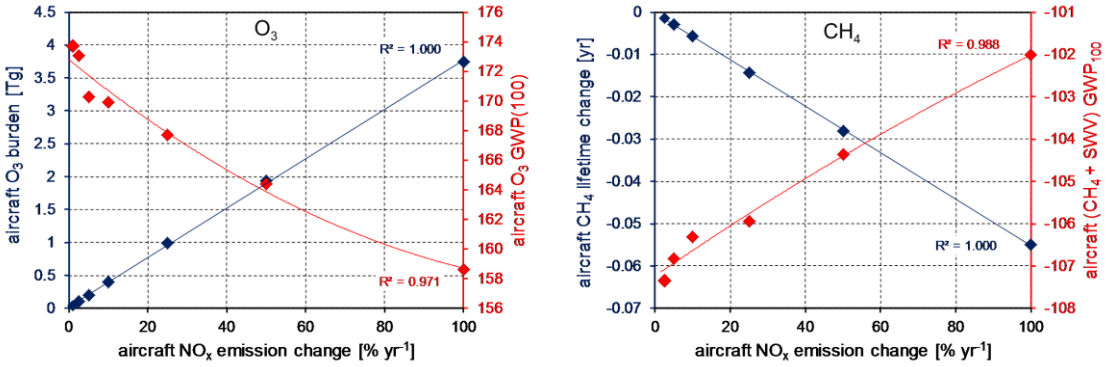

Figure 7.9: Scatter plots of O_3 burden change (blue) and the corresponding short-term O_3 GWP_{100} (red) on the left panel and CH_4 lifetime reduction (blue) and the corresponding (CH_4+SWV) GWP_{100} (red) on the right panel against series of small incremental aircraft NO_x emission rates (up to 1.42 Tg(N) yr^{-1} = 100% NO_x emission change).

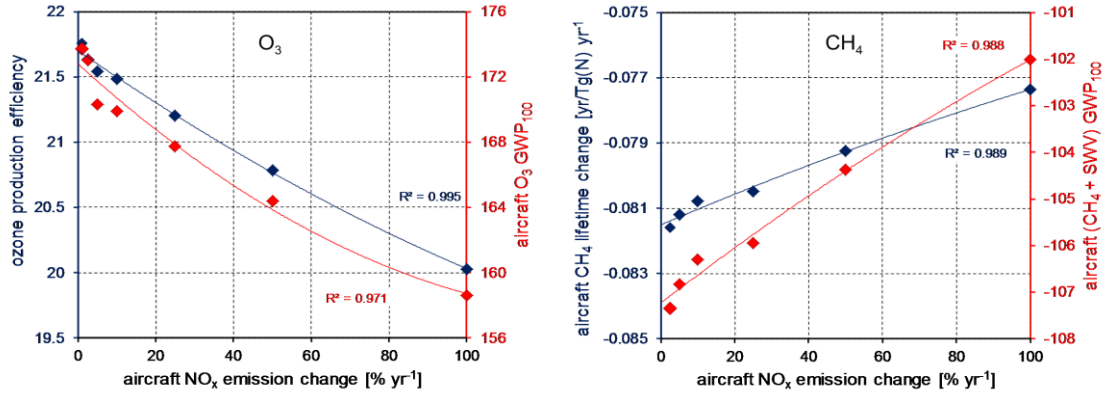

Figure 7.10: Scatter plots of normalized O_3 production efficiency (blue) and the corresponding short-term O_3 GWP_{100} (red) on the left panel and normalized CH_4 lifetime reduction (blue) and the corresponding (CH_4+SWV) GWP_{100} (red) on the right panel against series of small incremental aircraft NO_x emission rates (up to 1.42 Tg(N) yr^{-1} = 100% NO_x emission change).

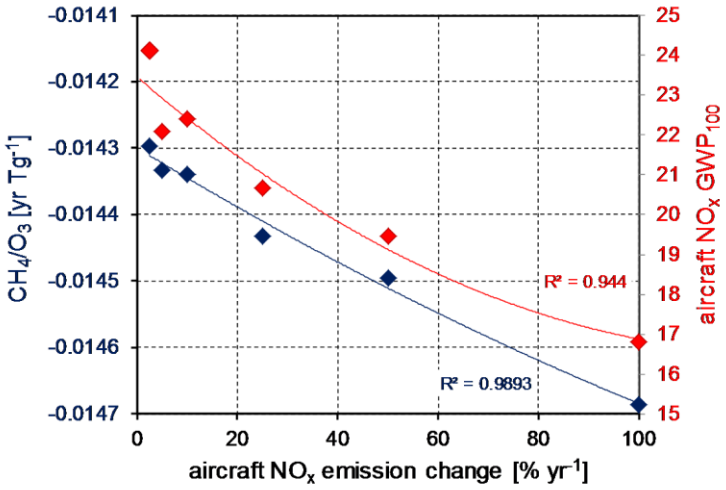

Figure 7.11: Scatter plot of CH_4 lifetime change per O_3 burden change (blue) and the corresponding net NO_x GWP_{100} (red) against series of small incremental aircraft NO_x emission rates (up to 1.42 Tg(N) yr^{-1} = 100% NO_x emission change).

The O_3 burden change and the CH_4 lifetime reduction increase with greater aircraft NO_x emissions and decrease with reduced[2] aircraft NO_x emissions (Figure 7.13). These processes proceed linearly when aircraft NO_x rates are relatively small[3]. However, the rates of changes become disparate for greater aircraft NO_x rates, where CH_4 lifetime reduction is more sensitive, by 9%, 18%, 35% for 25%, 50%, 100% aircraft NO_x emission change, respectively, than O_3 burden change to modified aircraft NO_x emission rates. This relation is observed to be symmetrical and the more pronounced CH_4 lifetime reduction over O_3 burden change is valid for both reduction and increase of aircraft NO_x emissions. The relative difference between O_3 and CH_4 changes constitute 30% for each aircraft NO_x emission rate.

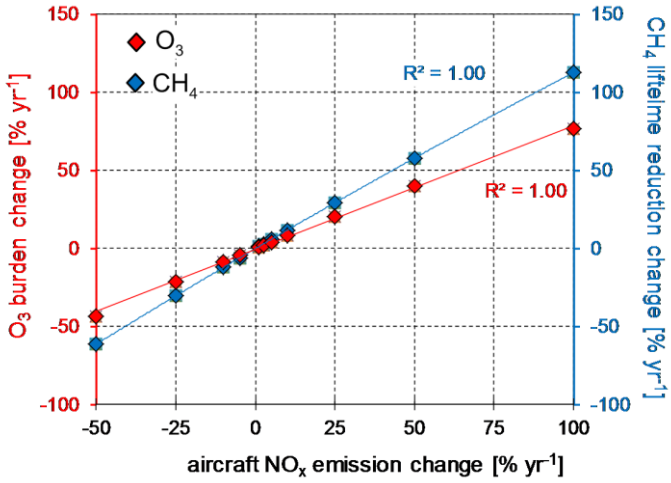

Figure 7.13: Scatter plots of O_3 burden change (red) and CH_4 lifetime reduction change (blue) for steady-state experiments against series of aircraft NO_x emission rates, ranging from 0.35 Tg(N) yr^{-1} (-50% NO_x emission change) to 1.42 Tg(N) yr^{-1} (100% NO_x emission increase).

The efficiency of ozone production decreases with increasing NO_x emission rates and conversely, increases with decreasing aircraft NO_x emissions (Figure 7.14). On the contrary, the CH_4 lifetime reduction is weakening with reduced NO_x rates and becomes more negative with greater aircraft NO_x emissions. There are 18% more O_3 molecules produced per emitted N when the aircraft NO_x emissions are reduced by 50% compared with 50% NO_x increase case. The CH_4 lifetime reduction is 26% stronger for 50% NO_x increase compared with 50% NO_x reduction. The greater O_3 burden change

[2] The aircraft NO_x reduction experiments were taken from Chapter 5 and combined with steady–state experiments performed for this Chapter.
[3] The aircraft NO_x ranging from 0.35 Tg(N) yr^{-1} (-50% NO_x emission change) to 1.42 Tg(N) yr^{-1} (100% NO_x emission increase) was taken into account. The 0% change constitute the 0.71 Tg(N) yr^{-1} of aircraft NO_x emissions.

per N and weaker CH_4 reduction per N leads to greater CH_4/O_3 ratio with decreasing aircraft NO_x emissions rates (Figure 7.15). Knowing that aviation net NO_x GWP is strongly and significantly correlated with ratio of CH_4 lifetime change per O_3 burden change, the distinct picture might be drawn where magnitudes of aviation net NO_x GWP increase with reduced aircraft NO_x emissions.

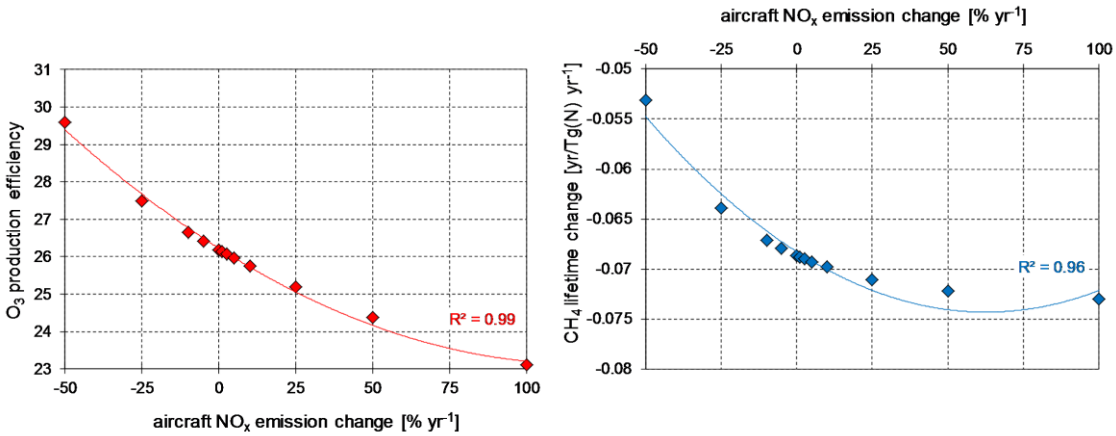

Figure 7.14: Scatter plots of normalized O_3 production efficiency (upper) and normalized CH_4 lifetime change (bottom) for steady-state experiments against series of global aircraft NO_x emission rates, ranging from 0.35 Tg(N) yr^{-1} (-50% NO_x emission change) to 1.42 Tg(N) yr^{-1} (100% NO_x emission increase).

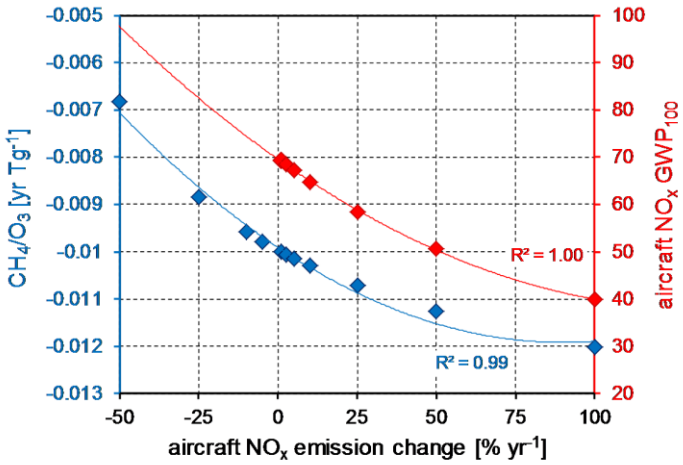

Figure 7.15: Scatter plot of CH_4 lifetime change per O_3 burden change (blue) and the corresponding net NO_x GWP_{100} (red) for steady-state experiments against series of global aircraft NO_x emission rates, ranging from 0.35 Tg(N) yr^{-1} (-50% NO_x emission change) to 1.42 Tg(N) yr^{-1} (100% NO_x emission increase) (dots are individual experiments, lines are the best fit curves).

7.5 Summary

The response of the chemical system varies with size of the aircraft NO_x emission rate, and in a non-linear way, which results in significant diversity of aviation NO_x GWPs. The chemical response is also sensitive to the level of aircraft NO_x background.

Twenty four experiments were performed, gathering both 'pulse' and steady-state experiments, leading to twenty four different dependencies between CH_4 lifetime change and O_3 burden change, giving twenty four different net NO_x GWP estimates. This sheds light on understanding the disparities between numbers reported in literature.

This study shows that even with one model and consistent experimental settings it is not possible to determine a unique value for an aircraft NO_x GWP. Additionally, the peculiarity of the relation between aircraft NO_x emissions and aviation NO_x GWP, where the GWP magnitudes increase with reduction of aircraft NO_x emissions and decrease with increasing aircraft NO_x emissions, also raises concern. It is not evident how policy might handle such behaviour.

Chapter 8

Variation of the effect of regional aviation NO_x emissions

8.1 Introduction

The geographical imbalance of climate impact from NO_x emissions is a result of both the short-term nature of the chemistry and the heterogeneous pattern of emissions. The geographical imbalance arises from complexity of the response of NO_x effect components. The short-lived O_3 change (positive climate forcing, warming) is inhomogeneous, concentrated mainly where the NO_x emissions occur. The CH_4 response (negative climate forcing, cooling), due to its decadal lifetime, is homogenously spread over the globe. Thus, even if these two effects might cancel as a global mean, they do not on a regional scale (e.g., Prather et al., 1999).

The same amount of NO_x emissions might lead to different regional climate impacts. The O_3 production formed from NO_x emissions strongly depends on the background conditions that are distinct for specific spatio-temporal locations. The O_3 response is influenced by the background NO_x concentrations (e.g., Isaksen et al.,1978, Berntsen and Isaksen, 1999), the abundance of HO_x, VOCs (e.g., Lin et al.,1988, Jaeglé et al., 1998) or the intensity of solar flux.

These different influences result in quite a specific behaviour, as different climate responses might result from equal global mean RFs arising from the same amount of emitted NO_x at different locations (e.g., Berntsen et al., 2005, Shine et al., 2005a).

There is an ongoing interest in investigations of regional climate impacts, including those from the effects of surface NO_x emissions (Fuglestvedt et al., 1999, Berntsen et al., 2005, Naik et al., 2005, Shine et al., 2005a, Derwent et al. 2008, Shindell et al., 2009, Fry et al., 2012). All these studies agree that the global O_3 change and its radiative forcings are more sensitive to NO_x emission fluxes near equator, than in mid- and high-latitude regions. Shine et al. (2005a) additionally pointed out that usually the hemisphere, where NO_x emissions occur, is related with a warming effect and the other hemisphere with cooling.

There are only few studies dealing with geographical effects from aircraft NO_x emissions (Grewe and Stenke, 2008, Stevenson and Derwent, 2009, Köhler et al., 2012). Grewe and Stenke (2008) and Köhler et al. (2012) have shown that different latitudinal bands give different RFs per unit aircraft NO_x emission. The RFs resultant from O_3 and CH_4 changes at low latitudes are significantly greater than RFs from those changes at higher latitudes. Köhler et al. (2012) also presented the aircraft NO_x impact over four geographical regions, where tropical locations, China and India, with their net NO_x RFs of 14.3 mW m^{-2} per Tg(N) yr^{-1} and 12.6 mW m^{-2} per Tg(N) yr^{-1}, substantially exceed the mid-latitudinal net NO_x RFs, of ~2 mW m^{-2} per Tg(N) yr^{-1}, over Europe and USA. On the contrary, the study of Stevenson and Derwent (2009) result in strong compensations between O_3 and CH_4 responses for July's pulse aircraft NO_x emissions at 112 different cruise altitude locations, where, in most cases, the short-term O_3 positive RFs was overwhelmed by long-term CH_4 negative RFs. They also highlighted the correlation between NO_x background concentration and the resultant RFs from aircraft NO_x perturbation.

Similarly as for the previous chapter, few and disparate estimates are the motivation of this study. In this chapter, the regional impacts of aviation NO_x emissions on tropospheric chemistry and their related climate forcings are investigated. The low-latitude emissions are usually highlighted in terms of their efficiency in O_3 production and O_3 RFs. However, aircraft NO_x emissions, injected in the mid-latitude remote oceanic regions, might also be influential in terms of their impact on climate.

The responses of Northern and Southern Hemisphere along with five regions: Europe, North America, Southeast Asia, North Pacific and North Atlantic are investigated. The dependence of experimental design (e.g. aircraft NO_x rates) on the perception of inter-regional dependencies is also discussed.

8.2 Methodology

8.2.1 Incremental aircraft NO_x emissions

In order to explore the impact of regional aircraft NO_x emissions on climate, seven geographical domains were defined: Europe (EUR), North America (NA), Southeast Asia (SE ASIA), North Pacific (NPAC), North Atlantic (NATL), Northern Hemisphere (NH) and Southern Hemisphere (SH) (Figure 8.1, Table 8.1). Incremental aircraft NO_x emissions were applied to one region per experiment. The injections of aircraft NO_x emissions are valid for all altitudes in the defined domains. Each incremental aircraft NO_x case is based on equal mass of emissions, 0.035 Tg(N) yr^{-1}. This constitutes different relative addition of emission to the total NO_x in each region (Table 8.1); whilst for continental regions, it is equal to ~30% increase of aircraft NO_x, for oceanic domains, it rises to ~160%.

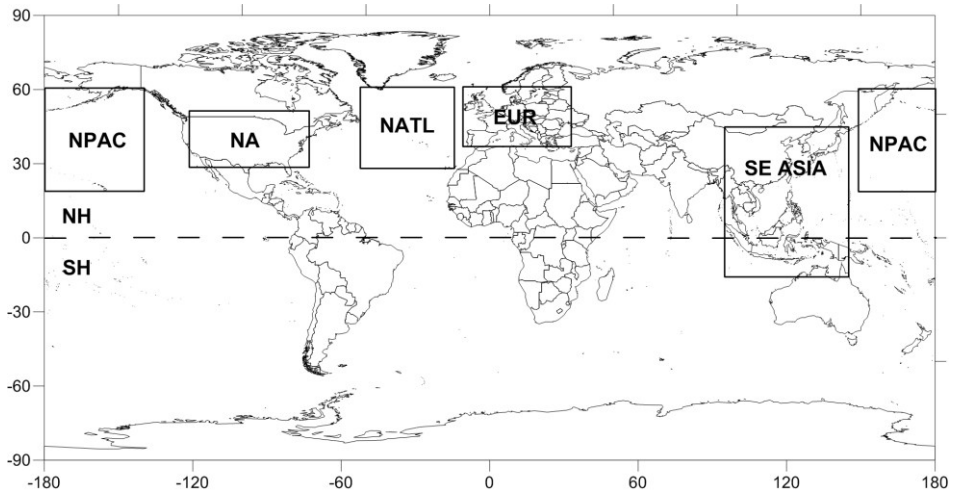

Figure 8.1: Regions with incremental aircraft NO_x emissions: Europe (EUR), North America (NA), Southeast Asia (SE ASIA), North Atlantic (NATL), North Pacific (NPAC), Northern Hemisphere (NH) and Southern Hemisphere (SH).

Table 8.1: Description of regional domains, along with the amount of emitted aircraft NO_x in each region (third column) and the increase (in %) of aircraft NO_x for three cases of incremental aircraft emissions in each region (three last columns).

REGION	Geographical extent	Aircraft NO_x [Tg(N)/yr]	Incremental aircraft N [Δ N/base N]		
			0.035 Tg(N)/yr	0.71 Tg(N)/yr	6.39 Tg(N)/yr
EUR	10°W-30°E; 40°N-60°N	0.112	0.32	6.3	57.2
NA	120°W-75°W; 30°N-50°N	0.132	0.27	5.4	48.5
SE ASIA	95°E-145°E; 12°S-45°N	0.128	0.28	5.5	50.0
NPAC	180°W-140°W; 150°E-180°E; 20°N-60°N	0.021	1.67	33.4	300.6
NATL	50°W-15°W; 30°N-60°N	0.023	1.54	30.8	276.8
NH	180°W-180°E; 0°-90°N	0.653	0.05	1.1	9.8
SH	180°W-180°E; 0°-90°S	0.057	0.62	12.4	111.9
Global	180°W-180°E; 90°S-90°N	0.71	0.05	1	9

Additionally, two other sizes of aircraft NO_x emissions rates were applied in each region: 0.71 Tg(N) yr^{-1} and 6.39 Tg(N) yr^{-1}. This choice is subjective and it is based on experiments in Chapter 7, where a global incremental NO_x emission of 0.71 Tg(N) yr^{-1} still belongs to a linear response regime, while injection of 6.39 Tg(N) yr^{-1} results in highly non-linear behaviour of NO_x–O_3–CH_4 system. Table 8.1 shows the relative increases of aircraft NO_x emissions for each incremental aircraft NO_x case.

8.2.2 Experimental design

The REACT4C 2006, aircraft emission dataset, was implemented into the 3D CTM, MOZART-3. Twenty two experiments were performed, one reference (base aircraft emission) run and twenty one perturbation (incremental aircraft emission) simulations, each starting in January 2006 and finishing in December 2006; each simulation was preceded by a multi-year spin-up, 2000–2005. The aircraft perturbation is derived by extracting the difference between 'aircraft' and 'incremental aircraft' experiments.

The details regarding model set-up, aircraft emission dataset, surface emissions and dynamical data applied for this study are described in Chapter 3.3. The description of radiative forcings and global warming potentials calculations is presented in Chapter 3.2.

8.3 Results

8.3.1 Hemispherical and regional aircraft NO_x emissions

Air traffic presents a highly heterogeneous geographical pattern: 92% of NO_x emissions are emitted in the Northern Hemisphere (Figure 8.2), from which 52% belongs to EUR, NA and SE ASIA and 6% to NPAC and NATL (based on the regional domains defined in this study, see Table 8.1). By contrast, the vertical distribution is similar world-wide, with most of the air traffic concentrated at 10–11 km (Figure 8.3). However, subtle differences in the peak of aircraft NO_x emissions exist: Northern Hemisphere, Europe and North Pacific have their peak of NO_x at 10.37 km; for Southern Hemisphere, North America, North Atlantic and Southeast Asia it is one level higher, 10.98 km.

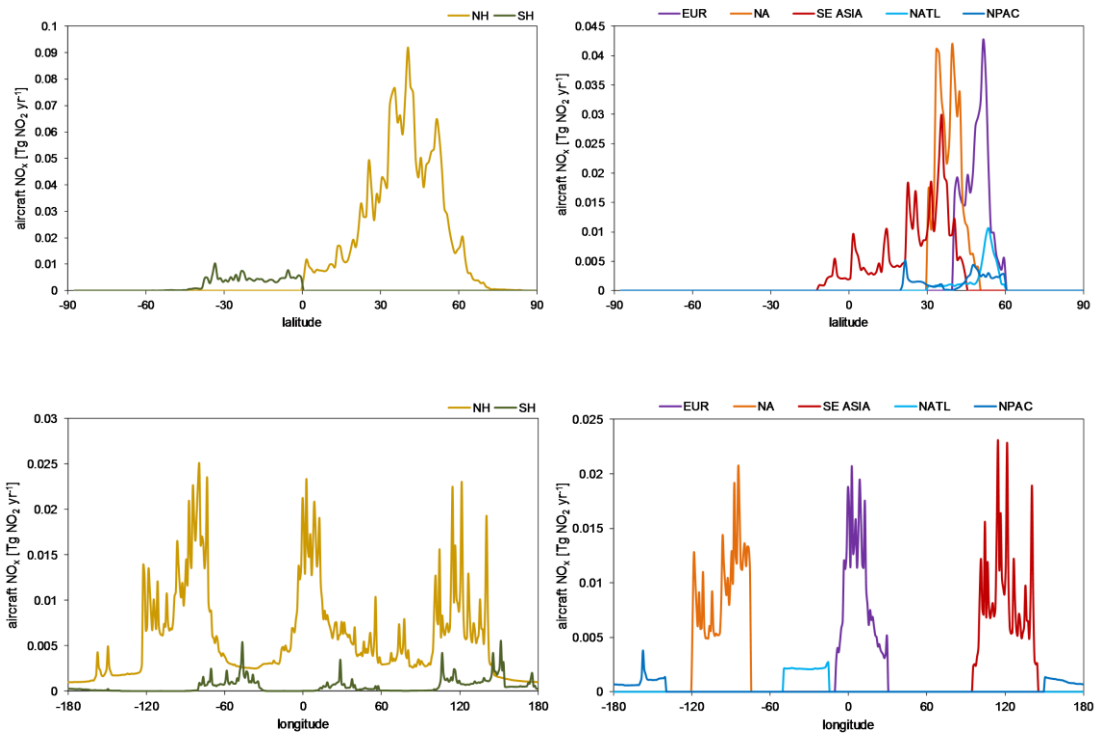

Figure 8.2: The latitudinal (upper row) and longitudinal (bottom row) profiles of aircraft NO_x emissions in seven regions: Northern and Southern Hemisphere (left panels); Europe (EUR), North America (NA), Southeast Asia (SE ASIA), North Atlantic (NATL) and North Pacific (NPAC) (right panels).

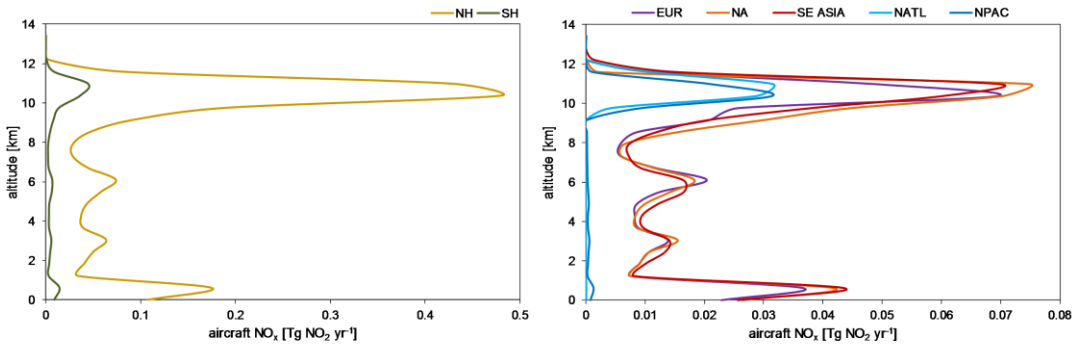

Figure 8.3: The vertical profiles of aircraft NO_x emissions in seven regions: Northern and Southern Hemisphere (left panel); Europe (EUR), North America (NA), Southeast Asia (SE ASIA), North Atlantic (NATL) and North Pacific (NPAC) (right panel).

8.3.2 Hemispherical and regional chemical perturbations for aviation NO_x emissions

The same amount of additional emitted aircraft NO_x (0.035 Tg(N)/yr) from various locations leads to different magnitudes and extents of O_3 perturbation. The specific patterns of response from the Northern and Southern Hemisphere are shown in Figure 8.4. The NH's O_3 perturbation is concentrated mainly at cruise altitudes of high latitudes, where most of the emissions occur. The SH's aircraft NO_x emissions are concentrated mostly in the low-latitudes (there are hardly any emissions for latitudes greater than 52°S), where the convective transport is strong. Thus, the SH's O_3 response is observed throughout the vertical domain, with peak of perturbed O_3 in mid-altitudes and over 35–15°S. The NH's relative O_3 change is concentrated mainly over Europe and North Atlantic, while O_3 from SH NO_x perturbation expands almost uniformly across the southern tropical belt. The regional dependencies also present their characteristic extent in O_3 change. Whilst the peak of O_3 perturbation is concentrated at cruise altitudes in all regions, convective transport, pronounced especially over low-latitudes (SE ASIA), causes that chemical impact has a greater vertical extent than for other regions (Figure 8.5). The peak magnitudes of O_3 changes vary among continental regions from 0.16 ppbv (SE ASIA), 0.24 ppbv (NA) to 0.29 ppbv (EUR); the oceanic regions O_3 response is observed to be much greater: 0.72 ppbv (NPAC) and 0.90 ppbv (NATL). The differences in magnitudes of O_3 perturbation originate from various background conditions specific for each region (e.g., EUR and SE ASIA on Figures C.1, 8.5; more details are presented in Chapter 8.4

and on Figure C.2). The spatial extent of O_3 perturbation is determined primarily by the transport of aircraft NO_x effect and it differs among different regions. The EUR emission leads to the O_3 perturbation being concentrated mostly over Europe and high-northern latitudes. The meridional transport is especially pronounced for NPAC and NATL, where the aircraft NO_x perturbation (Figure C.1), through westerly winds, is transported to the regions far from the aircraft NO_x emission locations. This affect the spread of O_3 perturbation, that is observed in Europe, North Atlantic and northern latitudes of America in the case of NPAC and in Europe and all northern Asia in the case of NATL. The NA's O_3 change occurs over Atlantic and Europe, while the SE ASIA's O_3 perturbation is transported to the Northern Pacific.

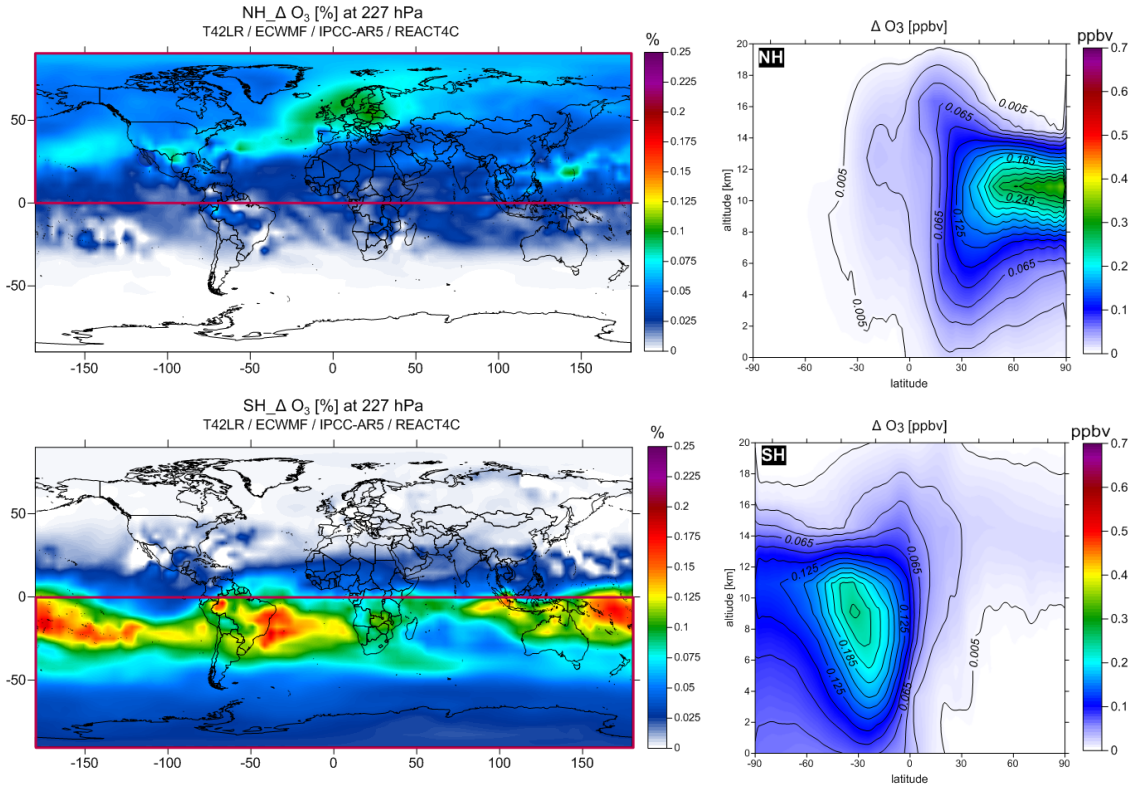

Figure 8.4: Annual O_3 changes calculated by MOZART-3 model for incremental aircraft NO_x emissions of 0.035 Tg(N) yr^{-1} in Northern Hemisphere (NH) (upper panel) and Southern Hemisphere (SH) (bottom panel). Figures on the left show the change (in %) of O_3 concentration at flight level, 227 hPa. Figures on the right show the zonal mean change (in ppbv) of O_3 concentration. The red rectangles indicate the geographical domains with incremental aircraft NO_x emissions.

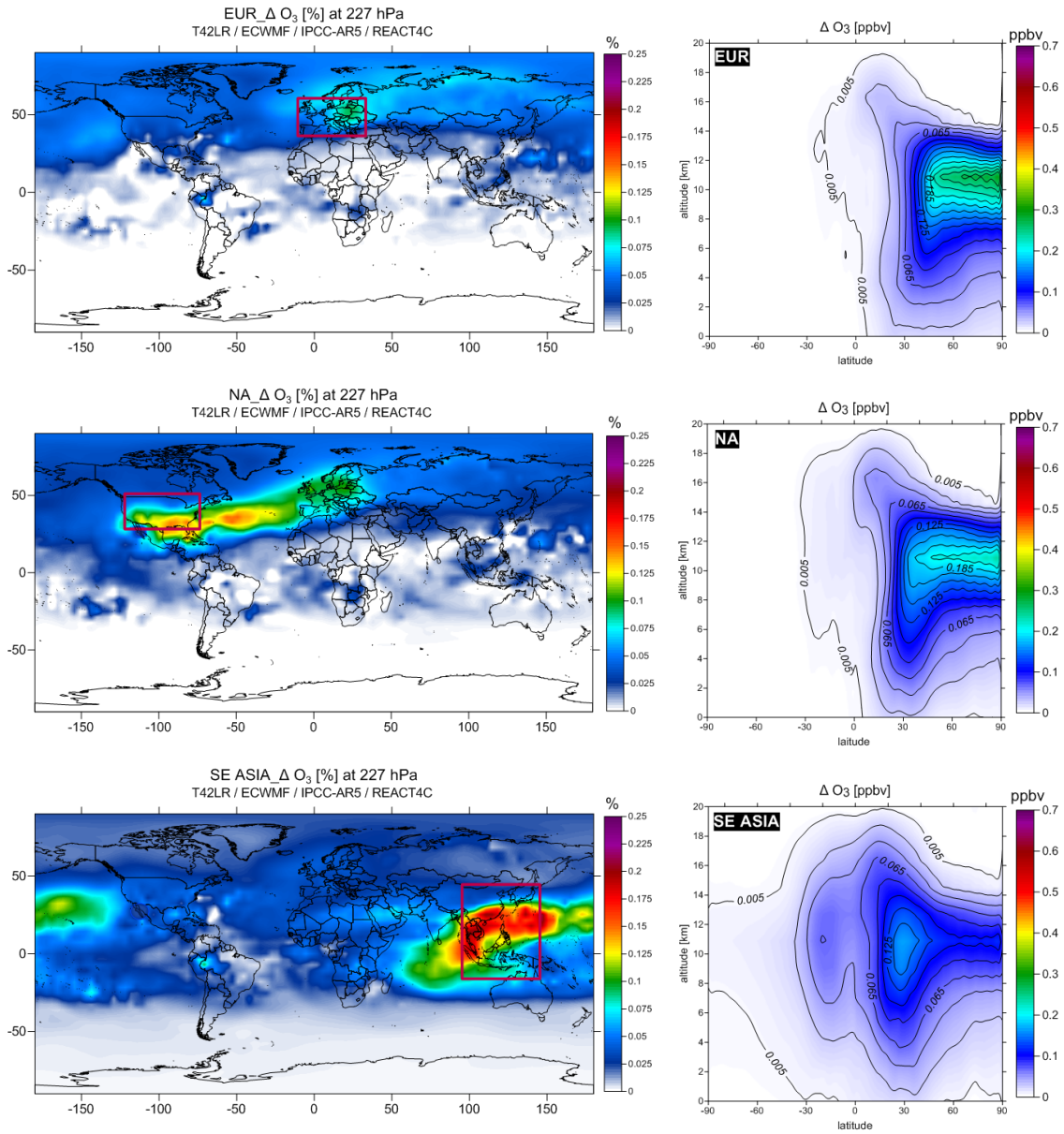

Figure 8.5: Annual O_3 changes calculated by MOZART-3 model for incremental aircraft NO_x emissions of 0.035 Tg(N) yr^{-1} in Europe (EUR) (upper panel), North America (NA) (middle panel) and Southeast Asia (SE ASIA) (bottom panel). Figures on the left show the change (in %) of O_3 concentration at flight level, 227 hPa. Figures on the right show the zonal mean change (in ppbv) of O_3 concentration. The red rectangles indicate the geographical domains with incremental aircraft NO_x emissions.

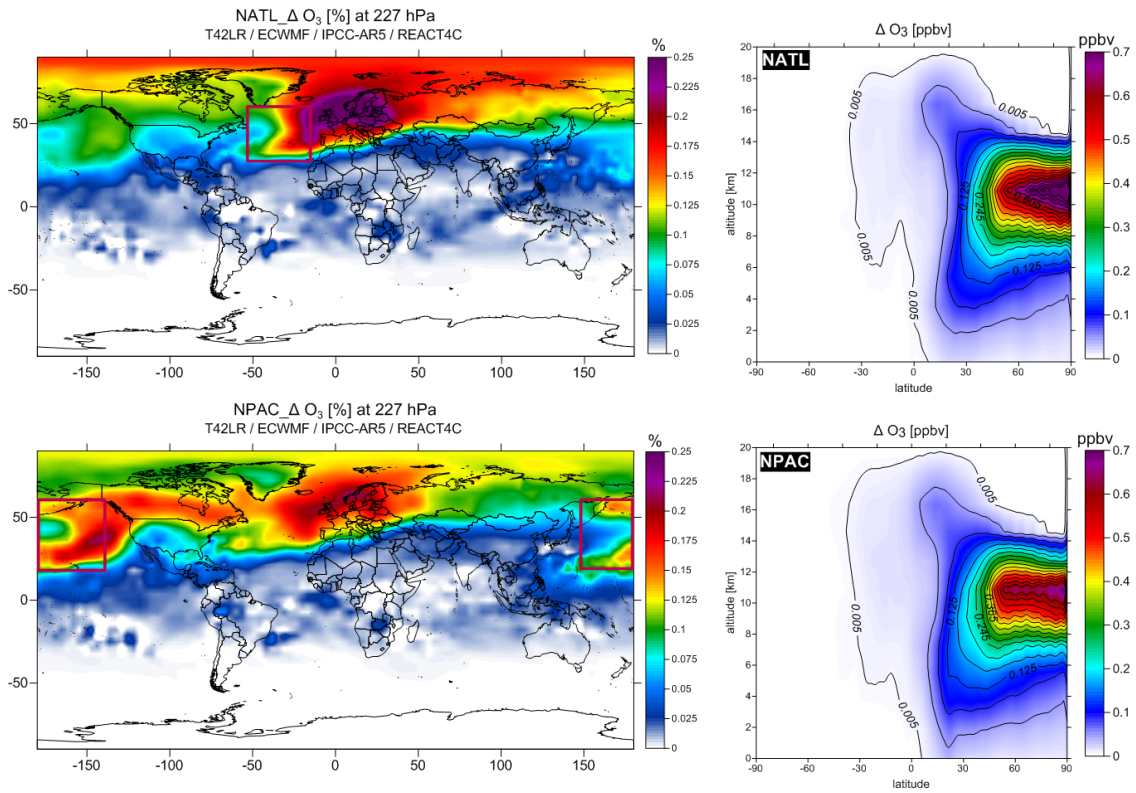

Figure 8.5: Figure 8.5 continuing, but for North Atlantic (NATL) (upper panel) and North Pacific (NPAC) (bottom panel).

The aircraft NO_x perturbation in different regions shows disparities in their impact on global O_3 burden and CH_4 lifetime change (Table 8.2). The Southern Hemisphere produces 40% more O_3 per emitted aircraft N, and is twice as efficient in CH_4 lifetime reduction, than the Northern Hemisphere. A similar pattern in O_3 change is observed if the North Pacific is compared with Europe. In general, the remote oceanic regions have a greater OPE and this results in the larger O_3 burden change, where NPAC and NATL exceed SE ASIA by 24% and 13%, respectively, in O_3 perturbation. Among continental regions, the low-latitudinal SE ASIA gives more O_3 by 23% and 14% compared with EUR and NA, respectively. The CH_4 lifetime reduction results from more convoluted dependencies and the largest O_3 change did not always introduce the greatest CH_4 reduction. The least efficient CH_4 loss occurs over NATL, the greatest efficiency in CH_4 lifetime reduction is observed over SE ASIA. The CH_4 lifetime reduction over NA (-0.036%) is almost as high as over SE ASIA (-0.039%), however NPAC's CH_4 follows the high O_3 burden change (0.26 Tg), which is not observed for SE ASIA's O_3 burden change (0.20 Tg). The explanations of these patterns are presented in the Discussion (Chapter 8.4).

Table 8.2: The global and annual mean O_3 burden change (in Tg) and the CH_4 lifetime reduction (in %) due to the aircraft NO_x emissions in different geographical regions. Calculations are done for surface–1hPa domain and are based on 0.035 Tg(N) yr^{-1} aircraft NO_x increase.

REGION	O_3 burden change (Tg)	CH_4 lifetime change (%)
Global	0.20	-0.034
NH	0.19	-0.031
SH	0.31	-0.067
EUR	0.15	-0.024
NA	0.17	-0.028
SE ASIA	0.20	-0.039
NPAC	0.26	-0.036
NATL	0.22	-0.024

The global response of the chemical system varies with the size of the pulse and in a non-linear way (Chapter 7). The non-linear O_3 and CH_4 responses are also observed from regional aircraft NO_x perturbations (Figure 8.6); the greater NO_x emission rates lead to weaker O_3 responses and less pronounced CH_4 reductions. However, each region has its own distinctive sensitivity in the response of chemical system. The O_3 response over Southeast Asia is much less sensitive to different aircraft NO_x emission rates than over oceans, where the O_3 change depends significantly on the amount of emitted NO_x. For example, as a result of 6.39 Tg(N) yr^{-1} experiments, SE ASIA has the greatest global O_3 burden change and NATL's O_3 is observed to be of similar magnitude as O_3 for EUR, which is in contrast to what was presented in the paragraph above. The CH_4 lifetime reduction also changes with aircraft NO_x emission rates. The non-linearity of CH_4 lifetime reduction is stronger at low latitudes, where conditions for CH_4 oxidation (high temperature and concentrations of OH) are advantageous, compared with mid-latitudes. Thus, CH_4 over SE ASIA and SH follows strictly the O_3 sensitivity to additional NO_x emissions: the weaker O_3 response causes the weaker CH_4 lifetime reduction, both at the same rates of deviation. For other regions, especially for NATL and NPAC, the weaker O_3 response does not necessarily lead to a weaker CH_4 lifetime reduction. Figure 8.7 shows these peculiarities. The CH_4 lifetime change per unit O_3 burden change over SE ASIA and SH remains almost the same for each incremental aircraft NO_x case (the ratio changes by 1.5% and -1.9%, respectively, with greater NO_x emission rates). This is not observed for other regions, especially oceanic

domains, where CH_4/O_3 ratio becomes significantly greater (44% for NATL) with larger NO_x emission rates. These results show that the variation in experimental design strongly influences the perception of inter-regional dependencies, e.g., the greatest O_3 burden change, can easily belong to, either NPAC, or SE ASIA depending on the size of aircraft NO_x emission rates.

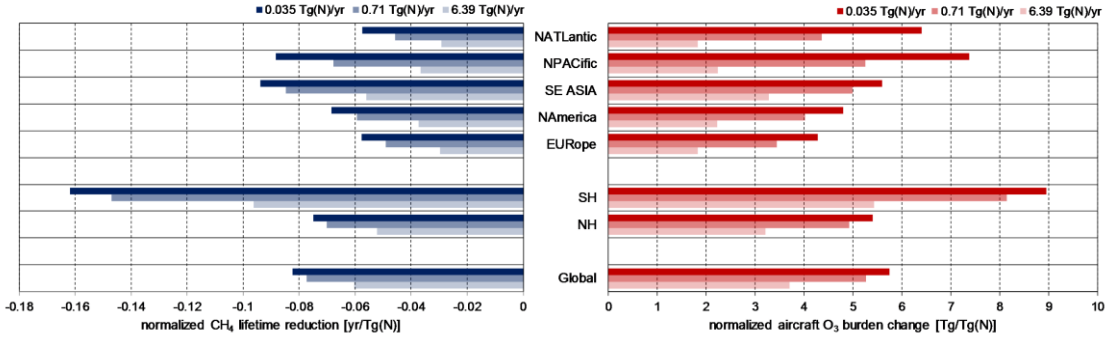

Figure 8.6: The normalized O_3 burden change (red bars) and CH_4 lifetime reduction (blue bars) in different geographical regions as a response to different sizes of incremental aircraft NO_x emissions.

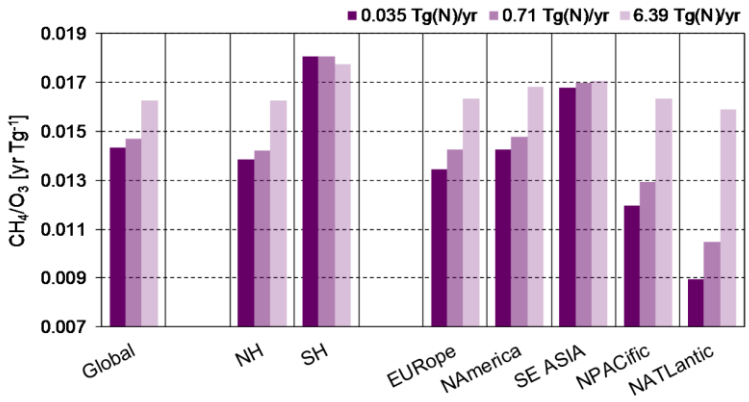

Figure 8.7: The absolute ratio of the CH_4 lifetime change to the O_3 burden change for different geographical regions for a series of aircraft NO_x emission rates.

8.3.3 Hemispherical and regional radiative forcings and global warming potentials for aviation NO_x emissions

The latitudinal distributions of short-term O_3 RF for different geographical regions are shown in Figure 8.8. In general, the pattern for each region shows similar latitudinal profiles as aircraft NO_x emissions. However, the magnitudes of O_3 RF responses differ: the SH's O_3 RF is much larger, by 52%, than NH's short-term forcing and NPAC,

NATL exceeds, by 29%, the O_3 responses from continental regions. The peak of short-term O_3 RF is different for each region being located at 21°S for SH (3.1 mW m^{-2}), 29°N (1.7 mW m^{-2}), 44°N for EUR (1.4 mW m^{-2}), 31°N for NA (1.9 mW m^{-2}), 24°N for SE ASIA (1.9 mW m^{-2}), 39°N for NATL (2.3 mW m^{-2}) and 31°N for (2.6 NPAC mW m^{-2}). The RFs mentioned above are zonal and annual values; locally, the differences in the short-term O_3 RF are much more pronounced. Both hemispherical perturbations show the strongest O_3 forcings over subtropical belts, for SH it is southern parts of the equator, for NH it is northern parts (Figure 8.9). The magnitudes of the responses differs, for NH O_3 RF reaches 2.5 mW m^{-2} over Northern Africa, for SH the maximums of O_3 RF (3.5–3.9 mW m^{-2}) are more spread and occur over South Atlantic and Australia. The North Pacific is the most powerful in terms of induced short-term O_3 RF among all investigated regions (Figure 8.10). The O_3 forcings reach 4.5 mW m^{-2} over northern Pacific and west coast of North America. The NPAC perturbation has the most extensive range of impact that is observed for most of the northern subtropical areas: Atlantic, Africa and southwest Asia. Similarly acts NATL, but the O_3 RF response is shifted more East with the highest values (3.5–3.9 mW m^{-2}) concentrated over Africa and southwest Asia. The smallest responses of O_3 RF are observed for EUR experiment, with maximum forcings (2.3 mW m^{-2}) located over Balkans and southwest Asia. The NA perturbation affects mainly subtropical Atlantic and Africa (3.0–3.1 mW m^{-2}) and SE ASIA – southeast Asian coast and subtropical Pacific (3.0–3.2 mW m^{-2}).

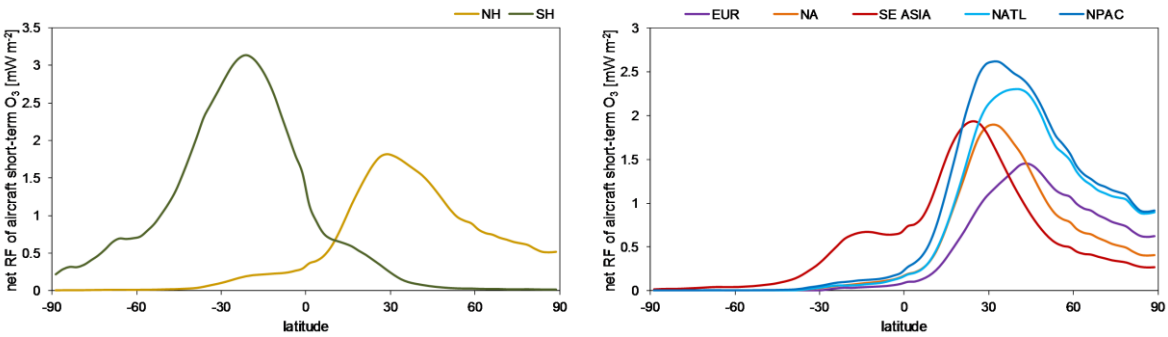

Figure 8.8: Zonal and annual mean net (long wave and shortwave) radiative forcing (mW m^{-2}) from short-term O_3 for Northern (NH) and Southern (SH) Hemisphere (left panel) and regions: Europe (EUR), North America (NA), Southeast Asia (SE ASIA), North Atlantic (NATL) and North Pacific (NPAC) (right panel). Based on 0.035 Tg(N)/yr aircraft NO_x increase experiments.

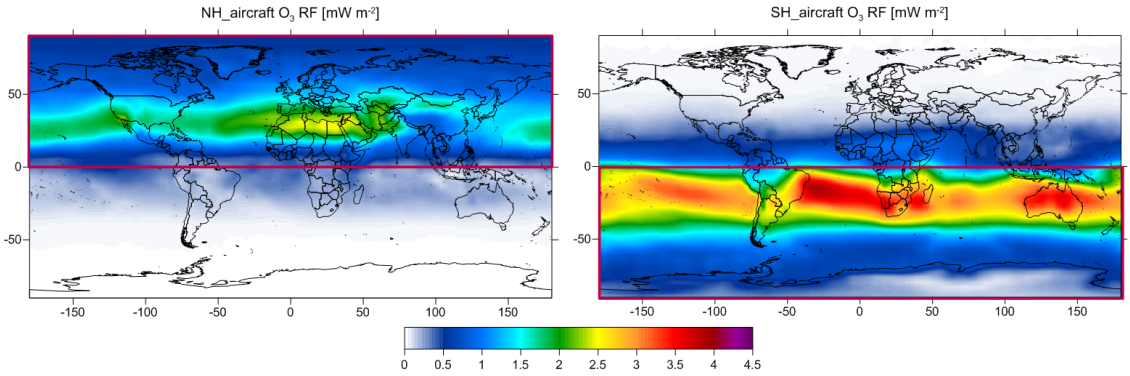

Figure 8.9: The annual distribution of the net (long wave and shortwave) radiative forcing (mW m^{-2}) from short-term O_3 for Northern (NH) and Southern (SH) Hemisphere. Based on 0.035 Tg(N)/yr aircraft NO_x increase experiments. The red rectangles indicate the geographical domains with incremental aircraft NO_x emissions.

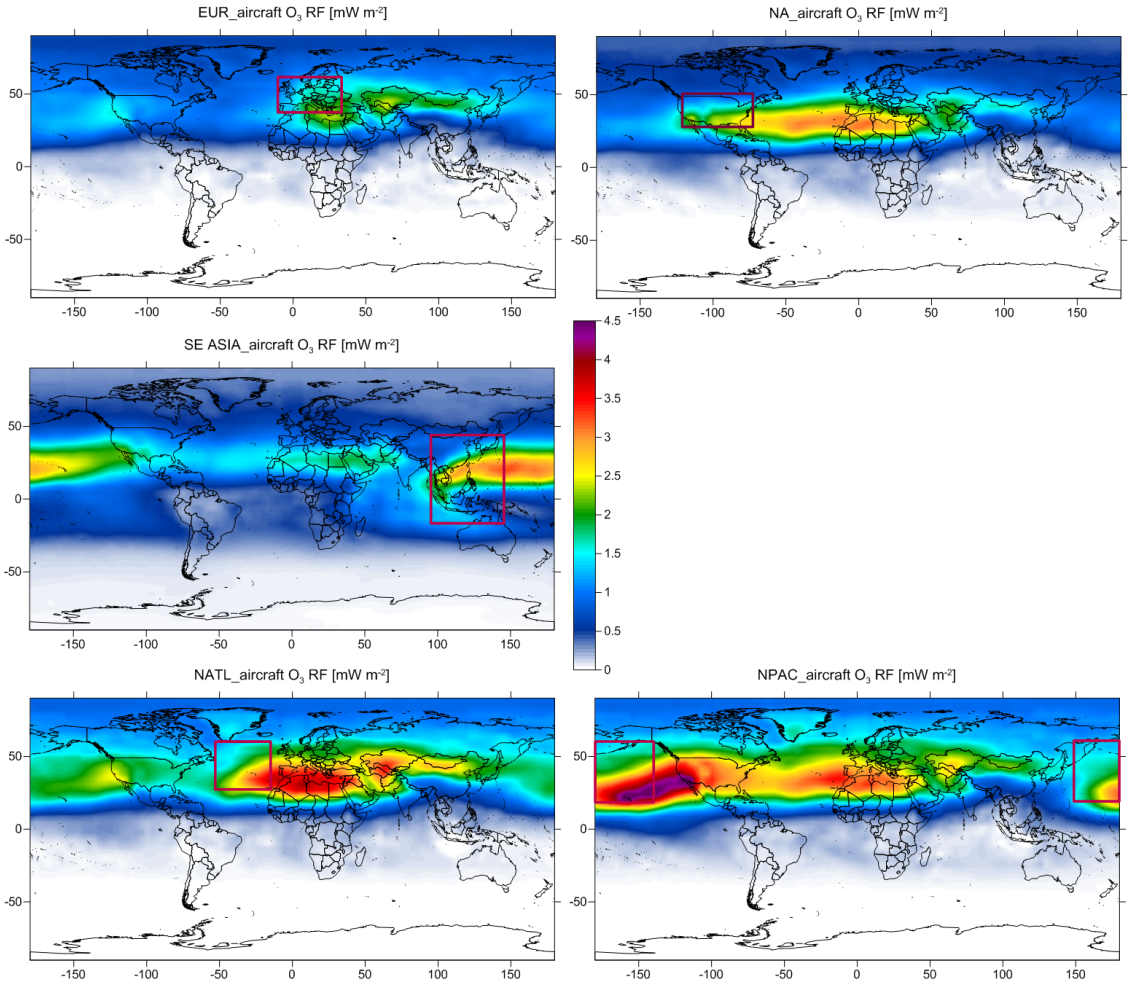

Figure 8.10: The annual distribution of the net (long wave and shortwave) radiative forcing (mW m^{-2}) from short-term O_3 for Europe (EUR), North America (NA), Southeast Asia (SE ASIA), North Atlantic (NATL) and North Pacific (NPAC). Based on 0.035 Tg(N)/yr aircraft NO_x increase experiments. The red rectangles indicate the geographical domains with incremental aircraft NO_x emissions.

Figure 8.11 shows the normalized net global annual mean RF and the four component forcings, for different geographical regions. The hemispheric differences in the resultant RFs are significant: net NO_x RFs vary from 3.7 mW m^{-2}/Tg(N) yr^{-1} for NH to 7.3 mW m^{-2}/Tg(N) yr^{-1} for SH. The differences between single components also are observed: both short-term O_3 RF and long-term negative RFs are twice as strong over SH than over NH (by 50% and 53%, respectively). The highest net NO_x RF value is observed over North Atlantic, 10.0 mW m^{-2}/Tg(N) yr^{-1}, which is the result of strong positive short-term O_3 RF and relatively weak long-term negative forcings. A similar pattern is observed for NPAC, in that the difference in short-term O_3 RF (22.9 mW m^{-2}/Tg(N) yr^{-1}) is larger than all the regions. Whilst the short-term O_3 RF over Southeast Asia is as large as that over the North Atlantic (20.0 mW m^{-2}/Tg(N) yr^{-1}), the negative forcings play a relatively larger role at low-latitudes, which efficiently reduce the net NO_x RF in SE ASIA to 4.9 mW m^{-2}/Tg(N) yr^{-1}. The net of positive and negative forcings over North America and over Europe are the smallest among all the regions, 3.3 and 2.3 mW m^{-2}/Tg(N)yr^{-1}, respectively.

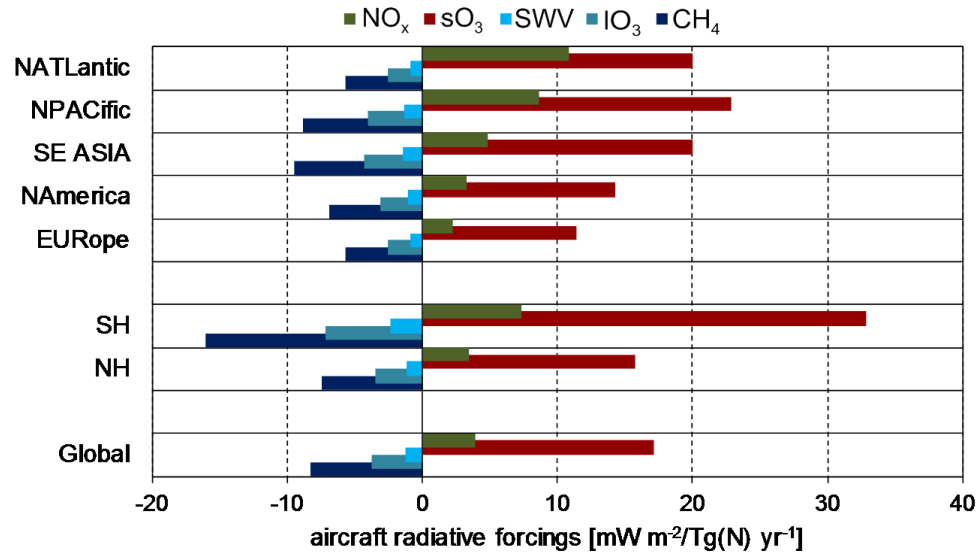

Figure 8.11: Radiative forcings per unit emission of N (in mW m^{-2}/Tg(N) yr^{-1}) due to short-term O_3 (sO_3), CH_4-induced O_3 (lO_3), CH_4 (CH_4), stratospheric water vapour (SWV) and NO_x (net of all 4 components) for Northern and Southern Hemisphere and regions: Europe, North America, Southeast Asia, North Atlantic and North Pacific. Based on 0.035 Tg(N)/yr aircraft NO_x increase experiments.

The net NO_x GWP values are positive for all regions and each time horizon (Figure 8.12). There are substantial differences in calculated GWPs; the greatest values are calculated for a 20-year time horizon for each region and the significant,

by ~80–70%, reduction of GWPs appears with larger time horizons. The largest differences in values are calculated for North Atlantic ($GWP_{20,\ 100,\ 500}$ = 511, 125, 38) and Europe ($GWP_{20,\ 100,\ 500}$ = 164, 26, 8) for each time horizon. The net NO_x GWPs of continental mid-latitude regions, EUR and NA, are smaller than low-latitudinal SE ASIA, by 48%, 31% for H=20 and by 53%, 33% for H=100, respectively. However, the net NO_x GWPs of oceanic mid-latitude regions, NPAC and NATL, are greater than low-latitudinal SE ASIA, by 32%, 38% for H=20 and by 44%, 55% for H=100, respectively. The Southern Hemisphere's GWPs for positive and negative components are twice larger than values for Northern Hemisphere. The net NO_x GWP presents significant dominance of SH over NH, by 51% for 20-time year horizon and by 49% for 100- and 500-time year horizon.

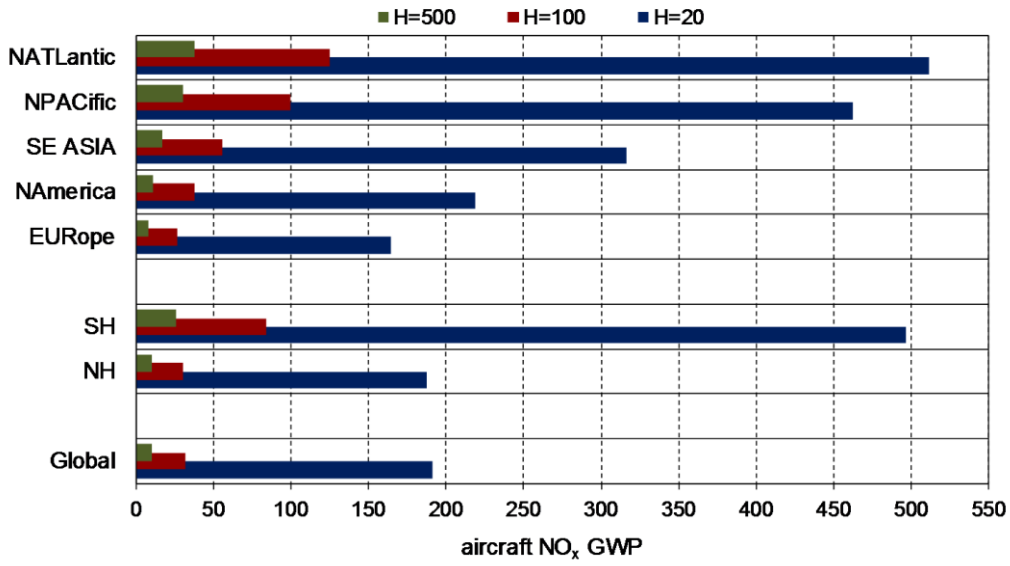

Figure 8.12: Aviation net NO_x GWPs for Northern and Southern Hemisphere and regions: Europe, North America, Southeast Asia, North Atlantic and North Pacific for 20-, 100- and 500-year time horizons. All values are on a per kg N basis relative to CO_2 and are based on 0.035 Tg(N)/yr aircraft NO_x increase experiments.

8.4 Discussion

The explanation for large O_3 response over remote oceanic regions might be unravelled by small background NO_x concentrations. The large O_3 response over SE ASIA might be additionally explained by the intensity of solar irradiance: taking into account the NO_x background conditions in this region, the magnitude of O_3 change is substantial. The mean concentration of NO_x at 227 hPa is 93 pptv. However, the NO_x emissions

from lightning over SE ASIA significantly modify its background at flight level, where mean local annual NO_x concentrations reach ~400 pptv, while these over mid-latitudinal regions are ~70 pptv (Figure 8.13a). Thus, indeed, intensity of solar flux, driving photochemistry, constitutes an important factor in local O_3 production.

The CH_4 perturbations depend highly on the place and extent (latitude and altitude) of the O_3 perturbation, as both temperature and concentrations of OH and CH_4 affect the efficiency of CH_4 oxidation (Köhler et al., 2008). The mean concentrations of OH and CH_4 at 227 hPa are 1.0 x 10^6 molecules cm^{-3} and 1717 ppbv, respectively; the mean temperature at 227 hPa is 220°K (Figure 8.13). The most efficient CH_4 lifetime reduction occurs over Southeast Asia, where OH concentrations and temperature are the greatest among the investigated domains. The concentrations of CH_4 differ between regions within 1% range. Despite the OH and CH_4 backgrounds are of similar magnitudes over NPAC and NATL, the temperature pattern reveals differences, being higher over North Pacific, by ~6°K (~3%). The lower temperature slows down the CH_4 oxidation, which might be the reason of the least efficient CH_4 lifetime reduction over North Atlantic.

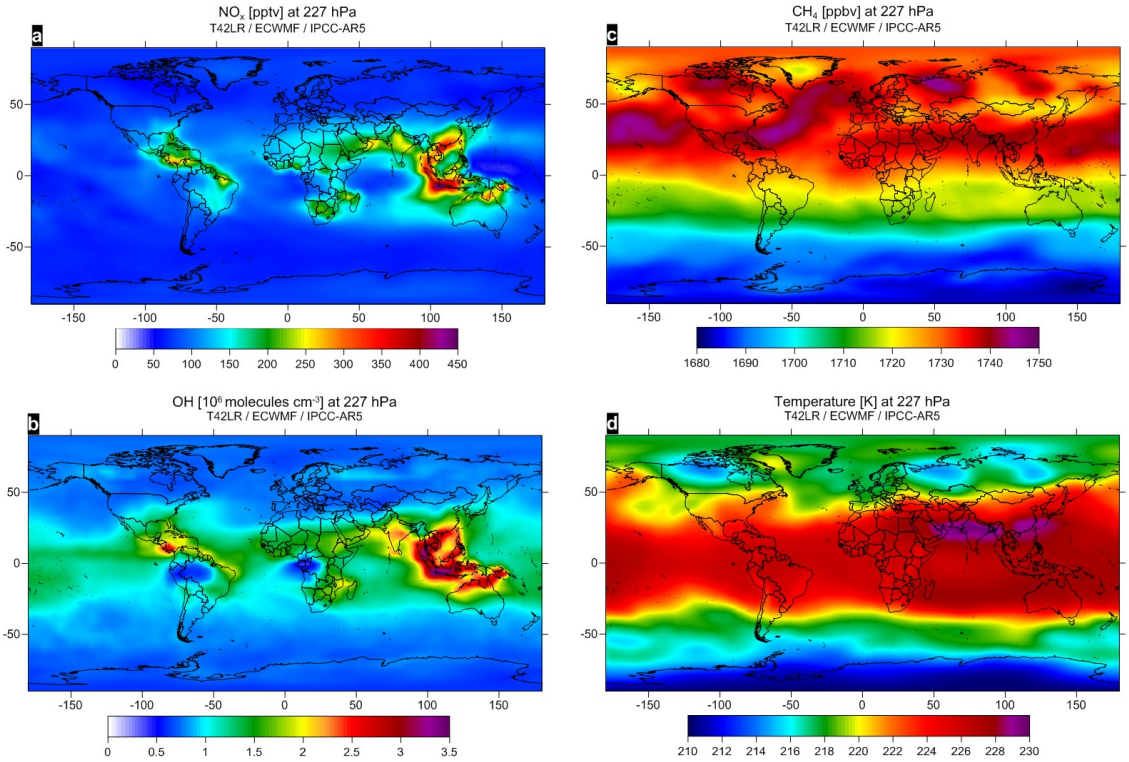

Figure 8.13: Annual mean distributions of NO_x (a), OH (b), CH_4 (c) concentrations and temperature pattern (d) at 227 hPa in 2006 modelled by MOZART-3.

The vast part of air traffic takes place in Northern Hemisphere, which results in a highly heterogeneous pattern of aircraft NO_x emissions, only ~8% belongs to the Southern Hemisphere (e.g. Figure 8.2). The response of the NO_x–O_3–CH_4 system consist of temporally diverse changes of its components; O_3 – short-lived and CH_4 – long-lived. Thus, it is expected the O_3 to roughly follow the NO_x source and the CH_4 perturbation to be more spread over the globe. In fact, 82% of increase of aircraft O_3 burden comes from the Northern Hemisphere, which is at the same time a dominant sphere for CH_4 lifetime reduction due to aircraft NO_x emissions, as only 31% of CH_4 reduction happens in Southern Hemisphere (Figure 8.14).

Both O_3 and CH_4 lifetime responses are found to be related to the hemisphere where the main NO_x source occurs. This behaviour is confirmed when aircraft NO_x emissions are injected in selected locations: for Europe, North America, North Pacific and North Atlantic more than 90% of O_3 and CH_4 is associated with Northern Hemisphere; for the Southern Hemisphere's NO_x emissions 88% of O_3 and 95% of CH_4 changes are related with this hemisphere.

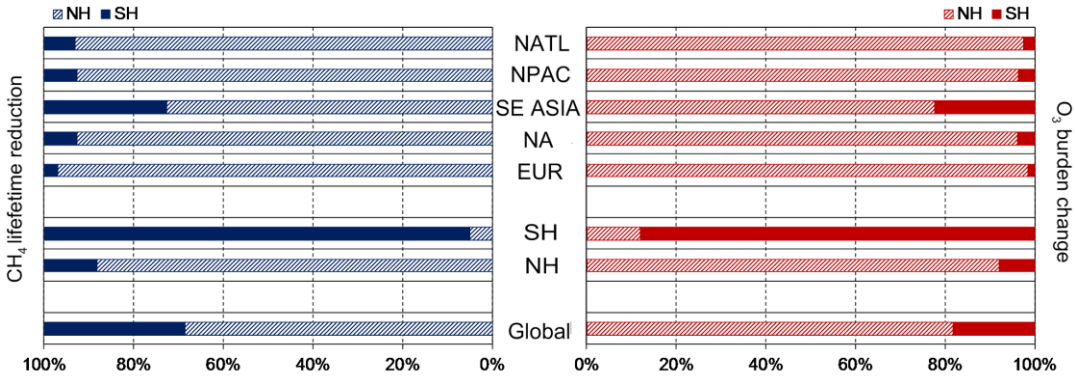

Figure 8.14: The O_3 burden change (right panel) and CH_4 lifetime reduction (left panel) in Northern and Southern Hemisphere for different aircraft NO_x emission locations.

The positive combined O_3+CH_4 forcings are associated with Northern Hemisphere and negative with southernmost latitudes for global aircraft NO_x perturbation (Prather et al., 1999). This geographical imbalance of the aircraft net NO_x effect is indirectly observed here. The CH_4 lifetime reduction is much more efficient in the Southern Hemisphere, where CH_4 changes per O_3 change are twice as large in Southern Hemisphere, compared with the Northern Hemisphere (Figure 8.15). Moreover, this effect is irrespective to the location of emission, which means that it is also the true for Southern Hemisphere as a NO_x emission receptor. These results suggest that aircraft

NO_x emissions have the potential to trigger the positive net NO_x RFs for the Northern Hemisphere and negative net NO_x RFs for the Southern Hemisphere's latitudes regardless of the aircraft NO_x emission location. Indeed, the aircraft NO_x emissions injected in Southern Hemisphere lead to the net NO_x RFs of 0.0[1] and 0.2 mWm^{-2} for SH and NH.

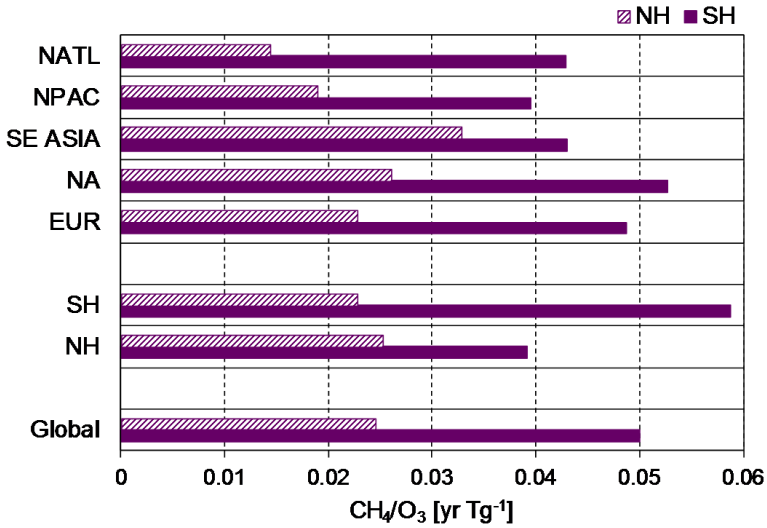

Figure 8.15: The absolute ratio of the CH_4 lifetime change to the O_3 burden change in Northern and Southern Hemisphere for different aircraft NO_x emission locations.

Recently Köhler et al. (2012) presented results for regional aircraft NO_x impacts from four regions: USA, Europe, India and China. The 0.036 Tg(N)/yr of aircraft NO_x was injected through all vertical layers into limited domains. The greatest O_3 mass change and O_3 forcings, as well as net NO_x forcings were found for low latitudinal regions and the net NO_x RFs and GWPs are positive. This is in agreement with results from this study. However, discrepancies appear when magnitudes of responses are compared. The continental mid-latitudinal O_3 chemical perturbation from this study are lower by ~16–20% and the low-latitudinal O_3 column change modelled by MOZART-3 is 50% weaker, than Köhler's et al. (2012). The magnitudes of O_3 RFs also differ and are smaller in this study by 17–29% for continental mid-latitudes and around twice smaller for low-latitudes. The net NO_x RFs differences are small for EUR (5%) and greater for NA, 28%. The geographical extent of low-latitudinal region taken into account in this study is different than Köhler's et al. (2012): here it reaches the 12°S circle of latitude,

[1] This is hemispherical mean; the sign of the net NO_x RF value changes to negative for 60-90°S latitudinal band.

in Köhler's et al. (2012) – 6°N. SE ASIA region in this study is characterized by very high NO_x background concentrations from lightning emissions, while Köhler's India and China are relatively 'free' from those high NO_x lightning emission, as modelled by MOZART-3 (e.g. Figure 8.12). This might be one of the reasons of the substantial differences in O_3 response and the resultant NO_x RFs over tropics.

The CH_4 lifetime change per unit O_3 change, as presented by Köhler et al. (2012), varies by 18%, between different regions of NO_x emission. This study presents similar range of regional differences, 20%, when continental regions are considered. However, by taking into account the oceanic locations, the variation in CH_4 lifetime change per unit O_3 change increases to 47% (Figure 8.7).

Whilst there is a general qualitative agreement in general properties of regional responses between Köhler et al. (2012) and this study, the comparison with Stevenson and Derwent (2009) becomes more complicated. Their study presents integrated radiative forcings (IRF) over 100-year time horizon of positive and negative responses of chemical system due to aircraft NO_x emissions. The aircraft NO_x increase (4 kg (NO_2) s^{-1} = 0.04 Tg(N)/yr) was injected for a period of month (July) at cruise altitudes (~200–300 hPa) in a limited geographical domains. Unfortunately, a detailed comparison is not possible as Stevenson and Derwent (2009) did not provide an exact number for their AGWPs. However, some peculiarities are noticed, e.g. the lowest O_3 IRFs values are observed for South Asia and the greatest for South Pacific; the smallest magnitudes of CH_4 IRFs are for Asia, next to North America and Europe and the most pronounced CH_4 reduction is observed for Pacific; the net IRFs are negative for most of the locations, with the greatest cancellation over Pacific and the smallest over South America. The certain characteristic of the model is visible in this case; however, other aspects exist as well.

Firstly, the aircraft NO_x increase was performed only for a period of one month, July. The small Asian short-term O_3 response may indicate that it can influence the results to some extent. The NO_x background (due to lightning) is much higher in this region during summer compared with winter months, when the lightning NO_x 'moves' more south from the equator. As an example on how a 'July's aircraft NO_x' may affect the results, the $AGWP_{100}$ were calculated for an annual mean and July perturbation based on the experiments performed with MOZART-3 (Table 8.3). It is observed that, when

July's numbers are derived, all values are greater, by ~50%, compared with yearly values (the photochemistry is much more efficient in northern latitudes in July, compared with the annual average); except the $AGWP_{100}$ for SE ASIA and SH, where July's calculations result in the reductions of calculated metrics by 18% and 2%, respectively. The response of a NO_x–O_3–CH_4 system is highly dependent on the state of the atmosphere into which aircraft NO_x is injected, thus, as it is shown above, a single month perturbation is not representative when the regional responses are investigated (even on the global scale a 35% difference in calculated values is observed).

Secondly, the amount of emitted NO_x during one month is the same as the amount of NO_x applied in this study and by Köhler et al. (2012), but for a period of year. As it was shown in chapter 8.3.2 the size of NO_x emission rates influence the regional response of the chemical system (Figures 8.6, 8.7).

Table 8.3: Calculated time integrated (H=100) radiative forcings of aircraft net NO_x (sum of positive and negative components) for annual mean perturbation and for July perturbation in different regions. Calculations are based on 0.035 Tg(N)/yr aircraft NO_x increase.

REGION	Year_ $AGWP_{100}$	July_ $AGWP_{100}$
Global	3.9	5.3
NH	3.7	5.7
SH	7.3	7.1
EUR	2.3	3.5
NA	3.3	5.1
SE ASIA	4.9	4.0
NPAC	8.7	17.6
NATL	10.8	20.1

8.5 Summary

The analyses presented in this chapter have shown how different locations of aircraft NO_x emission affect the sensitivity of global and hemispherical O_3 response and the compensating balance between O_3 and CH_4 perturbations. The spatial variation of O_3 burden change has a strong correlation with NO_x background concentration at flight level (Figure 8.16), which was also presented by Stevenson and Derwent (2009),

but for O_3 integrated RFs. Generally, the largest global and annual O_3 burden change is observed for locations where NO_x background is low and it is decreasing with greater NO_x concentrations. The SE ASIA, with large NO_x background, is an exception here, as the efficiency of O_3 production charged by the intensity of solar flux results in relatively large O_3 burden change. The July's correlation between aircraft O_3 change and NO_x background conditions confirms the effectiveness of sunlight in accelerating the photochemical reactions, as SE ASIA has lower ΔO_3 compared with low NO_x background northern location (Figure C.2, in Appendix C). Indeed, the efficiency of O_3 production depends on a mixture of various conditions (Appendix C, Figure C.2).

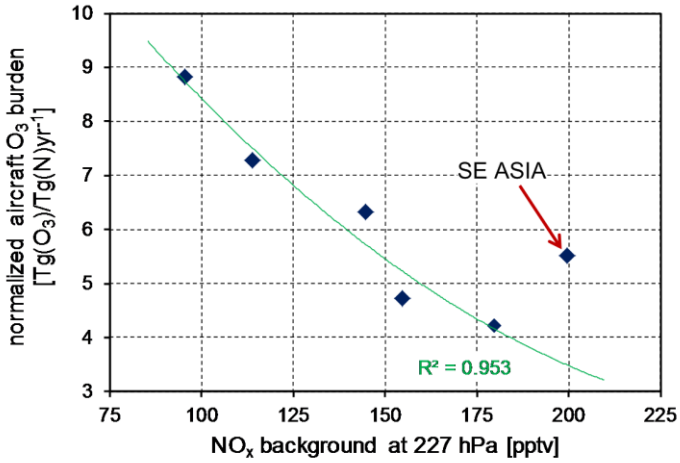

Figure 8.16: Scatter plot of global and annual O_3 burden change due aircraft NO_x emission increase by 0.035 Tg(N) yr^{-1} in different regions against background NO_x concentration at 227 hPa (dots are individual experiments, line is the best-fit curve).

The sensitivity of regional chemical responses varies with size of aircraft NO_x emissions (Figure 8.7), being especially pronounced over remote domains. The global O_3 and CH_4 responses saturate with greater aircraft NO_x emission rates (e.g., Figure 7.4). This saturation effect is also observed for regional dependencies (Chapter 9.4), where scale of this processes reach different limits for each region. Therefore, regional application of an equal mass of emission implies violation of the subtle balance of local NO_x–O_3–CH_4 system. The question addressed with 'fixed NO_x' experiments is the regional sensitivities to unit mass of emission. If the regional values of climate impact are required, then, experiments where the balance of local NO_x–O_3–CH_4 system is treated 'equally' should be applied and this is addressed in Chapter 9.

Chapter 9

Variation of the effect of regional aviation NO_x emissions – the revisited approach and its implications

9.1 Introduction

The sensitivity of global chemical response varies with size of the aircraft NO_x emissions and saturates at greater NO_x emission rates (e.g. Figure 7.4). Also, the varying regional chemical responses depends on the size of the aircraft NO_x emissions (Figure 8.7), being especially pronounced for regions with low background NO_x concentrations. Equal mass of aircraft NO_x emissions leads to substantially different relative increases of aircraft NO_x (Table 8.1, 9.1), which means that each regional domain is pushed to different regimes of its local NO_x–O_3–CH_4 system balance, when it 'deals' with additional NO_x.

In order to give an 'equal chance' for regions to respond to aircraft NO_x emissions and to estimate the un-biased values of regional aircraft net NO_x RFs and GWPs the experiments with equal relative aircraft NO_x emissions are employed . Additionally, separate calculations were performed in order to explore how the inclusion of regional aircraft NO_x responses into a global estimates influence the calculated metrics.

9.2 Methodology

9.2.1 Incremental aircraft NO_x emissions and experimental design

The relative incremental aircraft NO_x emissions were applied for a period of year to seven regions: Northern Hemisphere (NH), Southern Hemisphere (SH), Europe (EUR), North America (NA), Southeast Asia (SE ASIA), North Pacific (NPAC) and North Atlantic (NATL) (geographical extents of these regions are the same as in Chapter 8, Table 8.1). Incremental aircraft NO_x emissions were applied to one region per experiment. The injections of aircraft NO_x emissions are valid for all altitudes in the defined domains. Two different cases of incremental aircraft NO_x emission were applied: 5% (N) yr^{-1} and 100% (N) yr^{-1}. This constitutes different addition of mass of aircraft NO_x emission in each region, which for some regions is substantially different than 0.035 Tg(N) yr^{-1} experiments (Table 9.1). The 5% NO_x increase per year reduces the incremental aircraft NO_x emissions by ~80–95% compared with 0.035 Tg(N) yr^{-1} case for most regions. The 100% NO_x increase per year is greater than 0.035 Tg(N) yr^{-1} by ~70% for continental regions, but it is still smaller by ~40% for oceanic regions.

Table 9.1: The amount of emitted aircraft NO_x in each region in Tg(N) yr^{-1} (second column) and in % yr^{-1} (third column) is given. The two last columns present the increase (in Tg(N) yr^{-1}) of aircraft NO_x for two cases of relative incremental aircraft emissions, 5% and 100%, in each region. In the bracket the difference between the % (N) and 0.035 Tg(N) increases is shown.

REGION	Aircraft NO_x		Δ aircraft NO_x [Tg(N) yr^{-1}] ($\Delta \frac{\%N-0.035TgN}{0.035TgN}$)	
	[Tg(N) yr^{-1}]	[% yr^{-1}]	5% yr^{-1}	100% yr^{-1}
Global	0.71	100	0.035 (0%)	0.71 (+19.0)
NH	0.653	92	0.033 (-0.08)	0.653 (+17.4)
SH	0.057	8	0.003 (-0.92)	0.057 (+0.61)
EUR	0.112	16	0.006 (-0.84)	0.112 (+2.15)
NA	0.132	19	0.007 (-0.81)	0.132 (+2.71)
SE ASIA	0.128	18	0.006 (-0.82)	0.128 (+2.60)
NPAC	0.021	3	0.001 (-0.97)	0.021 (-0.40)
NATL	0.023	3	0.001 (-0.97)	0.023 (-0.35)
REST	0.294	41	0.015 (-0.58)	0.294 (+7.29)

9.2.3 Incorporation of aircraft NO_x regionalities into global estimates

The experiments with regional 5% yr^{-1} and 100% yr^{-1} incremental aircraft NO_x emissions were exploited. An additional geographical domain was defined (REST) covering all the longitude-latitude-altitude grids outside of the EUR, NA, SE ASIA, NATL, NPAC domains. The aircraft NO_x emissions characteristic for region REST along with the relative incremental aircraft NO_x emissions are presented in Table 9.1.

The magnitudes of the impact of aircraft NO_x are calculated in three different ways:

- global NO_x emissions, globally calculated and averaged aircraft deltas (chemical, RFs, AGWPs) (called later as Global),
- hemispherical NO_x emissions, hemispherically calculated aircraft deltas (chemical, RFs, AGWPs), then averaged globally (called later as Hemispherical),
- regional NO_x emissions, regionally calculated aircraft deltas (chemical, RFs, AGWPs), then averaged globally (called later as Regional).

Through relative increases in each region the sums of aircraft NO_x emissions in each, Global, Hemispherical and Regional, case are the same. Below the schematic structure for 5% yr^{-1} incremental aircraft NO_x case is presented:

$$5\%\_avi\_NO_x = 5\%\_avi\_NO_x^{Global} = 5\%\_avi\_NO_x^{Hemispherical} = 5\%\_avi\_NO_x^{Regional} = 0.035\ Tg(N)\ yr^{-1},$$

where:

$$5\%\_avi\_NO_x^{Global} = Global^{5\%\_NO_x},$$

$$5\%\_avi\_NO_x^{Hemispherical} = NH^{5\%\_NO_x} + SH^{5\%\_NO_x},$$

$$5\%\_avi\_NO_x^{Regional} = EUR^{5\%\_NO_x} + NA^{5\%\_NO_x} + SE\ ASIA^{5\%\_NO_x} + NPAC^{5\%\_NO_x} + NATL^{5\%\_NO_x} + REST^{5\%\_NO_x}.$$

The amount of emitted aircraft NO_x is the same for each 5%_avi_NO_x case (and consequently for 100%_avi_NO_x case), thus the influence of differences in the treatment of aircraft NO_x emissions and its effects (Global vs Hemispherical vs Regional) on the calculated chemical response, radiative forcing or global warming potential can be investigated.

9.2.2 Experimental design

The REACT4C, aircraft emission dataset, was implemented into the 3D CTM, MOZART-3. Nineteen experiments were performed, one reference (base aircraft emission) run and eighteen perturbation (incremental aircraft emission) simulations, each starting in January 2006 and finishing in December 2006; each simulation was preceded by a multi-year spin-up, 2000–2005. The aircraft perturbation is derived by extracting the difference between 'aircraft' and 'incremental aircraft' experiments.
The details regarding model set-up, aircraft emission dataset, surface emissions and dynamical data applied for this study are described in Chapter 3.3. The description of radiative forcings and global warming potentials calculations is presented in Chapter 3.2.

9.3 The linearity of chemical responses to regional aircraft NO_x emissions

The global O_3 burden changes linearly with additional NO_x emissions up to ~1.42 Tg(N) yr^{-1}, which constitute 100% incremental aircraft NO_x emissions increase. The deviation from linearity was found to be -7%. The O_3 burden changes from regional aircraft NO_x emissions also are calculated to be relatively linear, with certain deviations from 1:1 relation (Figure 9.1). The annual average O_3 response appears to be the most linear for SE ASIA and EUR where the annual mean value between 5% x 20 and 100% experiments differ by 0.3%, 3.5%, respectively. NA's O_3 change for 100% NO_x increase is 10% lower than for 5% x 20, similarly as NPAC, but the difference increases to 18%. NATL is the only region, where the variation in resultant O_3 is relatively large, 35% and it rises to 53% for winter months (DJF). The NATL O_3 burden change for 100% aircraft NO_x emission increase is significantly greater than the resultant O_3 form 5% x 20 case. In general, for remote oceanic regions (NPAC, NATL) and for EUR the deviation from linearity is increasing during winter and it is decreasing during the summer months (JJA). The opposite pattern, non-linearity is greater in the summer than during the winter, is observed for NA and SE ASIA.

Despite these deviations from linear response exist for regional aircraft O_3 responses, there are not as much pronounced, as the observed non-linearities of tropospheric O_3 changes due to surface anthropogenic NO_x reductions over North America and East Asia (Wu et al., 2009). These non-linearities are significantly less pronounced during the summer, which is inconsistent with aircraft NA and SE ASIA O_3 changes.

The values of CH_4 lifetime change per O_3 burden change are always greater for 100% aircraft NO_x increase than 5% x 20 case. Whilst the difference for continental regions varies from 5% for SE ASIA to 7% for NA, it becomes substantial for oceanic regions as it constitutes 42% for NPAC and 45% for NATL. This suggest that application of greater NO_x emission rates, which definitely is the case for 0.035 Tg(N) yr^{-1} over NPAC and NATL, might significantly decrease their net NO_x RFs.

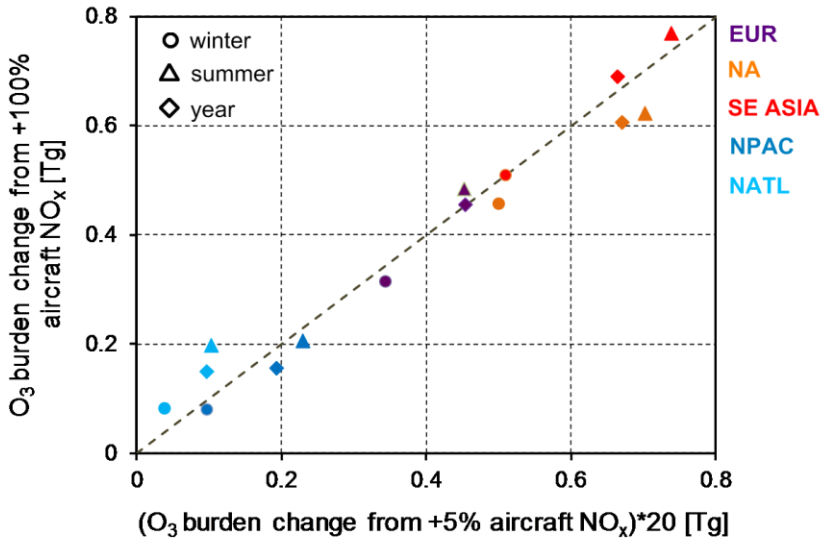

Figure 9.1: Ozone burden changes (in Tg) due to incremental aircraft NO_x emissions in different regions. The abscissa shows the responses from 5% x 20 NO_x increase and the ordinate shows the responses from 100% NO_x increase. The linear (1:1) relationship is presented by dashed line.

9.4 Variations of radiative forcings and global warming potentials for different rates of regional aircraft NO_x emissions

The global O_3 production efficiency and the efficiency of CH_4 lifetime reduction change with varying sizes of aircraft NO_x emission (e.g. Figure 7.7). This influence the resultant aircraft net NO_x RFs and GWPs, which magnitudes are, in general, decreasing with increasing aircraft NO_x emission rates. The similar pattern, to some extent, is observed on a regional scale.

The net NO_x radiative forcing from regional perturbations are found to be greater for experiments with lower aircraft NO_x emission rates, which is the 5% (N) yr^{-1} case and tend to decrease with greater aircraft NO_x emissions (Table 9.2). The net NO_x RFs of EUR, NA and NATL are larger by ~30% for 5% (N) yr^{-1} compared with 0.035 Tg(N) yr^{-1}, the difference for NPAC's net NO_x RF increases to 56%. The short-term O_3 RF variation ranges from 10% for EUR to 22% for NPAC; CH_4 RF variation ranges from up to 10% for continental regions and rises significantly for oceanic regions reaching 69% for NATL. In general, for smaller aircraft NO_x emissions rates short-term O_3 RF is calculated to be the greatest and CH_4 RF, and consequently CH_4-induced O_3 RF and SWV RF are calculated to be the smallest (less negative) compared with greater aircraft NO_x emissions rates, as it was observed on a global scale.

Table 9.2: Normalized regional aircraft net NO_x radiative forcings for different incremental aircraft NO_x emissions. Net NO_x accounts for short-term O_3 RF, CH_4-induced O_3 RF and CH_4 with SWV RF.

REGION	Net NO_x RF [mW m^{-2}/Tg(N) yr^{-1}]		
	0.035 Tg(N) yr^{-1}	5 %(N) yr^{-1}	100 %(N) yr^{-1}
Global	3.96	3.96	3.06
NH	3.41	3.46	3.22
SH	7.31	9.91	6.71
EUR	2.29	3.52	1.93
NA	3.26	4.29	3.20
SE ASIA	4.87	4.61	4.96
NPAC	8.67	19.91	9.64
NATL	10.86	14.52	12.59

There is one exception, SE ASIA: the values of net NO_x RFs for different incremental aircraft NO_x emission cases stay within a ~5% range and they are increasing with increasing NO_x emission rates. The same is observed for short-term O_3 RF, which is 10% lower for 5% (N) yr^{-1} compared with 0.035 Tg(N) yr^{-1}, and 2% different for 100% (N) yr^{-1} compared with 0.035 Tg(N) yr^{-1}.

The background atmospheric conditions of SE ASIA domain might explain this distinct behaviour. The HO_x background at flight level over SE ASIA is the highest among all investigated regions (Figure C.2 in Appendix C), having at the same time low NO_x background (< 1 pbbv). Under this condition an important termination chain for HO_2 would be HO_2 + HO_2 (Seinfeld and Pandis, 2006). This finds a further explanations in Lin et al. (1988) box model study, where it is shown that for low NO_x background the radical combination reactions (RO_2 and HO_2) supress the non-linearity of O_3 production efficiency.

The regional ratios of the CH_4 lifetime change per O_3 burden change vary, as observed on a global scale (Figure 7.11), with different sizes of emitted aircraft NO_x and they decrease with increasing aircraft NO_x emissions (Figure 9.2). The greatest differences are found to be over oceans, where the CH_4 lifetime change per O_3 burden change varies by 54% for NATL and 47% for NPAC between aircraft emissions of 0.71 and 1.42 Tg(N) yr^{-1}; the continental (EUR and NA) differences constitute ~10% between 0.71 and 1.8 Tg(N) yr^{-1}. The CH_4 lifetime change per O_3 burden change for SE ASIA varies only by 3% for different aircraft NO_x emissions rates, which results in relatively constant magnitudes of net NO_x RFs (Table 9.2). Similarly as for global net NO_x GWPs, the regional metric values are significantly correlated with ratio of CH_4 lifetime change per O_3 burden change ($r=0.7$, $p<0.001$). The remote oceanic regions, with small CH_4 lifetime change per O_3 burden change values, give larger net NO_x GWPs than continental regions with greater CH_4/O_3 ratios. Similarly as for global GWPs, regional aviation net NO_x GWPs decrease with increasing aircraft NO_x emissions (consequently, the SE ASIA is again an exception).

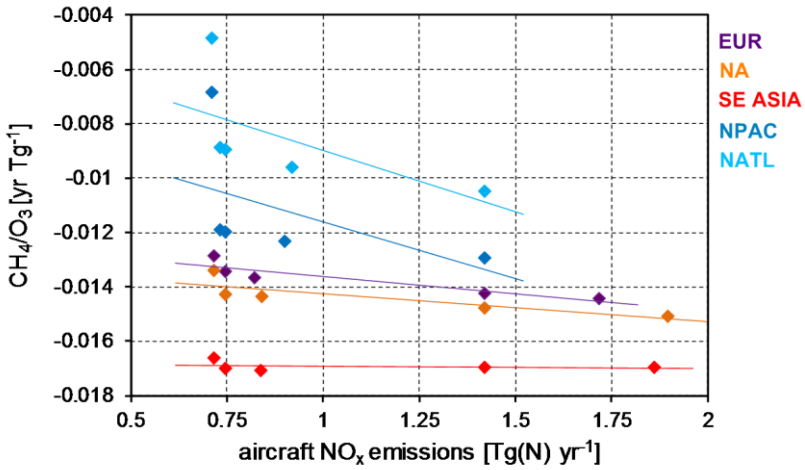

Figure 9.2: Scatter plot of CH_4 lifetime change per O_3 burden change for different regions and a series of aircraft NO_x emission (dots are individual experiments, lines are the linear best fit lines).

The spread in the reported regional net NO_x RFs and GWPs differs between different experimental designs (Figure 9.3). Experiments with 0.035 Tg(N) yr^{-1} have shown reduced variability of calculated metrics, mainly through supressed NPAC response. The aviation net NO_x GWP varies from 26 (EUR) to 125 (NATL) for 0.035 Tg(N) yr^{-1} incremental aircraft NO_x emissions experiments. The 5% (N) yr^{-1} incremental aircraft NO_x emissions case result in a new values ranging from 41 for EUR to 229 for NPAC.

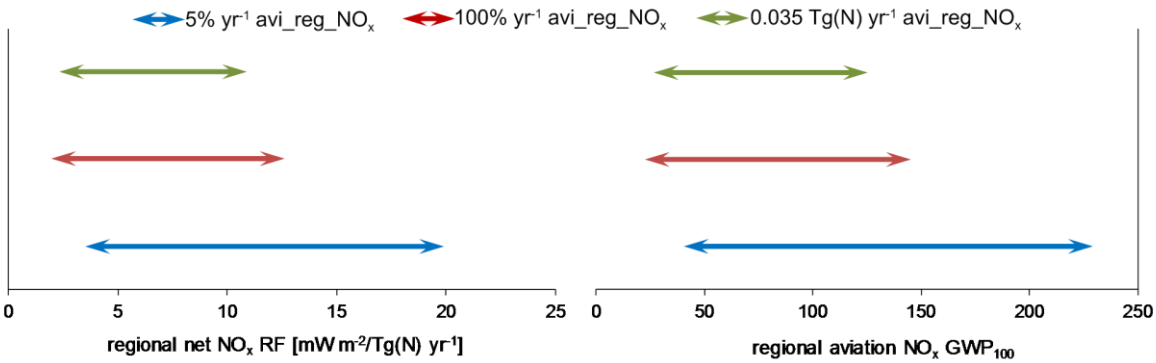

Figure 9.3: The spread in regional aviation net NO_x RFs (left) and aviation net NO_x GWPs (right) for different incremental aircraft NO_x emission, 5% (N) yr^{-1}(blue), 100% (N) yr^{-1} (red) and 0.035 Tg(N) yr^{-1} (green).

9.5 Incorporation of aircraft NO_x regionalities into a global metrics

Usually metrics utilize globally averaged estimates from globally averaged input. An aircraft NO_x perturbation leads to production of a heterogeneous pattern of chemical and radiative forcing responses and results in various sensitivities of changes depending on the location of emission. This is why an attempt to include this spatial variation in responses appeared. Previous chapters have shown the climate metrics for aircraft NO_x impacts based on global input and global estimates (Chapter 6, 7), as well as on regional input and global estimates (Chapter 8 and 9.4). Here an attempt of one step forward is presented and the climate metrics (RFs and GWPs) for aircraft net NO_x impact from regional input and regionally calculated responses are derived.

Different treatments of NO_x emissions and differences in calculations of chemical responses lead to disparity in estimates of O_3 burden change and CH_4 lifetime reduction (Table 9.3). The values based on global emissions and global calculations are the largest for aircraft O_3 burden change, whilst, for aircraft CH_4 lifetime reduction, the values based on regional emissions and regional calculations are the largest. The magnitude of O_3 burden change is affected mainly in Regional case, where values decrease by 47% and 45% for 5% (N) yr^{-1} and 100% (N) yr^{-1}, respectively, compared with Global case. The Hemispherical case decreases the O_3 burden change by 8% and 9% for 5% (N) yr^{-1} and 100% (N) yr^{-1}, respectively. The CH_4 lifetime reduction for Hemispherical case is found to be weaker by 7% and 9%, than global averages, for 5% and 100% (N) yr^{-1} incremental aircraft NO_x emissions, respectively. The Regional case increases the CH_4 lifetime reduction by 8% for both for 5% and 100% (N) yr^{-1}. Regional aircraft NO_x emissions modify the O_3 concentration fields, but not necessarily the chemical response is located in the receptor domain. Often the vast part of aircraft O_3 change is observed, due to meridional transport of aircraft NO_x perturbation (Appendix C, Figure C.1), outside of region where NO_x emissions were emitted (e.g. Figure 8.5). Thus, some mass of aircraft O_3 changes is lost for Hemispherical and Regional cases. Table 9.3 gives also an insight on how different might be the oxidizing environment of the atmosphere when it is analysed on the regional and global scale.

This fact that not all aircraft O_3 changes are captured through regional calculations of regional input affect also the resultant short-term O_3 RFs (Table 9.4). The Hemispherical and Regional O_3 RFs are ~10% and ~65%, respectively, lower than Global magnitudes. However, when the respective regional calculations are performed based on a global NO_x emissions input, the short-term O_3 RFs are 45% greater than the Global estimates. This visualise the challenges arising when dealing with short-lived species, as theoretically the more detailed study should allow to observe the more detailed patterns; the balance between the nature of investigated substances and the complexity of applied method is needed.

Table 9.3: The global and annual mean O_3 burden change (in Tg) and the CH_4 lifetime reduction (in yr) due to the aircraft NO_x emissions as a results of different treatment of aircraft NO_x emissions and calculated responses: global, hemispherical (NH+SH) and regional (EUR+NA+SE ASIA+NATL+NPAC+REST) for different incremental aircraft NO_x emissions.

Incremental case	NO_x treatment	O_3 burden change (Tg)	CH_4 lifetime change (yr)
5% (N) yr^{-1}	Global	0.18	-0.0026
	Hemispherical	0.17	-0.0024
	Regional	0.10	-0.0028
100% (N) yr^{-1}	Global	3.38	-0.0511
	Hemispherical	3.06	-0.0466
	Regional	1.85	-0.0555

Table 9.4: The short-term O_3 RF due to the aircraft NO_x emissions as a results of different treatment of aircraft NO_x emissions and calculated responses: global, hemispherical (NH+SH) and regional (EUR+NA+SE ASIA+NATL+NPAC+REST) for different incremental aircraft NO_x emissions.

Incremental case	NO_x treatment	Short-term O_3 RF [mW m^{-2}/Tg(N) yr^{-1}]	
		Global NO_x emissions–globally calculated ΔO_3 averages	
5% (N) yr^{-1}	Global	16.7	
100% (N) yr^{-1}		15.3	
		Regional NO_x emissions–regionally calculated ΔO_3–averaged globally	Global NO_x emissions–regionally calculated ΔO_3–averaged globally
5% (N) yr^{-1}	Hemispherical	15.3	16.7
	Regional	5.6	31.0
100% (N) yr^{-1}	Hemispherical	13.9	15.3
	Regional	5.5	28.0

The calculated net NO_x RFs for different NO_x treatments show continuation of these peculiarities: Hemispherical and Regional values are ~3% and ~155% smaller than Global RF magnitudes (Table 9.5). Whilst the Hemispherical net NO_x RF is, to great extent, consistent with Global estimates; the Regional net NO_x RF shows significant discrepancy, where even a sign changes to negative. This can be explained by the fact that short-term O_3 RFs are more than twice smaller for Regional estimates than the global averages. Additionally, there is a greater CH_4 lifetime reduction and thus stronger negative CH_4 RF response for Regional case. All these aspects reduce the magnitude of Regional net NO_x RF compared with Global and Hemispherical estimates.

Table 9.5: The aviation net NO_x RFs and GWPs as a results of different treatment of aircraft NO_x emissions and calculated responses: global, hemispherical (NH+SH) and regional (EUR+NA+SE ASIA+NATL+NPAC+REST) for different incremental aircraft NO_x emissions.

Incremental case	NO_x treatment	Net NO_x	
		RF [mW m^{-2}/Tg(N) yr^{-1}]	GWP_{100}
5% (N) yr^{-1}	Global	4.79	55
	Hemispherical	4.59	52
	Regional	-2.71	29
100% (N) yr^{-1}	Global	3.78	44
	Hemispherical	3.69	42
	Regional	-2.10	23

The relation between Global, Hemispherical and Regional estimates changes again, when different treatments of NO_x emissions and their effects are applied to GWP calculations. The regional effectiveness in aircraft chemical and RF responses per emitted N is significantly larger than the 'global potential' and the 'strength' is hidden especially over the remote locations, like SH, NPAC or NATL (Figure 9.4). The AGWP is a normalized value, thus, in order to deal with potentials of regional NO_x RF responses, the weighted (by emission of NO_x in each region) averages are applied for Hemispherical and Regional GWP calculations. The Hemispherical net NO_x GWP_{100} is, similarly as net NO_x RFs, in the same range of magnitudes as Global estimate: the differences are 5% and 2.5% for 5% and 100% (N) yr^{-1}, respectively (Table 9.5). The Regional net NO_x GWP_{100} decrease substantially being 47% and 48% smaller, for 5% and 100% (N) yr^{-1}, respectively, than Global net NO_x GWP_{100}.

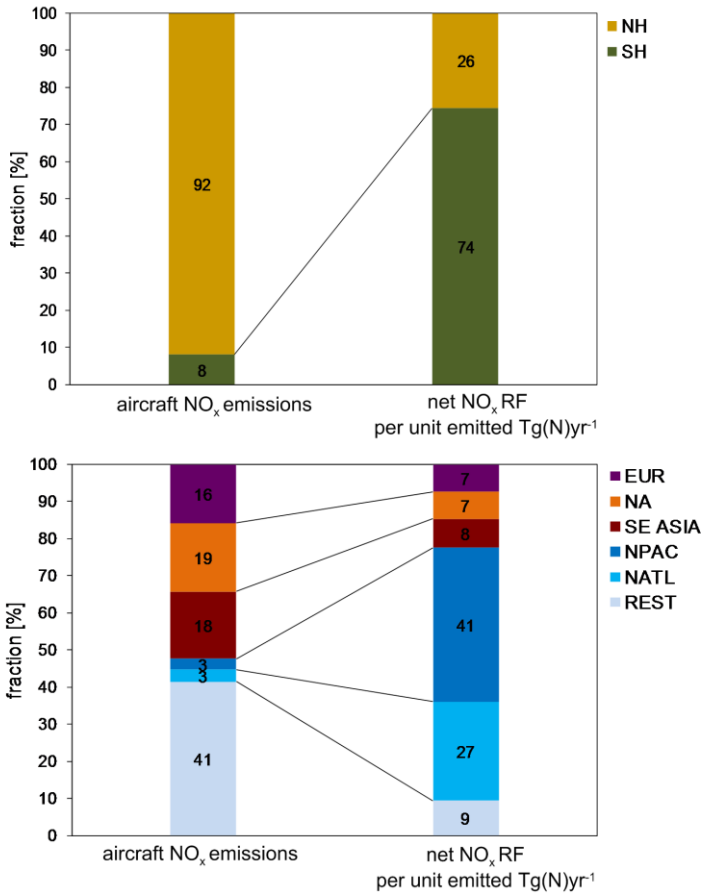

Figure 9.4: Regionally normalized (per unit emission of N) contributions (in %) of Northern and Southern Hemispheres (upper panel) and different regions (bottom panel) to the aircraft net NO_x RF. Based on 5% (N) yr^{-1} incremental aircraft NO_x emission experiments.

Indeed, different treatment of aircraft NO_x emissions and calculation of their effects influence the derived estimations. The dependencies between Global, Hemispherical and Regional magnitudes are driven by various factors, affecting this relation at different stages of calculated metrics. The inclusion of regionalities into a global metrics might be useful, but the methods to achieve this need to be applied with care, as well as the motivation of such procedure. Lund et al. (2012) highlighted that for transport sectors, taking into account regionalities in the calculations might become an important issue when this sector is considered in isolation, but it turns to be of importance when its climate impact is assessed in connection with an overall climate response.

Chapter 10

Overall summary of results

The series of global and regional aircraft NO_x experiments were conducted using 3D CTM, MOZART-3. The dependence of aviation NO_x effects on various factors, such as surface emissions of ozone precursors, aircraft inventories, the amount of emitted aircraft NO_x and region of aircraft NO_x emissions, have been shown (Chapters 5, 6, 7, 8, 9). A substantial variation in the relation between aircraft responses of O_3 and CH_4 were found: 82 different ratios of CH_4 lifetime change per O_3 burden change were derived in 82 CTM experiments. Consequently, a wide spectrum of aircraft net NO_x RFs and GWPs were calculated: 59 different experiments led to 59 different GWP values (Figure 10.1) with magnitudes ranging from positive (95% of results) to negative (5% of results).

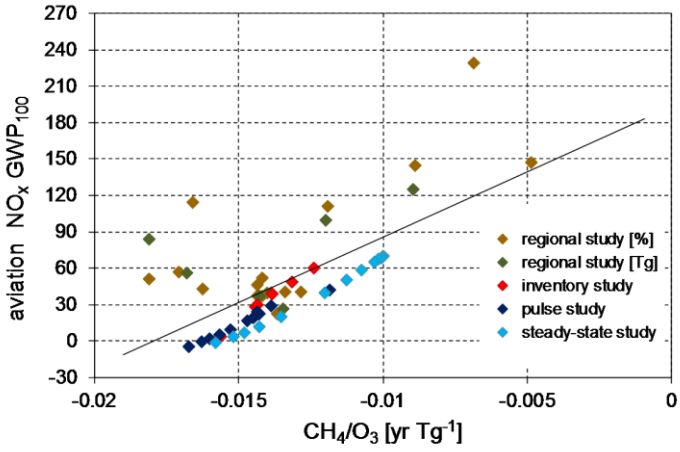

Figure 10.1: Scatter plot of aviation NO_x global warming potentials for 100-time year horizon against ratios of CH_4 lifetime change per O_3 burden change for global and regional aircraft NO_x perturbations (dots are the individual experiments, line is the linear fit line).

10.1 Do the surface emissions of ozone precursors influence the effect of aircraft NO_x emissions?

The effect of aircraft NO_x emissions depends on the condition of the atmosphere into which NO_x is injected. The results from Chapter 5 show that modified surface emissions of ozone precursors (NO_x, CO, NMVOC) alter the chemical perturbations from the aircraft NO_x perturbation. The 30% reductions of anthropogenic and biomass burning NO_x, CO and NMVOC fluxes were applied, while aircraft NO_x emissions were kept constant. Reductions of surface NO_x emissions decrease OH concentrations, increasing CO and CH_4 abundance. On the contrary, reductions of CO and NMVOC increase OH level, decreasing CH_4 lifetime by 3.4% and 0.7%, respectively. Reductions of surface NO_x, CO and NMVOC emissions caused the decrease of tropospheric O_3 concentrations. The resultant changes from surface emissions also affect the upper troposphere, where aircraft NO_x emissions are released. The greatest sensitivity of aircraft O_3 and CH_4 responses to modified background conditions were calculated for 30% reduction of surface NO_x emissions: the O_3 burden change increased by 20% along with the increase of CH_4 lifetime reduction by 46%. The 30% reductions of surface CO and NMVOC affected aircraft NO_x response with similar sensitivity, causing decrease of aircraft O_3 burden change by 3% and 4% and decrease of aircraft CH_4 lifetime reduction by 7% and 5%, respectively. The NO_x background conditions efficiently influenced aircraft O_3 response: the smaller NO_x concentrations the greatest O_3 change. However, aircraft NO_x emissions were found to be even more efficient (by 11% for 50% of reduced NO_x) in affecting O_3 changes.

10.2 Can aircraft inventories explain the variation in estimates of aircraft NO_x impact on RF?

Comparative modelling studies have usually focused on the inter-model variability, using the same emission databases. Chapter 6 presents a novel approach of using a single model with various aircraft emissions. Six different aircraft NO_x emission inventories were normalized to give the same global emissions of NO_x and were analysed using MOZART-3. Each of the emission datasets have slightly different assumptions and therefore vertical distributions of emissions. The normalized NO_x emissions differed by 23% at cruise altitudes, 283–200 hPa, where most of the aircraft

NO_x occurs in MOZART-3. The resultant short-term O_3 chemical perturbation varied by 15% and each of the datasets led to different O_3 production efficiency, being the greatest for inventories with more NO_x emissions at higher altitudes. The largest O_3 aircraft perturbation did not introduce the greatest CH_4 reduction, as the relationship between O_3 and CH_4 change is a function of altitude of NO_x emission; thus, it is inventory dependent. Once all the positive and negative effects were accounted for, the variability of the net NO_x radiative forcing reached 94%. Using these radiative effects to formulate a net aviation NO_x GWPs for 100-year time horizon resulted in values ranging from 60 to 4. The spread between aircraft NO_x estimates arising from usage of different aircraft inventories, and their vertical distribution of emissions, potentially explains a significant range of uncertainty in estimates of an overall aviation NO_x RF.

10.3 Why is there a significant discrepancy in the reported values of an aircraft NO_x GWP?

The magnitudes of aviation NO_x GWPs reported in the literature not only vary greatly in magnitude, but also in sign, from positive to negative. Chapter 7 presents some peculiarities of NO_x–O_3–CH_4 system, which reveal the explanation of these disparities. The response of the chemical system varied with the amount of aircraft NO_x emission and in a non-linear way. The aircraft O_3 perturbation along with CH_4 lifetime reduction saturated at higher aircraft NO_x emission rates, in accordance with current understanding of atmospheric chemistry. However, the extent of these effects was different and O_3 saturation was more pronounced than the weakening of CH_4 reduction. This resulted in a decreasing ratio of CH_4 lifetime reduction per O_3 burden change with greater aircraft NO_x emissions. A strong and significant ($r=0.99$, $p<0.001$) correlation between the variance in CH_4/O_3 dependencies and global aircraft NO_x GWPs was found. Consequently, the substantial diversity of aviation GWPs, with magnitudes ranging from positive to negative, net NO_x GWP_{100} varied from 22 to -4, could be reproduced with the same model and emissions distribution. Thus, even with one model and consistent experimental design, it was not possible to determine a unique value for an aviation NO_x GWP. Additionally, the magnitudes of aircraft net NO_x GWPs increase with reduction of aircraft NO_x emissions and decrease with increasing aircraft NO_x emissions.

10.4 What are the variations of the effect of regional aircraft NO_x emissions?

Aircraft NO_x emissions injected into different geographical locations affect the sensitivities of global and hemispherical chemical responses and the compensating balance between O_3 and CH_4 changes, as it was shown in Chapters 8 and 9. The resultant O_3 burden change varied by 42% between different regions; the aviation net NO_x GWP_{100} varied from 21 for Europe to 125 for the North Atlantic (based on 0.035 Tg(N) yr^{-1} incremental aircraft NO_x emission experiments). Significant hemispherical disparity in the resultant effects from aircraft NO_x perturbation was also found, where the net NO_x GWP_{100} for Northern and Southern Hemisphere differed by 49%, being greatest for the Southern Hemisphere. The dependence between spatial variation of O_3 burden change and NO_x background was shown: O_3 response decreases with greater NO_x concentrations.

Similarly as for global responses, regional chemical perturbations also varied with size of aircraft NO_x emission rate. Therefore, experiments based on equal mass of aircraft NO_x emissions applied into different regions leads to biased regional dependencies. This affects mainly geographical domains with low NO_x concentration (e.g., remote oceanic regions), where injected NO_x often constitutes a significant relative increase, which pushes the local NO_x–O_3–CH_4 balance into a saturation regime and reduces its aircraft NO_x effect. The experiments with equal relative aircraft NO_x emissions revealed the 'real' potential of regional aircraft NO_x effects. The 5% (N) yr^{-1} incremental aircraft NO_x emission case resulted in a net aviation NO_x GWP_{100} ranging from 41 for Europe to 224 for North Pacific.

The regional ratios of CH_4 lifetime change per O_3 burden change decrease with increasing aircraft NO_x emissions: the remote oceanic regions experienced the most substantial variation (54–47%) compared with more stable continental regions (~10% of divergence). This pattern affects the magnitudes of resultant metrics, which were found to be smaller for greater aircraft NO_x emissions. The only region, among investigated, which was an exception to the above dependencies, is Southeast Asia, where the non-linearity of NO_x–O_3–CH_4 system was found to be supressed. The CH_4 lifetime change per O_3 burden change varied by only 3% and the calculated RF and GWP values were almost insensitive to the amount of emitted aircraft NO_x emissions.

Chapter 11

Conclusions and recommendations for further work

The impact of aircraft NO_x emissions on a coupled NO_x–O_3–CH_4 system was investigated and some previously unexplored uncertainties associated with aircraft NO_x estimates were identified. The applied framework, which consisted of two main tools, 3D CTM MOZART 3 and RTM Edwards–Slingo, have been found suitable for representing aircraft responses properly and in agreement with other studies, both on a global and regional scale. The aircraft net NO_x effects estimated in this study arise from four components, short-term O_3, CH_4-induced O_3, CH_4 and CH_4 impact on SWV, which differ in their spatial and temporal scale of responses. This study has shown that a consistent consensus in aviation net NO_x estimates is going to be a difficult to achieve due to the intrinsic characteristics of NO_x chemistry. The aircraft NO_x uncertainties originate not only from inter-model differences (Myhre et al., 2011) or background NO_x concentrations (Holmes et al., 2011), but also the usage of different aircraft NO_x inventories and the size of emitted aircraft NO_x contribute to these disparities (Figure 11.1). The increasing uncertainty with increasing policy and societal relevance is a conventional process when moving along the cause–effect chain: however, the aviation NO_x GWP can be over an order of magnitude different for constant aircraft NO_x emissions, which represents a significant uncertainty before one steps to 'real-world impacts' uncertainties. One of the main challenges with incorporating aircraft NO_x emissions into climate agreements might be the fact that a unique aviation NO_x GWP does not exist, or that global aviation net NO_x impact *decreases* with increased aircraft NO_x emissions and *increases* with reduction of aircraft NO_x emissions, a behaviour that is different to most other emissions.

UNCERTAINTIES ASSOCIATED WITH AIRCRAFT NO_x ESTIMATES FOR SELECTED CASE STUDIES

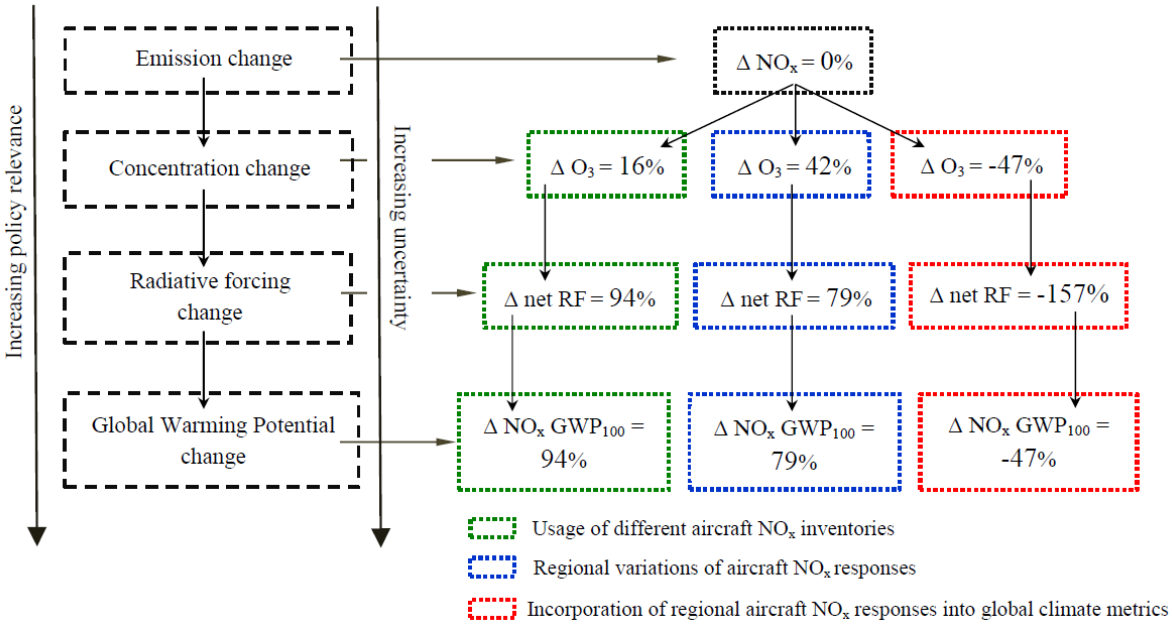

Figure 11.1: Scheme presenting a cause–effect chain from aircraft NO_x emissions to aviation NO_x GWP. The increasing disparity in calculated values at different steps of this chain based on selected 3D CTM case studies is shown (Figure adapted from Fuglestvedt et al., 2003)

Recently, a new HNO_3 forming channel resulting from the reaction between NO and HO_2 has been found (Butkovskaya et al., 2005). It was shown that it leads to a reduction in tropospheric O_3 burden of 11%, a decrease of global mean OH of ~13–14% and an increase in CH_4 lifetime of ~5–11% (Cariolle et al., 2008, Søvde et al., 2011). These modified background changes of atmospheric constituents will affect aircraft NO_x response and as it was presented by Gottschaldt et al. (2013) by accounting for $HO_2 + NO \rightarrow HNO_3$ the magnitude of aircraft net NO_x RF is significantly reduced, mainly through enhanced CH_4 lifetime reduction. Further worthwhile points of consideration are: the inclusion of plume processes, that might reduce the aircraft O_3 response by 10–25% (Cariolle et al., 2009), new NMHC oxidation scheme (Taraborrelli et al., 2012), that might increase OH background and consequently affect CH_4 and CH_4 related aircraft NO_x components or new cloud scavenging parameterisation (Neu and Prather, 2011), that might influence the upper tropospheric O_3 budget. These aspects might be considered in the future modelling studies and their impact on aircraft NO_x effects.

Studies presented in this thesis give some perspectives and inspiration for further research. Firstly, whilst it was interesting to investigate the non-linearities of a NO_x–O_3–CH_4 system on global and regional scales, the altitudinal dimension

also sounds equally interesting. Taking into that aircraft chemical perturbation, even for relatively close altitudinal bands (9–10km and 10–11km in Figure 6.17), can be already very different, the series of incremental aircraft NO_x emissions at different altitudinal level might give an additional view on the dependencies between NO_x chemistry and background conditions. Secondly, the performed analysis of the effects of regional aircraft NO_x emissions give some insight into the hemispherical radiative imbalance (Figure 8.15) that are characteristic for aviation NO_x. The presented results suggest the potential of Southern Hemispheric cooling regardless of the location of aviation NO_x emissions, which seems to be an important aspect to explore. In order to fully investigate and prove this behaviour, more regions over Southern Hemisphere need to be defined, along with detailed analysis of their RF latitudinal variation. Finally, this thesis presents the dependencies between the coupled NO_x–O_3–CH_4 system and climate forces. However, an investigation of climate responses to saturation of O_3 production efficiency with increasing aircraft NO_x emissions rates might be also an interesting prospect for a further study[1], where of special interest might constitute the interactions among chemical non-linearities and *band saturation effects* under different background conditions.

The denominators for GWP calculations applied in this study constituted data given by IPCC AR4 (Forster et al., 2007). However, Joos et al. (2013) has recently presented the re-evaluated CO_2 AGWPs. If values from this latest study were applied, the aviation NO_x GWPs presented within this thesis would be reduced by ~5% for GWP_{20}, 6% for GWP_{100} and 12% for GWP_{500}. Consideration of different scenarios of future emissions also might lead to verified aircraft NO_x GWP values. In the light of results presented by Reisinger et al. (2011), where CO_2 AGWPs decrease for greater CO_2 concentrations, the calculated aviation NO_x GWPs would increase, with differences pronounced especially under RCP 8.5 scenario.

The aircraft NO_x characteristics are emphasised by the integrative nature of the GWP and its 'artificial' memory of short-lived effects long after their occurrence. This explains the fact that the variance in the CH_4 change per O_3 change in the year of emission drives the variability of NO_x GWPs; since there is no unique GWP value, there is also no unique ratio of CH_4 lifetime change per O_3 mass change. However, the variance in the resultant global CH_4 lifetime change per O_3 column change

[1] This would require a different model framework, than applied in this thesis.

is reduced significantly, by 95%, for time horizons representing the long-term decay responses (Figure 11.2). This gives the chance for an end-point metrics, like GTP, to reduce the disparity in aircraft NO_x estimates, as the effect is accounted only for one chosen year in the future. This possibly might be viewed, as a trade-off with relatively wider range of uncertainties associated with GTP and related with additional assumptions on the climate sensitivity and heat exchange between the ocean and atmosphere. Nevertheless, the non-linearities of NO_x–O_3–CH_4 system need further investigations in order to capture responses of other metric types on such attribute.

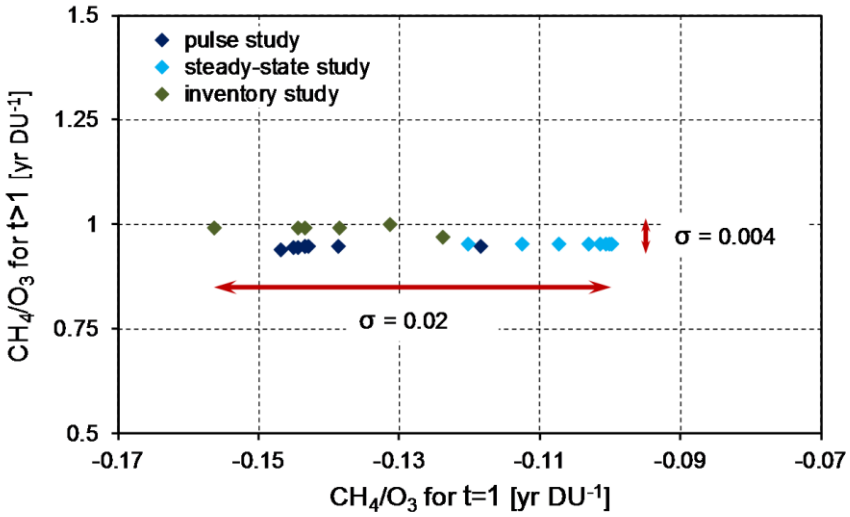

Figure 11.2: Scatter plot of CH_4 lifetime change per O_3 column change for different case studies of aircraft NO_x perturbations. The abscissa shows the ratios of responses of the first year effect and the ordinate shows the ratios of the long-term decay responses. The standard deviation values are given next to arrows.

The aviation impact on climate arises from CO_2 emissions and non-CO_2 emissions and effects, causing the long-term and short-term impacts, respectively. The scientific understanding is assigned to be high only for CO_2, the non-CO_2 factors are still very uncertain, which becomes an urgent matter as they constitute a significant contribution to the total aviation RF. Currently, the effects of aircraft NO_x are considered to be the best known, among the unknowns. The assessment of the impact of aviation on aerosol, the RF from contrails and contrail cirrus, or the effect of aircraft aerosol on contrail cirrus are especially uncertain, where often both magnitude and sign are questionable. Recent studies, e.g., Burkhardt and Kärcher (2011), Righi et al. (2013), Chen and Gettelman (2013), highlight the significance of those aircraft climate effects and show that their RF magnitudes might even outweigh the impact of aircraft CO_2 emissions. Thus, all the more, further investigations of aviation non-CO_2 climate impacts, other than NO_x, are particularly in need.

Appendix A

Table A.1. Updated rate constants for second-order reactions in 2D CTM, TROPOS.

Reaction	k rate_old	k rate_new	Ref
(KR1) O1D + N2O → NO + NO	7.2E-11	6.7E-11*exp(20/T)	1
(KR2) O1D + H2OC → OH + OH	2.2E-10	1.63E-10*exp(60/T)	1
(KR3) O1D + MOLS → O3P	2.1E-11*exp(100/T)	2.15E-11*exp(110/T)	1
(KR4) O3P + O2 → O3	See Table A.2		
(KR5) O3P + NO → NO2	See Table A.2		
(KR6) O3P + NO2 → NO3	See Table A.2		
(KR7) O3P + NO2 → NO	6.5E-12*exp(120/T)	5.1E-12*exp(210/T)	1
(KR8) HO2 + OH → H2O	4.8E-11*exp(250/T)	4.8E-11*exp(250/T)	1
(KR9) O3 + OH → HO2	1.9E-12*exp(-1000/T)	1.7E-12*exp(-940/T)	1
(KR10) HO2 + O3 → OH	1.4E-14*exp(-600/T)	1.0E-14*exp(-490/T)	1
(KR11) HO2 + HO2 → H2O2	See A.3		
(KR12) OH + OH → H2O2	See Table A.2		
(KR13) H2O2 + OH → HO2	2.9E-12*exp(-160/T)	1.8E-12	1
(KR14) H2 + OH → H2O + HO2	7.7E-12*exp(-2100/T)	2.8E-12*exp(-1800/T)	1
(KR15) H2 + O1D → HO2 + OH	1.1E-10	1.1E-10	1
(KR16) NO2 + OH → HNO3	See Table A.2		
(KR17) NO + O3 → NO2	2.0E-12*exp(-1400/T)	3.0E-12*exp(-1500/T)	1
(KR18) NO2 + O3 → NO3	1.2E-13*exp(-2450/T)	1.2E-13*exp(-2450/T)	1
(KR19) NO + HO2 → NO2 + OH	3.7E-12*exp(240/T)	3.5E-12*exp(250/T)	1
(KR20) NO2 + HO2 → HO2NO2	See Table A.2		
(KR21) HO2NO2 → NO2 + HO2	See Table A.2		

Reaction	k rate_old	k rate_new	Ref
(KR22) NO + NO3 → NO2 + NO2	1.6E-11*exp(150/T)	1.5E-11*exp(170/T)	1
(KR23) HNO3 + OH → NO3	See A.4		
(KR24) HO2NO2 + OH → NO2	1.5E-12*exp(360/T)	1.3E-12*exp(380/T)	1
(KR25) NO2 + NO3 → N2O5	See Table A.2		
(KR26) N2O5 → NO2 + NO3	See Table A.2		
(KR27) CO + OH → HO2	1.5E-13* (1.0+(0.6+PATM))	1.3E-13* (1.0+(0.6*PATM))	3
(KR28) CH4 + OH → CH3O2 + H2O	1.59E-20*($T^{2.84}$)* exp(-978/T)	1.85E-20*($T^{2.82}$)* exp(-987/T)	3
(KR29) CH4 + O1D → CH3O2 + OH	1.4E-10	1.05E-10	3
(KR30) CH4 + O1D → HCHO + H2	1.5E-11	7.5E-12	3
(KR31) CH3O2 + NO → HCHO + HO2 + NO2	4.2E-12*exp(180/T)	2.8E-12*exp(300/T)	1
(KR32) CH3O2 + HO2 → CH3OOH	1.7E-13*exp(1000/T)	4.1E-13*exp(750/T)	1
(KR33) CH3O2 + CH3O2 → products	1.7E-13*exp(220/T)	9.5E-14*exp(390/T)	1
(KR34) CH3O2 + NO2 → CH3O2NO2	See Table A.2		
(KR35) CH3O2NO2 → CH3O2 + NO2	See Table A.2		
(KR36) CH3OOH + OH → products	1.1E-11	3.8E-12*exp(200/T)	1
(KR37) HCHO + OH → CO + HO2	1.6E-11*exp(-110/T)	5.4E-12*exp(135/T)	3
(KR38) HCHO + NO3 → HNO3 + HO2 + CO	6.0E-16	5.6E-16	3
(KR41) C2H6 + OH → C2H5O2	1.37E-17*T2* exp(-444/T)	8.7E-12*exp(-1070/T)	1
(KR42) C3H8 + OH → products	1.27E-17* T2*exp(14/T)	8.7E-12*exp(-615/T)	1
(KR43) C4H10 + OH → products	1.55E-11*exp(-540/T)	1.75E-17* T^2*exp(114/T)	4
(KR44) C5H12 + OH → products	3.9E-12	2.48E-17* T^2*exp(158/T)	4
(KR45) C6H14 + OH → products	5.6E-12	2.61E-14*T* exp(-112/T)	4
(KR46) C2H5O2 + NO → products	1.16*KR31	2.6E-12*exp(365/T)	1

Reaction	k rate_old	k rate_new	Ref
(KR47) CH3CHO + OH → CH3COO2	5.6E-12*exp(310/T)	4.4E-12*exp(365/T)	3
(KR48) CH3CHO + NO3 → HNO3 + CH3COO2	1.4E-12*exp(-1860/T)	1.4E-12*exp(-1900/T)	1
(KR49) CH3COO2 + NO2 → PAN	See Table A.2		
(KR50) PAN → CH3COO2 + NO2	See Table A.2		
(KR51) PAN + OH → HCHO + NO2	1.2E-12*exp(-650/T)	2E-14	1
(KR52) CH3COO2 + NO → CH3O2 + NO2	1.85*KR31	8.1E-12*exp(270/T)	1
(KR53) C4H9O2 + NO → products	1.16*KR31	2.54E-12*exp(360/T)	5
(KR54) C2H5COCH3 + OH → CH3CH(O2)COCH3	1.8E-11*exp(-890/T)	2.53E-18*(T^2)*exp(503/T)	4
(KR55) CH3CH(O2)COCH3 + NO → products	KR31	2.54E-12*exp(360/T)	5
(KR56) C6H13O2 + NO → products	1.16*KR31	2.54E-12*exp(360/T)	5
(KR57) C2H4 + OH → HOCH2CH2O2	See Table A.2		
(KR58) HOCH2CH2O2 + NO → HO2+NO2, *FRAA:HCHO, *FRBB:CH3CHO	KR31	9.0E-12	3
(KR59) C2H4 + O3 → products	1.2E-14*exp(-2633/T)	1.2E-14*exp(-2630/T)	1
(KR60) C3H6 + OH → CH3CH(O2)CH2OH	See Table A.2		
(KR61) CH3CH(O2)CH2OH + NO → CH3CHO + HCHO + HO2 + NO2	KR31	2.54E-12*exp(360/T)	5
(KR62) C3H6 + O3 → products	1.3E-14*exp(-2105/T)	6.5E-15*exp(-1900/T)	1
(KR63) C2H2 + OH → HCOCHO + OH	See Table A.2		
(KR64) C6H6 + OH → *0.47:ARO2	7.57E-12*exp(-529/T)	2.33E-12*exp(-193/T)	4
(KR65) C7H8 + OH → *0.82: ARO2	2.1E-12*exp(322/T)	1.18E-12*exp(338/T)	4
(KR66) ARO2 + NO → CH3COCHO + HCOCHCHCHO + HO2 + NO2	KR31	2.54E-12*exp(360/T)	5
(KR67) HCOCHCHCHO + OH → HCOCHCHCOO2	3E-11	5.2E-11	5

Reaction	k rate_old	k rate_new	Ref
(KR68) HCOCHCHCOO2 + NO → products	KR31	8.1E-12*exp(270/T)	5
(KR69) HCOCHO + OH → CO + CO + HO2	1.15E-11	1.15E-11	1
(KR70) CH3COCHO + OH → CH3COO2 + CO	1.7E-11	1.5E-11	3
(KR71) C2H5O2 + HO2 → C2H5OOH	6.5E-13*exp(650/T)	7.5E-13*exp(700/T)	1
(KR72) C4H9O2 + HO2 → C4H9OOH	KR71	(2.91E-13* exp(1300/T))*0.625	5
(KR73) C6H13O2 + HO2 → C6H13OOH	KR71	(2.91E-13* exp(1300/T))*0.770	5
(KR74) CH3COO2 + HO2 → CH3COO2H	KR71	4.3E-13*exp(1040/T)	1
(KR75) CH3CH(O2)COCH3 + HO2 → products	KR71	(2.91E-13* exp(1300/T))*0.625	5
(KR76) HOCH2CH2O2 + HO2 → products	KR71	1.2E-11	3
(KR77) CH3CH(O2)CH2OH + HO2 → products	KR71	(2.91E-13* exp(1300/T))*0.520	5
(KR78) ARO2 + HO2 → ;	KR71	(2.91E-13* exp(1300/T))*0.820	5
(KR79) HCOCHCHCOO2 + HO2 → ;	KR71	4.3E-13*exp(1040/T)	5
(KR80) CH3O2 + CH3COO2→ products	2.2E-12*exp(490/T)	2.0E-12*exp(500/T)	1
(KR81) CH3COO2 + CH3COO2 → 2CH3O2	2.8E-12*exp(490/T)	2.9E-12*exp(500/T)	1
(KR82) C2H5OOH + OH → products	2.0E-11	1.16E-11 (298K; 69%:31%)	5
(KR83) C4H9OOH + OH → products	2.0E-11	1.24E-11	5
(KR84) C6H13OOH + OH → C6H13O2	3.0E-12	6.4E-12	5
(KR85) CH3COO2H + OH → CH3COO2	5.0E-12	3.7E-12	5

Reaction	k rate_old	k rate_new	Ref
(KR86) Isoprene + OH → ISOPO2	-	2.7E-11*exp(390/T)	3
(KR87) ISOPO2 + NO → products	-	2.54E-12*exp(360/T)	5
(KR88) ISOPO2 + HO2 → 2.75 CO + 0.9 H2	-	(2.91E-13* exp(1300/T))*0.706	
(KR89) Isoprene + O3 → products	-	1.03E-14* exp(-1995/T)	3
(KR91) MVKETONE + OH → MVKO2	3.0E-12*exp(500/T)	2.6E-12*exp(610/T)	3
(KR92) MVKO2 + NO → products	KR31	2.54E-12*exp(360/T)	5
(KR93) MVKO2 + HO2 → products	KR71	(2.91E-13* exp(1300/T))*0.625	5
(KR94) MVKETONE + O3 → products	4.0E-15*exp(-2000/T)	8.5E-16*exp(-1520/T)	3
(KR95) MACR + OH → MACRO2	3.86E-12*exp(500/T)	8.0E-12*exp(380/T)	3
(KR96) MACRO2 + NO → products	KR31	8.1E-12*exp(270/T)	5
(KR97) MACRO2 + HO2 → products	KR71	4.3E-13*exp(1040/T)	5
(KR98) MACR + O3 → products	4.4E-15*exp(-2500/T)	1.4E-15*exp(-2100/T)	3

A.3: Old values: k_{11} = (2.2E-13*exp(600/T))+(MOLS*1.8E-33*exp(980/T))
New values: k_{11} = (3.5E-13*exp(430/T))+(MOLS*1.7E-33*exp(1000/T))
Ref.: 1

A.4: Old values: k_o = 7.2E-15*exp(785/T), k_2 = 4.1E-16*exp(1440/T),
k_3 = MOLS*1.9E- 33*exp(725/T)
New values: k_o = 2.4E-14*exp(460/T), k_2 = 2.7E-17*exp(2199/T),
k_3 = MOLS*6.5E-34*exp(1335/T)
Ref.: 1

Table A.2. Updated rate constants for termolecular reactions in 2D CTM, TROPOS.

Reaction	Old values			New values			Ref
	k_0	k_∞	F_c	k_0	k_∞	F_c	
(KR4) O3P + O2 → O3	[M]*5.6E-34*(T/300)$^{-2.6}$	2.8E-12	exp(-T/696)	[M]*6.0E-34*(T/300)$^{-2.4}$	—		1
(KR5) O3P + NO → NO2	[M]*9.7E-32*(T/300)$^{-1.6}$	3.0E-11*(T/300)$^{0.3}$	exp(-T/1850)	[M]*1.0E-31*(T/300)$^{-1.6}$	3.0E-11*(T/300)$^{0.3}$	0.85	2
(KR6) O3P + NO2 → NO3	[M]*9.0E-32*(T/300)$^{-2.0}$	2.2E-11	exp(-T/1300)	[M]*1.3E-31*(T/300)$^{-1.5}$	2.3E-11*(T/300)$^{-0.24}$	0.6	2
(KR12) OH + OH → H2O2	[M]*6.9E-31*(T/300)$^{-0.8}$	3.0E-11	exp(-T/913)	[M]*6.9E-31*(T/300)$^{-0.8}$	2.6E-11	0.5	2
(KR16) NO2 + OH → HNO3	[M]*2.5E-30*(T/300)$^{-2.9}$	5.2E-11	exp(-T/353)	[M]*3.3E-30*(T/300)$^{-3.0}$	4.1E-11	0.4	2
(KR20) NO2 + HO2 → HO2NO2	[M]*1.8E-31*(T/300)$^{-3.2}$	4.7E-12	0.6	[M]*1.8E-31*(T/300)$^{-3.2}$	4.7E-12	0.6	2
(KR21) HO2NO2 → NO2 + HO2	[M]*4.7E-6*(-10000/T)	3.4E+14*(-10420/T)	0.6	[M]*4.1E-5*(-10650/T)	4.8E+15*(-11170/T)	0.6	2
(KR25) NO2 + NO3 → N2O5	[M]*2.7E-30*(T/300)$^{-3.4}$	2.0E-12*(T/300)$^{0.2}$	0.34	[M]*3.6E-30*(T/300)$^{-4.1}$	1.9E-12*(T/300)$^{0..2}$	0.35	2
(KR26) N2O5 → NO2 + NO3	[M]*2.2E-3*(-11080/T) *(T/300)$^{-4.4}$	9.7E+14*(-11080/T) *(T/300)$^{0.1}$	0.34	[M]*1.3E-3*(-11000/T) *(T/300)$^{-3.5}$	9.7E+14*(-11080/T) *(T/300)$^{0.1}$	0.35	2
(KR34) CH3O2 + NO2 → MEO2NO2	[M]*2.3E-30*(T/300)$^{-4.0}$	8.0E-12	exp(-T/327)	[M]*2.5E-30*(T/300)$^{-5.5}$	1.8E-11	0.36	3
(KR35) MEO2NO2 → CH3O2 + NO2	[M]*9.0E-5*(-9690/T)	1.1E+16*(-10560/T)	0.4	[M]*9.0E-5*(-9690/T)	1.1E+16*(-10560/T)	0.6	3
(KR49) CH3COO2 + NO2 → PAN	[M]*2.0E-28	8.4E-12	0.27	[M]*2.7E-28*(T/300)$^{-7.1}$	1.2E-11*(T/300)$^{-0.9}$	0.3	3
(KR50) PAN → CH3COO2 + NO2	[M]*6.3E-2*(-12785/T)	2.2E+16*(-13435/T)	0.27	[M]*4.9E-3*(-12100/T)	5.4E+16*(-13830/T)	0.3	3
(KR57) C2H4 + OH → ETHEO2	[M]*9.5E-29*((T/300)$^{-3.1}$	9.0E-12	exp(-T/840)	[M]*8.6E-29*(T/300)$^{-3.1}$	9.0E-12*((T/300)$^{-0.85}$	0.48	3
(KR60) C3H6 + OH → PRPEO2	[M]*8.0E-27*(T/300)$^{-3.5}$	3.0E-11	exp(-T/433)	[M]*8.0E-27*((T/300)$^{-3.5}$	3.0E-11*((T/300)$^{-1}$	0.5	3
(KR63) C2H2 + OH → HCOCHO + OH	[M]*5.0E-30	8.3E-13*(T/300)$^{2.0}$	0.6	[M]*5.0E-30	8.3E-13*(T/300)$^{2.0}$	0.6	1

References :

1. Sander S. P., Friedl R. R., Ravishankara A. R., Golden D. M., Kolb C. E., Kurylo M. J., Molina M. J., Moortgat G. K. and Finlayson-Pitts B. J., 2006. Chemical Kinetics and Photochemical Data for Use in Atmospheric Studies, JPL Publ. 06-2, No. 15.

2. Atkinson R., Baulch D. L., Cox R.A., Crowley J. N., Hampson R. F., Hynes R. G., Jenkin M. E., Rossi M. J. and Troe J., 2004. Evaluated kinetic and photochemical data for atmospheric chemistry: Volume I – gas phase reactions of O_x, HO_x, NO_x and SO_x species, Atmos. Chem. Phys., 4, 1461–1738.

3. Atkinson R., Baulch D. L., Cox R.A., Crowley J. N., Hampson R. F., Hynes R. G., Jenkin M. E., Rossi M. J. and Troe J., 2006. Evaluated kinetic and photochemical data for atmospheric chemistry: Volume II – gas phase reactions of organic species, Atmos. Chem. Phys., 6, 3625–4055.

4. Atkinson R., Arey J., 2003. Atmospheric degradation of Volatile Organic Compounds, Chem. Rev., 103, 4605-4638.

5. Master Chemical Mechanism (MCM), http://mcm.leeds.ac.uk/MCM/

Appendix B

By taking into account the $O(^1D)$ production from O_3 photolysis at wavelengths longer than 310 nm, which leads to existence of so-called 'tail', the overall rate increases by ~10% (Seinfeld and Pandis, 2006). This is an important modification of the specificity of the oxidizing capacity of the atmosphere.

An updated quantum yield for production of $O(^1D)$ in 2D CTM, TROPOS (in FACSIMILE format):

```
*;
 TUHERE = TEMP<#70,#8> ;
*;
 DO 49 FOR #3 = 0(1)34 ;
  P1O3<#3> = 0.9 ;
  LABEL 49;

 DO 52 FOR #3 = 35(1)38 ;
 Q1 = EXP(-0/(0.695*TUHERE)) ;
 Q2 = EXP(-825.518/(0.695*TUHERE)) ;
 ATAU = (304.225-LAMBDA<#3>)/5.576 ;
 BTAU = (314.957-LAMBDA<#3>)/6.601 ;
 CTAU = (310.737-LAMBDA<#3>)/2.187 ;
 X1 = ((Q1/(Q1+Q2))*0.8036*EXP(-(ATAU@4))) ;
 X2 = ((Q2/(Q1+Q2))*8.9061*((TUHERE/300)@2)*EXP(-(BTAU@2)));
 X3 = (0.1192*((TUHERE/300)@1.5)*EXP(-(CTAU@2))) ;
```

```
 PTEMP = X1+X2+X3+0.0765 ;
   P1O3<#3> = PTEMP ;
   LABEL 52 ;

  DO 54 FOR #3 = 39(1)46 ;
   P1O3<#3> = 0.08 ;
   LABEL 54 ;

 DO 55 FOR #3 = 47(1)105 ;
   P1O3<#3> = 0.00 ;
   LABEL 55 ;
*;
```

Appendix C

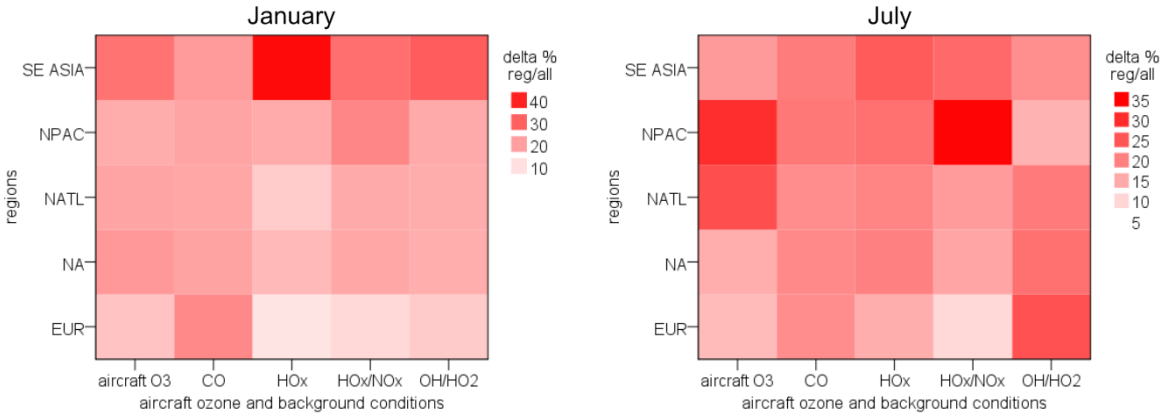

Figure C.2: Relationship between background conditions (CO concentrations, HO_x concentrations, OH/HO_2 ratio and NO_x/HO_x ratio) at 250–200 hPa and aircraft O_3 burden change (aircraft O_3) for different regions: Europe (EUR), North America (NA), Southeast Asia (SE ASIA), North Atlantic (NATL) and North Pacific (NPAC). The percentage fraction presents how the specific combination of region and background condition contribute to the specific total regional background condition.

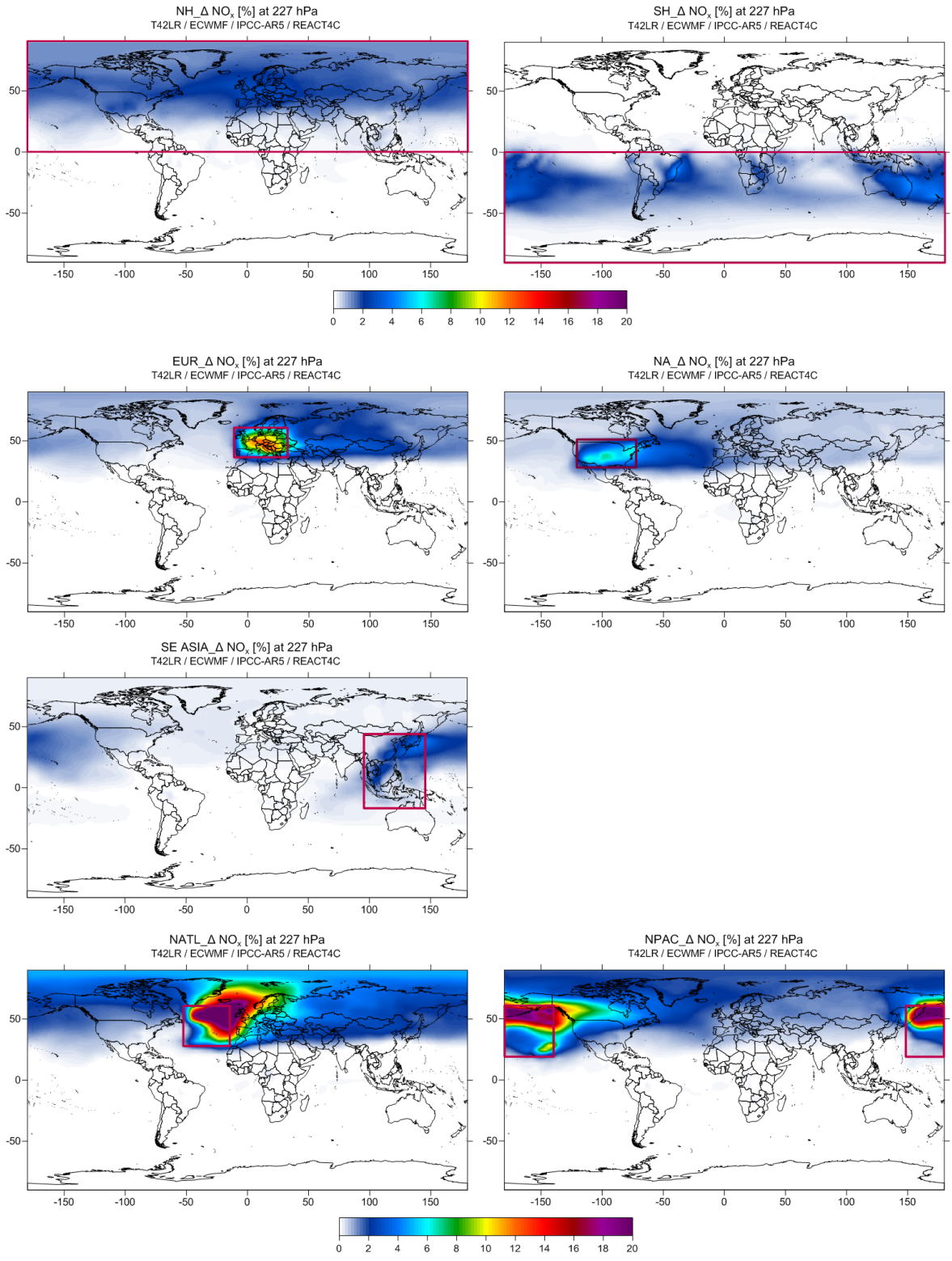

Figure C.1: Annual NO_x changes (in %) at 227 hPa calculated by MOZART-3 model for incremental aircraft NO_x emissions of 0.035 Tg(N) yr^{-1} in Northern Hemisphere (NH), Southern Hemisphere (SH), Europe (EUR), North America (NA), Southeast Asia (SE ASIA), North Atlantic (NATL) and North Pacific (NPAC). The red rectangles indicate the geographical domains with incremental aircraft NO_x emissions.

Peer-reviewed publication

The peer-reviewed paper published in Atmospheric Environment prior to the publication of this thesis is attached.

Atmospheric Environment 74 (2013) 159–168

Contents lists available at SciVerse ScienceDirect

Atmospheric Environment

journal homepage: www.elsevier.com/locate/atmosenv

The assessment of the impact of aviation NO_x on ozone and other radiative forcing responses – The importance of representing cruise altitudes accurately

A. Skowron*, D.S. Lee, R.R. De León

Dalton Research Institute, Manchester Metropolitan University, John Dalton Building, Chester Street, Manchester M1 5GD, United Kingdom

HIGHLIGHTS

- The series of aircraft inventories are investigated using 3D CTM, MOZART v3.
- The discrepancies in altitudinal distribution of aircraft NO_x emissions are observed.
- The resultant O_3 chemical perturbation varied by 15%.
- The variability of net NO_x radiative forcing is observed to be 94%.
- Future efforts should focus on accurate representation of emissions at cruise altitudes.

ARTICLE INFO

Article history:
Received 13 December 2012
Received in revised form
15 March 2013
Accepted 18 March 2013

Keywords:
Aviation
Radiative forcing
Emissions
Nitrogen oxides
Ozone response

ABSTRACT

Aviation emissions of NO_x result in the formation of tropospheric ozone (warming) and destruction of a small amount of methane (cooling), positive and negative radiative forcing effects. In addition, the reduction of methane results in a small long-term reduction in tropospheric ozone (cooling) and, in addition, a long-term reduction in water vapour in the stratosphere (cooling) from reduced oxidation of methane, both negative radiative forcing impacts. Taking all these radiative effects together, aircraft NO_x is still thought to result in a positive (warming) radiative effect under constant emissions assumptions. Previously, comparative modelling studies have focussed on the variability between models, using the same emissions database. In this study, we rather quantify the variability and uncertainty arising from different estimations of present-day aircraft NO_x emissions. Six different aircraft NO_x emissions inventories were used in the global chemical transport model, MOZART v3. The inventories were normalized to give the same global emission of NO_x in order to remove one element of uncertainty. Emissions differed in the normalized cases by 23% at cruise altitudes (283–200 hPa, where the bulk of emission occurs, globally). However, the resultant short-term ozone chemical perturbation varied by 15% between the different inventories. Once all the effects that give rise to positive and negative radiative impacts were accounted for, the variability of net radiative forcing impacts was 94%. Using these radiative effects to formulate a net aviation NO_x Global Warming Potential (GWP) for a 100-year time horizon resulted in GWPs ranging from 60 to 4, over an order of magnitude. It is concluded that the detailed placement of emissions at chemically sensitive cruise altitudes strongly affects the assessment of the total radiative impact, introducing a hitherto previously unidentified large fraction of the uncertainty of impacts between different modelling assessments. It is recommended that future formulations of aircraft NO_x emissions focus efforts on the detailed and accurate placement of emissions at cruise altitudes to reduce the uncertainty in future assessments of aviation NO_x impacts.

1. Introduction

The impact of aviation NO_x emissions on the production of tropospheric ozone (O_3) has been investigated since the early 1970s (Hidalgo and Crutzen, 1977). Several thematic research programmes in the US and Europe investigated aircraft NO_x effects on

* Corresponding author.
E-mail address: a.skowron@mmu.ac.uk (A. Skowron).

1352-2310/$ – see front matter © 2013 Elsevier Ltd. All rights reserved.
http://dx.doi.org/10.1016/j.atmosenv.2013.03.034

tropospheric chemistry in the 1980s and 1990s (see Lee et al., 2010 for a summary).

Despite the length of time over which this effect has been investigated, it still represents an active research area. One particular milestone was the IPCC (1999) Special Report on 'Aviation and the Global Atmosphere', which summarized results of a number of 3D global chemical transport models (CTMs), which were relatively newly developed over 2D models. The IPCC (1999) highlighted the finding that whilst NO_x emissions from the existing fleet of subsonic aircraft resulted in a small increase in tropospheric O_3, there was also a small but significant reduction in ambient CH_4 (for an equilibrium calculation of constant emissions), since CH_4 has a lifetime of approximately 8–12 years and takes some time to respond to an additional NO_x increase. The IPCC thus identified a positive ozone radiative forcing (RF) and a negative RF associated with a NO_x increase from aircraft.

Wild et al. (2001) also identified that with this long-term CH_4 decrease, a small decrease in O_3 also resulted (again, for equilibrium conditions). However, it has taken some time to realise that this O_3 decrease could be significant over the longer time-period and that the overall RF response from aircraft NO_x arises from one positive and two negative RF responses. More recently, Myhre et al. (2011) summarized a number of model responses to an aircraft NO_x increase and also highlighted a fourth RF response in that a decrease in CH_4 also ultimately resulted in a small negative RF response from water vapour in the stratosphere. Any CH_4 response takes decades to come to an equilibrium response and its mixing time means that it can enter the stratosphere where it can be oxidised to water vapour. The water vapour results in a positive forcing in the stratosphere, so that any reduction in CH_4 will result in a reduction in water vapour forcing in the stratosphere and can therefore be viewed as a negative RF from aviation NO_x.

The complexity of NO_x–O_3–CH_4 system is intensified not only through different timescales of responses of its components (positive forcing is short-term, negative responses are long-term), but also by differences of their spatial extents: the short-term O_3 enhancement is regional, the CH_4, CH_4-induced O_3 and stratospheric water vapour (SWV) act on a global scale.

Many studies have been published over the past 20 years assessing the impact of aviation NO_x emissions on tropospheric chemistry and RF (see Lee et al., 2010 for a recent review, along with Myhre et al., 2011). Among them, the investigations regarding the impact of aircraft NO_x from modified cruise altitudes also exist (Gauss et al., 2006; Frömming et al., 2012). However, these studies are not always straightforward to compare, since the models have had varying degrees of complexity in terms of completeness of representation of tropospheric and stratospheric chemistry, horizontal and vertical resolution.

There are numbers of tools which are utilized in order to place on a common scale different climate impacts. The most traditional are radiative forcing (RF) and global warming potential (GWP). Radiative forcing (RF) is an accepted measure of the strength of the perturbation of Earth-atmosphere system caused by natural agents and human activity. The global warming potential (GWP) is a ratio of the RF from the emission of a species relative to that of CO_2 for a nominal kg release of both gases, integrated over given time horizon. Whilst RF is a backward looking measure, the GWP through its relativity is one step further in the cause–effect chain.

In this paper, we revisit the NO_x impact on chemical composition of the troposphere using a 3D CTM, MOZART v3 (Kinnison et al., 2007) and quantify the individual RF responses from short-term O_3 increases, long-term CH_4 and O_3 decreases, and CH_4 feedback effects on stratospheric water vapour. Most importantly, the impact of using different emission inventories is investigated in this work, since all previous comparative studies have utilised different models. Here, we take a novel approach of using a single model with different (normalized) emissions that have slightly different assumptions and therefore vertical distributions of emissions in order to better understand the impact of height distribution of aircraft NO_x emissions and their representation in emission inventories.

2. Methodology and experimental design

2.1. Aircraft emission inventories

The aircraft inventory datasets are usually generated from an aircraft movement database, the characteristic of a global fleet in terms of type of aircraft and engines, fuel-flow model, calculation of emissions at vertical scale from fuel flow, landing and take-off emissions (LTO). The aircraft movement databases are a mixture of a flight plan data, flight operation data, radar data, Official Aviation Guide (OAG) data (www.oag.com) and idealized great circle routes analysis. A comprehensive comparison of global aviation inventories was recently presented by Olsen et al. (2013).

Here, six different aircraft inventories were investigated:

1. AEDT (Aviation Environmental Tool) for the year 2006 (Wilkerson et al., 2010). The global aircraft data was provided by Volpe National Transportation Systems Centre. The aircraft fuel burn and emissions were estimated based on an individual flight by flight analysis. This inventory is based on radar data for Europe and North America, which account for 70–80% of global aircraft movements, and for the remaining flight movements the OAG data were used.
2. AEM (Advanced Emission Model) for the year 2006 (www.eurocontrol.int/services/advanced-emission-model). AEM is a stand-alone system (developed and maintained by EUROCONTROL), which calculates aviation emissions and fuel burn. It uses a few basic databases: aircraft, aircraft engines, fuel burn rates and emissions indices. AEM is aimed to analyse the flight profile data, on a flight by flight bases, for different air traffic scenarios.
3. AERO2K inventory for the year 2002 (Eyers et al., 2005) was developed under the EC 5th Framework Programme. The dataset is based on a radar tracked flight data for North America and Europe. Data for the rest of the world are covered by scheduled flights data from Back Aviation database (Back, 2002) and by routing information. Forty representative aircraft types were applied in order to calculate the fuel burn and emissions for each flight using means from the PIANO (www.piano.aero) aircraft performance model.
4. REACT4C (EC 7th Framework Programme Reducing Emissions from Aviation by Changing Trajectories For the benefits of Climate) for the year 2006 (www.react4c.eu). The input data are the CAEP-8 comprehensive set of aircraft movements, which are individual movements for 6 weeks of the year, scaled to a full year's movements. The air traffic movements are from radar data for flights for Europe and North America and the remaining global flight movements are taken from OAG. The models used to generate this inventory are: the fuel-flow model PIANO (Project Interactive Analysis and Optimization model) and global emissions model FAST (The Future Aviation Scenario Tool) (Owen et al., 2010), similarly as for QUANTIFY and TRADEOFF data presented below.
5. QUANTIFY (Quantifying the Climate Impact of Global and European Transport Systems) for a year 2000 (Owen et al., 2010). The inventory consists of OAG data for scheduled flights and AERO2K's traffic for non-scheduled aircraft movements. The QUANTIFY dataset, once released, was scaled to the

International Energy Aviation (IEA) aviation fuel burn total for year 2000.

6. TRADEOFF for the year 1992 (Gauss et al., 2006). The dataset was created based on a flight track data from the EUROCONTROL and FAA from the year 1991/1992. Four months of aircraft movements: July 1991, October 1991, January 1992 and April 1992 were scaled to a full year's movement. The global aircraft movement data are a combination of air traffic control and scheduled data. Sixteen civil aircraft-engine type combinations represent the global fleet of aircraft.

Aircraft inventories used in this study are three dimensional gridded datasets, with a $1^\circ \times 1^\circ$ horizontal resolution and a vertical resolution which varies from 1 km through 610 m to 500 ft. An overview of the characteristics of each inventory is presented in Table 1. Military emissions have not been taken into account in this study.

Each dataset represents different years of emissions, which results in different amounts of burned fuel ranging from 210 Tg yr^{-1} for AEDT (2006) to 114 Tg yr^{-1} for TRADEOFF (1992) which affects the emitted NO_x. In order to exclude the differences in the amount of injected NO_x and consequently its impact on O_3 response, the NO_x emissions of each inventory were scaled to the same global total as the REACT4C, which is 2.33 Tg (NO_2) yr^{-1}.

2.2. Global chemical transport model of the atmosphere

The Model for Ozone and Related Tracers, version 3 (MOZART-3) was used in this study. It is a 3D Chemistry Transport Model (CTM) comprehensively evaluated by Kinnison et al. (2007) and extensively used for different applications, e.g. impact of El Niño and La Niña events on dynamical, thermal and chemical structure of the middle atmosphere (Sassi et al., 2004), distribution of stratospheric O_3 and downward O_3 transport in the UTLS region during the sudden stratospheric warming event in January 2004 (Liu et al., 2009), forecast analysis of the ozone hole over Antarctica in 2008 (Flemming et al., 2011), evaluation of Ozone Depletion Potentials for n-propyl bromide (Wuebbles et al., 2011).

MOZART-3 is built on the framework of the transport model MATCH (Model for Atmospheric Transport and Chemistry) (Rasch et al., 1997) and accounts for advection (flux-form semi-Lagrangian scheme of Lin and Rood (1996)); convection (shallow and mid-level convection scheme of Hack (1994) and deep convective transport of Zhang and McFarlane (1995)); boundary layer exchanges (Holstag and Boville, 1993) and wet and dry deposition (Brasseur et al., 1998; Müller, 1992, respectively).

MOZART-3 represents detailed chemical and physical processes from the troposphere through the stratosphere. The chemical mechanism consists of 108 species, 218 gas-phase reactions, 71 photolytic reactions (including the photochemical reactions associated with organic halogen compounds) and 17 heterogeneous reactions. The kinetic and photochemical data is from NASA/JPL (Sander et al., 2006).

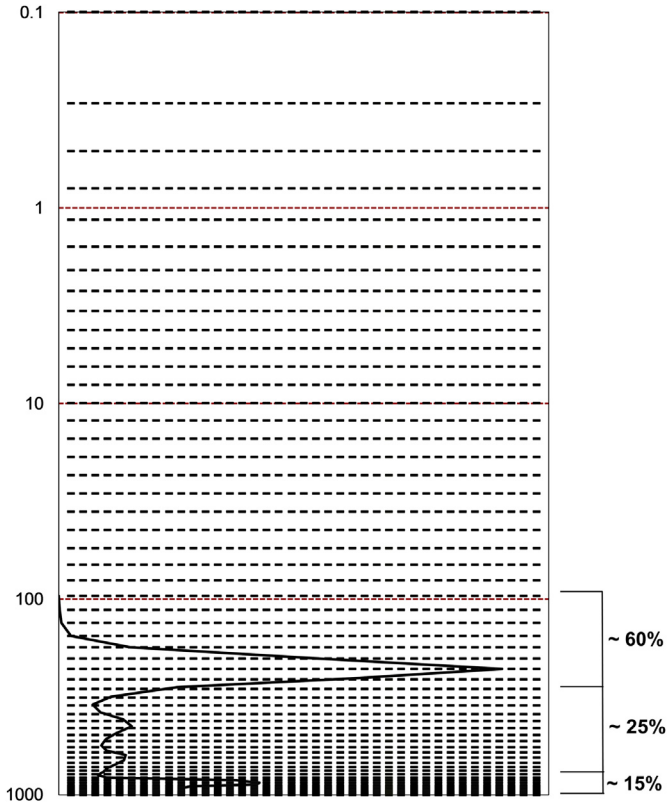

Fig. 1. The vertical domain of MOZART-3. The dashed lines (black lines in the web version) represent model's 60 hybrid sigma pressure layers and solid lines (red lines in the web version) show the 1000, 100, 10, 1 and 0.1 pressure (hPa) levels. The percentage numbers are the schematic illustration of a vertical distribution of aircraft NO_x emissions in MOZART-3.

The anthropogenic (non-aviation) and biomass burning emissions are taken from Lamarque et al. (2010) and represent the year 2000. The biogenic surface emissions are taken from the European Union project POET (Precursors of Ozone and their Effects on Troposphere) (Granier et al., 2005).

The horizontal resolution applied in this study is T42 ($\sim 2.8^\circ \times 2.8^\circ$) and the vertical domain extends from the surface to 0.1 hPa with 60 hybrid layers (Fig. 1). The transport of chemical compounds is driven by the meteorological fields from European Centre for Medium Range Weather Forecasting (ECMWF), reanalysis ERA-Interim for the year 2000 (Simmons et al., 2007).

Seven experiments were performed, one reference (no-aircraft) run and six perturbation (aircraft) simulations, each starting in January 2000 and finishing in December 2000; each simulation was

Table 1
The summary of specifications of six aircraft inventories used in this study: AEDT, AEM, AERO2K, REACT4C, QUANTIFY and TRADEOFF.

Inventory	AEDT	AEM	AERO2K[a]	REACT4C	QUANTIFY	TRADEOFF
Year	2006	2006	2002	2006	2000	1992
Fuel (Tg $year^{-1}$)	187	210	156	178	152	114
Distance (billion km $year^{-1}$)	38.9	43.6	33.2	38.9	30.5	17.4
CO_2 (Tg $year^{-1}$)	590	508	492	562	479	n/a
NO_x (Tg(NO_2) $year^{-1}$)	2.72	2.99	2.06	2.33	1.98	1.61
Vertical spacing	1 km	500 ft	500 ft	610 m	610 m	610 m
Temporal resolution	Annual	Monthly	Monthly	Monthly	Monthly	Seasonal
Air traffic movements	Radar data, OAG	Radar data, OAG	Radar data, BACK	Radar data, OAG	OAG for schedule & AERO2K for non-schedule traffic	OAG, scheduled data
Modelling tool	SAGE, BADA	AEM, BADA	AERO2K, PIANO	FAST, PIANO	FAST, PIANO	FAST, PIANO

[a] Based on civil aviation data only.

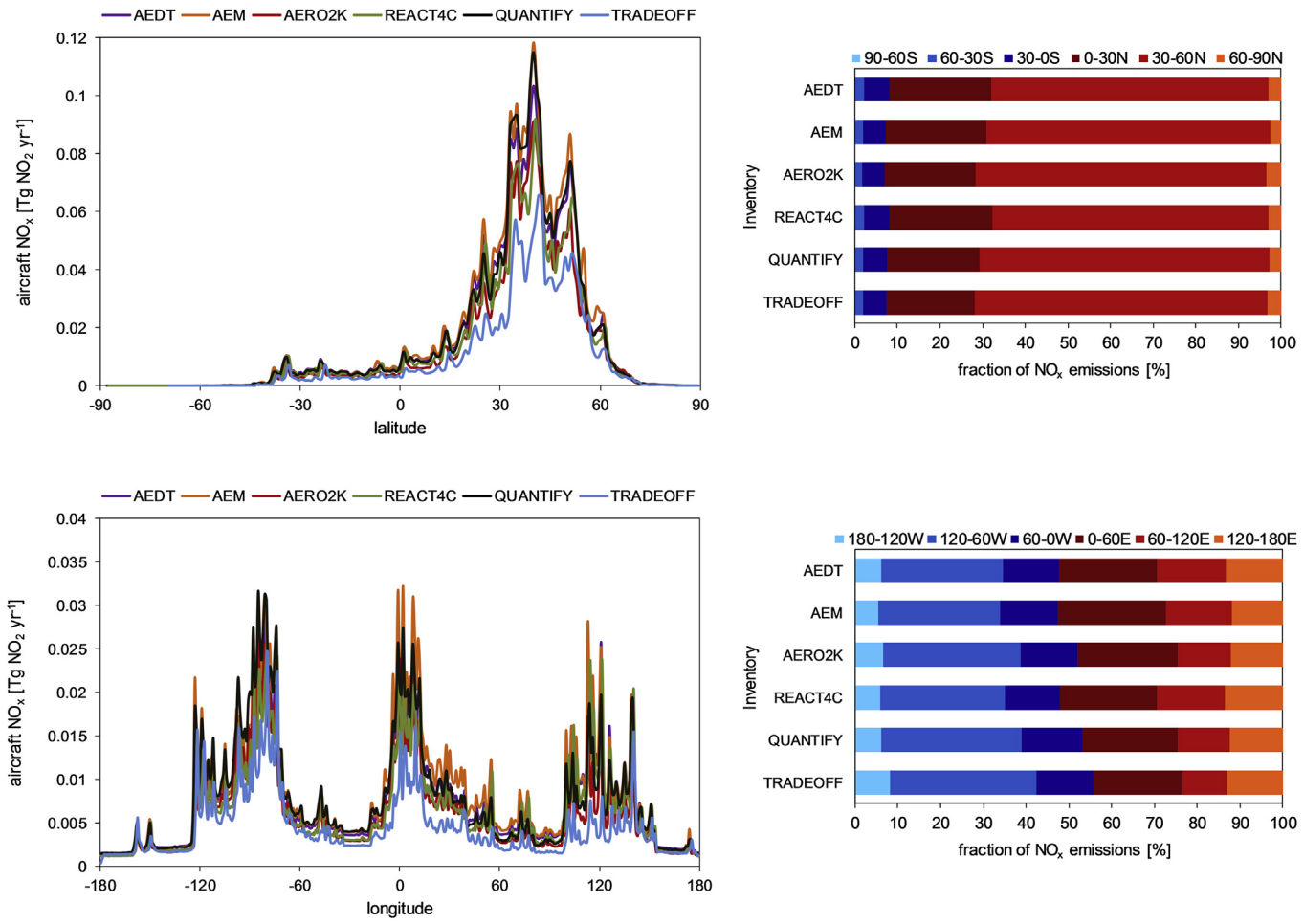

Fig. 2. The globally and annually averaged latitudinal (upper row) and longitudinal (bottom row) distributions of aircraft NO_x emission (left column) and the fraction of aircraft NO_x emission occurring in latitudinal and longitudinal bands (right column) for six aircraft inventories: AEDT, AEM, AERO2K, REACT4C, QUANTIFY and TRADEOFF. The figure presents the original, not scaled datasets.

preceded by one year spin-up. The aircraft perturbation is derived by extracting the difference between aircraft and no-aircraft experiments. The calculations of O_3 change and CH_4 lifetime change, along with RFs, covers the surface-1 hPa domain. Since our experiments are performed for 2 years, the magnitude of aircraft stratospheric response is not fully representative. The O_3 depletion due to aircraft NO_x emissions, from current fleets, is relatively small (−0.01 DU), thus it does not affect O_3 changes significantly. However, the O_3 column change, presented in this paper is overestimated by 5.1% for surface-1 hPa domain and the short-term O_3 RF is underestimated by 0.6%. The CH_4 lifetime reduction and its negative RF are overestimated by 0.2%.

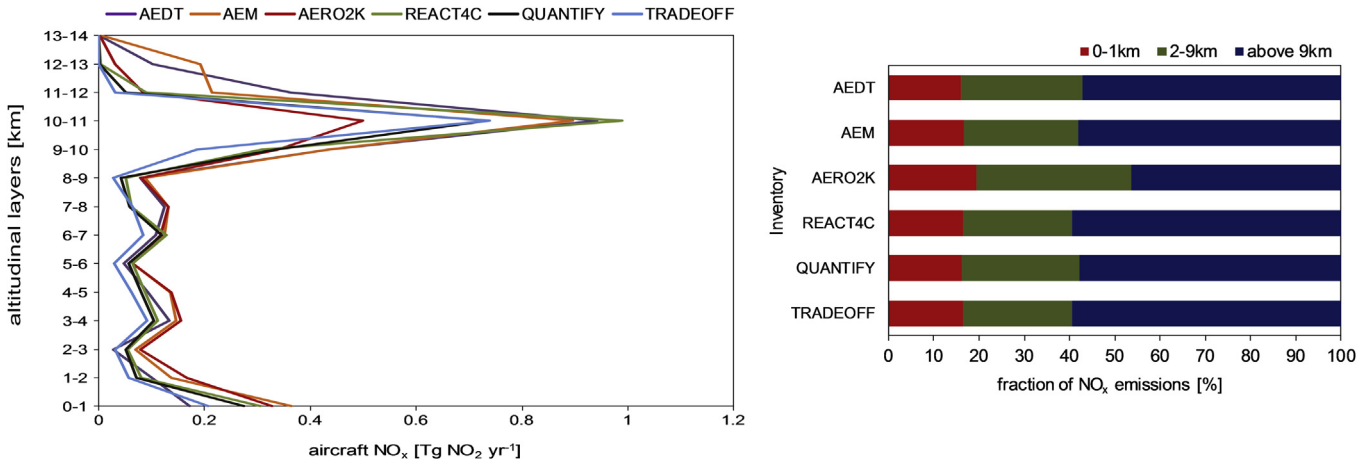

Fig. 3. The globally and annually averaged altitudinal distributions of aircraft NO_x emission for six different inventories (left) and the fraction of aircraft NO_x emission occurring in three altitudinal bands (right) for six aircraft inventories: AEDT, AEM, AERO2K, REACT4C, QUANTIFY and TRADEOFF. The figure presents the original, not scaled datasets.

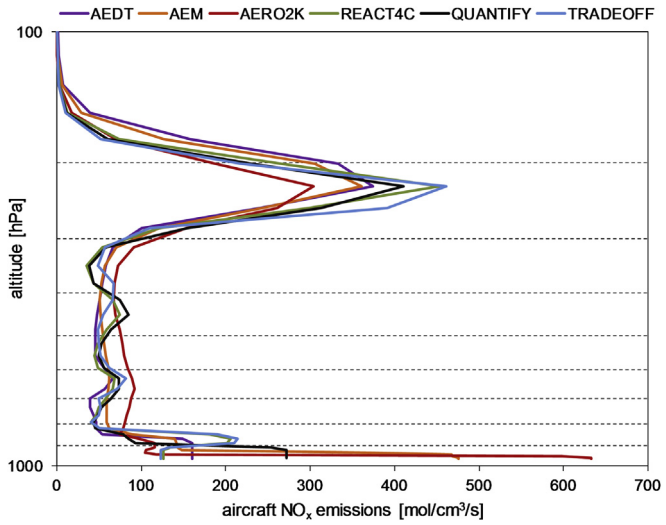

Fig. 4. The globally and annually averaged vertical distribution of aircraft NO_x emissions in MOZART-3 for six aircraft inventories: AEDT, AEM, AERO2K, REACT4C, QUANTIFY and TRADEOFF. The NO_x emissions are scaled to the same global total, which is 2.33 $Tg(NO_2)\ yr^{-1}$.

2.3. Radiative forcings and global warming potentials calculations

The short-term O_3 radiative forcings are calculated off-line using the Edwards – Slingo radiation code (Edwards and Slingo, 1996). This comprehensive radiative transfer model was developed in the UK Meteorological Office and is based on the two-stream equations in both the long-wave and short-wave spectral regions. Cloud treatment is based on averaged ISCCP D2 data (Rossow and Schiffer, 1999). Climatological fields of temperature and specific humidity are based on ERA-Interim data (Simmons et al., 2007). The calculations were performed on monthly O_3 MOZART-3 output. To account for a stratospheric adjustment a 20% reduction was applied to the O_3 RF, following the work of Stevenson et al. (1998).

A one year CTM simulation is not long enough to calculate the change in CH_4 concentration, as it takes decades for CH_4 to come into equilibrium with the perturbed OH fields. That is why to obtain the steady state concentrations of CH_4 in the perturbation runs the change in CH_4 lifetime owing to reaction with OH was calculated for each inventory, which then, based on Fuglestvedt et al. (1999), was multiplied by the reference CH_4 concentration and a feedback factor of 1.4 (Prather et al., 2001) to reflect the effect of changes of CH_4 on its own lifetime: $[CH_4]_{ss} = [CH_4]_{ref} * (1 + 1.4 * \Delta\alpha_0/\alpha_{ref})$, where $\Delta\alpha_0 = \alpha_{per} - \alpha_{ref}$ and $[CH_4]_{ref}$ is a reference run concentration.

The RF of CH_4 is calculated using a simplified expression defined in Ramaswamy et al. (2001). The impact of CH_4 change on

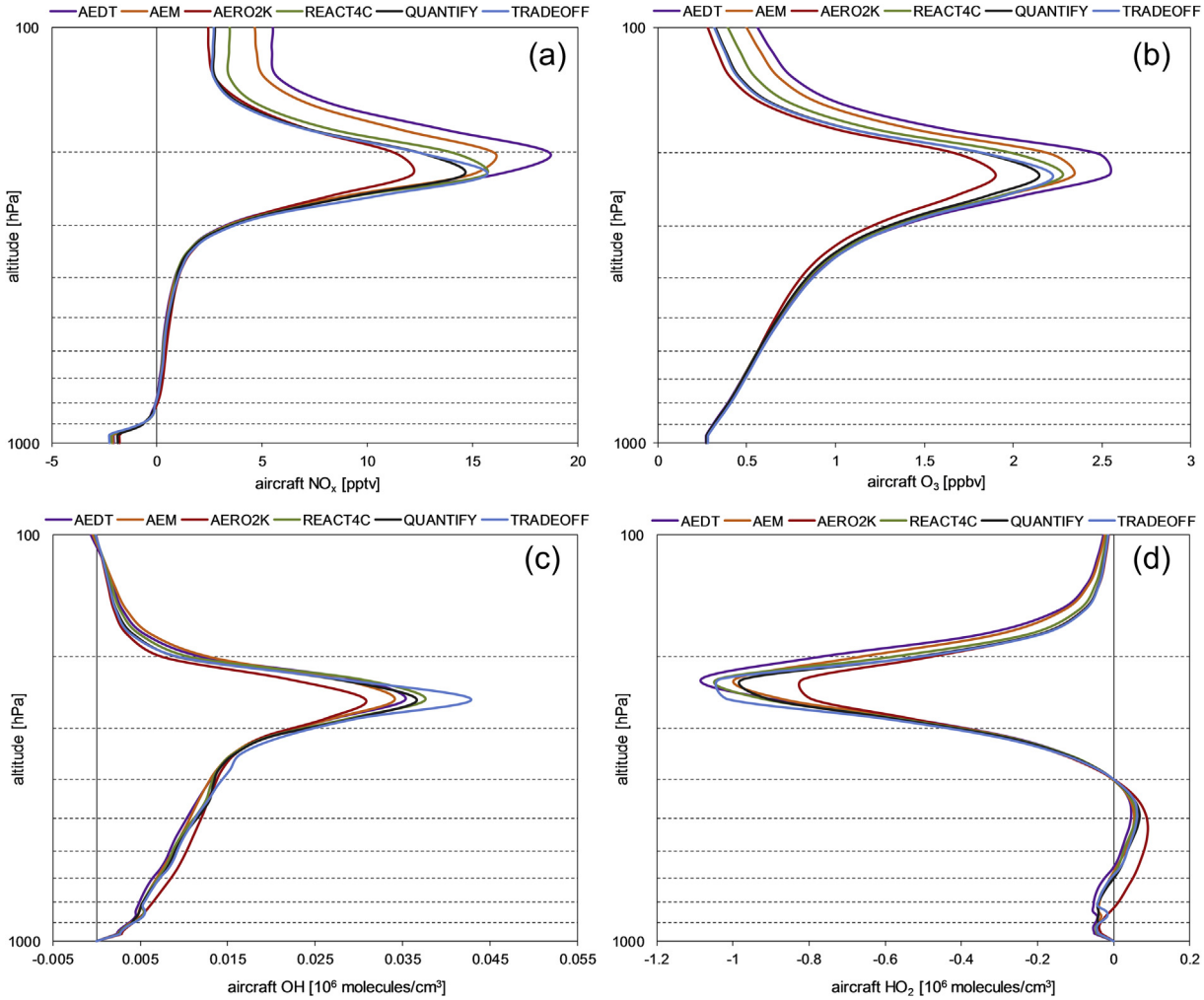

Fig. 5. The globally and annually averaged vertical distributions of aircraft perturbations of NO_x (a), O_3 (b), OH (c) and HO_2 (d) concentrations for a series of normalized aircraft inventories.

Table 2
The short-term global and annual mean O_3 column change (in DU) and O_3 production efficiency (OPE; the number of O_3 molecules produced per emitted NO_x molecule) for a series of normalized aircraft inventories.

Inventory	O_3 (DU)	OPE
AEDT	0.56	30.1
AEM	0.54	29.1
AERO2K	0.48	25.4
REACT4C	0.52	28.2
QUANTIFY	0.50	27.0
TRADEOFF	0.52	27.7

Table 3
CH_4 lifetime (in year) due to destruction by OH (between the surface and 1 hPa) and the CH_4 lifetime reduction (in year) due to the aircraft NO_x emissions for a series of normalized aircraft inventories.

Inventory	CH_4 lifetime (year)	CH_4 lifetime change (year)
Reference run	8.882	
AEDT	8.813	−0.070
AEM	8.811	−0.071
AERO2K	8.808	−0.074
REACT4C	8.810	−0.073
QUANTIFY	8.809	−0.073
TRADEOFF	8.808	−0.074

stratospheric water vapour (SWV) is also included and as described in Myhre et al. (2007) the RF of SWV is assumed to be 0.15 times that of CH_4 RF. The CH_4-induced O_3 is computed based on an assumption that 10% increase of CH_4 leads to 0.64 DU increase of ozone (Prather et al., 2001) and this ozone has a specific RF of 42 mW m^{-2} DU^{-1} (Ramaswamy et al., 2001).

The temporal evolution of net RF following the NO_x emission is required in order to calculate GWP. It can be assumed that the constant one year emission is a step emission followed by a decay of the resulting forcing from the end of the year onwards. The GWP calculations are based on a methodology described by Fuglestvedt et al. (2010). The primary-mode lifetime is taken into account for integrations of long-term effects (CH_4 with SWV and CH_4-induced O_3).

3. Results

3.1. Aircraft NO_x emissions

Since various methodologies have been applied to derive different inventories, the distribution of NO_x emissions reveals some discrepancies. The geographical distribution shows rather common picture (Fig. 2). The image of altitudinal spacing is not so unique (Fig. 3).

The Northern Hemisphere is the main location of aircraft NO_x emissions: emissions in 30–60N and 0–30N regions constitute 65% and 24%, respectively, for AEDT, AEM and REACT4C inventories; AERO2K, QUANTIFY and TRADEOFF have slightly more emissions in mid northern latitudes (68%) and less over the northern tropical region (21%). Most of aircraft NO_x emissions occur over North America, Europe and South-East Asia. AERO2K, QUANTIFY and TRADEOFF have a bit lower emissions, by ~4%, in 60–120E region and a bit more, by ~4%, in 120–60W region than AEDT, AEM and REACT4C.

The largest part of the NO_x emissions are injected between 9 and 12 km for most of the inventories, only AEDT and AEM have more aircraft NO_x over 12 km than the other inventories. AERO2K's NO_x emissions at cruise altitudes constitute only 43% of its total aircraft NO_x emissions (Fig. 3), which, when compared with 57% of QUANTIFY, 58% of AEM, 59% of REACT4C and TRADEOFF and 63% of AEDT, is quite low. The 'missing' ~10% is hidden under AERO2K's relatively high NO_x emissions at mid-altitudes, which is 34%, while for all the rest of inventories it is around 25%. The difference in the vertical structure of NO_x emissions between AERO2K and the other datasets is significant.

The original aircraft emission data, with their regular vertical gridding (500 ft, 610 m or 1 km) are interpolated by MOZART-3 to its irregular (with hybrid sigma layers every ~1 km in the upper troposphere and lower stratosphere (UTLS) region) vertical spacing (Fig. 1). Fig. 4 shows the vertical distribution of aircraft NO_x emissions in MOZART-3 for the six aircraft inventories. Each dataset represents the same amount of global total aircraft NO_x (2.33 Tg NO_2). The initial resolution of dataset plays a significant role when it is redistributed into the lowest CTM's vertical layers. Taking into account that the vertical resolution in MOZART-3 near surface is high (~45 m) the datasets with higher resolution (AEM and AERO2K) have more aircraft NO_x emissions near ground (1000–950 hPa).

In MOZART-3 most of aircraft NO_x emissions are injected in the 283–200 hPa region, where the emissions differ by 23% when the greatest (TRADEOFF) and the smallest (AERO2K) numbers are taken into account. The peak of aircraft NO_x emissions is observed at 227 hPa, with the greatest values occurring for REACT4C and TRADEOFF. AEDT and AEM have more emissions at 200 hPa and at higher altitudes, than other inventories, which raises the possibility of more efficient accumulation of N molecules (Seinfeld and Pandis, 2006).

3.2. Chemical perturbation

The response of the NO_x–O_3–CH_4 system affected by aviation NO_x emissions is presented in Fig. 5. The positive peak of NO_x

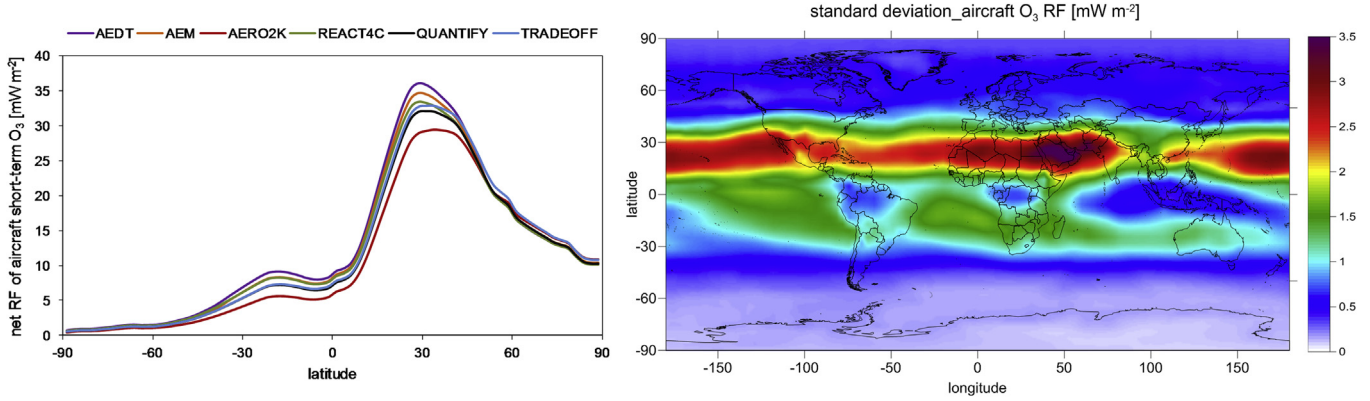

Fig. 6. Zonal and annual mean net (long-wave and shortwave) radiative forcing (mW m^{-2}) from short-term O_3 (left) and the standard deviation of net radiative forcing from short-term O_3 (right) for a series of normalized aircraft inventories.

Table 4
Absolute radiative forcings (in mW m^{-2}) due to short-term O_3, CH_4-induced O_3, CH_4, stratospheric water vapour (SWV) and NO_x (net of all 4 components) for series of normalized aircraft inventories. The radiative forcings per unit emission of N (in mW m^{-2} Tg(N) yr^{-1}) are presented in the brackets.

Inventory	Radiative forcings				
	Short-term O_3	CH_4-induced O_3	CH_4	SWV	Net NO_x
AEDT	14.3 (20.5)	−3.0 (−4.3)	−6.7 (−9.5)	−1.0 (−1.4)	3.6 (5.2)
AEM	13.8 (19.7)	−3.0 (−4.2)	−6.8 (−9.7)	−1.0 (−1.5)	3.0 (4.2)
AERO2K	11.5 (16.5)	−3.1 (−4.5)	−7.1 (−10.4)	−1.1 (−1.5)	0.2 (0.3)
REACT4C	13.4 (19.2)	−3.1 (−4.4)	−7.0 (−10.0)	−1.1 (−1.5)	2.3 (3.3)
QUANTIFY	12.8 (18.3)	−3.1 (−4.4)	−7.0 (−10.0)	−1.1 (−1.5)	1.7 (2.4)
TRADEOFF	13.1 (18.7)	−3.1 (−4.5)	−7.1 (−10.2)	−1.1 (−1.5)	1.8 (2.6)

response is observed at 227 hPa for all inventories, except for AEDT and AEM, which have their maximum one level higher, at 201 hPa. This suggests that potential of NO_x perturbation is greater for higher NO_x emissions. The greatest NO_x response is observed for AEDT and the smallest for AERO2K, which consequently affects the O_3 perturbation, which follows the same pattern of differences between datasets in terms of emissions. The largest O_3 response takes place at 227 hPa level for all inventories. The enhanced O_3 changes the oxidizing capacity of the troposphere. In general, aircraft NO_x perturbs the OH/HO_2 ratio: increases OH and decreases HO_2. The positive OH response is observed through all tropospheric domain, the negative HO_2 response is observed mainly at flight altitudes. While the impact of AERO2K inventory on NO_x and O_3 in UTLS region is relatively weak, it is responsible for greater aircraft OH in mid-altitudes and consequently CO and CH_4 changes, than other datasets. The more efficient CO oxidation results in a greater AERO2K's HO_2 perturbation in mid-altitudes compared to other inventories.

The same amount of emitted NO_x, but different vertical distributions of NO_x emissions lead to significant differences in short-term O_3 response between inventories. Table 2 gives global and annual means of total column O_3 change (in DU) and ozone production efficiency values for six different inventories. The greatest column change is observed for AEDT (0.56 DU) and AEM (0.54 DU) and the smallest is for AERO2K (0.48 DU). Also QUANTIFY shows a relatively lower O_3 perturbation (0.50 DU) compared with the other FAST inventories REACT4C and TRADEOFF (0.52 DU).

The O_3 production in the troposphere has been shown to be sensitive to the height of the initial precursor emissions (Köhler et al., 2008). This is indirectly observed in our results, where more molecules of ozone are produced per molecule of N emitted for inventories with NO_x emissions at higher altitudes, it being 30 for AEDT, 29 for AEM, 28 for REACT4C, 27 for QUANTIFY and TRADEOFF and 25 for AERO2K (Table 2). This shows that a lower potential, by 15%, is observed for AERO2K inventory compared to AEDT dataset in terms of ozone production, which is consistent with the spread of O_3 column change.

The methane lifetime due to destruction by OH in a reference case was observed as 8.88 years. In contrast to the O_3 responses, the CH_4 lifetime reductions are observed to be quite uniform among different inventories (Table 3) ranging from −0.074 years for AERO2K and TRADEOFF, −0.073 years for REACT4C to −0.070 years for AEDT.

3.3. Radiative forcing and global warming potential for aviation NO_x emissions

The latitudinal distributions of short-term O_3 RF for the six inventories are shown in Fig. 6. The pattern for each inventory shows similar characteristics and it is consistent with zonal-mean distributions of NO_x emissions (Fig. 2) (both rather short-lived), with dominating role of short-term O_3 RF over the Northern Hemisphere. While agreement in the resultant short-term O_3 RF between inventories at high southern and northern latitudes is observed the tropical region (30°S–40°N) shows discrepancies. The largest spread in the short-term O_3 RF between inventories occurs over northern tropical belt (15–30°N), where locally the standard deviation reaches 3.0–3.5 mW m^{-2}, over Middle East, Pacific and North Africa.

Table 4 presents the global and annual mean RF (mW m^{-2}) for short-term O_3, CH_4–induced O_3, CH_4, and SWV for a series of inventories. The standard deviation of short-term O_3 values is 1.0 mW m^{-2} (with AEDT and AERO2K resulting in highest and lowest numbers, 14.3 and 11.5 mW m^{-2}, respectively). The CH_4 responses are much more consistent, the standard deviation is 0.2 mW m^{-2} (with values ranging from −7.1 mW m^{-2} for AERO2K and TRADEOFF to −6.7 mW m^{-2} for AEDT). The net aircraft NO_x RF values ranges from 3.6 mW m^{-2} for AEDT, 2.3 mW m^{-2} for REACT4C to 0.2 mW m^{-2} for AERO2K, with 1.2 mW m^{-2} standard deviation.

Myhre et al. (2011) reported GWP values for aviation NO_x emissions using the same aircraft emissions, the same experimental design and a range of five models. The differences in their results constitute a good insight into uncertainties which arise from usage of different global chemistry models. In contrast, the spread in results which are presented in this study gives a measure of differences that arise from usage of different aircraft inventories. The resulting GWP values for three time horizons (20, 100 and 500 years) are given in Table 5. The values show significant differences, which are enhanced with larger time horizons; however, the sign of calculated responses shows a consistently net positive value. The largest differences come from the AEDT and AERO2K inventories, being 57%, 93% different for 20, 100 time horizons respectively. The increase of discrepancy with larger time horizons can be explained by CH_4, as its response 'remains' for a few decades after NO_x emission.

The GWP reduction between a 20 year time horizon and a 100 year horizon is larger for inventories where the CH_4 lifetime reduction is more enhanced, e.g. it is 82% for AEDT, 83% for AEM, 85% for REACT4C, 87% for QUANTIFY and TRADEOFF, 97% for AERO2K. Due to relatively short lifetimes of the net NO_x

Table 5
Global warming potentials (GWP) for aircraft NO_x emissions for a series of aircraft inventories for 20, 100 and 500 time horizon (sO_3 = short-term O_3, lO_3 = CH_4-induced O_3, CH_4 = CH_4 + SWV, net NO_x = sO_3 + lO_3 + CH_4). All values are on a per kg N basis and are relative to CO_2.

Inventory	GWP(20)				GWP(100)				GWP(500)			
	sO_3	lO_3	CH_4	Net NO_x	sO_3	lO_3	CH_4	Net NO_x	sO_3	lO_3	CH_4	Net NO_x
AEDT	828	−140	−356	332	235	−50	−126	60	72	−15	−38	18
AEM	796	−137	−364	295	226	−49	−129	49	69	−15	−39	15
AERO2K	666	−146	−379	142	189	−52	−134	4	58	−16	−41	1
REACT4C	777	−143	−372	262	221	−51	−132	39	67	−15	−40	12
QUANTIFY	740	−143	−372	225	210	−51	−132	28	64	−15	−40	8
TRADEOFF	759	−146	−380	233	216	−52	−134	30	66	−16	−41	9

components the GWP ($H = 500$) differs between inventories only by the CO_2 integral in the denominator.

4. Discussion

Fig. 7 shows the vertical profiles of the relative difference of NO_x, O_3 and OH responses to that of the AEDT inventory (chosen simply as it gives the largest overall response). The aircraft NO_x perturbation for AEDT occurring at 227 hPa is about 25% greater than that for AERO2K. The difference increases with higher altitudes and constitutes 55% at 100 hPa. On the contrary, AERO2K's NO_x significantly exceeds that of AEDT at mid-altitudes, where the difference reaches 500% at 762 hPa. The response of the O_3 for these discrepancies is not the same. It is observed that AERO2K's O_3 response indeed dominates in the low-troposphere region (1000–600 hPa) but only by about 4%, whereas AEDT's dominance at cruise altitudes reaches 25% and 50% at 100 hPa. The same pattern is observed for all inventories, just the scale of differences is not so well pronounced. The linear correlation between additional NO_x and O_3 response is observed in UTLS region, being the strongest at 227 hPa and becoming weaker at higher altitudes, for AERO2K the ratio of O_3 to NO_x is 1 at 227 hPa and 0.9 at 100 hPa (e.g. for AEM it is 1 at 227 hPa and 0.7 at 100 hPa, for REACT4C it is 1.5 at 227 hPa and 0.8 at 100 hPa).

Interestingly, the greatest O_3 aircraft perturbation did not introduce the strongest CH_4 reduction, as might be expected from the chemistry. The altitudinal distribution of emissions can hide the explanation: a significant fraction of AERO2K's NO_x emissions occurs in the mid-troposphere. The ~4%'s dominance of AERO2K's O_3 in 900–700 hPa region significantly changes the oxidizing capacity of the low troposphere (there is more OH by about 30% than for AEDT). Annual mean concentrations of OH and CH_4 and temperature are greater at lower altitudes which catalyse OH production and CH_4 destruction.

Another implication of AERO2K's enhancement of O_3 concentrations at lower altitudes is that this O_3 is not as radiatively efficient as O_3 at higher altitudes (Lacis et al., 1990; Köhler et al., 2008).

It is worth to mention, that not only the height is important, also the geographical distribution of aircraft NO_x emissions plays a certain role in terms of O_3 RF response. The NO_x emissions from low latitudes have a greater impact on climate forcings than the NO_x emissions from high latitudes (Berntsen et al., 2005; Köhler et al., 2012) The AERO2K dataset has lower, compared to other inventories, NO_x emissions at cruise altitudes over East Asia and over the Pacific (not shown here), which was also noted by Olsen et al. (2013). Even though certain regional differences in the distribution of aircraft NO_x emissions occur, they are not as powerful as altitudinal discrepancies in terms of O_3 production (based on work to be published).

Fig. 8 shows a short-term O_3 RF and net NO_x RF responses normalized to 1 Tg of emitted N reported for a number of model simulations (Stordal et al., 2006; Hoor et al., 2009; Myhre et al., 2011; Hodnebrog et al., 2011, 2012). The inter-model mean O_3 and NO_x RF values are 22.2 and 5.0 mW m^{-2} Tg^{-1}(N) yr^{-1}, respectively. While for short-term O_3 responses most of the model results are placed within a one standard deviation range, the net NO_x RF values constitute a more diverse picture. This can be explained by the inter-study differences in the components taken into account for net NO_x calculation. Myhre et al. (2011) pointed out that the ratio of the CH_4 lifetime change to the O_3 column change is very specific for each model, which also influence the net NO_x numbers. The results produced by MOZART-3 are in good agreement with other studies.

The spread in RF values (20% for O_3 RF and 94% for net NO_x RF) between six aircraft inventories is of a smaller magnitude to that of uncertainties between models; however, it is still significant. Myhre et al. (2011) reported a 36% spread in O_3 RF values and 54% in net NO_x

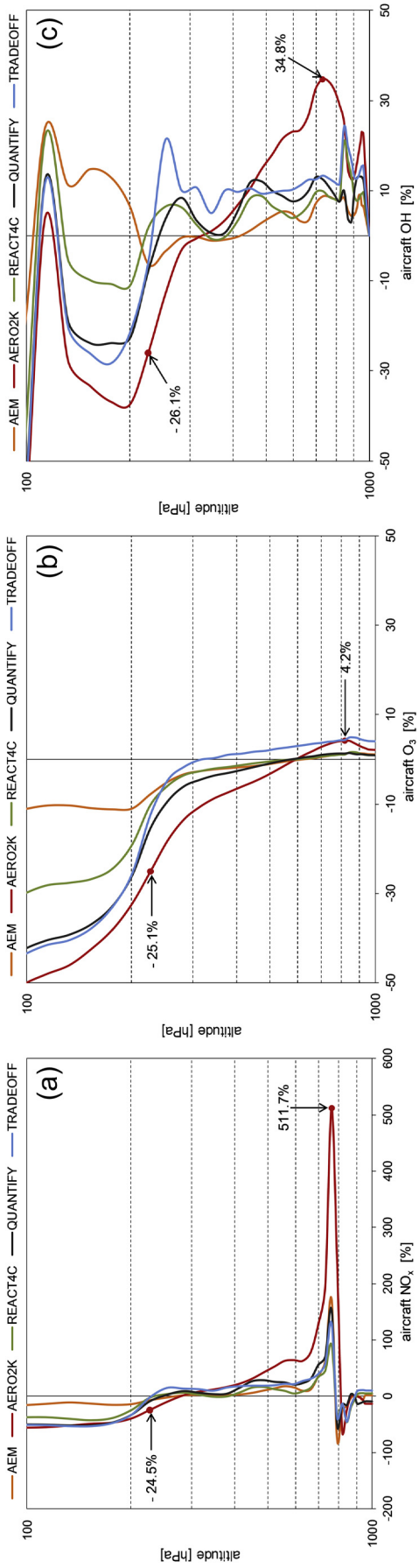

Fig. 7. The globally and annually averaged vertical distributions of relative differences (in %) of aircraft perturbations of NO_x (a), O_3 (b) and OH (c) concentrations for a normalized inventories; results from each inventory were related to the results from AEDT inventory.

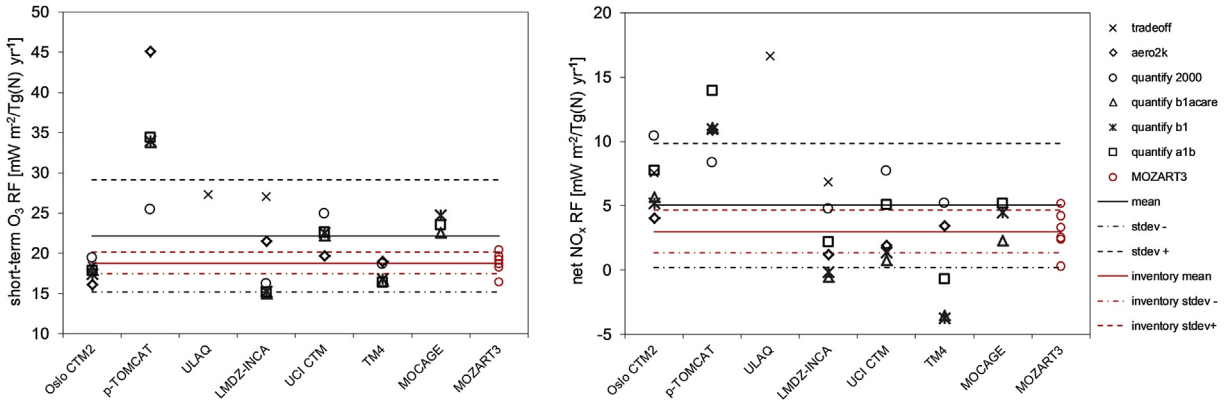

Fig. 8. Global and annual radiative forcings from a short-term O_3 (left) and net NO_x (right) per unit emission of aircraft N (mW m^{-2} Tg^{-1} N yr^{-1}) reported in literature (black font) and shown by this study (red font). Each point represents a particular model study, solid lines denote the mean value, dashed lines show the one standard deviation range of results. The components taken into account as a 'net NO_x' differ from study to study; more information is included in the text.

RF values between a set of five different models (note that Myhre et al. (2011) account for the time-history emissions (Grewe and Stenke, 2008) in their long-term effects); Hoor et al. (2009) reported a 64% spread in O_3 RF and 89% in net NO_x (net is without SWV) values between five different models and Stordal et al. (2006) showed a 33% spread in O_3 RF and 59% in net NO_x RF (net is a sum of short-term O_3 and CH_4 only) values between three different models. This places the discrepancies between different inventories on the same scale of importance as inter-model differences.

5. Conclusions

The coupled NO_x–O_3–CH_4 system, as affected by aviation NO_x emissions, results in a regional short-term O_3 positive radiative forcing and a global long-term O_3, CH_4 and SWV negative responses. Nonetheless the overall radiative forcing induced by current day emissions of aviation NO_x from 3D CTM MOZART-3 is positive as shown by this study, ranging from 3.6 to 0.2 mW m^{-2}.

By using one model (3D CTM MOZART-3) and a series of aircraft inventories (AEDT, AEM, AERO2K, REACT4C, QUANTIFY, TRADEOFF) scaled to the same global total (2.33 Tg (NO_2) yr^{-1}), the sensitivity of O_3 response due to the discrepancies in vertical distribution of aircraft NO_x emissions was investigated. It is observed that the differences in the vertical distribution of aircraft NO_x emissions between inventories, with AEDT and AERO2K being the most different, strongly influence the aircraft short-term O_3 response and consequently the net NO_x effect.

The aviation impact on RF per unit emission of NO_x differs from inventory to inventory and ranges from 5.2 to 0.3 mW m^{-2} Tg^{-1}(N) yr^{-1} (for AEDT and AERO2K, respectively). The responses of short-term O_3 RF range from 20.5 to 16.5 mW m^{-2} Tg^{-1}(N) yr^{-1} (for AEDT and AERO2K, respectively). It is observed that both, the O_3 and net NO_x RF are greater for inventories with higher peak of perturbation of NO_x concentrations, which is a result of the amount of emitted NO_x at higher altitudes.

The spread between aircraft short-term O_3 RF (20%) and aircraft net NO_x RF (94%) values, which emerges from usage of different aircraft inventories should not be neglected as it constitutes a significant range of uncertainty. Careful attention should be paid to formulating aircraft emission inventories where precise cruise altitudes are defined.

Acknowledgements

Two anonymous reviewers are thanked for their constructive comments. We thank Bethan Owen, Ling Lim and Emily Gray for help in understanding the aircraft inventory peculiarities and Ole Amund Søvde for helpful remarks on the manuscript. The CAEP/MDG, EUROCONTROL (http://www.inventair.eurocontrol.int/home) and projects: AERO2K (http://cate.mmu.ac.uk/aero2k.asp), REACT4C (http://www.react4c.eu), QUANTIFY (http://www.pa.op.dlr.de/quantify), TRADEOFF (http://www.iac.ethz.ch/tradeoff) are acknowledged for providing aircraft datasets. This study was funded by the UK Department of Transport.

References

Back, 2002. Back Information Services, Aviation Link: OAG User's Guide for Software, Version 2.3. A Division of Back Associates, Inc.
Berntsen, T.K., Fuglestvedt, J.S., Joshi, M.M., Shine, K.P., Stuber, N., Ponater, M., Sausen, R., Hauglustaine, D.A., Li, L., 2005. Response of climate to regional emissions of ozone precursors: sensitivities and warming potentials. Tellus, Series B: Chemical and Physical Meteorology 57, 283–304.
Brasseur, G.P., Hauglustaine, D.A., Walters, S., Rasch, P.J., Müller, J.-F., Granier, C., Tie, X.X., 1998. MOZART, a global chemical transport model for ozone and related tracers, Part 1: model description. Journal of Geophysical Research 103 (21), 28265–28289.
Edwards, J.M., Slingo, A., 1996. Studies with a flexible new radiation code. I: choosing a configuration for a large-scale model. Quarterly Journal of the Royal Meteorological Society 122, 689–719.
Eyers, C.J., Addleton, D., Atkinson, K., Broomhead, M.J., Christou, R.A., Elliff, T.E., Falk, R., Gee, I.L., Lee, D.S., Marizy, C., Michot, S., Middel, J., Newton, P., Norman, P., Plohr, M., Raper, D.W., Stanciou, N., 2005. AERO2k Global Aviation Emissions Inventories for 2002 and 2025. QinetiQ Ltd., Farnborough, Hampshire. QINETIQ/04/01113.
Flemming, J., Inness, A., Jones, L., Eskes, H.J., Huijnen, V., Schultz, M.G., Stein, O., Cariolle, D., Kinnison, D., Brasseur, G., 2011. Forecasts and assimilation experiments of the Antarctic ozone hole 2008. Atmospheric Chemistry and Physics 11, 1961–1977.
Frömming, C., Ponater, M., Dahlmann, K., Grewe, V., Lee, D.S., Sausen, R., 2012. Aviation-induced radiative forcing and surface temperature change in dependency of the emission altitude. Journal of Geophysical Research 117, D19104.
Fuglestvedt, J.S., Berntsen, T.K., Isaksen, I.S.A., Mao, H., Liang, X.Z., Wang, W.C., 1999. Climatic forcing of nitrogen oxides through changes in tropospheric ozone and methane: global 3D model studies. Atmospheric Environment 33, 961–977.
Fuglestvedt, J.S., Shine, K.P., Cook, J., Berntsen, T., Lee, D.S., Stenke, A., Skeie, R.B., Velders, G.J.M., Waitz, I.A., 2010. Transport impacts on atmosphere and climate: metrics. Atmospheric Environment 44, 4648–4677.
Gauss, M., Isaksen, I.S.A., Lee, D.S., Søvde, O.A., 2006. Impact of aircraft NO_x emissions on the atmosphere – tradeoffs to reduce the impact. Atmospheric Chemistry and Physics 6, 1529–1548.
Granier, C., Guenther, A., Lamarque, J.F., Mieville, A., Muller, J.F., Olivier, J., Orlando, J., Peters, G., Petron, G., Tyndall, G., Wallens, S., 2005. POET, a Database of Surface Emissions of Ozone Precursors. Available at: http://www.aero.jussieu.fr/projet/ACCENT/POET.php.
Grewe, V., Stenke, A., 2008. Airclim: an efficient tool for climate evaluation of aircraft technology. Atmospheric Chemistry and Physics 8, 4621–4639.
Hack, J.J., 1994. Parameterization of moist convection in the NCAR community climate model (CCM2). Journal of Geophysical Research 99, 5551–5568.
Hidalgo, H., Crutzen, P.J., 1977. The tropospheric and stratospheric composition perturbed by NO_x emissions of high-altitude aircraft. Journal of Geophysical Research 82 (37), 5833–5866.
Hodnebrog, Ø., Berntsen, T.K., Dessens, O., Gauss, M., Grewe, V., Isaksen, I.S.A., Koffi, B., Myhre, G., Olivié, D., Prather, M.J., Pyle, J.A., Stordal, F., Szopa, S.,

Tang, Q., van Velthoven, P., Williams, J.E., Ødemark, K., 2011. Future impact of non-land based traffic emissions on atmospheric ozone and OH – an optimistic scenario and a possible mitigation strategy. Atmospheric Chemistry and Physics 11, 11293–11317.

Hodnebrog, Ø., Berntsen, T.K., Dessens, O., Gauss, M., Grewe, V., Isaksen, I.S.A., Koffi, B., Myhre, G., Olivié, D., Prather, M.J., Stordal, F., Szopa, S., Tang, Q., van Velthoven, P., Williams, J.E., 2012. Future impact of traffic emissions on atmospheric ozone and OH based on two scenarios. Atmospheric Chemistry and Physics 12, 12211–12225.

Holstag, A., Boville, B.A., 1993. Local versus nonlocal boundary-layer diffusion in a global climate model. Journal of Climate 6, 1825–1842.

Hoor, P., Borken-Kleefeld, J., Caro, D., Dessens, O., Endresen, O., Gauss, M., Grewe, V., Hauglustaine, D., Isaksen, I.S.A., Jockel, P., Lelieveld, J., Myhre, G., Meijer, E., Olivie, D., Prather, M., Schnadt Poberaj, C., Shine, K.P., Staehelin, J., Tang, Q., van Aardenne, J., van Velthoven, P., Sausen, R., 2009. The impact of traffic emissions on atmospheric ozone and OH: results from QUANTIFY. Atmospheric Chemistry and Physics 9, 3113–3136.

IPCC, 1999. Aviation and the global atmosphere. In: Penner, J.E., Lister, D.H., Griggs, D.J., Dokken, D.J., McFarland, M. (Eds.), Intergovernmental Panel on Climate Change. Cambridge University Press, Cambridge, UK.

Kinnison, D.E., Brausser, G.P., Walters, S., Garcia, R.R., Marsh, D.R., Sassi, F., Harvey, V.L., Randall, C.E., Emmons, L., Lamarque, J.F., Hess, P., Orlando, J.J., Tie, X.X., Randel, W., Pan, L.L., Gettelman, A., Granier, C., Diehl, T., Niemeier, U., Simmons, A.J., 2007. Sensitivity of chemical tracers to meteorological parameters in the MOZART-3 chemical transport model. Journal of Geophysical Research 112, D20302. http://dx.doi.org/10.1029/2006JD007879.

Köhler, M.O., Radel, G., Dessens, O., Shine, K.P., Rogers, H.L., Wild, O., Pyle, J.A., 2008. Impact of perturbations of nitrogen oxide emissions from global aviation. Journal of Geophysical Research 113, D11305.

Köhler, M.O., Radel, G., Shine, K.P., Rogers, H.L., Pyle, J.A., 2012. Latitudinal variation of the effect of aviation NO_x emissions on atmospheric ozone and methane and related climate metrics. Atmospheric Environment 64, 1–9.

Lacis, A., Wuebbles, D., Logan, J.A., 1990. Radiative forcing of climate by changes in the vertical distribution of ozone. Journal of Geophysical Research 95, 9971–9981.

Lamarque, J.F., Bond, T.C., Eyring, V., Granier, C., Heil, A., Klimont, Z., Lee, D., Liousse, C., Mieville, A., Owen, B., Schultz, M.G., Shindell, D., Smith, S.J., Stehfest, E., Van Aardenne, J., Cooper, O.R., Kainuma, M., Mahowald, N., McConnell, J.R., Naik, V., Riahi, K., van Vuuren, D.P., 2010. Historical (1850–2000) gridded anthropogenic and biomass burning emissions of reactive gases and aerosols: methodology and application. Atmospheric Chemistry and Physics 10, 7017–7039.

Lee, D.S., Pitari, G., Grewe, V., Gierens, K., Penner, J.E., Petzold, A., Prather, M., Schumann, U., Bais, A., Berntsen, T., Iachetti, D., Lim, L.L., Sausen, R., 2010. Transport impacts on atmosphere and climate: aviation. Atmospheric Environment 44, 4678–4734.

Lin, S.J., Rood, R.B., 1996. A fast flux form semi-Lagrangian transport scheme on the sphere. Monthly Weather Review 124, 2046–2070.

Liu, Y., Liu, C.X., Wang, H.P., Tie, X.X., Gao, S.T., Kinnison, D., Brasseur, G., 2009. Atmospheric tracers during the 2003–2004 stratospheric warming event and impact of ozone intrusions in the troposphere. Atmospheric Chemistry and Physics 9, 2157–2170.

Müller, J.-F., 1992. Geographical distribution and seasonal variation of surface emissions and deposition velocities of atmospheric trace gases. Journal of Geophysical Research 97, 3787–3804.

Myhre, G., Nilsen, J.S., Gulstad, L., Shine, K.P., Rognerud, B., Isaksen, I.S.A., 2007. Radiative, forcing due to stratospheric water vapour from CH_4 oxidation. Geophysical Research Letters 34, L01807.

Myhre, G., Shine, K.P., Rädel, G., Gauss, M., Isaksen, I.S.A., Tang, Q., Prather, M.J., Williams, J.E., van Velthoven, P., Dessens, O., Koffi, B., Szopa, S., Hoor, P., Grewe, V., Borken-Kleefeld, J., Berntsen, T.K., Fuglestvedt, J.S., 2011. Radiative forcing due to changes in ozone and methane caused by the transport sector. Atmospheric Environment 45, 387–394.

Olsen, S.C., Wuebbles, D.J., Owen, B., 2013. Comparison of global 3-D aviation emissions datasets. Atmospheric Chemistry and Physics 13, 429–441.

Owen, B., Lee, D.S., Lim, L., 2010. Flying into the future: aviation emissions scenarios to 2050. Environmental Science & Technology 44, 2255–2260.

Prather, M., Ehhalt, D., Dentener, F., Derwent, R., Dlugokencky, E., et al., 2001. Atmospheric chemistry and greenhouse gases. In: Houghton, J.T. (Ed.), Climate Change 2001: The Scientific Basis, Contribution of Working Group I to the Third Assessment Report of the Intergovernmental Panel on Climate Change. Cambridge University Press, Cambridge, United Kingdom and New York, NY, USA, pp. 239–287.

Ramaswamy, V., Boucher, O., Haigh, J., Hauglustaine, D., Haywood, J., et al., 2001. Radiative forcing of climate change. In: Houghton, J.T., et al. (Eds.), Climate Change 2001: The Scientific Basis, Contribution of Working Group I to the Third Assessment Report of the Intergovernmental Panel on Climate Change. Cambridge University Press, Cambridge, United Kingdom and New York, NY, USA, pp. 349–416.

Rasch, P.J., Mahowald, N.M., Eaton, B.E., 1997. Representations of transport, convection, and the hydrological cycle in chemical transport models: implications for the modelling of short-lived and soluble species. Journal of Geophysical Research 102, 28,127–28,138.

Rossow, W.B., Schiffer, R.A., 1999. Advances in understanding clouds from ISCCP. Bulletin of the American Meteorological Society 80, 2261–2288.

Sander, S., Friedl, R., Ravishankara, A., Golden, D., Kolb, C., Kurylo, M., Molina, M., Moortgat, G., Finlayson-Pitts, B., Wine, P., Huie, R., Orkin, V., 2006. Chemical Kinetics and Photochemical Data for Use in Atmospheric Studies – Evaluation Number 15. Technical report. Jet Propulsion Laboratory (JPL) of the National Aeronautics and Space Administration (NASA).

Sassi, F., Kinnison, D.E., Boville, B.A., Garcia, R.R., Roble, R., 2004. Effect of El Niño – southern oscillation on the dynamical, thermal, and chemical structure of the middle atmosphere. Journal of Geophysical Research 109, D17108.

Seinfeld, J.H., Pandis, S.N., 2006. Atmospheric Chemistry and Physics From Air Pollution to Climate Change, second ed., vol. 1. John Wiley & Sons, Inc., pp. 210–211.

Simmons, A.J., Uppala, S., Dee, D., Kobayashi, S., 2007. ERA-Interim: new ECWMF reanalysis products from 1989 onwards. ECMWF Newsletter 110, 25–35.

Stevenson, D.S., Johnson, C.E., Collins, W.J., Derwent, R.G., Shine, K.P., Edwards, J.M., 1998. Evolution of tropospheric ozone radiative forcing. Geophysical Research Letters 25 (20), 3819–3822.

Stordal, F., Gauss, M., Myhre, G., Mancini, E., Hauglustaine, D.A., Köhler, M.O., Berntsen, T., Stordal, E.J.G., Iachetti, D., Pitari, G., Isaksen, I.S.A., 2006. TRADEOFFs in climate effects through aircraft routing: forcing due to radiatively active gases. Atmospheric Chemistry and Physics Discussions 6, 10733–10771.

Wild, O., Prather, M.J., Akimoto, H., 2001. Indirect long-term global radiative cooling from NOx emissions. Geophysical Research Letters 28, 1719–1722.

Wilkerson, J.T., Jacobson, M.Z., Malwitz, A., Balasubramanian, S., Wayson, R., Fleming, G., Naiman, A.D., Lele, S.K., 2010. Analysis of emission data from global commercial aviation: 2004 and 2006. Atmospheric Chemistry and Physics 10, 6391–6408.

Wuebbles, D.J., Patten, K.O., Wang, D., Youn, D., Martínez-Avilíes, M., Francisco, J.S., 2011. Three-dimensional model evaluation of the ozone depletion potentials for n-propyl bromide, trichloroethylene and perchloroethylene. Atmospheric Chemistry and Physics 11, 2371–2380.

Zhang, G.J., McFarlane, N.A., 1995. Sensitivity of climate simulations to the parameterization of cumulus convection in the Canadian climate centre general circulation model. Atmosphere-Ocean 33, 407–446.

Bibliography

Azar C., Johansson D. J. A., 2012. On the relationship between metrics to compare greenhouse gases – the case of IGTP, GWP and SGTP. Earth System Dynamics 3, 139-147.

Back, 2002. Back Information Services, Aviation Link: OAG user's guide for software version 2.3. A division of Back Associates, Inc.

Barnett J. J., Corney M., 1985. Middle atmosphere temperature reference model from satellite observations. Advances in Space Research 5, 125-134.

Berntsen T. K., Isaksen I.S.A., 1999. Effects of lightning and convection on changes in tropospheric ozone due to NO_x emissions from aircraft. Tellus 51B, 766-788.

Berntsen, T. K., Fuglestvedt J. S., Joshi M. M., Shine K. P., Stuber N., Ponater M., Sausen R., Hauglustaine D. A., Li L., 2005. Response of climate to regional emissions of ozone precursors: sensitivities and warming potentials. Tellus, Series B: Chemical and Physical Meteorology 57, 283-304.

Berntsen T., Tanaka K., Fuglestvedt J., 2010. Does black carbon abatement hamper CO_2 abatement? Climatic Change 103, 627-633.

Brasseur G.P., Cox R.A., Hauglustaine D., Isaksen I., Lelieveld J., Lister D.H., Sausen R., Schumann U., Wahner A., Wiesen P., 1998. European scientific assessment of the atmospheric effects of aircraft emissions. Atmospheric Environment 32 (13), 2329-2418.

Brasseur G. P., Hauglustaine D. A., Walters S., Rasch P. J., Müller J.-F., Granier C., Tie X. X., 1998b. MOZART, a global chemical transport model for ozone and related tracers, Part 1: Model description. Journal of Geophysical Research 103 (21), 28265-28289.

Buriez J.-C., Bonnel B., Fouquart Y., Geleyn J.-F., Morcrette J.-J., 1988. Comparison of model-generated and satellite-derived cloud cover and radiation budget. Journal of Geophysical Research 93, 3705-3719.

Burkhardt U., Kärcher B., 2011. Global radiative forcing from contrail cirrus, Nature Climate Change, 1, 54-58.

Butkovskaya N., Kukui A., Pouvesle N., Le Bras, G., 2005. Formation of nitric acid in the gas phase HO_2+NO reaction: effects of temperature and water vapour. Journal of Physical Chemistry A 109, 6509-6520.

Cariolle D., Evans M. J., Chipperfield M. P., Butkovskaya N., Kukui A., Le Bras G., 2008. Impact of the new HNO3-forming channel of the HO2+NO reaction on tropospheric HNO_3, NO_x, HO_x and ozone. Atmospheric Chemistry and Physics 8, 4061-4068.

Cariolle D., Caro D., Paoli R., Hauglustaine D. A., Cuénot B., Cozic A., Paugam R., 2009. Parameterization of plume chemistry into large scale atmospheric models: Application to aircraft NO emissions. Journal of Geophysical Research 114, D19.

Chen C.-C., Gettelman A., 2013. Simulated radiative forcing from contrails and contrail cirrus. Atmospheric Chemistry and Physics 13, 12525-12536.

Cherubini F., Peters G., Berntsen T., Strømman A., Hertwich E., 2011. CO_2 emissions from biomass combustion for bioenergy: atmospheric decay and contribution to global warming. Global Change Biology Bioenergy 3, 413-29 426.

Cherubini F., Guest G., Strømman A., 2012. Application of probablity distributions to the modelleing of biogenic CO_2 fluxes in life cycle assessment. Global Change Biology 4 (6), 784-798.

Collins W. J., Fry M. M., Yu H., Fuglestvedt J. S., Shindell D. T., West J. J., 2013. Global and regional temperature change potentials for near-term climate forcers. Atmospheric Chemistry and Physics 13, 2471-2485.

Daniel J., Solomon S., Sanford T., McFarland M., Fuglestvedt J., Friedlingstein P., 2012. Limitations of single basket trading: lessons from the Montreal Protocol for climate policy. Climatic Change 111, 241-248.

Dee D. P., Uppala S. M., Simmons A. J., Berrisford P., Poli P., Kobayashi S., Andrae U., Balmaseda M. A., Balsamo G., Bauer P., Bechtold P., Beljaars A. C. M., van de Berg L., Bidlot J., Bormann N., Delsol C., Dragani R., Fuentes M., Geer A. J., Haimberger L., Healy S. B., Hersbach H., Hólm E. V., Isaksen L., Kållberg P., Köhler M., Matricardi M., McNally A. P., Monge-Sanz B. M., Morcrette J. J., Park B. K., Peubey C., de Rosnay P., Tavolato C., Thépaut J. N., Vitart F., 2011. The ERA-interim reanalysis: configuration and performance of the data assimilation system. Quarterly Journal of the Royal Meteorological Society 137, 553-597.

Denman K. L., Brasseur G., Chidthaisong A., Ciais P., Cox P. M., Dickinson R. E., Hauglustaine D., Heinze C., Holland E., Jacob D., Lohmann U., Ramachandran S, da Silva Dias P. L., Wofsy S. C., Zhang X., 2007. Couplings Between Changes in the Climate System and Biogeochemistry. In: Solomon S., et al. (Eds), Climate Change 2007: The Physical Science Basis. Contribution of Working Group I to the Fourth Assessment Report of the Intergovernmental Panel on Climate Change. Cambridge University Press, Cambridge, United Kingdom and New York, NY, USA, pp. 499-587.

Derwent R. G., 1990. Trace Gases and their Relative Contribution to the Greenhouse Effect. Harwell: Atomic Energy Research Establishment. Document: AERE R13716.

Derwent R., Friedl R., Karil I. I., Kelder H., Kirchoff V. W. J. H., Ogawa T., Rossi M. J., Wennberg P., 1999. Impacts of aircraft emissions on atmospheric ozone. Chapter 2 of 'Aviation and the Global Atmosphere'. In: Penner J.E. et al. (Eds.), Special Report of the Intergovernmental Panel on Climate Change. Cambridge University Press, Cambridge, pp. 36.

Derwent R. G., Collins W. J., Johnson C. E., Stevenson D. S., 2001. Transient behaviour of tropospheric ozone precursors in a global 3-D CTM and their indirect greenhouse effects. Climatic Change 49, 463-487.

Derwent R.G., Stevenson D.S., Doherty R.M., Collins W.J., Sanderson M.G., Johnson C.E., 2008. Radiative forcing from surface NO_x emissions: spatial and seasonal variations. Climatic Change 88, 385-401.

Dlugokencky E., Nisbet E., Fisher R., Lowry D, 2011. Global atmospheric methane: budget, changes and dangers. Philosophical Transactions of the Royal Society a-Mathematical Physical and Engineering Sciences, 369, 2058-2072.

Edwards J. M., Slingo A., 1996. Studies with a flexible new radiation code. I: Choosing a configuration for a larqe-scale model. Quarterly Journal of the Royal Meteorological Society 122, 689-719.

Ehhalt D., Rohrer F., 1994. The impact of commercial aircraft on tropospheric ozone. Proceedings of the 7th Priestley Conference, 24-27 June 1994, Lewisburs, Pennsylvania, USA.

Emmons L. K., Walters S., Hess P. G., Lamarque J.-F., Pfister G. G., Fillmore D., Granier C., Guenther A., Kinnison D., Laepple T., Orlando J., Tie X., Tyndall G., Wiedinmyer C., Baughcum S. L., Kloster S., 2010. Description and evaluation of the model for ozone and related chemical tracers, version 4 (MOZART-4). Geoscience Model Development 3, 43-67.

Eyers C. J., Addleton D., Atkinson K., Broomhead M. J., Christou R. A., Elliff T. E., Falk R., Gee I. L., Lee D. S., Marizy C., Michot S., Middel J., Newton P., Norman P., Plohr M., Raper D. W., Stanciou N., 2005. AERO2k Global Aviation Emissions Inventories for 2002 and 2025. QinetiQ Ltd, Farnborough, Hampshire QINETIQ/04/01113.

Fiore A. M., Jacob D. J., Field B. D., Streets D. G., Fernandes S. D., Jang C., 2002. Linking ozone pollution and climate change: The case for controlling methane. Geophysical Research Letters 29 (19), 1919.

Fisher D. A., Hales C. H., Wang W. C., Ko M. K. W., Sze N. D., 1990. Model calculations of the relative effects of CFCs and their replacements on global warming. Nature 344, 513-516.

Flemming J., Inness A., Jones L., Eskes H. J., Huijnen V., Schultz M. G., Stein O., Cariolle D., Kinnison D., Brasseur G., 2011. Forecasts and assimilation experiments of the Antarctic ozone hole 2008. Atmospheric Chemistry and Physics 11, 1961-1977.

Forster P., Shine K. P., Stuber N., 2006. It is premature to include non-CO_2 effects of aviation in emission trading schemes. Atmospheric Environment 40, 1117-1121.

Forster P., Ramaswamy V., Artaxo P., Berntsen T., Betts R., Fahey D. W., Haywood J., Lean J., Lowe D. C., Myhre G., Nganga J., Prinn R., Raga G., Schulz M., Van Dorland R., 2007. Changes in Atmospheric Constituents and in Radiative Forcing. In: Solomon S., et al. (Eds), Climate Change 2007: The Physical Science Basis. Contribution of Working Group I to the Fourth Assessment Report of the Intergovernmental Panel on Climate Change. Cambridge University Press, Cambridge, United Kingdom and New York, NY, USA, pp. 129-234.

Frömming C., Ponater M., Dahlmann K., Grewe V., Lee D. S., Sausen R., 2012. Aviation-induced radiative forcing and surface temperature change in dependency of the emission altitude. Journal of Geophysical Research 117, D19104.

Fry M., Naik V., West J. J., Schwarzkopf M. D., Fiore A. M., Collins W. J., Dentener F. J., Shindell D. T., Atherton C., Bergmann D., Duncan B. N., Hess P., MacKenzie I. A., Marmer E., Schultz M. G., Szopa S., Wild O., Zen G., 2012. The influence of ozone precursor emissions from four world regions on tropospheric composition and radiative climate forcing. Journal of Geophysical Research 117, D07306.

Fuglestvedt J. S., Berntsen T. K., Isaksen I. S. A., Mao H., Liang X. Z. and Wang W. C., 1999. Climatic forcing of nitrogen oxides through changes in tropospheric ozone and methane; global 3D model studies. Atmospheric Environment 33, 961-77.

Fuglestvedt J., Berntsen T., Godal O., Skodvin T., 2000. Climate implications of GWP-based reductions in greenhouse gas emissions. Geophysical Research Letters 27, 409-412.

Fuglestvedt J., Berntsen T., Godal O., Sausen R., Shine K., Skodvin T., 2003. Metrics of climate change: Assessing radiative forcing and emission indices. Climatic Change 58, 267-331.

Fuglestvedt J., Berntsen T., Myhre G., Rypdal K., Skeie R.B., 2008. Climate forcing from the transport sectors. Proceedings of the National Academy of Sciences of the United States of America 105, 2, 454-458.

Fuglestvedt J. S., Shine K. P., Cook J., Berntsen T., Lee D. S., Stenke A., Skeie R. B., Velders G. J. M., Waitz I. A., 2010. Transport impacts on atmosphere and climate: Metrics. Atmospheric Environment 44, 4648-4677.

Gauss M., Isaksen I. S. A., Lee D. S., Søvde O. A., 2006. Impact of aircraft NO_x emissions on the atmosphere – tradeoffs to reduce the impact. Atmospheric Chemistry and Physics 6, 1529-1548.

Gettelman A., Kinnison D. E., Brasseur G., Dunkerton T., 2004. Impact of monsoon circulations on the upper troposphere and lower stratosphere. Journal of Geophysical Research 109, D22101.

Gillett N. P., Matthews H. D., 2010. Accounting for carbon cycle feedbacks in a comparison of the global warming effects of greenhouse gases. Environmental Research Letters 5, 034011.

Godal O., Fuglestvedt J., 2002. Testing 100-year global warming potentials: Impacts on compliance costs and abatement profile. Climatic Change 52, 93-127.

Gottschaldt K., Voigt C., Jöckel P., Righi M., Deckert R., Dietmüller S., 2013. Global sensitivity of aviation NO_x effects to the HNO_3-forming channel of the HO_2 + NO reaction. Atmospheric Chemistry and Physics 13, 3003-3025.

Granier C., Guenther A., Lamarque J. F., Mieville A., Muller J. F., Olivier J., Orlando J., Peters G., Petron G., Tyndall G., Wallens S., 2005. POET, a database of surface emissions of ozone precursors. (available at http://www.aero.jussieu.fr/projet/ACCENT/POET.php).

Grewe V., Dameris M., Hein R., Köhler I., Sausen R., 1999. Impact of future subsonic aircraft NO_x emissions on the atmospheric composition. Geophysical Research Letters 26 (1), 47-50.

Grewe V., Dameris M., Fichter C., Lee D.S., 2002. Impact of aircraft NO_x emissions. Part 2: effects of lowering the flight altitude. Meteorologische Zeitschrift 11 (3), 197-205.

Grewe V., Stenke A., 2008. Airclim: an efficient tool for climate evaluation of aircraft technology. Atmospheric Chemistry and Physics 8, 4621-4639.

Grewe V., Dahlmann K., Matthes S., Steinbrecht W., 2012. Attributing ozone to NO_x emissions: Implications for climate mitigation measures. Atmospheric Environment 59, 102-107.

Hack J. J., 1994. Parameterization of moist convection in the NCAR community climate model (CCM2). Journal of Geophysical Research 99, 5551-5568.

Hansen J., Sato M., Ruedy R., 1997. Radiative forcing and climate response. Journal of Geophysical Research 102, D6, 6831-6864.

Harvey L. D. D., 2000. Global Warming: The Hard Science. Published Harlow: Prentice Hall, pp. 336.

Hidalgo H., Crutzen P.J., 1977. The tropospheric and stratospheric composition perturbed by NO_x emissions of high-altitude aircraft. Journal of Geophysical Research 82 (37), 5833-5866.

Holstag A., Boville B. A., 1993. Local versus nonlocal boundary-layer diffusion in a global climate model. Journal of Climate 6, 1825-1842.

Hodnebrog Ø., Berntsen T. K., Dessens O., Gauss M., Grewe V., Isaksen I. S. A., Koffi B., Myhre G., Olivié D., Prather M. J., Pyle J. A., Stordal F., Szopa S., Tang Q., van Velthoven P., Williams J. E., Ødemark K., 2011. Future impact of non-land based traffic emissions on atmospheric ozone and OH – an optimistic scenario and a possible mitigation strategy. Atmospheric Chemistry and Physics 11, 11293-11317.

Hodnebrog Ø., Berntsen T. K., Dessens O., Gauss M., Grewe V., Isaksen I. S. A., Koffi B., Myhre G., Olivié D., Prather M. J., Stordal F., Szopa S., Tang Q., van Velthoven P., Williams J. E., 2012. Future impact of traffic emissions on atmospheric ozone and OH based on two scenarios. Atmospheric Chemistry and Physics 12, 12211-12225.

Holmes C. D., Tang Q., Prather M. J., 2011. Uncertainties in climate assessment for the case of aviation NO. Proceedings of the National Academy of Sciences of the United States of America 108, 10997-11002.

Hoor P., Borken-Kleefeld J., Caro D., Dessens O., Endresen O., Gauss M., Grewe V., Hauglustaine D., Isaksen I. S. A., Jockel P., Lelieveld J., Myhre G., Meijer E., Olivie D., Prather M., Schnadt Poberaj C., Shine K. P., Staehelin J., Tang Q., van Aardenne J., van Velthoven P., Sausen R., 2009. The impact of traffic emissions on atmospheric ozone and OH: results from QUANTIFY. Atmospheric Chemistry and Physics 9, 3113-3136.

Horowitz L. W., Walters S., Mauzerall D. L., Emmons L. K., Rasch P. J., Granier C., Tie X., Lamarque J.-F., Schultz M. G., Tyndall G. S., Orlando J. J., Brasseur G.P., 2003. A global simulation of tropospheric ozone and related tracers: Description and evaluation of MOZART, version 2, Journal of Geophysical Research 108 (D24), 4784.

Hough A. M., 1989. The development of a two-dimensional global tropospheric model. 1. The model transport. Atmospheric Environment, 23, 1235-1261.

Hough A. M, 1991. Development of a two-dimensional global tropospheric model: model chemistry. Journal of Geophysical Research, 96, 7325-7362.

Hough A.M., Johnson C. E., 1991. Modelling the role of nitrogen oxides, hydrocarbons and carbon monoxide in the global formation of tropospheric oxidants. Atmospheric Environment 25A, 1819-1835.

Houghton J. T., Jenkins G. J., Ephraums J. J. (Eds.), 1990. Climate Change: The IPCC Scientific Assessment. Cambridge University Press, Cambridge, Great Britain, New York, NY, USA and Melbourne, Australia, pp. 410.

Isaksen I. S. A., Hov Ø., Hesstvedt E., 1978. Ozone generation over rural areas. Environmental Science and Technology 12, 1279-1284.

Isaksen I., Jackman C., Baughcum S., Dentener F., Grose W., Kasibhatla P., Kinnison D., Ko M.K.W., McConnell J.C., Pitari G., Wuebbles D.J., 1999. Modeling the chemical composition of the future atmosphere. Chapter 4 of 'Aviation and the Global Atmosphere'. In: Penner J.E., et al. (Eds.), Special Report of the Intergovernmental Panel on Climate Change. Cambridge University Press, Cambridge, pp. 43.

Isaksen I.S.A., Berntsen T.K., Wang W.-C., 2001. NO_x emissions from aircraft: its impact on the global distribution of CH_4 and O_3 and on radiative forcing. Terrestrial, Atmospheric and Oceanic Sciences 12 (1), 63-78.

Isaksen I., Granier C., Myhre G., Berntsen T.K., Dalsøren S.B., Gauss M., Klimont Z., Benestad R., Bousquet P., Collins W., Cox T., Eyring V., Fowler D., Fuzzi S., Jöckel P., Laj P., Lohmann U., Maione M., Monks P., Prevot A.S.H., Raes F., Richter A., Rognerud B., Schulz M., Shindell D., Stevenson D.S., Storelvmo T., Wang W.-C., van Weele M., Wild M., Wuebbles D., 2009. Atmospheric composition change: Climate-Chemistry interactions. Atmospheric Environment 43, 5138-5192.

Jaeglé L., Jacob D. J., Brune W. H., Tan D., Faloona I. C., Weinheimer A. J., Ridley B. A., Campos T. L., Sachse G. W., 1998. Sources of HO_x and production of ozone in the upper troposphere over the United States. Geophysical Research Letters 25, 1709-1712.

Johansson D. J. A, Persson U. M., Azar C., 2006. The cost of using global warming potentials: analysing the trade off between CO_2, CH_4 and N_2O. Climatic Change 77, 291-309.

Johnson C. E., Derwent R. G., 1996. Relative radiative forcing consequences of global emissions of hydrocarbons, carbon monoxide and NO_x from human activities estimated with a zonally-averaged two-dimensional model. Climatic Change, 34, 439-462.

Johnson C., Henshaw J., McInnes G.,1992. Impact of aircraft and surface emissions of nitrogen oxides on tropospheric ozone and global warming. Nature 355, 69-71.

Jones N., 2013. Troubling milestone for CO_2. Nature Geoscience 6, 589.

Joos F., Roth R., Fuglestvedt J. S., Peters G. P., Enting I. G., von Bloh W., Brovkin V., Burke E. J., Eby M., Edwards N. R., Friedrich T., Frölicher T. L., Halloran P. R., Holden P. B., Jones C., Kleinen T., Mackenzie F. T., Matsumoto K., Meinshausen M., Plattner G.-K., Reisinger A., Segschneider J., Shaffer G., Steinacher M., Strassmann K., Tanaka K., Timmermann A., Weaver A. J., 2013. Carbon dioxide and climate impulse response functions for the computation of greenhouse gas metrics: a multi-model analysis. Atmospheric Chemistry and Physics 13, 2793-2825.

Kandlikar M., 1995. The relative role of trace gas emissions in greenhouse abatement policies. Energy Policy 23 (10), 879-883.

Kärcher B., 1996. Aircraft-generated aerosols and visible contrails. Geophysical Research Letters 23, 1933-1936.

Kinnison D. E., Brausser G. P., Walters S., Garcia R. R., Marsh D. R., Sassi F., Harvey V. L., Randall C. E., Emmons L., Lamarque J. F., Hess P., Orlando J. J., Tie X. X., Randel W., Pan L. L., Gettelman A., Granier C., Diehl T., Niemeier U., Simmons A. J., 2007. Sensitivity of chemical tracers to meteorological parameters in the MOZART-3 chemical transport model, Journal of Geophysical Research 112, D20302.

Köhler M. O., Rädel G., Dessens O., Shine K. P., Rogers H. L., Wild O., Pyle J. A., 2008. Impact of perturbations of nitrogen oxide emissions from global aviation. Journal of Geophysical Research 113, D11305.

Köhler M. O., Rädel G., Shine K. P., Rogers H. L., Pyle J. A., 2012. Latitudinal variation of the effect of aviation NO_x emissions on atmospheric ozone and methane and related climate metrics. Atmospheric Environment 64, 1-9.

Lacis A., Wuebbles D., Logan J. A., 1990. Radiative forcing of climate by changes in the vertical distribution of ozone. Journal of Geophysical Research 95, 9971-9981.

Lamarque J. F., Bond T. C., Eyring V., Granier C., Heil A., Klimont Z., Lee D., Liousse C., Mieville A., Owen B., Schultz M. G., Shindell D., Smith S. J., Stehfest E., Van Aardenne J., Cooper O. R., Kainuma M., Mahowald N., McConnell J. R., Naik V., Riahi K., van Vuuren D. P., 2010. Historical (1850–2000) gridded anthropogenic and biomass burning emissions of reactive gases and aerosols: methodology and application. Atmospheric Chemistry and Physics 10, 7017-7039.

Lamarque J., Kyle G. P., Meinshausen M., Riahi K., Smith S. J., van Vuuren D. P., Conley A., Vitt F., 2011. Global and regional evolution of short-lived radiatively-active gases and aerosols in the Representative Concentration Pathways. Climatic Change 109, 191-212.

Lashof D. A., 2000. The use of global warming potentials in the Kyoto Protocol. Climatic Change 44, 423-425.

Lashof D. A., Ahuja D. R., 1990. Relative contributions of greenhouse gas emissions to global warming. Nature 344, 529-531.

Lee D. S., Fahey D., Forster P., Newton P. J., Wit R. C. N., Lim L. L., Owen B., Sausen R., 2009. Aviation and global climate change in the 21st century. Atmospheric Environment 43, 3520-3537.

Lee D. S., Pitari G., Grewe, V., Gierens K., Penner J. E., Petzold A., Prather M., Schumann U., Bais A., Berntsen T., Iachetti D., Lim L. L., Sausen R., 2010. Transport impacts on atmosphere and climate: Aviation. Atmospheric Environment 44, 4678-4734.

Leibensperger E. M., Mickley L. J., Jacob D. J., Barrett S. R. H., 2011. Intercontinental influence of NO_x and CO emissions on particulate matter air quality, Atmospheric Environment 45, 3318-3324.

Lin S. J., Rood R. B., 1996. A fast flux form semi-Lagrangian transport scheme on the sphere. Monthly Weather Review 124, 2046-2070.

Lin X., Trainer M., Liu S. C., 1988. On the nonlinearity of the tropospheric ozone production. Journal of Geophysical Research 93, 15879-15888.

Liu Y., Liu C. X., Wang H. P., Tie X. X., Gao S. T., Kinnison D., Brasseur G., 2009. Atmospheric tracers during the 2003–2004 stratospheric warming event and impact of ozone intrusions in the troposphere. Atmospheric Chemistry and Physics 9, 2157-2170.

Lund M., Berntsen T., Fuglestvedt J., Ponater M., Shine K., 2012. How much information is lost by using global mean climate metrics? an example using the transport sector. Climatic Change, 113, 949-963.

Mahlman J. D., Levy H., Moxim W. J., 1980. Three-dimensional tracer structure and behaviour as simulated in two ozone precursor experiments, Journal of Atmospheric Sciences 37, 655-685.

Manne A., Richels R., 2001. An alternative approach to establishing trade-offs among greenhouse gases. Nature 29, 410, 675-677.
Manning M., Reisinger A., 2011. Broader perspectives for comparing different greenhouse gases. Philosophical Transactions of the Royal Society A – Mathematical Physical and Engineering Sciences, 369, 1891-1905.

Michaelis P., 1992. Global warming: efficient policies in the case of multiple pollutants. Environmental and Resource Economics 2, 61-77.

Müller J.-F., 1992. Geographical distribution and seasonal variation of surface emissions and deposition velocities of atmospheric trace gases. Journal of Geophysical Research 97, 3787-3804.

Myhre G., Nilsen J.S., Gulstad L., Shine K.P., Rognerud B., Isaksen I. S. A., 2007. Radiative forcing due to stratospheric water vapour from CH_4 oxidation. Geophysical Research Letters 34, L01807.

Myhre G., Kvalevåg M., Rädel G., Cook J., Shine K., Clark H., Karcher F., Markowicz K., Kardas A., Wolkenberg P., Balkanski Y., Ponater M., Forster P., Rap A., Rodriguez De Leon R., 2009. Intercomparison of radiative forcing calculations of stratospheric water vapour and contrails. Meteorologische Zeitschrift 18, 585-596.

Myhre G., Shine K. P., Rädel G., Gauss M., Isaksen I. S. A., Tang Q., Prather M. J., Williams J. E., van Velthoven P., Dessens O., Koffi B., Szopa S., Hoor P., Grewe V., Borken-Kleefeld J., Berntsen T. K., Fuglestvedt J. S., 2011. Radiative forcing due to changes in ozone and methane caused by the transport sector. Atmospheric Environment 45, 387-394.

Naik V., Mauzerall D., Horowitz L., Schwarzkopf M. D., Ramaswamy V., Oppenheimer M., 2005. Net radiative forcing due to changes in regional emissions of tropospheric ozone precursors, Journal of Geophysical Research 110, D24306.

Neu J., Prather M., 2012. Toward a more physical representation of precipitation scavenging in global chemistry models: cloud overlap and ice physics and their impact on tropospheric ozone. Atmospheric Chemistry and Physics 12, 3289-3310.

Olsen S. C., Wuebbles D. J., Owen B., 2013. Comparison of global 3-D aviation emissions datasets. Atmospheric Chemistry and Physics 13, 429-441.

O'Neill B. C., 2000. The jury is still out on global warming potentials. Climatic Change 44, 427-443.

O'Neill B. C., 2003. Economics, natural science, and the costs of global warming potentials – an editorial comment. Climatic Change 58, 251-260.

Oort A. H., 1983. Global atmospheric circulation statistics, NOAA Professional Paper 14, Geophysical Fluid Dynamics Laboratory, Princeton, N.J.

Owen B., Lee D. S., Lim L., 2010. Flying into the future: Aviation Emissions Scenarios to 2050. Environmental science and Technology 44, 2255-2260.

Pan L. L., Wei J. C., Kinnison D. E., Garcia R. R., Wuebbles D. J., Brasseur G. P., 2007. A set of diagnostics for evaluating chemistry climate models in the extratropical tropopause region. Journal of Geophysical Research 112, D09316.

Park M., Randel W. R., Kinnison D. E., Garcia R. R., Choi W., 2004. Seasonal variations of methane, water vapor, ozone, and nitrogen dioxide near the tropopause: Satellite observations and model simulations, Journal of Geophysical Research 109, D03302.

Penner J. E., Lister D. H., Groggs D. J., Dokken D. J., McFarland M. (Eds.), 1999. Aviation and the global atmosphere: a special report of IPCC Working Groups I and III in collaboration with the Scientific Assessment Panel to the Montreal Protocol on Substances that Deplete the Ozone Layer. Cambridge University Press, UK, pp. 373.

Peters G., Aamaas B., Berntsen T., Fuglestvedt J., 2011. The integrated global temperature change potential (iGTP) and relationships between emission metrics. Environmental Research Letters 6, 044021.

Pitari G., Mancini E., Bregman A., 2002. Climate forcing of subsonic aviation: indirect role of sulfate particles via heterogeneous chemistry. Geophysical Research Letters 29 (22), 14 1-4.

Plumb R. A., Mahlman J. D., 1987. The zonally-averaged transport characteristics of the GFDL general circulation/transport model. Journal of Atmospheric Sciences 44, 298-327.

Prather M. J., 1994. Lifetimes and eigenstates in atmospheric chemistry. Geophysical Research Letters 21 (9), 801-804.

Prather M., Sausen R., Grossmann A. S., Haywood J. M., Rind D., Subbaraya B. H., 1999. Potential climate change from aviation. Chapter 6 of 'Aviation and the global atmosphere'. In: Penner J. E., et al. (Eds.), Special Report of the Intergovernmental Panel on Climate Change. Cambridge University Press, Cambridge.

Prather M., Ehhalt D., Dentener F., Derwent R., Dlugokencky E., et al., 2001. Atmospheric chemistry and greenhouse gases. In: Houghton J.T. (Eds.), Climate Change 2001: The Scientific Basis, Contribution of Working Group I to the Third Assessment Report of the Intergovernmental Panel on Climate Change. Cambridge University Press, Cambridge, United Kingdom and New York, NY, USA, pp. 239-287.

Ramaswamy V., Boucher O., Haigh J., Hauglustaine D., Haywood J., et al., 2001. Radiative forcing of climate change. In: Houghton J.T., et al. (Eds.), Climate Change 2001: The Scientific Basis, Contribution of Working Group I to the Third Assessment Report of the Intergovernmental Panel on Climate Change. Cambridge University Press, Cambridge, United Kingdom and New York, NY, USA, pp. 349-416.

Rasch P. J., Mahowald N. M., Eaton B. E., 1997. Representations of transport, convection, and the hydrological cycle in chemical transport models: Implications for the modelling of short-lived and soluble species, Journal of Geophysical Research 102, 28127-28138.

Reisinger A., Meinshausen M., Manning M., 2011. Future changes in global warming potentials under representative concentration pathways. Environmental Research Letters 6, 024020.

Righi M., Hendricks J., Sausen R., 2013. The global impact of the transport sectors on atmospheric aerosol: simulations for year 2000 emissions. Atmospheric Chemistry and Physics 13, 9939-9970.

Rogers H. L., Lee D. S., Raper D. W., Forster P. M. D., Wilson C. W., Newton P. J., 2002. The impact of aviation on the atmosphere. Aeronautical Journal 106 (1064), 521-546.

Rossow W. B., Schiffer R. A., 1999. Advances in understanding clouds from ISCCP, Bulletin of the American Meteorological Society 80, 2261-2288.

Royal Society, 2008. Ground-level ozone in the 21st century: future trends, impacts and policy implications. Science Policy Report 15/08. Available at: http:// royalsociety.org/policy/ publications/2008/ground-level-ozone/.

Rypdal K., Berntsen T., Fuglestvedt J. S., Aunan K., Torvanger A., Stordal F., Pacyna J. M., Nygaard L. P., 2005. Tropospheric ozone and aerosols in climate agreements: scientific and political challenges. Environmental Science and Policy 8, 29-43.

Sander S., Friedl R., DeMore W., Ravishankara A., Golden D., Kolb C., Kurylo M., Molina M., Hampson R., Huie R., Moortgat G., 2003. Chemical kinetics and photochemical data for use in stratospheric modelling – evaluation number 13. Technical report, Jet Propulsion Laboratory (JPL) of the National Aeronautics and Space Administration (NASA).

Sander S., Friedl R., Ravishankara A., Golden D., Kolb C., Kurylo M., Molina M., Moortgat G., Finlayson-Pitts B., Wine P., Huie R., Orkin V., 2006. Chemical kinetics and photochemical data for use in atmospheric studies – evaluation number 15. Technical report, Jet Propulsion Laboratory (JPL) of the National Aeronautics and Space Administration (NASA).

Sassi F., Kinnison D. E., Boville B. A., Garcia R. R., Roble R., 2004. Effect of El Niño – Southern Oscillation on the dynamical, thermal, and chemical structure of the middle atmosphere. Journal of Geophysical Research 109, D17108.

Sausen R., Isaksen I., Grewe V., Hauglustaine D., Lee D.S., Myhre G., Köhler M.O., Pitari G., Schumann U., Stordal F., Zerefos C., 2005. Aviation radiative forcing in 2000: an update of IPCC (1999). Meteorologische Zeitschrift 14 (4), 555-561.

Seinfeld J. H., Pandis S. N., 2006. Atmospheric Chemistry and Physics From Air Pollution to Climate Change, volume 1. John Wiley & Sons, Inc., second edition, pp. 1203.

Shindell D. T., Faluvegi G., Bell N., Schmidt G. A., 2005. An emissions-based view of climate forcing by methane and tropospheric ozone. Geophysical Research Letters 32, L04803.

Shindell D. T., Faluvegi G., Koch D. M., Schmidt G. A., Unger N., Bauer S. E., 2009. Improved attribution of climate forcing to emissions, Science, 326, 716-718.

Shine K., 2009. The global warming potential–the need for an interdisciplinary retrial. Climatic Change 8, 467-472.

Shine K., Berntsen T., Fuglestvedt J., Sausen R., 2005a. Scientific issues in the design of metrics for inclusion of oxides of nitrogen in global climate agreements. Proceedings of the National Academy of Sciences of the United States of America 102, 44, 15768-15773.

Shine K., Fuglestvedt J., Hailemariam K., Stuber N., 2005b. Alternatives to the global warming potential for comparing climate impacts of emissions of greenhouse gases. Climatic Change 68, 281-302.

Shine K., Berntsen T., Fuglestvedt J., Skeie R., Stuber N., 2007. Comparing the climate effect of emissions of short- and long-lived climate agents. Philosophical Transactions of the Royal Society A – Mathematical Physical and Engineering Sciences 365, 1903-1914.

Schoeberl M. R., Douglass A. R., Zhu Z., Pawson S., 2003. A comparison of the lower stratospheric age spectra derived from a general circulation model and two data assimilation systems, Journal of Geophysical Research 108 (D3), 4113.

Skodvin T., 1999. Making climate change negotiable: the development of the global warming potential index. Working Paper 1999:9. CICERO, Oslo, Norway. Available at http://www.cicero.uio.no/media/194.pdf.

Skowron A., Lee D. S., Hurley J., 2009. Aviation NO_x Global Warming Potential. 2nd International Conference on Transport, Atmosphere and Climate, 25-28 June 2009, Aachen/Maastricht, Germany/Netherlands.

Skowron A., Lee D. S., De Leon R. R., 2013. The assessment of the impact of aviation NO_x on ozone and other radiative forcing responses – The importance of representing cruise altitudes accurately. Atmospheric Environment 74, 159-168.

Smith S. J., Wigley T. M. L., 2000a. Global Warming Potentials: 1. Climatic implications of emissions reductions. Climatic Change 44, 445-457.

Smith S. J., Wigley T. M. L., 2000b. Global Warming Potentials: 2. Accuracy. Climatic Change, 44, 459-469.

Smith S. M., Lowe J. A., Bowerman N. H. A., Gohar L. K., Huntingford C., Allen M. R., 2012. Equivalence of greenhouse-gas emissions for peak temperature limits. Nature Climate Change, 2, 535-538.

Søvde O. A., Gauss M., Isaksen I. S. A., Pitari G., Marizy C., 2007. Aircraft pollution – a futuristic view, Atmospheric Chemistry and Physics 7, 3621-3632.

Søvde O. A., Hoyle C. R., Myhre G., Isaksen I. S. A., 2011. The HNO_3 forming branch of the HO_2+NO reaction: pre-industrial to present trends in atmospheric species and radiative forcings. Atmospheric Chemistry and Physics 11, 8929-8943.

Solomon S., Qin D., Manning M., Chen Z., Marquis M., Averyt K. B., Tignor M., Miller H. L. (Eds.), 2007. Contribution of Working Group I to the Fourth Assessment Report of the Intergovernmental Panel on Climate Change. Cambridge University Press, Cambridge, United Kingdom and New York, NY, USA.

Stevenson D. S., Johnson C. E., Collins W. J., Derwent R. G., Shine K. P., Edwards J. M., 1998. Evolution of tropospheric ozone radiative forcing. Geophysical Research Letters 25, 20, 3819-3822.

Stevenson D. S., Doherty R. M., Sanderson M. G., Collins W. J., Johnson C. E., Derwent R.G., 2004. Radiative forcing from aircraft NO_x emissions: Mechanisms and seasonal dependence. Journal of Geophysical Research 109, D17307.

Stevenson D. S., Dentener F. J., Schultz M. G., Ellingsen K., van Noije T. P. C., Wild O., Zeng G., Amann M., Atherton C. S., Bell N., Bergmann D. J., Bey I., Butler T., Cofala J., Collins W. J., Derwent R. G., Doherty R. M., Drevet J., Eskes H. J., Fiore A. M., Gauss M., Hauglustaine D. A., Horowitz L. W., Isaksen I. S. A., Krol M. C., Lamarque J.-F., Lawrence M. G., Montanaro V., Müller J.-F., Pitari G., Prather M. J., Pyle J. A., Rast S., Rodriguez J. M., Sanderson M. G., Savage N. H., Shindell D. T., Strahan S. E., Sudo K., Szopa S. Multimodel ensemble simulations of present-day and near-future tropospheric ozone. Journal of Geophysical Research 111, D08301

Stevenson D.S. and Derwent R.G., 2009. Does the location of aircraft nitrogen oxide emissions affect their climate impact? Geophysical Research Letters 36, L17810.
Stiller G. P., von Clarmann T., Haenel F., Funke B., Glatthor N., Grabowski U., Kellmann S., Kiefer M., Linden A., Lossow S., López-Puertas M., 2012. Observed temporal evolution of global mean age of stratospheric air for the 2002 to 2010 period. Atmospheric Chemistry and Physics 12, 3311-3331.

Stordal F., Gauss M., Myhre G., Mancini E., Hauglustaine D. A., Köhler M. O., Berntsen T., Stordal E. J. G., Iachetti D., Pitari G., Isaksen I. S. A., 2006. TRADEOFFs in climate effects through aircraft routing: forcing due to radiatively active gases. Atmospheric Chemistry and Physics Discussions 6, 10733-10771.

Tanaka K., O'Neill B., Rokityanskiy D., Obersteiner M., Tol R., 2009. Evaluating Global Warming Potentials with historical temperature. Climatic Change 96, 443-466.

Tanaka K., Peters G. P., Fuglestvedt J. S., 2010. Multicomponent climate policy: why do emission metrics matter? Carbon Management 1(2), 191-197.

Tanaka K., Johansson D., O'Neill B., Fuglestvedt J., 2013. Emission metrics under the 2°C climate stabilization. Climatic Change Letters 117, 933-941.

Taraborrelli D., Lawrence M. G., Crowley J. N., Dillon T. J., Gromov S., Groß C. B. M., Vereecken L., Lelieveld J., 2012. Hydroxyl radical buffered by isoprene oxidation over tropical forests, Nature Geoscience 5, 190-193.

Tol R., Berntsen T., O'Neill B., Fuglestvedt J., Shine K., 2012. A unifying framework for metrics for aggregating the climate effect of different emissions. Environmental Research Letters 7, 044006.

Trenberth K. E., Fasullo J. T., Kiehl J., 2009. Earth's global energy budget. Bulletin of the American Meteorological Society 90, 311-324.

Unger N., 2011. Global climate impact of civil aviation for standard and desulfurized jet fuel. Geophysical Research Letters 38, L20803.

Unger N., Shindell D. T., Koch D. M., Streets D. G., 2006. Cross influences of ozone and sulfate precursor emissions changes on air quality and climate, Proceedings of the National Academy of Sciences of the United States of America, 103, 4377-4380.

van Noije T. P. C., Eskes H. J., Dentener F. J., Stevenson D. S., Ellingsen K., Schultz M. G., Wild O., Amann M., Atherton C. S., Bergmann D. J., Bey I., Boersma K. F., Butler T., Cofala J., Drevet J., Fiore A. M., Gauss M., Hauglustaine D. A., Horowitz L. W., Isaksen I. S. A., Krol M. C., Lamarque J.-F., Lawrence M. G., Martin R. V., Montanaro V., Müller J.-F., Pitari G., Prather M. J., Pyle J. A., Richter A., Rodriguez J. M., Savage N. H., Strahan S. E., Sudo K., Szopa S., van Roozendael M., 2006. Multi-model ensemble simulations of tropospheric NO_2 compared with gome retrievals for the year 2000. Atmospheric Chemistry and Physics 6 (10), 2943-2979.

West J. J., Fiore A. M., Naik V., Horowitz L. W., Schwarzkopf M. D., Mauzerall D. L., 2007. Ozone air quality and radiative forcing consequences of changes in ozone precursor emissions, Geophysical Research Letters 34, L06806.

Wigley T. M. L., 1998. The Kyoto Protocol: CO_2, CH_4, and climate implications. Geophysical Research Letters 25, 2285-2288.

Wilcox L., Shine K., Hoskins B., 2012. Radiative forcing due to aviation water vapour emissions. Atmospheric Environment 63, 1-13.

Wild O., Prather M. J., Akimoto H., 2001. Indirect long-term global radiative cooling from NOx emissions. Geophysical Research Letters 28, 1719-1722.

Wilkerson J. T., Jacobson M. Z., Malwitz A., Balasubramanian S., Wayson R., Fleming G., Naiman A. D., Lele S. K., 2010. Analysis of emission data from global commercial aviation: 2004 and 2006. Atmospheric Chemistry and Physics 10, 6391-6408.

Wu S. L., Duncan B. N., Jacob D. J., Fiore A. M., Wild O., 2009. Chemical nonlinearities in relating intercontinental ozone pollution to anthropogenic emissions. Geophysical Research Letters 36, L05806.

Wuebbles D., 1983. Chlorocarbon emission scenarios: potential impact on stratospheric ozone. Journal of Geophysical Research 88, 1433-43.

Wuebbles D. J., Patten K. O., Wang D., Youn D., Martínez-Avilíes M., Francisco J. S., 2011. Three-dimensional model evaluation of the Ozone Depletion Potentials for n-propyl bromide, trichloroethylene and perchloroethylene. Atmospheric Chemistry and Physics 11, 2371-2380.

Zhang G. J., McFarlane N. A., 1995. Sensitivity of climate simulations to the parameterization of cumulus convection in the Canadian climate centre general circulation model. Atmosphere-Ocean 33, 407-446.